Dietary and pharmacological interventions to improve mammalian healthspan and lifespan

Inaugural-Dissertation

zur

Erlangung des Doktorgrades

der Mathematisch-Naturwissenschaftlichen Fakultät

der Universität zu Köln

vorgelegt von

Lisonia Gkioni

aus Athens, Griechenland

Köln, 2022

This is a dissertation accepted by the Faculty of Mathematics and Natural Sciences of the University of Cologne

Date of thesis defense: 03.02.2023

Gutachter: **Prof. Dr. Linda Partridge**

Prof. Dr. Matteo Bergami

I. Table of Contents

II. Acknowledgements

First, I would like to thank Prof. Dr. Linda Partridge for her trust, patient guidance and invaluable feedback throughout my time as a PhD student. I am grateful for her words of advice always aimed at getting the most out of the projects I was involved in. Thanks to her, I was shown the path to independence, resilience and responsibility in performing high quality research. I also want to express my gratitude to Dr. Sebastian Grönke for bringing his thorough knowledge and experience through all the stages of completing this thesis. His feedback was instrumental to the integrity of my research. This endeavour would not have been possible without their expertise and supervision.

I would like to extend my thanks to my thesis committee members, Prof. Dr. Dario Valenzano and Prof. Dr. Manolis Pasparakis for their support and constructive feedback. I am extremely thankful to Prof. Dr. Matteo Bergami and Prof. Dr. Jan Riemer for being part of the defence committee and evaluating my work. A special thanks to Dr. Andromachi Pouikli for agreeing to write the thesis protocol and being part of the defence.

I am deeply indebted to my forever twin, Dr. Carolina Monzó for being the best lab-partner I could ever hope for. She is a brilliant researcher, incredible friend and inspirational person and none of the work that was carried out during these years would have been possible without her. I feel very lucky to have shared multiple projects and many moments with her. Together with Nathalie Jauré, they are the smartest and coolest bioinformatic brains I have ever known. Nathalie is an amazing researcher, caring and reliable friend and wonderful person who I admire and hope to share the date of defence with (fingers crossed!). Special thanks to Mehdi (or actually Mehdis) for sustaining this group of troubled researchers and knowing first-hand what being a PhD means. He always made sure we could push through and was a source of fun and wisdom. Words cannot express my gratitude to Carolina, Nathalie and Mehdi for their immense support and friendship and I cannot wait to share many more moments with them in the future; still we rise!

Additionally, I am extremely thankful to a great crew of people who directly or indirectly contributed to this thesis. Special thanks should go to Maarouf who is an amazing scientist I have learned so much from and a brain expert, who, instead of mocking me when I knew nothing about his favourite organ (the brain), he had tireless discussions with me and helped with everything he could. I am also grateful to Bruna and Sophie who shared their fly work experience with me and with whom I shared so many great nights of gaming, trips and holidays. During these years as a PhD student, I had the pleasure of working with a brilliant group of technicians who put their experience and skills to my disposal. I will be forever grateful to Sandra, who is such a kind soul, strong and compassionate and greatly helped me with mouse work. The dissection days were a lot more entertaining because of her and I will always remember our motto: ‘Teamwork makes the dream work!’ A really successful teamwork was also the one behind the microbiome project and I cannot thank Jenny and Ramona enough for their hard work, incredible organisation skills and fun discussions during the countless metabolite extractions. I would like to also acknowledge Ola and Jens for their involvement in this project and tireless discussions on optimisations. Many thanks to Oliver Hendrich for always making sure I had assistance in keeping up with a demanding mouse experimental schedule and for directly being involved in dissections, as well as to André and Ramona for their help in performing various mouse experiments. Furthermore, I am sincerely grateful to

Sarah for her huge help with the brain stainings; Lisa and Tobias for sharing their expertise in mouse work with me and setting the experimental foundation on which parts of this thesis were based; Elisa for helping me move and being an amazing buddy; Helena, Pingze and Larissa for always being supportive and fun to talk to; Javi for the great talks and encouragement (Ánimo); Joris for the moral and scientific support, as well as Dennis, Jonathan, Annika and Sina. They have all contributed to creating an open, motivating and pleasant atmosphere during these past years. I would also like to thank Christine, for making sure that everything was running smoothly and Daniela Morrick for her advice and support.

Moreover, I would like to acknowledge the fantastic core facilities of the MPI for Biology of Ageing and external collaborators that were instrumental for the completion of the current work. Many thanks to the Comparative Biology Facility and especially Dr. Bettina Bertalan and Dr. Sandra Buhl and all animal caretakers in the experimental and quarantine barrier. Special thanks to my primary caretakers Doreen Briel, Karina Pilger and Sabrina Seyfarth for feeding and ensuring the wellbeing of the animals on a daily basis and especially to Doreen Briel for the excellent collaboration. I am also thankful to the members of the Phenotyping Core Facility, Martin for being our mentor of mouse oral gavages, and Andrea for her enormous help during glucose tolerance and insulin sensitivity tests. A big thanks to Patrick, Frederik and Yvonne from the Metabolomics and Xinping from the Proteomics Facility. Many thanks should go to the FACS & Imaging Facility, especially Dr. Christian Kukat and Marcel, for their help with the microscopy sessions. A special thank you to Heiko Backes from the MPI for Metabolism research, who was always willing to answer my questions and provided me with everything I needed to complete parts of this thesis.

My sincere thanks to my greek gang in Cologne, Machi, Danae and Chrysanthi (κορίτσια μου!) for their scientific help, friendship and emotional support. All three are brilliant scientists and great friends that I cannot put into words how thankful I am to have met them. We have shared smiles, stories and worries together and, although I cannot promise to visit you if you stay in Cologne (!) I will make sure you come wherever I will be!

Getting through my dissertation would not have been possible without the unwavering emotional support of Mar, who was always there for me with her word of advise and devilish humour to keep me going (αγαπημένη ζέβρα); Laz, who bothered to know every single detail of my work, did so much to lift my spirits during the past months and whose project ideas might at some point shake the world of science (εσύ κι αν προλαβαίνεις να αλλάξεις καριέρα μπέστιε!); Anja, with her heartfelt encouragement who never stopped trusting I could do this (ζουλιτσίσι); and of Kris, Chris, Ioanna and Thaleia for their incredible friendship and understanding. I count on all of you to make sure I will not lose my sanity (έχετε προϋπηρεσία). Σας αγαπάω και σας ευχαριστώ!

Finally, my deepest appreciation and thanks go to my family. Words cannot express how grateful I am to my beloved parents, Leta and Niko, for their endless patience, support, encouragement, love and devotion. I could have never undertaken this journey without their unconditional trust and help along the way. Μαμά, μπαμπά, thank you for being inspiring role models and know that you are the two most influential people in my life! Special thanks also to my grandparents and aunt who have been generous with their love and encouragement. You are the best family ever!!! Σας αγαπάω πολύ και σας υπερευχαριστώ για όλα!!!

III. Abbreviations

AD	Alzheimer's disease
AIRR	Adaptive Immune Receptor Repertoire
ANOVA	Analysis of variance
AL	Ad libitum
ALP	Alkaline phosphatase
AL_DR16M	Midlife onset DR at 16 months of age
AL_DR20M	Late-life onset DR at 20 months of age
AP-1	Activator protein-1
AST	Aspartate transaminase
BAT	Brown adipose tissue
BCR	B-Cell Receptor
BSA	Bovine Serum Albumin
c	Controls
C. elegans	Caenorhabditis elegans
CMRglc	Cerebral metabolic rate of glucose
DAPI	4′,6-diamidino-2-phenylindole
DR	Dietary Restriction
DUSP/DUSP1/2	Dual-specificity phosphatase/Dual-specificity phosphatase1/2
ERK	Extracellular signal-regulated kinase
FELASA	Federation of European Laboratory Animal Science Associations
18F-FDG	2-deoxy-2-[fluorine-18] fluoro-D-glucose
FFPE	Formalin-fixed paraffin embedded
Foxo	Forkhead Box O
GAPs	GTPase-activating proteins
GDP	Guanosine diphosphate
GEFs	Guanine nucleotide exchange factors
GFAP	Glial fibrillary acidic protein
γ-GT	γ-Glutamyl transferase

GSK-3	Glycogen synthase kinase-3
GTP	Guanosine triphosphate
H&E	Hematoxylin and eosin
HR	Heart rate
HRP	Horseradish peroxidase
HSC	Haematopoietic Stem Cells
Iba-1	Ionised calcium-binding adaptor molecule 1
IF	Intermittent fasting
IGF	Insulin-like growth factor
Igh	Immunoglobulin Heavy Chain Complex
IghC	Immunoglobulin heavy chain constant domain
IghD	Immunoglobulin heavy chain diversity domain
IghJ	Immunoglobulin heavy chain joining domain
IghV	Immunoglobulin heavy chain variable domain
IIS	Insulin and insulin-like growth factor signalling
INF-γ	Interferon-γ
IMGT	International immunogenetics information
IL-1β	Interleukin-1β
IL-6	Interleukin-6
NF-kb	Nuclear factor 'kappa-light-chain-enhancer' of activated B-cells
LC-MS	Liquid chromatography–mass spectrometry
MAPK	Mitogen-activated protein kinase
MTBE	Methyl-tert-butyl-ether
MRM	Multiple reaction monitoring
P20	Frequency of 20 most present BCR clones
PGE2	Prostaglandin E2
PI3K	Phosphatidylinositol 3-kinase
PBS	Phosphate-buffered saline
PBST	PBS + 0.2% Triton X-100
PET	Positron emission tomography

r	Rapamycin at 42 mg/kg
RDI	Repertoire Dissimilarity Index
rt	Rapamycin and trametinib at 1.44 mg/kg
RTKs	Receptor tyrosine kinases
SHM	Somatic Hypermutation
S6K	Ribosomal S6 kinase
TBS	Tris-buffered saline
TBS-T	Tris-buffered saline with Tween 20
t-high	Trametinib at 1.44 mg/kg
TNF/TNF-α	Tumour necrosis factor/Tumour necrosis factor-α
t-low	Trametinib at 0.58 mg/kg
TLRs	Toll-like receptors
TOR	Target of rapamycin
TORC1	Target of rapamycin complex 1
TPL2	Tumour progression locus 2
Tsc1	Tuberous sclerosis complex 1
Tsc2	Tuberous sclerosis complex 2
UMI	Unique Molecular Identifier
WAT	White adipose tissue

1. Aim of the thesis

1.1 Summary

Advances in the field of ageing over recent years have led to the discovery that pharmacological and dietary interventions can slow the ageing process. Genetic alterations to the insulin/insulin-like growth factor (IGF) signalling (IIS) and mechanistic target of rapamycin (mTOR) network in multiple organisms have provided promising targets for pharmacological interventions. mTOR inhibition by rapamycin robustly extends lifespan and is associated with marked health improvements in multiple model organisms. Similarly, pharmacological manipulation of Ras signalling by trametinib prolongs lifespan in flies, and treatment with a combination of trametinib, rapamycin and lithium induced an additive increase in fly lifespan. However, whether trametinib alone or in combination with rapamycin can also extend mouse lifespan is currently unknown. Although combinatorial drug treatments hold great promise to maximise longevity, and potentially to reduce drug dosage and hence side-effects, to date, the most effective environmental intervention known to extend healthy lifespan in various animal species is Dietary Restriction (DR). DR alleviates a plethora of age-related pathologies, including immune dysregulation with age. The adaptive immune system is highly sensitive to DR feeding and DR delays age-associated T-cell immune senescence. Nevertheless, the impact of DR on B-cell immune responses, and whether the improved health and lifespan of DR mice can be attributed to some extent to enhanced B-cell immunity under DR, remain largely unexplored. My PhD thesis first explores the potential of a novel pharmacological intervention to promote mouse healthy ageing. Second, the work elucidates the role of adaptive immunity as a contributor to the benefits of a robust dietary intervention on mouse health and longevity. Specifically the thesis work addresses the following: (I) Does trametinib administration extend lifespan in mice and is there an additive effect by combining trametinib and rapamycin on mouse health and/or longevity. (II) Does B-cell immunity change in response to DR and could these changes contribute to the increased health and lifespan under DR.

Chapter 3 of the thesis encompasses a detailed characterization of the effects of trametinib, alone and in combination with rapamycin, on the lifespan and healthspan of female and male mice. For this purpose, I assessed the survival of mice treated with trametinib at two doses, with rapamycin alone, and with their combination, with untreated controls. Trametinib-only treated female and male mice were significantly longer lived compared to the controls and mice receiving the double combination of trametinib and rapamycin showed a lifespan extension that was greater compared to the single trametinib and rapamycin treatments. Rapamycin and trametinib combination induced a mild attenuation of the age-related decline in heart rate in males and improvement in exploratory capacity in old females. The combination of trametinib and rapamycin also reduced tumour formation in the spleen and liver of old animals, progression of spleen tumours between 12 and 24 months of age, and kidney inflammation in old female mice. Finally, by studying brain glucose metabolism and the activation of microglia and astrocytes, I showed that the double combination of trametinib and rapamycin attenuated the age-related increase in brain glucose uptake and significantly reduced the accumulation of striatal microglia and astrocytes in females, suggesting that trametinib and rapamycin might alleviate age-related brain inflammation.

In Chapter 4 of the thesis, I examined the effects of chronic and late-onset DR on the ageing B-cell receptor (BCR) repertoire in the mouse spleen and ileum. Given that the critical time period wherein DR can prolong lifespan lies between 16 and 20 months, I assessed the changes in the BCR repertoire in response to chronic DR and DR initiated at 16 and 20 months of age. Chronic DR attenuated the age-associated decline in spleen BCR repertoire diversity and the increased occupation by expanded clones. DR onset at 16 months of age, which has been found to extend lifespan to a similar extent as chronic DR, showed diversity and maintenance of the clonal population structure similar to chronic DR. In contrast, DR onset at 20 months was associated with a profile that was more similar to ad libitum feeding. Further, by studying the ileum BCR changes upon the chronic and late-onset DR, I demonstrated that chronic DR is only accompanied by few changes in the ileum, which facilitate antigen-binding capacity. Despite the mild response of the ileum, the microbiome strongly responded to chronic DR and late-onset DR, with initiation of DR at both 16 and 20 months of age inducing microbiome diversification similar to chronic DR. Finally, I found a negative correlation between the increased within-individual diversity and decreased clonal expansions under chronic DR and DR onset at 16 months in the spleen and ileum with morbidity, suggesting that these adaptive immunity traits may contribute to the responsiveness in lifespan to DR feeding.

1.2 Zusammenfassung

Fortschritte auf dem Gebiet der Altersforschung in den letzten Jahren haben gezeigt, dass pharmakologische und diätetische Eingriffe den Alterungsprozess positiv beeinflussen können. Durch genetische Veränderungen im Insulin/IGF (IIS) bzw. mTOR-Netzwerks wurden vielversprechende Angriffspunkte für pharmakologische Eingriffe in diese ernährungsabhängigen Signalwegen aufgedeckt. So führt die Hemmung des mTOR-Signalweges durch das Medikament Rapamycin zu einer längeren Lebensspanne und verbesserten Gesundheit in verschiedensten Modellorganismen einschließlich der Taufliege Drosophila und bei Mäusen. Auch die pharmakologische Hemmung des Ras/MEK/ERK Signalweges durch das Medikament Trametinib verlängert die Lebenszeit von Fliegen. Interessanterweise führte eine Kombinationsbehandlung mit Trametinib und Rapamycin zu einer additiven Verlängerung der Lebensspanne von Fliegen. Ob Trametinib allein oder in Kombination mit Rapamycin auch die Lebensspanne von Mäusen verlängern kann, ist derzeit noch unbekannt. Kombinatorische Arzneimittelbehandlungen sind ein vielversprechender Ansatz, um die Langlebigkeit zu maximieren und möglicherweise die Arzneimitteldosierung und damit auch die Nebenwirkungen zu reduzieren. Allerdings ist der wirksamste zurzeit bekannte Eingriff um die gesunde Lebensspanne zu verlängern, eine reduzierte Nahrungsaufnahme (Fachbegriff: "Dietary Restriction", DR). Die DR-Behandlung lindert eine Vielzahl altersbedingter Pathologien, einschließlich der altersbedingten Abnahme der Funktion des Immunsystems. Dabei ist der Einfluß von DR auf die altersbedingte Abnahme der Funktion der T-Zellen bereits bekannt. Inwieweit DR auch die Funktion der B-Zellen beeinflußt und ob die verbesserte Gesundheit und Lebensdauer von DR-Mäusen auf einem verbessertem Immunsystem beruht, ist jedoch noch weitgehend unerforscht. In meiner Doktorarbeit habe ich die folgenden zwei Fragestellungen untersucht: (I) Verlängert die Verabreichung von Trametinib die Lebensspanne von Mäusen und gibt es einen zusätzlichen Effekt durch die Kombination von Trametinib und Rapamycin auf die Gesundheit und die Langlebigkeit von Mäusen? (II) Verändert sich die Zusammensetzung des B-Zell-Rezeptorrepertoires wenn Mäuse mit DR behandelt werden, und tragen diese Veränderungen eventuell zu der erhöhten Gesundheit und Lebenserwartung der DR Tiere bei?

Kapitel 3 der Dissertation beinhaltet eine detaillierte Untersuchung wie Trametinib, allein und in Kombination mit Rapamycin, die Lebenszeit und Gesundheit von Mäusen beeinflußt. Um dies zu untersuchen, wurden männliche und weibliche Tiere mit zwei verschiedenen Dosierungen von Trametinibbehandelt. Diese Mäuse lebten signifikant länger als die Kontrolltiere, was zeigt, dass eine Trametinibbehandlung auch in Säugetieren die Lebenszeit verlängern kann. Interessanterweise führte die Kombination aus Trametinib und Rapamycin zu einer deutlichen verlängerten Lebenszeit, im Vergleich zu den Einzelbehandlungen. Die Kombination von Rapamycin und Trametinib bewirkte auch eine leichte Abschwächung des altersbedingten Rückgangs der Herzfrequenz bei männlichen Tieren und eine Verbesserung der Erkundungsfähigkeit bei alten weiblichen Tieren. Desweiteren war die Tumorbildung in Milz und Leber, und Entzündungen in der Niere durch die doppelte Medikamentengabe reduziert. Die Kombination von Trametinib und Rapamycin verringerte auch den altersbedingten Anstieg der Glukoseaufnahme im Gehirn und die Anhäufung von Mikroglia und Astrozyten, was darauf hindeutet, dass Trametinib und Rapamycin altersbedingte Gehirnentzündungen lindern könnten.

In Kapitel 4 der Dissertation beschreibe ich, wie DR das B-Zell-Rezeptor (BCR)-Repertoire der der Maus in Milz und Ileums während des Alterungsprozess beinflußt. Mittels BCR-Sequenzierung konnte ich zeigen, dass eine kontinuierliche DR Behandlung den altersbedingten Rückgang der Vielfalt des BCR-Repertoires in der Milz verlangsamt und die Entstehung von B Zellklonen reduziert. Mäuse verlieren im Alter zwischen 16 und 20 Monaten die Eigenschaft auf die DR Behandlung mit einer Lebenszeitverlängerung zu reagieren, so daß Unterschiede in diesen zwei Zeitpunkten Hinweise auf Faktoren geben können, die ursächlich für die verlängerte Lebenszeit der DR Tiere sind. Wurde die DR Behandlung mit 16 Monaten begonnen, zeigten die Mäuse eine ähnliche Diversität und Aufrechterhaltung der klonalen Populationsstruktur im BCR-Repertoire der Milz wie unter der chronischen DR Behandlung. Im Gegensatz dazu zeigten Tiere bei denen die DR Behandlung erst mit 20 Monaten begonnen wurde, ein BCR-Repertoire, was den Ad-libitum Kontrolltieren ähnelte. Dieses Ergebnis deutet darauf hin, dass diese Veränderung im BCR-Repertoire eventuell eine Rolle für DR bedingte Lebenszeitverlängerung spielt. Im Gegensatz zur Milz, gab es im Ileum nur wenige Veränderungen im BCR-Repertoire mit dem Alter oder unter der DR Diät. Dies war erstaunlich, da die DR Behandlung die Zusammensetzng des Darm-Mikrobioms stark veränderte, was zeigt dass die Zusammensetzung des BCR Repertoire im Darm unabhängig von der Zusammensetzung des Darmmikrobioms ist. Weiterhin konnte ich zeigen, dass die Morbidität der Mäuse negativ mit bestimmten Parametern des BCR-Repertoire in der Milz korreliert war, was darauf hindeutet, dass diese Merkmale der adaptiven Immunität eine Rolle in der Lebensszeitverlängerung unter DR Bedingungen haben könnten.

2. Methods

2.1 Mouse work

All mice were kept in the Comparative Biology facility of the Max Planck Institute for Biology of Ageing. Female and male F1 hybrid mice (C3B6F1) were generated in-house by crossing C3H/HeOuJ females with C57BL/6NCrl males (strain codes 626 and 027, respectively, Charles River Laboratories).

2.1.1 Mouse Husbandry, DR and drug treatments

2.1.1.1 Mouse Husbandry

All protocols involving animals were carried out in accordance with the guidelines of the Federation of the European Laboratory Animal Science Association (FELASA) with all protocols approved by the Landesamt für Natur, Umwelt und Verbraucherschutz, Nordrhein-Westfalen, Germany (reference no. 84-02.04.2017.A074 and 81-02.04.2019.A313, and AZ: 84-02.04.2015.A437). All mice were housed in individually ventilated cages (GM500 Mouse IVC Green Line, Techniplast), in groups of five mice per cage, under specific-pathogen-free conditions, at 21°C, with 50-60% humidity and a 12h light/dark cycle. For environmental enrichment, mice had constant access to nesting material and chew sticks. Mice had ad libitum access to chow (Ssniff Spezialdiäten GmbH; Ssniff, R/MH low phytoestrogen content) and sterile-filtered water at all times, unless withdrawal or reduction of chow was necessary for specific experiments or feeding regimes.

In the first study (Chapter 3), directly after birth, litters with more than 8 pups were reduced to a maximum of 8 pups, while litters with fewer than 4 pups were excluded to avoid lifespan-modulating effects of mal- or overfeeding during the nursing period. After weaning at 3 weeks of age, females were randomly allocated to cages, while male mice were weaned litter-wise to avoid aggression and fighting. If males of different litters had to be combined, a ratio of 2:3 was preferred over a 4:1 ratio. After randomization and cage allocation, cages were randomly assigned to treatment groups, to which researchers were blinded. To rule out that the drugs interfere with the water uptake of the mice, consumption of drinking water was measured weekly during the pretest experiment. For that purpose, water bottles were weighed when placed into the holding cage and when replaced. Average drinking water consumption per cage and day was determined from the weight difference. Additionally, body weight was measured weekly during the 4-weeks of the pretest experiment and every 8 weeks from animals of the lifespan cohort. Weighing of lifespan animals was started 4 weeks before the start of the drug treatment at 6 months of age.

In the second study (Chapter 4), litter size was adjusted to a maximum of 8 pups, after removal of male pups within 3 days of birth. After weaning at 3-4 weeks of age, the pups were randomly allocated to cages and subsequently to groups, to which researchers were blinded.

2.1.1.2 DR treatment

To elucidate the effects of DR on the adaptive immune system, C3B6F1 hybrid female mice were used. C3B6F1 hybrids have been successfully used by the LP lab and respond well to DR treatment (Hahn et al. 2019, 2017). The study consisted of four treatment groups: mice fed ad libitum (AL), mice under chronic DR feeding (DR), mice switched from AL to DR at 16 (AL_DR16M) and 20 months (AL_DR20M) of age. Lifespan was assessed in the lifespan cohort (n = 220 mice), and spleen and ileum tissues were collected from a separate cohort of mice (Drews et al. 2021). To avoid developmental effects, the chronic DR treatment was initiated at the age of 12 weeks. Food consumption of the AL group was measured weekly, and DR animals received 60% of the food amount consumed by AL-fed animals, i.e. food intake was reduced by 40%. DR animals were fed once per day in the morning, while AL animals had constant access to food. All animals had constant access to water. The chow diet (Ssniff Spezialdiäten GmbH; Ssniff, R/MH low phytoestrogen content) was enriched with all essential vitamins and minerals, ensuring that DR animals were adequately supplied with all essential nutrients, despite their lower food intake. All animals were checked daily for their well-being and deaths were recorded.

2.1.1.3 Drug treatments

C3B6F1 females and males were used to study the effect of trametinib and rapamycin single and combined treatments on health- and lifespan in mice. 5 treatment groups were included in the study: (I) Control mice received a standard rodent diet (Rat/Mouse - Low phytoestrogen (R/M-phyto low), Ssniff Spezialdiäten Gmbh, Germany) supplemented with the corresponding amount of the encapsulation material Eudragit S100 (1-207-490-4242, Evonik CYRO LLC, 480 mg/kg diet) and PEG-400 (3,2 ml/kg), (II) Rapamycin mice received R/M-phyto low food containing 42 mg/kg rapamycin (522 mg encapsulated rapamycin/kg diet) and PEG-400 (3,2 ml/kg), (III+IV) Trametinib mice received R/M-phyto low food containing trametinib at 0.58 mg/kg (low) or 1,44 mg/kg of diet (high), respectively, and Eudragit S100 (480 mg/kg diet) and PEG-400 (3,2 ml/kg), and (V) Rapamycin/Trametinib mice received food containing rapamycin at 42 mg/kg and trametinib at 1.44 mg/kg of diet and PEG-400 (3,2 ml/kg). Calculations on the amount of trametinib in the diet were based on the assumption of a mouse body weight of 30 g with daily food consumption of 5 g per mouse. Rapamycin was obtained from LC Laboratories and encapsulated by Southwest Research Institute (SwRI). Trametinib was obtained from Biozol (1187431-43-1).

Drug treatments for the lifespan, phenotyping and tissue collection experiments were started at the age of 6 months. Before that, mice were fed the standard chow diet supplemented with Eudragit S100 (1-207-490-4242, Evonik CYRO LLC, 480 mg/kg diet). Trametinib was administered continuously. Rapamycin was administered intermittently, with the mice alternating between rapamycin and control food on a weekly basis. Double treatment with rapamycin and trametinib was also done intermittently, with weekly alternations of rapamycin/trametinib and trametinib food. The dose of 42 mg/kg of rapamycin was chosen based on the robust lifespan extension in genetically heterogeneous mice receiving this dose (Richard A. Miller et al. 2014). Trametinib doses were determined based on the results of a pretest experiment and were according to the assessment report of the European Medicines Agency (EMA/CHMP/258608/2014).

2.1.2 Mouse phenotyping

Phenotyping was performed in a separate mouse cohort (phenotyping cohort) to evaluate healthspan, behaviour and fitness. A total of 75 C3B6F1 female and 75 male mice were bred and 15 mice per treatment group were tested. Experiments were performed in middle-aged animals at 12 months of age and at old age at 20-22 months age. All tests were carried out during the light phase of the light/dark cycle and experimenters were blinded to the treatment group. Experimental apparatus was cleaned with Bacilol AF between the various tests, as well as between cages of the same testing run.

2.1.2.1 Electrocardiography

Electrocardiography (ECG) was performed to examine heart rate and function. The electrical activity of the heart was recorded non-invasively via the paws of conscious mice using the ECGenie system (Mouse Specifics: https://mousespecifics.com/heart/ecgenie/). The ECGenie system is a raised platform enclosed in red Plexiglas. Mice were placed on the training platform (i.e. an additional platform on each side of the measurement platform) for 10 minutes, which allows for acclimatisation prior to the test. Subsequently, each mouse was placed on the measurement platform on interchangeable electrodes that transmit the electrical signals to a computer for a maximum of 10 minutes. Signals with a heart rate variation that exceeded 35 bpm were excluded (Thireau et al. 2008) and the average heart rate per mouse was evaluated in the analysis.

2.1.2.2 Rotarod

Rotarod was performed to assess motor coordination and learning. Mice were placed onto the Rotarod (TSE Systems, type 3375-M5) as it was rotating at a low speed (5 rpm). After starting the measurement, the revolving rate was continuously increased from 5 rpm to 40 rpm over a total period of 300 seconds. The total time that each mouse spent on the rod, with a cut-off time of 300 seconds was measured. The test was performed on four consecutive days to assess learning capability.

2.1.2.3 Treadmill

To measure endurance, mice were placed onto the treadmill (TSE Systems, type 3033401-M-04/C) and allowed to warm up and acclimatise to the experimental setup for 5 minutes under low speed (0.1m/sec). Subsequently, a progressively accelerating speed was applied from 0.1 m/sec for another ten minutes to 1.3 m/s within 60 min. A mild electroshock (0.3 mA) was applied for 5 seconds, followed by 5 seconds of refractory period as soon as mice slowed down beyond a critical point and crossed the laser beam for more than 2 seconds to ensure that mice only stopped running upon exhaustion. Exhaustion was defined as the willingness of a mouse to withstand three consecutive shocks instead of continuing running.

2.1.2.4 Open field

The open field experiment was carried out to determine locomotion, exploratory drive and anxiety-like behaviour (ActiMot2, TSE Systems). Mice were placed in a box of approximately 50 cm x 50 cm x 40 cm and were allowed to freely explore for 10 minutes. The test chamber

was illuminated to 20-30 lux. At 5 and 10 minutes, their total activity, speed and time spent in the centre was recorded via infrared sensors.

2.1.3 Mouse tissue collection, macro-pathological and histopathological examination

2.1.3.1 Tissue collection

For tissue collection from drug treated mice (chapter 3) 24-month old female and male mice were sacrificed using cervical dislocation. Mice were decapitated and the skull and body were dissected in parallel to limit tissue deterioration. Liver, spleen, kidney, WAT and brain tissues were harvested, snap-frozen in liquid nitrogen and stored at -80°C for subsequent molecular analysis. Plasma-EDTA was isolated by adding 1µl of 500 mM EDTA per 100 µl of blood and subsequent centrifugation at 1,000g for at least 10 min at 4 °C, followed by aliquoting and storage at −80 °C. Liver, spleen, white adipose tissue (WAT), brown adipose tissue (BAT), heart, kidney, pancreas ovaries or testis, femur and brain samples were dissected and fixed in 10% neutral-buffered formalin (HT501320-9.5L, Sigma) for preparation of formalin-fixed paraffin embedded (FFPE) tissues or cryosections for subsequent histological analysis.

For tissue collection of DR mice, (chapter 4), spleen and ileum tissues were harvested and snap-frozen using liquid nitrogen at 5, 16, 20, 24 and 28 months of age, followed by storage at -80°C until further use. Tissue collection was done by Lisa F. Drews.

2.1.3.2 Post mortem macro-pathology analysis

Post-mortem macroscopical examination of drug-treated mice (chapter 3) was performed by the care-takers. Mice that died naturally and those that had to be sacrificed due to bad health, were examined and pathologies were documented. Tumour load and location, organ enlargement and abnormalities, including organ discoloration or granulation were documented. The presence and severity of tumours was scored with 0 (absence), 1 (one tumour in one organ), 2 (multiple tumours or tumour diameter > 3 cm in one organ or metastasis in two organs), 3 (severe metastasis in 3 or more organs) (Ikeno et al. 2009). The presence of other lesions was scored with 1 or 0 (absence). The severity of pathology was adjusted upon combination of multiple pathological findings (i.e. if one organ was affected by both tumours and discoloration, the score was adjusted from 1 to 2) (Ikeno et al. 2009).

2.1.3.3 Mouse histopathology

Histopathological examination of liver, heart, pancreas, kidney, WAT, BAT, spleen, ovaries, testes and femur of 24 months old drug treated animals was carried out by Prof. Robert Klopfleisch (Institute of Veterinary Pathology, Freie Universitaet Berlin). Hematoxylin and eosin (H&E) stainings were performed and each organ was scored for the following pathological lesions: liver was examined for the presence of lymphomas, sarcomas, benign or malignant tumours, as well as for the presence of lipidosis (diffuse or focal) or necrosis. Liver tumour grade was determined as low (scored with 1), moderate (scored with 2), high (scored with 3) and very high (scored with 4). Heart was assessed for the presence of hypertrophy and fibrosis. In pancreas, the presence of inflammation, fat necrosis, lymphoma and exocrine

atrophy was evaluated. For both the heart and the pancreas, the presence of each of the pathologies was scored with 1 and the absence with 0. The presence of kidney lesions, lymphoma, oxalate crystals and hydronephrosis were documented and kidney inflammation and glomerulopathy were scored with 1 (mild), 2 (moderate) and 3 (severe). WAT and BAT were scored for the presence of lymphoma, sarcoma, necrosis or granuloma and inflammation with 1, whereas the absence of pathological findings was scored with 0. In spleen, the presence of extramedullary hematopoiesis, lymphomas, sarcomas, germinal centre and mantle zone hyperplasia was scored with 1 or 0 (absence). Testes were examined for atrophy or degeneration and ovaries for the presence of cysts, lymphoma and endometrial hyperplasia. Lastly, the femur was inspected for the presence of sarcoma.

2.1.3.4 Generation of a 'macro-morbidity' index

A macro-morbidity index, adapted from (Ikeno et al. 2009; Bokov et al. 2011; Treuting et al. 2008) was generated for DR animals. This index encompasses the collected macro-pathology of these mice, previously described in detail by (Drews, 2021). For each mouse, the macro-morbidity index was calculated as the sum of the non-neoplastic pathologies burden, and the neoplasia grade. A degree of 1 was assigned to each non-neoplastic pathological finding at dissection, while neoplasia was graded as 0 (absence of tumours), 1 (1 organ affected by tumours), or 2 (2 or more organs affected by tumours, representing metastatic cancer). The index was generated in a way that the presence of a non-neoplastic pathology was equally weighted to the presence of tumours in one organ affected by tumours, while the state of metastasis was double-weighted. In this context, a high macro-morbidity index was indicative of a high degree of sickness at time of death, while a lower index represented a healthy state at time of death.

2.2 Molecular biology and biochemistry methods

2.2.1 LC-MS/MS for trametinib plasma levels measurement

For the analysis of trametinib levels in plasma, 20 uL of plasma from mice fed with either 0, 0.29, 0.58, 1.44, 2.88 or 11.52 mg/kg of diet were extracted using a standard protocol from the mass-spectrometry facility of the Max Planck Institute for Biology of Ageing (Cologne, Germany). In brief, metabolites were extracted from 20 uL of plasma, which was carefully defrosted on ice. After that, 1 ml of a -20 °C methyl-tert-butyl-ether (MTBE):methanol:water (5:3:2 (v:v:v)) mixture, containing 10 ng/mL of Everolimus as an internal standard, was added to each plasma sample. The samples were immediately vortexed and subsequently incubated for 30 min at 4 °C on an orbital shaker. Protein pellets were then obtained by centrifugation at 21.000 x g and 4°C for 10 min. The supernatant was transferred to a fresh 2 mL Eppendorf tube and separation of the polar and the lipid-containing phases was facilitated by addition of 150 µl of MTBE and 100 µL of UPC/MS-grade water (Biosolve). The samples were vortexed briefly and subsequently mixed for 15 min at 15 °C on an orbital shaker. Phase separation was performed by a 5 min centrifugation at 16.000×*g* at 15°C. Finally, 600 µl of the upper MTBE phase, containing the hydrophobic compounds (including the Everolimus and trametinib), was sampled to a fresh 1.5 ml microcentrifuge tube, while the remaining polar phase was not used for further processing. The obtained metabolite extracts were dried down in a Speed Vacuum concentrator (Eppendorf) at 30°C, followed by resuspending in 80µl of 70:30 [v:v]

acetonitrile:isopropanol (Biosolve, Valkenswaard, Netherlands) containing 5% dimethylsulfoxid (Sigma-Aldrich). Samples were thoroughly vortexed and incubated for 5 min in a sonication bath and subsequently filtered through a 0.2µm filter (Merck). After that, the resuspended samples were transferred to autosampler vials (Chromatography Accessories Trott, Germany).

Liquid chromatography–mass spectrometry (LC-MS) analysis was performed using a Xevo-TQs triple quadrupole mass spectrometer (Waters) coupled to an Acquity iClass liquid chromatography system (Waters). The LC was equipped with a BEH C18 column (100 x 2.1 mm, Waters). Mobile phase A was UPLC-grade water (Biosolve), containing 10 mM ammonium acetate and 0.1% acetic acid (Sigma Aldrich). Mobile phase B contained acetonitrile: isopropanol 70:30 [v:v] (Biosolve). LC-based separation was performed using a 6 min gradient starting with 300 µL/min of 45% mobile phase B. This flow was held constant for 0.5 min, before ramping to 100% mobile phase B within the next minute. After keeping this composition constant for the next 2 min, ramping down within 0.1 min to the starting conditions of 45% mobile phase B followed. In the last step, the column was equilibrated for 2.4 min (45% mobile phase B), before the next samples could be injected. The MS parameters were set to: Capillary voltage 1.5 kV, desolvation temperature 550°C, desolvation gas flow 800 l/h, cone gas flow 50 L/h and collision cell gas flow 9 L/h. Samples were analysed using a multiple reaction monitoring (MRM) method. For this purpose, quantitative and qualitative scans were used. For the quantitative scan, quadrupole 1 was set to m/z 616.01 and quadrupole 3 was set to m/z of 254.09. For the qualitative scan, quadrupole 1 was set to m/z 616.01 and quadrupole 3 was set to m/z 226.08. For the internal standard correction, Everolimus (LC labs) was spiked into the extraction buffer, thus enabling correction for pipetting and sample handling. The quantitative MRM transitions for Evereolimus were m/z 980.59 on quadrupole 1, while quadrupole 3 was set to m/z 389.22. The qualitative transition was m/z 980.59 on quadrupoles 1 and m/z 908.5 on quadrupoles 3. For the absolute quantification of trametinib levels, authentic standards were diluted to concentrations of 0, 2, 4, 10, 40, 200, 600, 1200, 2400 and 3600 ng/mL. The LC-MS data was analysed using the TargetLynx software (Version 4.1, Waters).

To assess the effects of the different trametinib doses on liver function, plasma measurements of AST, ALP and y-GT levels were performed by Laboklin GmbH & Co. KG, Diagnostic Laboratory, Bad Kissingen, Germany.

2.2.2 Protein extraction for Western blot

5-10mg of mouse liver tissue was lysed with 400 µl of RIPA buffer (Pierce) containing Complete mini protease inhibitor without EDTA (Roche) and PhosStop phosphatase inhibitors (Roche) (1 tablet per 10 mL RIPA buffer) in precooled FastPrep™ Lysing Matrix D tubes (MP Biomedicals™, 116913100) using FastPrep®-24 (ThermoFisher Scientific, 4x25Hz, 30 sec). Protein extracts were incubated on ice for 10 min and subsequently placed in a sonicator water bath filled with ice for another 10 min. Centrifugation for 15 min at 13.000 rpm and 4°C followed. Protein quantification was performed using the BCA Protein Assay Kit (Pierce™, 23225). Samples were boiled, Laemmli buffer at ¼ of the total volume and 5% β-mercaptoethanol were added and protein extracts were stored at -80°C.

2.2.3 Western Blotting

20 µg of proteins were loaded and separated using 12% acrylamide gels (Criterion™ TGX Stain-Free™ Protein Gel (Biorad, 5678044) and blotted on PVDF membranes (AmershamTM Hybond®, GE10600023, Merck) at 80V, for 1 hour, on ice. Membranes were blocked using 5% non-fat dry milk powder (PanReac AppliChem, A0830) in Tris-buffered saline (TBS) 0.1% Tween 20 (PanReac AppliChem, A4974.0500) (TBS-T) at room temperature for at least 1 hour. Subsequently, membranes were incubated with primary antibodies for phosphorylated ERK1/2 (1:1000, anti-rabbit, Cell Signaling Technology, 4370) and total ERK1/2 (1:1000, anti-rabbit, Cell Signaling Technology, 4695) in 5% fatty-acid free bovine serum albumin (BSA, ThermoFisher Scientific, BP9704-100) in TBS-T at 4°C overnight. Blots were then washed 3x15 min in TBS-T and incubated with HRP-coupled secondary antibodies (ThermoFisher) diluted in 5% milk in TBS-T for 1h at room temperature, followed by 3x15 min washes in TBS-T at room temperature. For signal development, ECL Select Western Blotting Detection Reagent (GE Healthcare) was applied and image acquisition was performed using the ChemiDoc™ XRS+ System (Bio-Rad, 1708265). Western Blot signals were quantified using the Image Lab™ Software (Bio-Rad) with alpha tubulin (1:1000, anti-rabbit, Cell Signaling Technology, 2125) as internal control and normalised against non-drug treated controls.

2.2.4 Immunostaining of mouse brains

Brains of 5 female 6-month old control mice and 24-month old control, rapamycin, trametinib (1.44 mg/kg) and rapamycin/trametinib (1.44 mg/kg) mice were dissected and cut in half to facilitate fixative penetration in 10% neutral-buffered formalin (HT501320-9.5L, Sigma) for 2-4 hours at room temperature. Brains were fixed overnight at 4°C and then dehydrated in 30% sucrose (S7903-5KG, Sigma) in 1x phosphate-buffered saline (PBS) (P4417-50TAB, Sigma) for 2-4 hours at room temperature and subsequently overnight. All incubation steps were carried out in 50 ml falcon tubes (SKU 05-00001-01, pluriSelect) on a rocking shaker platform (88882018, ThermoFisher Scientific). Following dehydration, brains were frozen in Tissue-Tek® OCT (Labtech) on dry ice and stored at −80 °C until further processing. Brains were cut using a cryostat (CM1850, Leica Biosystems, FACS and Imaging core facility of the Max Planck Institute for Biology of Ageing). 25-µm sections were mounted on Superfrost Plus microscope slides (ThermoFisher Scientific) and stored at −80 °C until used for immunostainings. For immunostainings, slides were washed with 1xPBS (P4417-50TAB, Sigma) for 10 min and subsequently permeabilized with PBS + 0.2% Triton X-100 (85111, ThermoFisher Scientific) (PBST) for 15 min. An additional washing step in PBST for 5 minutes was carried out and followed by one-hour blocking with 2% normal goat serum (PCN5000, Life Technologies) in PBST at room temperature. Slides were afterwards incubated with primary antibodies in 2% normal goat serum in PBST overnight at 4 °C. The following primary antibodies were used: Ionised calcium-binding adaptor molecule 1 (Iba-1, 1:500, 019-19741, Wako) and Glial fibrillary acidic protein (GFAP, 1:1000, G3893, Sigma). The next day, slides were washed 3x15 min in PBST and incubated for one hour with Alexa Fluor-conjugated secondary antibodies at 1:1000 in 2% normal goat serum at room temperature. The following secondary antibodies were used: Alexa Fluor 488-goat anti-rabbit IgG (A-11008, coupled with Iba-1) and Alexa Fluor 633-goat anti-mouse IgG (A-21126, coupled with GFAP). For immunostaining controls to test unspecific binding of the secondary antibodies, primary antibody incubation was omitted, and slides were incubated with Alexa Fluor-conjugated

secondary antibodies (Alexa Fluor 488 and 633). Slides were then washed 2x10 min in PBST and 1x10 min in PBS and incubated for 30 min with DAPI (1:10000 in PBS, D1306, ThermoFisher Scientific). Slides were then washed with PBS for 10 min and embedded using VectaShield Antifade Mounting Medium without DAPI (Vectorlabs).

2.2.5 Confocal imaging and quantification of mouse brains

Imaging was performed using a Leica SP8-Upright confocal microscope (Leica Microsystems). HyD detectors for Alexa Fluor 488 and 663 with 6% and 10% power respectively and the corresponding gating and the excitation wavelength settings to maximise fluorophore emission were used. 40-µm *z*-stack confocal images were acquired at 2-µm intervals, with 40×/1.3 oil objective at 1× zoom. The same settings were used for all treatment groups during image acquisition. Representative montages from *z*-stack confocal images were used and image processing was performed using Image J (Fiji) software v2.3.0/1.53q (Image J, Maryland, USA). For quantification of astrocytes and microglia density in the brain cerebellum, striatum, hippocampus and cortex, the cell counter tool was used to count GFAP+ or Iba-1+ cells that overlapped with DAPI+ nuclei, respectively. Average astrocyte and microglia density was determined in 10-15 images per brain region per mouse brain.

2.2.6 RNA isolation

4-10 mg of spleen and ileum samples were homogenised in 1 mL TRIzol (Life Technologies) using a FastPrep-24 (MP Biomedicals) with 6 times bead-beating at 4 m/s for 30 sec. Homogenised samples were incubated at RT for 5 min. 200 µl of chloroform (0.2ml of chloroform per 1 ml of TRIzol) was added and mixed by vortexing. Samples were incubated at RT for 10 min and subsequently centrifuged at 12000 g for 15 min at 4 °C. The aqueous upper phase was collected and transferred to a new RNAse-free tube. 500 µl of isopropanol, 50 µl of 3.0 M NaOAc and 1.5 µl of glycogen (ThermoFisher Scientific) were added and tubes were shaken by hand. Samples were incubated at -80 °C for 30 to 45 min to precipitate RNA and then centrifuged at 12.000 g for 10 min at 4 °C. RNA pellets were washed twice with 1 ml of ice-cold 70% ethanol, air-dried for 5-10 min and then resuspended in 30 µl RNAse free water (ddH2O DMPC). As negative control, an extra RNA extraction with no RNA template (no template control) was performed.

2.2.7 DNAse Treatment

To remove possible DNA contaminations, RNA samples were treated with DNAse. Therefore, 3 µl of 10x TURBO DNAse Buffer and 1 µl of DNAse (ThermoFisher Scientific) was added to 30 µl RNA and samples were incubated for 30 min at 37 °C. Subsequently, another 1 µl of DNAse was added and samples were incubated for an additional 30 min. 3 µl of DNAse Inactivation buffer was added and samples were incubated at room temperature with occasional mixing. Samples were then centrifuged at 10000 g for 1.5 min and the supernatant including the DNA-free RNA was transferred to a new tube.

2.2.8 RNA quantification

RNA quantity and quality were measured with the Qubit® RNA BR Assay kit (ThermoFisher Scientific) and Agilent TapeStation 4200 System (Agilent Technologies), respectively. For the Qubit® assay, a master mix containing 199 µl of Qubit® RNA BR buffer and 1µl of Qubit® RNA BR reagent was prepared. 199 µl of the master mix and 1 µl of RNA were added to Qubit™ Assay Tubes (ThermoFisher Scientific, Q32856). For the standards, 190 µl of master mix and 10 µl of each Qubit broad range standard were added. Quantification was done using a Qubit 4 Fluorometer (ThermoFisher Scientific). RNA quality was assessed in a random subset of 30 samples on a TapeStation 4200. Therefore, 1 µl of RNA was mixed with 5 µl of RNA Sample Buffer, denatured at 72 °C for 3 min and incubated on ice for 2 min. Samples were subsequently measured using a D5000 Screen Tape. All obtained RIN values were above 7, in accordance with the recommendations for BCR-Seq (Turchaninova et al. 2016).

2.2.9 Reverse transcription and library preparation for BCR-Sequencing

SMARTScribe Reverse Transcriptase (Clontech) was used to reverse-transcribe RNA according to Turchainova and colleagues (Turchaninova et al. 2016). Therefore, 600 ng of RNA were mixed with 2 µl 10 µM isotype-specific primer mix including: IgM, IgD, IgG, IgA and IgE (Appendix 5.1). Samples were incubated for 2 min at 70 °C to denature RNA, and 3 min at 42°C to anneal isotype-specific primers. The mixture was then combined with 12 µl of reverse-transcription master-mix: 4 µl 5x First-strand buffer (Clontech) + 2 µl 20 mM DTT + 2 µl 10 µM 5'-Template switch adaptor (Appendix 5.2) + 2 µl 10 mM dNTP solution + 2 µl 10xSMARTScribe Reverse Transcriptase (Clontech). The reaction was incubated at 42 °C for 1 hour and then mixed with 1 µl of uracil DNA glycosylase (New England Biolabs), and incubated for 40 min at 37 °C to digest the template-switch adapter. Finally, the reaction product was purified using MinElute PCR Purification columns (Qiagen) and eluted in a total volume of 10 µl. Subsequently, a three-stage PCR amplification of the synthesised cDNA was performed. The amount of cDNA input was determined after testing various quantities of cDNA as input for the first PCR reaction. Sequencing depth per tissue was determined after performing deep sequencing of one spleen and one ileum sample and determining the rate of unique molecular identifier (UMI) duplicates. After that, the minimum amount of reads to obtain adequate coverage was calculated. 1 µl of Spleen cDNA with a target of 5 million reads and 5 µl of Ileum cDNA with a target of 3 million reads were identified as the optimal conditions to obtain a minimum coverage of 5 reads per UMI. In the first PCR, a second strand is added to the reverse-transcribed cDNA using the following reaction mix: 1 µl of Spleen or 5 µl of Ileum cDNA + 12.5 µl of 2x Kapa HiFi HotStart polymerase (Roche) + 1 µl 10 µM 5'- template switch primer (Appendix 5.3) + 1 µl 10 µM 3'-nested immunoglobulin isotype primer mix (Appendix 5.3) + nuclease-free water to 25µl. Samples were incubated for 90 s at 95 °C, followed by 18 cycles of 95 °C for 10 s, 60 °C for 20 s and 72 °C for 40 s, and finally an extension at 72°C for 4 min. PCR products were purified using 0.8x Agencourt AMPure XP beads (Beckman Coulter) and eluted with 30 µl water. During the second PCR, internal sample barcodes and Illumina sequencing adapters were added and the libraries were further amplified. 1 µl of purified PCR product was mixed with 2 µl 10 µM primer mix (5' and 3' primers with the respective sample barcodes) (Appendix 5.4), 12.5 µl of 2x Kapa HiFi HotStart polymerase (Roche) and 9.5 µl nuclease-free water. The following conditions were applied: 1 x 95 °C for 1 min 30 s; 13 x: 95 °C for 10 s, 60 °C for 20 s, 72 °C for 40 s and 72 °C for 4 min. PCR products were purified using 0.8x Agencourt AMPure XP beads (Beckman Coulter) to remove

unspecific amplifications of a length below ~400 nt. Samples were eluted in 20 µl water and size distribution of amplified DNA fragments was determined using TapeStation 4200 (Agilent, D1000 tape). Samples tagged with different internal barcodes were then pooled in equal molar amounts in groups of 10 samples, resulting in a total of 10 libraries. An extra library, containing no DNA was generated and sequenced and served as a negative control. Libraries were purified using 0.8x Agencourt AMPure XP beads (Beckman Coulter) and sequenced at the sequencing core facility of the Max Planck Institute for Molecular Genetics (Berlin, Germany). Spleen and ileum BCR repertoire libraries of a total of 50 mice (5 mice per treatment group (i.e. 5-month AL and DR; 16 months AL; 20 months AL, DR and ALDR16M; and 24 months AL, DR, ALDR16M and ALDR20M) were subjected to Illumina adaptor ligation (i5 and i7 indices), library pooling and asymmetric 400+100-nt paired-end sequencing on an Illumina NovaSeq 6000 platform.

2.2.10 Faecal samples collection, DNA extraction and 16S-rRNA sequencing library preparation

Faecal samples were provided by Dr Sebastian Grönke and Dr Lisa Drews. In brief, faecal pellets were directly collected from each mouse in 1.5 ml tubes (Eppendorf) by means of a forceps and subsequent collection of the excreted pellets. All samples were snap-frozen and stored at − 80 °C until they were weighed and cut to obtain 5 to 40 mg. Each faecal sample was homogenised by bead-beating on a TissueLyzer II (Qiagen, 85300) for 30 sec at 25 Herz/s in the presence of two 7 mm diameter stainless steel beads. 2 full spoons (43 mm) of zirconia beads (BioSpec) and 300 ul of DNA extraction buffer (27 ml 20% SDS (Sigma, 151-21-3) and 540 mg lysozyme (Sigma, L2879-5G) shaked at 100 rpm for 20 min at 38ºC) were added and bead-beaten twice for 3 min at 30 Herz/s. Samples were centrifuged for 6 min at 4000 g (15ºC) and 80 µl of the homogenate was transferred to a 96 well plate. 2 µl RNAse A solution (Qiagen) was added, and plates were incubated for 30 min at 37ºC. Then, 10 µl of Proteinase K (ThermoFisher) and 10 µl 20% SDS (ThermoFisher) were added and samples were incubated for 1 hour at 56ºC. After that, 40 µl of IRS solution (Qiagen) was added, plates were mixed and subsequently incubated for 5 min at 4ºC. Plates were centrifuged for 5 minutes at 2000 g and subsequently 100 µl of the supernatant was transferred to a new 96 well plate. DNA was purified using CleanNGS beads (GC biotech BV) at 1x concentration.

Purified DNA was quantified using a PicoGreen assay (Lumiprobe) and diluted to 5 ng/µl with nuclease-free water. In order to generate libraries for 16S sequencing, two successive rounds of PCR according to a standard Illumina protocol (“Website,” n.d.) were used. The V4 region was amplified using 515F-806R primers (Caporaso et al. 2011) in the following PCR reaction mix: 10 µl of DNA, 12 µl of 2x Kapa Hifi HotStart polymerase (Roche), 3 µl of 515F-806R primers in a 10 mM mixture and nuclease-free water to 25 µl. The resulting mix was incubated at: 98 °C for 3 min, followed by 7 cycles of: 98 °C for 30 s, 61 °C for 30 s and 72 °C for 30 s, finishing with a last extension at 72 °C for 5 min. Dual-index barcodes of the Nextera XT kit were added and the PCR products were purified using 0.8x CleanNGS beads (GC biotech BV) in order to remove contaminants and unspecific amplifications. DNA was eluted in 30 µl of water and DNA concentration was determined using PicoGreen (Lumiprobe) and Agilent TapeStation 4200 System (Agilent Technologies). The concentration of the libraries were adjusted to 1 ng/µl by adding nuclease-free water and libraries were pooled in equal molar

portions. 250x2 paired-end sequencing was performed on an Illumina HiSeq 2500 (Admera Health).

2.3 Statistics

2.3.1 Survival analysis

Survival of animals treated with trametinib and rapamycin was assessed in a total of 492 females and 605 males, which were bred in three generations from the same breeding pairs. 256 female and 261 male mice belonged to a cohort designated only for lifespan analysis (51-53 per treatment group). 75 females and 75 males were used for phenotyping experiments and the remaining 161 females and 269 males were used for the molecular and pathological analysis. Mice of the phenotyping and tissue collection cohorts that survived until 24 months of age were used for organ collection and the histopathological examination and were then censored for the lifespan analysis.

Throughout the course of the study, the health status of all mice was monitored daily by the caretakers and early signs of tumour growth were documented along with natural deaths. Mice with poor health status were closely monitored and weighed daily. A scoring sheet was used to assess the health status of mice and animals were euthanized when they reached a predefined score. Mice were otherwise left undisturbed until they died naturally. Kaplan-Meier survival curves were generated using birth and death dates of the mice. Differences between groups were analysed using log-rank test in Prism (GraphPad) and Cox Proportional Hazard in R (R Core Team).

2.3.2 Statistical analysis

Experiments were performed in a randomised and blinded fashion whenever possible. Statistical analysis was performed using GraphPad Prism 9.0, except for Cox Proportional Hazard analysis which was performed in R (R Core Team). Number of animals for each treatment group, as well as individual statistical tests are mentioned in the figure legends. For multiple comparison testing, One-way and two-way Analysis of variance (ANOVA) were followed by Bonferroni post-hoc test. To test for differences in the proportion of mice affected by pathologies, Chi Square test and Poisson regressions were used. The counts of mice where the pathological finding was present or absent was set as the dependent variable and the absence of pathology (score 0) was set as the reference classification. Comparisons were performed against the control mice (reference level). All error bars correspond to standard deviation. Significance was determined according to the P-value as follows: *P < 0.05; **P < 0.01; ***P < 0.001; ****P < 0.0001.

2.3.3 Sequencing data analysis and processing

2.3.3.1 BCR-Sequencing data processing

The pRESTO tool from the Immcantantion framework was used for data processing (v0.5.13) (Heiden et al. 2014). In brief, quality filtering (minQ = 20), demultiplexing by internal barcodes, primer masking, UMI extraction, generation of consensus reads from common UMIs, assembly of read pairs and annotation of IgH isotypes were performed. A mean of 208089

UMI-consensus reads per sample were studied in the spleen, and 61724 in the ileum. There were no batch effects in the number of UMI-consensus reads evaluated per mouse due to age or diet. IgBLAST (v1.17) (J. Ye et al. 2013) was used for V(D)J gene annotation from reference mouse BCR sequences obtained from IMGT (v3.40) (Giudicelli 2004). A data-table in AIRR (v1.3) standard format (Vander Heiden et al. 2018) was built for analysis using the Change-O tool (v1.1) (Gupta et al. 2015). Un-productive sequences were filtered out and clones were defined using sample-specific thresholds calculated with the R (v4.0.3) package SHazaM (v1.1). Novel alleles were identified using TIgGER (v1.0) (Gadala-Maria et al. 2015), and germlines were defined and annotated with Change-O. Quantification of clonal diversity, expansion and CDR3 region analysis were performed using Alakazam (v1.1). The P20 metric, calculated as the sum of frequencies of all clones with rank above or equal to 20 was used to assess clonal expansion rates. SHM was quantified with SHazaM and RDI (v1.0) (Bolen et al. 2017) was used to calculate the repertoire dissimilarity index for inter-individual dissimilarity. Isotype frequency was calculated as the percentage of the total reads corresponding to each isotype. CDR3 lengths were fitted on a normal distribution using Scipy (v1.4.2; (Virtanen et al. 2020)), and Alakazam was used to calculate V-J gene usage.

2.3.3.2 BCR-Sequencing data analysis

Statistical analysis was performed in python (v3.7.3). Linear regressions were calculated to analyse increase or decrease in BCR metrics on AL and DR mice with age (Scipy, v1.4.2; (Virtanen et al. 2020)). 2-way-ANOVA (Statsmodels, v0.11; (Seabold and Perktold 2010)) was used to compare DR to AL. Mann-whitney U tests with Bonferroni multiple testing corrections were used to compare the treatments within each timepoint. The relationship between each BCR metric and morbidity index was calculated using linear regression and Spearman correlation (Scipy; (Virtanen et al. 2020)). Seaborn (v0.10.1) was used for the generation of all plots.

2.3.3.3 16S-rRNA sequencing data processing and analysis

Raw-sequencing data were processed using cutadapt (v3.4) (M. Martin 2011) for quality filtering (minQ = 20), removing reads with no primers, as well as full primer sequences. Dada2 (v1.18) (Callahan et al. 2016) was used for error correction, chimaera removal, assembly of read pairs and taxa annotation with the Silva database (v132) (Yilmaz et al. 2014). Bacterial phylogenetic trees were calculated using phyloseq (v1.34) (McMurdie and Holmes 2013) for microbial within-individual diversity (Shannon and Simpson) and inter-individual dissimilarity (Bray Curtis). Statistical analyses were performed using vegan (v2.5.7) in R (v4.0.2), and were corrected for multiple testing using Benhamini Hochberg.

3. Double treatment with trametinib and rapamycin maximises longevity in mice

Author contributions:

Conception of the study predominantly by Tobias Nespital, Sebastian Grönke and Linda Partridge.

Execution of experiments predominantly by Lisonia Gkioni and Tobias Nespital. Lisonia Gkioni, Sandra Buschbaum, André Pahl, Jenny Fröhlich and Oliver Hendrich carried out tissue collection experiments. Andrea Mesaros and Martin Purrio performed metabolic phenotyping. Jitin Bali conceived the Positron Emission Tomography (PET) experiments. Franziska Dzialkowsky and Heiko Backes performed the PET experiments. Lisonia Gkioni executed brain stainings. Advised by Sarah Veugelen and Maarouf Baghdadi.

Statistical evaluation of data by Lisonia Gkioni. Graphical representation of data by Lisonia Gkioni.

Writing of the manuscript predominantly by Lisonia Gkioni, Sebastian Grönke and Linda Partridge

Double treatment with trametinib and rapamycin maximises longevity in mice

Authors:

Lisonia Gkioni[1]*, Tobias Nespital[1]*, Sandra Buschbaum[1], André Pahl[1], Andrea Mesaros[1], Martin Purrio[1], Heiko Backes[2], Sebastian Grönke[1] and Linda Partridge[1,3]

Affiliations:

1. Max Planck Institute for Biology of Ageing, Cologne, Germany

2. Max Planck Institute for Metabolism Research, Cologne, Germany

3. Institute of Healthy Ageing, University College of London, United Kingdom

3.1. Introduction

3.1.1 Ageing

3.1.1.1 Definition of ageing and hallmarks of ageing

Ageing is characterised by a declining organismal function, ultimately leading to increased vulnerability to death (López-Otín et al. 2013; Niccoli and Partridge 2012). This overall health deterioration is the major risk factor for a plethora of prevalent pathological conditions, including cancer and neurodegeneration, and metabolic disorders such as diabetes and cardiovascular disease (López-Otín et al. 2013; Niccoli and Partridge 2012). Therefore, ageing and age-associated diseases are subjected to scientific scrutiny, as they are emerging as among the greatest healthcare and financial threats on a global scale (Longo et al. 2015; Atella et al. 2019; United Nations 2019; Sheridan, Mair, and Quiñones 2019).

Thanks to extensive research and leading discoveries in the field of ageing over recent years, our current understanding of the fundamental processes that determine mammalian ageing at a molecular and cellular level has been expanded. Lopez-Otin and colleagues have proposed nine highly interconnected hallmarks of ageing, namely genomic instability, telomere attrition, stem cell exhaustion, cellular senescence, altered nutrient signalling, epigenetic alterations, loss of proteostasis, altered intracellular communication and mitochondrial dysfunction (López-Otín et al. 2013). Thus, ameliorating these hallmarks is an inviting prospect to modulate human ageing and extend lifespan. Indeed, several of these processes have been targeted pharmacologically. For example, administration of metformin attenuated the accumulation of senescence in human adipocytes and lung fibroblasts and in mouse osteoarthritis models (Le Pelletier et al. 2021; Feng et al. 2020; Moiseeva et al. 2013). Further, stem cell exhaustion was successfully targeted by rapamycin in the context of muscle tissue regeneration (Haller et al. 2017; García-Prat et al. 2016). It is, thus, becoming apparent that the hallmarks of ageing can be targeted pharmacologically and this might pave the way to successful interventions to combat the deteriorating organismal function at old age (Fontana and Partridge 2015).

3.1.1.2 Controlling the rate of ageing through genetic and pharmacological interventions

The discovery that genetic and pharmacological interventions can slow ageing (Partridge 2010; Fontana et al. 2014; Fontana and Partridge 2015) has opened novel therapeutic and preventive avenues for human ageing and ageing-associated diseases.

3.1.1.2.1 Genetic interventions

Genetic alterations in the two major and highly interconnected nutrient sensing pathways, namely the insulin/insulin-like growth factor (IGF) signalling (IIS) and mechanistic target of rapamycin (mTOR) in multiple organisms have revolutionised ageing research. The first to show that IIS signalling is implicated in the aetiology of ageing were Kenyon and colleagues, who discovered that nematode worms *Caenorhabditis elegans (C. elegans)* with a mutation in the insulin receptor homologue, *daf-2*, lived more than twice as long as their wild type counterparts (Kenyon et al. 1993). This increased longevity was shown to depend upon the worm Forkhead Box-O (FoxO) orthologue, DAF-16, a direct downstream target of IIS (K. Lin et al. 1997). Since then, research on insulin/IGF-1 signalling, FOXO and their roles in ageing has exploded. Especially with the discovery that reduced activity of IIS leads to increased lifespan in *Drosophila*, this pathway was proven to have an evolutionarily conserved role in ageing (Slack et al. 2011; Piper and Partridge 2018; Kenyon 2011; Yamamoto and Tatar 2011; Altintas, Park, and Lee 2016). Indeed, genetic down-regulation of IIS network activity can extend healthy lifespan in various organisms besides worms (Kenyon et al. 1993) and flies (Clancy et al. 2001; Grönke et al. 2010; Giannakou et al. 2004; Tatar et al. 2001), including mice (Blüher, Kahn, and Kahn 2003; Holzenberger et al. 2003; Selman et al. 2008; Fontana, Partridge, and Longo 2010) and potentially even humans, with the identification of *FOXO3A* as a longevity locus (Kuningas et al. 2007; Willcox et al. 2008; Pawlikowska et al. 2009).

A second major signalling branch of the IIS pathway downstream of the receptors is the oncogenic Ras pathway. Ras proteins belong to the family of small guanosine triphosphatases (GTPases) and are instrumental in transmitting signals from receptor tyrosine kinases (RTKs) bound in the cell membrane in response to external stimuli, including hormones, cytokines and growth factors (McKay and Morrison 2007). The signal transduction cascade initiated by Ras activates numerous downstream cell signalling processes, including differentiation, proliferation, metabolism and apoptosis (Schlessinger 2000). Ras proteins display an oscillation between an active guanosine triphosphate (GTP)-bound and an inactive guanosine diphosphate (GDP)-bound state (Goitre et al. 2014; Rajalingam et al. 2007). The balance between these two states is maintained by the opposing actions of guanine nucleotide exchange factors (GEFs) and GTPase-activating proteins (GAPs), which control the replacement of GDP by GTP and GTP hydrolysis, respectively (Goitre et al. 2014; Rajalingam et al. 2007). In its activated GTP-bound state, structural conformation changes take place, facilitating high affinity and specificity of Ras for numerous downstream effectors of the RTK pathway, such as Raf (Wittinghofer and Nassar 1996). Activation of Raf leads to activation of the Mek1/2 kinases, which subsequently initiates the extracellular signal-regulated kinase (ERK)/mitogen-activated protein kinase (MAPK) signalling cascade (Mendoza, Er, and Blenis 2011). Ras hyperactivation is highly oncogenic and, based on the finding that a third of human cancers present with a Ras mutation, Ras signalling has been established as central in cancer research (Stephen et al. 2014). However, Ras proteins are also important ageing modulators.

The role of Ras signalling in ageing was first demonstrated through the lifespan extension upon deletion of two Ras homologues, RAS1 and RAS2 in yeast (Fabrizio et al. 2003). Further investigation of the Ras signal transduction pathway in flies revealed that genetic inhibition of Ras, as well as ERK extends fly lifespan (Alic et al. 2014; Slack et al. 2015). The pro-longevity effects of Ras inhibition may therefore be conserved in higher organisms, such as mammals. Mice deficient for the tissue-specific GEF for Ras, which led to Ras inhibition, were longer-lived and exhibited enhanced motor function compared to their control littermates in old age (Borrás et al. 2011). Since the contribution of other effectors besides Ras to the observed effects cannot be ruled out (Mirisola and Longo 2011), further direct evidence for the role of Ras/Erk signalling in mammalian ageing is yet to come.

Genetic down-regulation of TOR pathway activity also extends lifespan in an evolutionary conserved manner. Inhibition of SCH9, the yeast homolog of ribosomal protein S6 kinase (S6K), as well as TOR depletion by RNA interference was shown to lead to a lifespan extension in *C. elegans* (Urban et al. 2007; Vellai et al. 2003). Similarly, overexpression of the *Drosophila* homologs of tuberous sclerosis complex 1 and 2 (Tsc1, Tsc2), as well as dominant negative forms of S6K and TOR itself increase fly lifespan (Kapahi et al. 2004). In mice, S6K1 deletion was also found to cause lifespan extension in females along with several health benefits in both sexes (Selman et al. 2009).

Collectively, the remarkable evolutionary conservation of IIS and mTOR modulations in ageing indicates that these pathways are crucial for the development of pro-longevity interventions.

3.1.1.2.2 Pharmacological interventions

The IIS/mTOR signalling network is implicated in the aetiology of a plethora of age-related diseases, including cancer and neurodegenerative disorders (Partridge et al. 2011). Thereby, the development of pharmacological interventions targeting specific nodes within the IIS/mTOR network has spurred increasing interest in promoting longevity and enhancing health later in life. One such example is the pharmacological inhibition of mTOR by rapamycin, which is an FDA-approved drug, commonly administered in patients as an immunosuppressive agent after organ transplantation (Chueh and Kahan 2005; Baroja-Mazo et al. 2016). Rapamycin robustly extends lifespan in multiple model organisms, ranging from worms (Robida-Stubbs et al. 2012) and flies (Bjedov et al. 2010) to mice, where rapamycin administration later in life (i.e. at 600 days of age) increases median and maximal lifespan in both male and female mice (Harrison et al. 2009). Next to the lifespan benefits, rapamycin also ameliorates ageing-related comorbidities, including cardiac dysfunction (Dai et al. 2014; Flynn et al. 2013) and impaired immune responses (C. Chen et al. 2009). Intriguingly, rapamycin was shown to restore immune function after influenza infection in old mice (C. Chen et al. 2009) and administration of another mTOR inhibitor in a cohort of elderly subjects also led to enhanced immune response to influenza vaccine and reduced infection rate (Mannick et al. 2014, 2018). These findings suggest that some of the anti-ageing benefits upon rapamycin treatment may be, at least partly, conserved in humans, and thereby support the idea that rapamycin and related TOR complex 1 (TORC1) inhibitors, are appealing agents to delay human ageing.

The IIS signalling network is highly complex and is characterised by extensive crosstalk between its branches. Reduced signalling through the phosphatidylinositol 3-kinase (PI3K) branch of the IIS signalling network can extend lifespan in *C. elegans* and *Drosophila* (Kenyon

et al. 1993; Slack et al. 2011), and has for long been viewed as the primary route by which the anti-ageing effects of reduced IIS upstream are effected. More recently, another important signalling intermediary of lifespan extension by lowered IIS was identified in flies, the Ras branch (Slack et al. 2015). The Ras signalling pathway is another target for pharmacological manipulation, as it can be directly targeted by many drugs including trametinib. Trametinib, a small molecule inhibitor of MEK, resulting in inhibition of Ras-Erk signalling, is an FDA-approved drug for the treatment of melanoma (Yamaguchi et al. 2011). The prolongevity effect of trametinib in flies was established by Slack and colleagues, with the discovery that oral administration of trametinib increased *Drosophila* lifespan, even when administered later in life (Slack et al. 2015). Nonetheless, it is yet to be determined whether the lifespan extending effects of trametinib are evolutionarily conserved.

In summary, ageing can be ameliorated through genetic and pharmacological interventions, with the latter being at the centre of attention in human ageing research and for translation to human health during ageing. The IIS/mTOR and Ras signalling network provides multiple drug targets and their individual manipulation is associated with lifespan benefits (Slack 2017). Interestingly, recent efforts driven by the extensive feedback present in these networks have been channelled into combinatorial drug treatments in order to maximise prolongevity effects, potentially with reduced side-effects. Indeed, simultaneous targeting of mTOR, MEK, and glycogen synthase kinase-3 (GSK-3) by rapamycin, trametinib and lithium, respectively, showed an additive effect in *Drosophila* lifespan, yielding a median lifespan extension by 48% in the flies receiving this triple drug regimen (Castillo-Quan et al. 2019). However, it is currently unknown whether such a combination would exert similar benefits in mammalian ageing.

In this study, we addressed whether the administration of trametinib alone or in combination with rapamycin can extend mouse lifespan, and we characterised the effects of trametinib single and combined treatment with rapamycin on mouse health. To this end, we orally treated male and female mice with trametinib at two different doses, or intermittently with rapamycin, as well as with both trametinib and rapamycin combined and we assessed their survival, fitness, brain metabolism and organismal health. Here, we showed that the single administration of trametinib significantly increased male and female mouse lifespan and that trametinib and rapamycin combination produced a greater lifespan prolongation compared to the single treatments in both males and females. We demonstrated mild beneficial effects of the combined trametinib and rapamycin treatment in the male mouse cardiac function and female mouse exploratory drive at old age. Additionally, the double combination of trametinib and rapamycin reduced tumour formation in the spleen and liver at old age, spleen tumour progression from middle to old age, and alleviated the increased glucose uptake and activation of microglia and astrocytes in the ageing brain. Finally, we elucidated on the beneficial effects of trametinib and rapamycin on systemic inflammation, by providing evidence of reduced brain and kidney inflammation under co-administration of trametinib and rapamycin.

3.2. Results

3.2.1. Trametinib effects on mouse lifespan and healthspan

3.2.1.1. Lifespan assessment under trametinib administration

3.2.1.1.1. Trametinib administration extends mouse lifespan

Trametinib, a small molecule inhibitor of MEK, resulting in inhibition of Ras-Erk signalling, is an FDA-approved drug for the treatment of melanoma (Yamaguchi et al. 2011). In *Drosophila*, oral administration of trametinib increased lifespan, even when administered later in life (Slack et al. 2015). To examine whether the lifespan-extending effect of trametinib is evolutionarily conserved between flies and mammals, we dosed female and male mice with trametinib in their food, and measured their survival.

To determine the dose range that efficiently inhibited the Ras-Mek-Erk pathway in vivo, and was not associated with any adverse effects on organismal health, we performed a pre-experiment (Figure 3.1 A). Three-month old male and female mice were fed for 4 weeks with 5 different doses of trametinib: 0.29, 0.58, 1.44, 2.88 and 11.52 mg/kg of diet, and the effects on pathway activity, body growth and pathology were measured. The dose range of trametinib was chosen based on a previous report (Wright and McCormack 2013; Research and Case Medical Research 2019). To test whether the drug was efficiently taken up by the mice, levels of trametinib in plasma were measured by mass spectrometry (Figure 3.1 B-C). Trametinib levels in plasma increased in a dose-dependent manner in both male and female mice (Figure 3.1 B-C), indicating efficient uptake of the drug. While at low drug concentrations plasma levels were comparable between male and female mice, females showed higher plasma levels of trametinib at drug concentrations of 1.44 mg/kg and above (Figure 3.1 B-C).

We next addressed the effect of trametinib on Ras-Mek-Erk pathway activity by performing a Western blot analysis on liver samples using phosphorylation of Erk as read-out. A trend for decreased Erk1/2 phosphorylation levels was observed for trametinib concentrations of 1.44 mg/kg and above in both females and males (Figure 3.1 D-E), with the reduction in Erk1/2 phosphorylation being significant only for trametinib at 11.52 mg/kg (Figure 3.1 D-E). Macropathological and histopathological inspection showed that trametinib doses of 0.29-2.88 mg/kg caused no adverse effects on body weight, water consumption or spleen weight (Supplementary Figure 3.1). Furthermore, no detrimental effects on liver function were observed, based on histopathological inspection of the liver for inflammation, lipidosis and necrosis and plasma levels of known markers for liver injury and dysfunction, including aspartate transaminase (AST), alkaline phosphatase (ALP) and γ-Glutamyl transferase (γ-GT) (Giannini, Testa, and Savarino 2005) (Supplementary Figure 3.1). In contrast, male and female animals that were fed with 11.52 mg/kg trametinib failed to gain body weight in the 4 weeks measurement period and showed increased spleen weight (Supplementary Figure 3.1 A-G), indicating detrimental side effects. Thus, for subsequent experiments we chose to feed animals with 0.58 and 1.44 mg/kg trametinib, based on the absence of any detectable pathology in the pre-test but indications of down-regulation of Ras-Mek-Erk pathway activity.

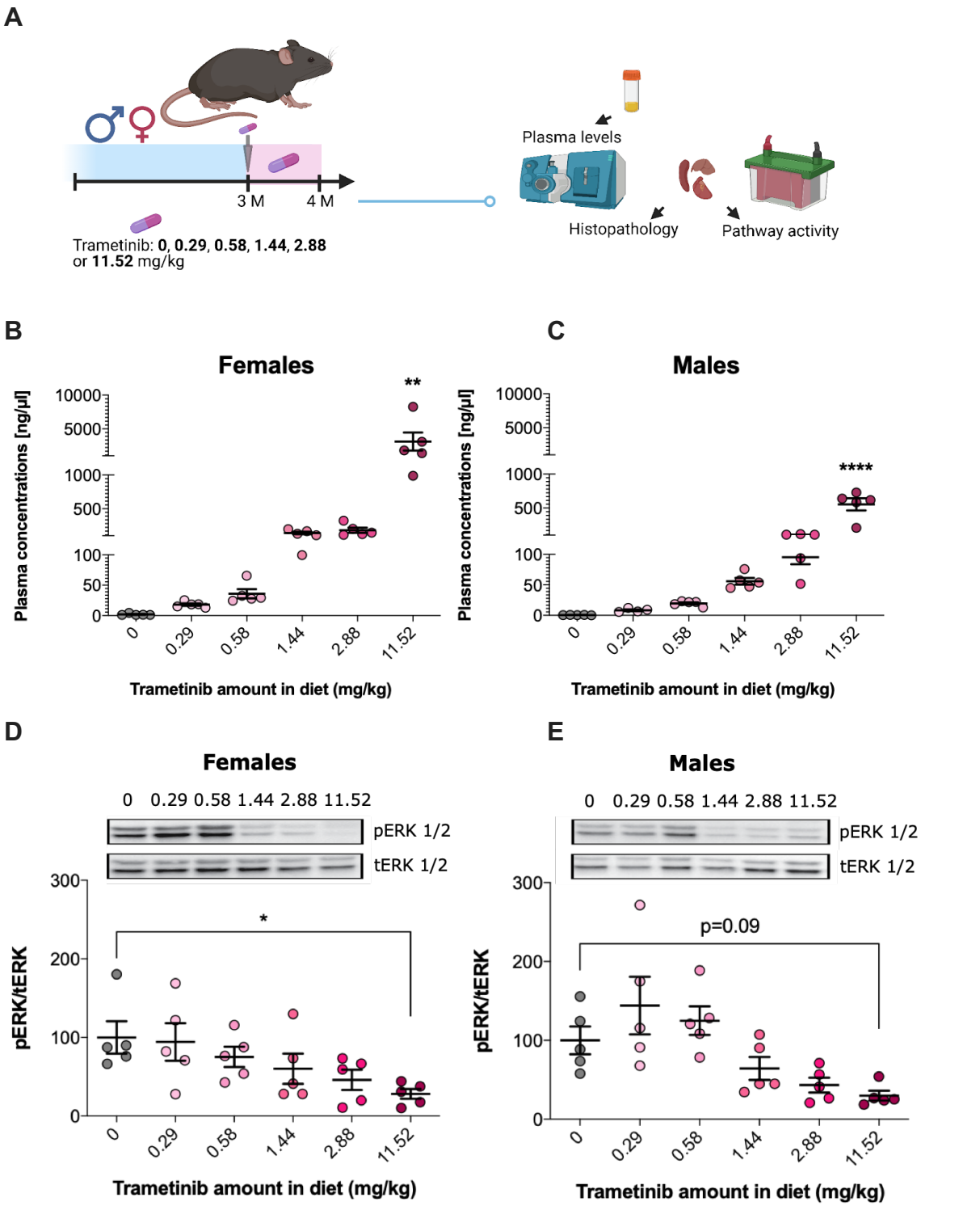

Figure 3.1. Trametinib at various doses shows efficient plasma uptake and inhibition of Ras-Mek-Erk pathway activity. (A) Outline of the pretest experiment to determine an effective dose of trametinib in mice. **(B-C)** Plasma concentration of trametinib in **(B)** female (n=5) and **(C)** male mice (n=5) fed with 0, 0.29, 0.58, 1.44, 2.88 or 11.52 mg/kg of trametinib. Data are presented as mean ± SD. Statistical analyses were performed using One-Way ANOVA. Females: p-value=0.024; Males: p-value<0.0001. **(D-E)** Western blot analysis of Erk phosphorylation and quantification of Western blot results in mouse livers of **(D)** female and **(E)** male mice. Statistical analyses were performed using One-Way ANOVA. Females: p-value=0.0317; Males: p-value=0.0915.

To determine whether trametinib treatment extended lifespan, male and female mice were fed with 0.58 and 1.44 mg/kg of trametinib starting from 6 months of age and their survival was measured (Figure 3.2 A-B, Supplementary Figure 3.2). Interestingly, trametinib treatment significantly extended lifespan in both male and female mice (Figure 3.2 A-B). However, while in females both the low and the high drug dose caused a similar extension in median lifespan by 6.7% and 7.2% (Figure 3.2 A), respectively, in males only the high drug dose significantly extended median lifespan by 10.2% (Figure 3.2 B). Thus, while trametinib treatment can extend lifespan in both males and females, we observed a dose-dependent effect only in males.

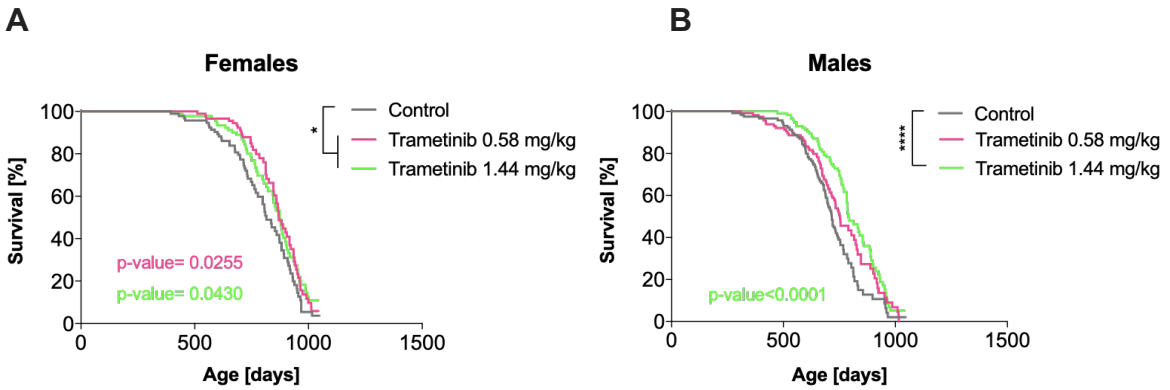

Figure 3.2. Trametinib extends mouse lifespan. (A-B) Trametinib extends lifespan in female **(A)** and male **(B)** mice. Survival curves and associated pairwise log-rank tests of control mice (grey, ♂ n=119, ♀ n=97), and mice treated with trametinib at 0.58 mg/kg (pink, ♂ n=120, ♀ n=97), and trametinib at 1.44 mg/kg (green, ♂ n=121, ♀ n=97). Data are expressed as *P < 0.05; **P < 0.01; ****P < 0.0001.

3.2.1.2. Healthspan assessment under trametinib administration

Given that trametinib extends lifespan in both male and female mice, we investigated whether the drug also ameliorated other phenotypic features of ageing. Therefore, we measured several health parameters that change with age in mice including heart rate, motor coordination, endurance, anxiety behaviour and memory.

3.2.1.2.1. Trametinib maintains heart rate with age

Cardiac ageing in mice is commonly manifested by an age-related decline in heart rate (Comelli et al. 2020; Piantoni et al. 2021; Larson et al. 2013; Mangoni and Nargeot 2008). To address whether trametinib administration attenuated the decline in heart rate with age, we performed non-invasive electrocardiography on 12 and 20-22-month old male and female mice. Consistent with previous data, heart rate significantly declined with age in control mice (c) (Figure 3.3 A, B). Female mice treated with the lower dose of trametinib (i.e. 0.58 mg/kg, t-low) also showed a decline in heart rate with age comparable to controls (Figure 3.3 A), while female mice receiving trametinib at 1.44 mg/kg (t-high) exhibited higher heart rate levels compared to controls at 22 months of age (Figure 3.3 A). However, trametinib at 1.44 mg/kg did not ameliorate the age-related decline in heart rate observed in control mice (slope of change not significantly different) (Figure 3.3 A). In the males, the age-related decline in heart rate observed in control mice was significantly attenuated in mice under trametinib at 1.44

mg/kg (significant slope of change compared to controls) and these mice (trametinib-treated) maintained their heart levels with age (Figure 3.3 B). Previous reports in melanoma patients and preclinical safety data in mice have been indicative of cardiotoxic effects and a lower heart rate after trametinib administration at levels corresponding to 1.44 mg/kg (M. Banks et al. 2017; Research and Case Medical Research 2019). Nonetheless, our results suggest that trametinib-treated females show increased heart rate levels at old age and do not undergo a decline in heart rate with age at this dose. Similar findings have been observed in DR animals, representing a model of healthy ageing characterised by higher heart rate compared to AL controls (Drews, 2021). Further, studies on centenarians demonstrate that they are able to maintain an increased heart rate compared to old individuals, suggesting that attenuating the age-related decline in heart rate might be important for longevity (Piccirillo et al. 1998; Paolisso et al. 1999; Hernández-Vicente et al. 2020). Therefore, our results indicate a mild effect of trametinib in maintaining heart rate at old age.

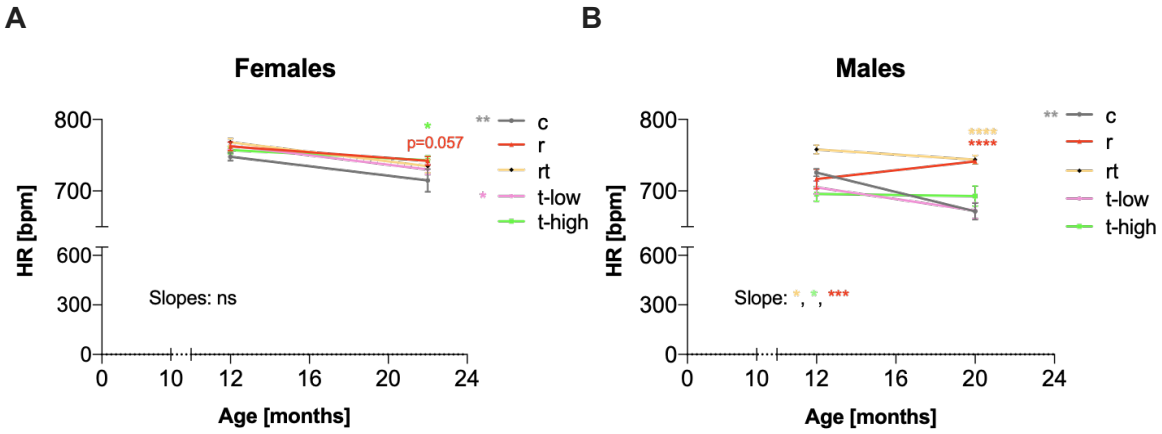

Figure 3.3. Trametinib, rapamycin and their combination maintain heart rate at old age. (A-B) Heart rate (HR) measured by electrocardiography in **(A)** female and **(B)** male control mice (c, grey, ♂ n=7-8, ♀ n=9-15), mice treated with single rapamycin at 42 mg/kg (r, red, ♂ n=8, ♀ n=10-15), mice treated with single trametinib at 0.58 mg/kg (t-low, dark green, ♂ n=8, ♀ n=8-10), and trametinib at 1.44 mg/kg of diet (t-high, green, ♂ n=9, ♀ n=8-10), as well as double combinations of rapamycin and trametinib at 1.44 mg/kg (rt, yellow, ♂ n=8, ♀ n=7-8) at 12 and 20-22 months of age. Female t-high mice showed higher heart rate compared to c at 22 months and a stable heart rate with age. Male mice receiving rapamycin alone or in combination with trametinib showed higher heart rate compared to single trametinib-treated mice at 20 months of age. Data are presented as mean ± SD. Statistical analyses were performed using Two-Way ANOVA with post hoc Bonferroni test and simple linear regression. Females: t-high vs c at 22 months p-value= 0.0398; r at 22 months vs c at 22 months p-value= 0.0570; c at 12 months vs c at 22 months p-value=0.0161; t-low at 12 months vs t-low at 22 months p-value=0.0361. Slope of t-high vs c at 12-22 months p-value=0.2884; Slope of rt vs c at 12-22 months p-value=0.9872; Slope of r vs c at 12-22 months p-value=0.4325. Males: c at 12 months vs c at 20 months p-value=0.0038; r at 20 months vs c at 20 months p-value<0.0001; rt at 20 months vs c at 20 months p-value<0.0001; rt at 12 months vs r at 12 months p-value=0.0162; rt at 12 months vs t-low at 12 months p-value=0.0011; rt at 20 months vs t-low at 20 months p-value<0.0001; r at 20 months vs t-low at 20 months p-value<0.0001; rt at 12 months vs t-high at 12 months p-value=0.0001; rt at 20 months vs t-high at 20 months p-value=0.0013; r at 20 months vs t-high at 20 months p-value=0.0023; Slope of r vs c at 12-22 months p-value=0.0002; Slope of t-high vs c at 12-22 months p-value=0.0282; Slope of rt vs c at 12-22 months p-value=0.0120. Data are expressed as *P < 0.05; **P < 0.01; ***P < 0.001; ****P < 0.0001.

3.2.1.2.2. Trametinib administration induces mild improvement in motor coordination at middle and old age

To assess the motor-coordination and motor learning of the mice under trametinib administration we used the rotarod test. Consistent with previous work (Baquer et al. 2009; Barreto, Huang, and Giffard 2010), we observed a decline in motor performance with age in female control mice as indicated by the significant decline in latency to fall at 22 compared to 12 months of age (Supplementary Figure 3.3 A). Although the same trend was observed in male mice, we did not detect significant differences in rotarod performance at 20 compared to 12 months of age (Supplementary Figure 3.3 B). At 12 months of age, all male and female mice showed motor learning, as indicated by the significantly increased latency to fall from the rotarod at the end of the training (day four) compared to the start of the training (day 1) (Figure 3.4 A,C), suggesting that none of the groups showed any deficits in motor learning. The total time spent on the rod was indistinguishable among the three groups at day four of the rotarod test at 12 months of age (Figure 3.4 A,C), indicating that motor performance is not improved under trametinib treatment at middle age. Similar to our findings at 12 months, at 20 months all female mice showed improved performance over consecutive trials and there were no differences in performance among the control and trametinib treated mice (Figure 3.4 B). In contrast, 20 month-old male mice dosed with 1.44 mg/kg of trametinib showed no motor performance improvement with training, as opposed to controls and mice dosed with 0.58 mg/kg of trametinib that had significantly increased latency to fall at day 4 versus day 1 of the rotarod (Figure 3.4 D). Although these findings are indicative of absence of motor learning in mice receiving the higher trametinib dose, the significantly higher latency to fall compared to control mice during the first two days of the test might account for the lack of improvement with further training (Figure 3.4 D). Our results are corroborated by previous reports on young mice that demonstrate a motor coordination profile that is similar to the trametinib-treated mice; young animals start from a better baseline compared to older mice, but by the end of the training both young and old mice improve to a similar extent (Barreto, Huang, and Giffard 2010). Collectively, our findings indicate that trametinib administration was not associated with an overall improved motor performance or motor learning, but might lead to a slight improvement in baseline motor performance at old age.

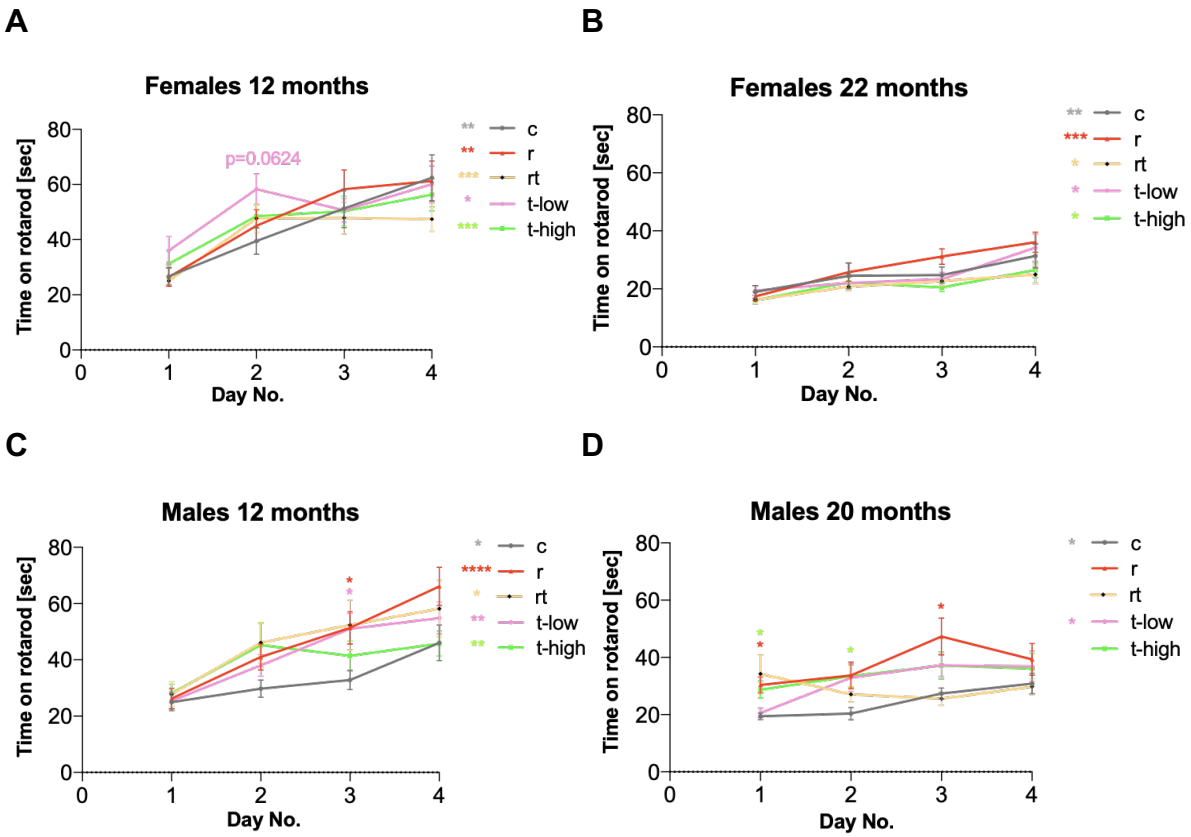

Figure 3.4. Trametinib does not affect overall motor performance at old age but rapamycin improves motor coordination in middle-aged and old mice. (A-D) Total time spent on the rod in rotarod test for **(A-B)** female and **(C-D)** male control mice (c, grey, ♂ n=10-14, ♀ n=13-15), mice treated with trametinib at 0.58 mg/kg (t-low, pink, ♂ n=11-15, ♀ n=15), and trametinib at 1.44 mg/kg (t-high, green, ♂ n=13-15, ♀ n=10-15), as well as double combinations of rapamycin and trametinib at 1.44 mg/kg (rt, yellow, ♂ n=15, ♀ n=15) at **(A,C)** 12 and **(B,D)** 20-22 months of age. Female and male mice under t-low and t-high showed higher latency to fall compared to c mice at 12 months of age (males and strong trend in females) and at 20-22 months of age (only males). Male mice under r administration showed higher latency to fall compared to c mice at 12 and 20 months of age. Data are presented as mean ± SD. Statistical analyses were performed using Two-Way ANOVA with post hoc Bonferroni test. Females: 12 month old c at day 1 vs day 4 of rotarod p-value= 0.0044; 12 month old r at day 1 vs day 4 of rotarod p-value= 0.0028; 12 month old rt at day 1 vs day 4 of rotarod p-value= 0.0005; 12 month old t-low at day 1 vs day 4 of rotarod p-value= 0.0121; 12 month old t-high at day 1 vs day 4 of rotarod p-value= 0.0002; 22 month old c at day 1 vs day 4 of rotarod p-value= 0.0094; 22 month old r at day 1 vs day 4 of rotarod p-value= 0.0003; 22 month old rt at day 1 vs day 4 of rotarod p-value= 0.0408; 22 month old t-low at day 1 vs day 4 of rotarod p-value= 0.0299; 22 month old t-high at day 1 vs day 4 of rotarod p-value= 0.0141; 12 month old t-low vs c at day 2 of rotarod p-value= 0.0624. Males: 12 month old cs at day 1 vs day 4 of rotarod p-value= 0.0414; 12 month old r at day 1 vs day 4 of rotarod p-value<0.0001; 12 month old rt at day 1 vs day 4 of rotarod p-value= 0.0388; 12 month old t-low at day 1 vs day 4 of rotarod p-value= 0.0010; 12 month old t-high at day 1 vs day 4 of rotarod p-value= 0.0018; 20 month old c at day 1 vs day 4 of rotarod p-value= 0.0319; 20 month old r at day 1 vs day 3 of rotarod p-value= 0.0342; 20 month old t-low at day 1 vs day 4 of rotarod p-value= 0.0352; 12 month old r vs c at day 3 of rotarod p-value= 0.0442; 12 month old t-low vs c at day 3 of rotarod p-value= 0.0360; 20 month old r vs c at day 1 of rotarod p-value= 0.0112; 20 month old t-high vs c at day 1 of rotarod p-value= 0.0417; 20 month old t-high vs c at day 2 of rotarod p-value= 0.0385; 20 month old r vs c at day 3 of rotarod p-value= 0.0443; 20 month old r vs 20 month old t-low at day 1 of rotarod p-value= 0.0324; 20 month old r vs 20 month old rt at day 3 of rotarod p-value= 0.0280. Data are expressed as *P < 0.05; **P < 0.01; ***P < 0.001; ****P < 0.0001.

3.2.1.2.3. Trametinib has no effect on mouse exploratory drive, anxiety or endurance at old age

To address whether trametinib affects the general spontaneous locomotor activity, anxiety and exploratory behaviour of old mice we used the open field test. We detected no significant differences in locomotion speed, exploration or anxiety in trametinib-treated mice compared to the controls in either sex (Figure 3.5 A-D, Supplementary Figure 3.4 A-F). Based on the rotarod results (Figure 3.4), it is unlikely that the trametinib-treated animals undergo a decline in muscular strength that is stronger than the controls and would not allow them to show enhanced exploration in the open field test. However, as there were no differences in anxiety-like behaviour, the increased emotional response is not likely to explain the lack of improvement in exploration by trametinib. To rule out that muscle weakness might account for the lack of differences in exploration between control and trametinib-treated mice, we also performed treadmill. We did not detect any significant differences in the endurance capacity between trametinib-treated and control male or female mice at 20 months of age (Supplementary Figure 3.4 G-H), suggesting that no deficits in endurance and muscle strength could be the drivers of the lack of improvement in exploration under trametinib administration. Collectively, our results suggest that there is no improvement in the capacity and motivation of old trametinib mice to explore and that old trametinib mice show anxiety and endurance levels that are comparable to control mice.

Taken together, trametinib administration was able to extend lifespan in female and male mice, but was not associated with marked improvements in the health of the mice. More specifically, trametinib administration might be beneficial to cardiac function at old age, but did not improve motor coordination, exploration or endurance capacity in old mice.

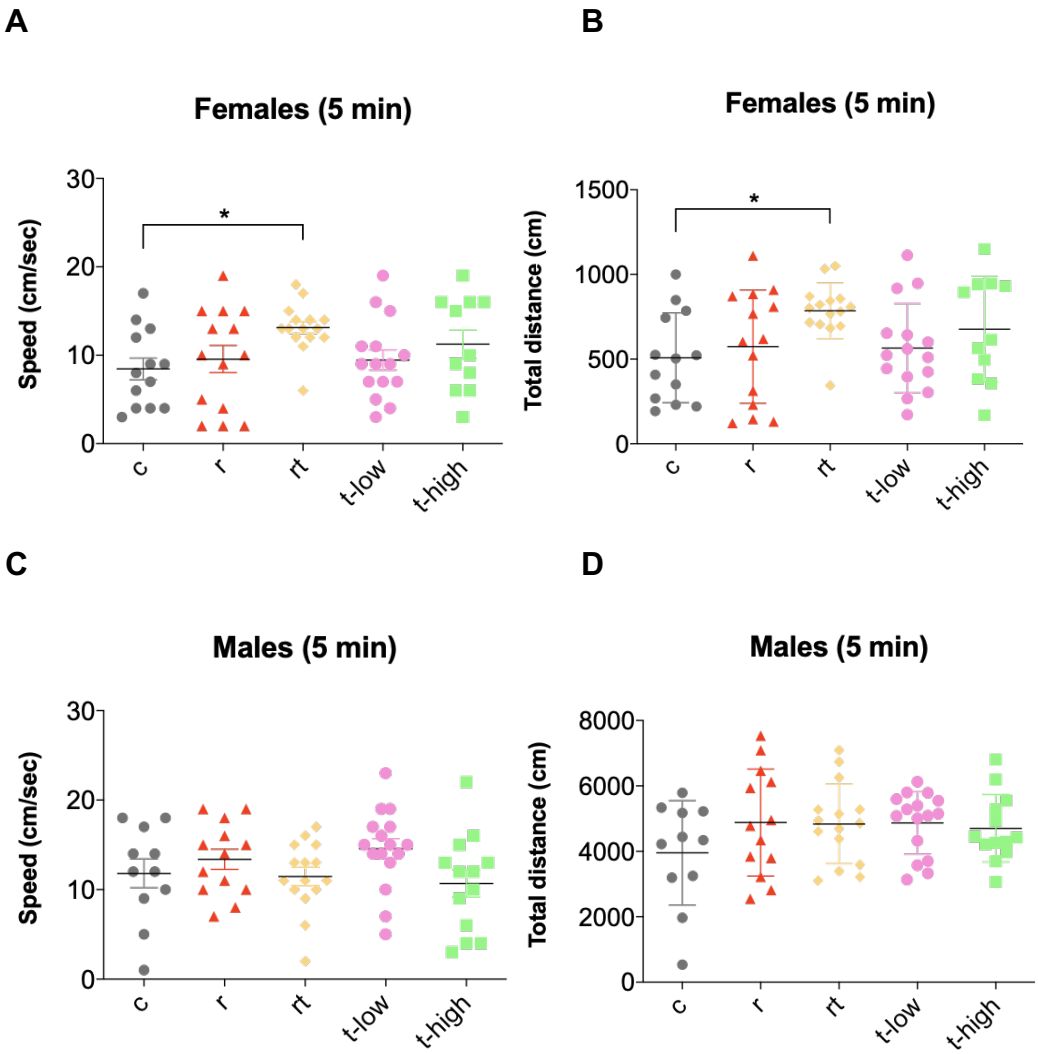

Figure 3.5. Trametinib does not affect exploration or anxiety behaviour in old mice, but its combination with rapamycin improves female mouse exploration. (A-C) Locomotion speed and **(B-D)** total distance travelled on the open field test at 5 min for **(A-B)** female and **(C-D)** male control mice (c, grey, ♂ n=11, ♀ n=13), mice treated with single rapamycin at 42 mg/kg (r, red, ♂ n=13, ♀ n=14), mice treated with trametinib at 0.58 mg/kg (t-low, pink, ♂ n=15, ♀ n=15), and trametinib at 1.44 mg/kg (t-high, green, ♂ n=13, ♀ n=12), as well as double combinations of rapamycin and trametinib at 1.44 mg/kg (rt, yellow, ♂ n=15, ♀ n=15) at **(A-B)** 22 and **(C-D)** 20 months of age. Old female rt mice showed increased locomotion speed and total distance travelled compared to 20-month old c mice. Data are presented as mean ± SD. Statistical analyses were performed using One-Way ANOVA with post hoc Bonferroni test. Females: speed of 22 months old rt mice at 5 min vs speed of 22 months old c mice at 5 min p-value= 0.0368; total distance of 22 months old rt mice at 5 min vs total distance of 22 m months old c mice at 5 min p-value= 0.0347. Data are expressed as *P < 0.05.

3.2.2. Effects of combined trametinib and rapamycin treatment on mouse lifespan and healthspan

3.2.2.1. Lifespan assessment under joint treatment with trametinib and rapamycin

3.2.2.1.1. Joint treatment with trametinib and rapamycin increases lifespan more than does treatment with either drug singly

Treatment of *Drosophila* with a combination of rapamycin and trametinib at the dose of each that maximised lifespan, produced an additive increase in lifespan in *Drosophila* (Castillo-Quan et al. 2019). In order to test whether these two drugs also have additive effects on mammalian lifespan, we fed mice with a diet containing both rapamycin and trametinib and compared their survival to mice fed with only rapamycin or only trametinib. In order to maximise the effect, we used the high dose of trametinib (1.44 mg/kg), which caused a robust lifespan extension in both male and female mice (Figure 3.2 A-B). Rapamycin was administered at a dose of 42 mg/kg, the maximum dose that has previously been shown to extend lifespan in genetically heterogeneous mice (Richard A. Miller et al. 2014). Intermittent rapamycin treatment improves health and increases lifespan in mice and in parallel ameliorates some of the side effects of chronic rapamycin treatment (C. Chen et al. 2009; Bitto et al. 2016). Thus, mice were treated with rapamycin intermittently, alternating between the rapamycin and control diets on a weekly basis. Trametinib treatment was continuous. Drug treatments were initiated at 6 months of age and survival of male and female mice was measured (Figure 3.6, Supplementary Figure 3.2). Treating mice with the rapamycin diet intermittently resulted in a robust extension in median lifespan in both female (17.4%, Figure 3.6 A) and male (16.6% Figure 3.6 A) C3B6F1 mice. Double treatment with rapamycin and trametinib caused a greater lifespan extension compared to the single drug treatments in both sexes, extending male median lifespan by 27.4% (Figure 3.6 A-B, the median lifespan for the rt group is yet to be reached in females). Similarly, cox proportional hazard analysis demonstrated a significantly reduced risk of dying in mice under rapamycin versus controls, trametinib at 1.44 mg/kg versus controls and joint treatment with trametinib and rapamycin versus controls in males and females (Supplementary Figure 3.5). Compared to control treatment, rapamycin reduced the risk of dying by 0.809 in females and 0.666 in males and trametinib at 1.44 mg/kg by 0.418 in females and 0.584 in males, while the combined rapamycin and trametinib treatment reduced the risk of dying as much as the two single treatments combined, by 1.229 in females and 1.122 in males (Supplementary Figure 3.5). Thus, as in flies, trametinib and rapamycin act additively to extend mouse lifespan, indicating that simultaneous downregulation of the Ras-Mek-Erk and mTOR pathways is needed to achieve maximum effects on survival.

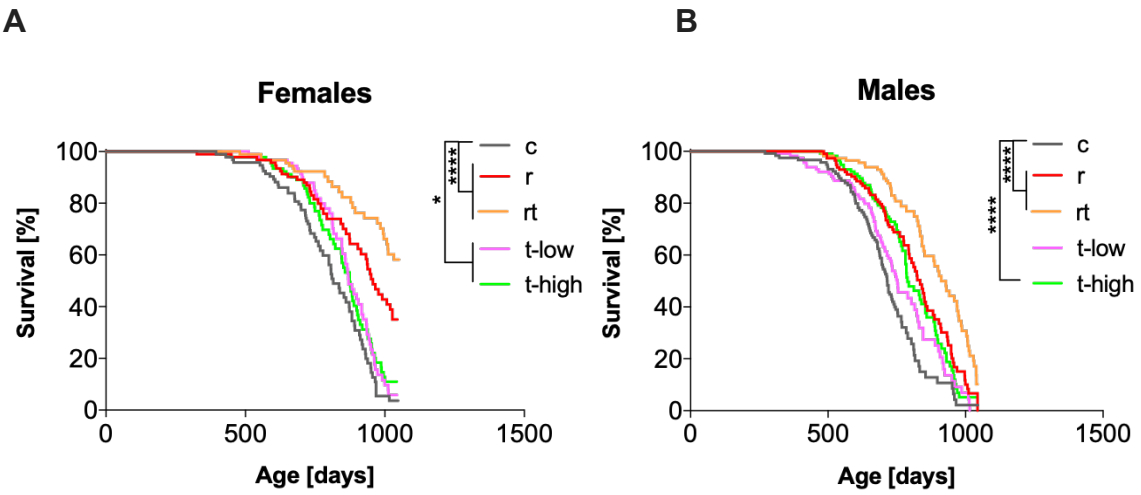

Figure. 3.6. Double treatment with trametinib and rapamycin increases mouse longevity more than does treatment with either drug alone. Survival curves and associated pairwise log-rank tests of female **(A)** and **(B)** male control mice (c, grey, ♂ n=119, ♀ n=97), mice treated with single, weekly intermediate rapamycin at 42 mg/kg (r, red, ♂ n=119, ♀ n=97), single trametinib at 0.58 mg/kg (t-low, pink, ♂ n=120, ♀ n=97), and trametinib at 1.44 mg/kg (t-high, green, ♂ n=121, ♀ n=97), or with double combinations of rapamycin and trametinib at 1.44 mg/kg (rt, yellow, ♂ n=120, ♀ n=97). Female median lifespan: c: 815 days; r: 957 days; t-low: 870 days; t-high: 874 days; rt: nd. Males median and maximum lifespan: c: 716 days (median); r: 835 days (median) and 1044 days (maximum); t-low: 752 days (median) and 1015 days (maximum); t-high: 789 days (median); rt: 912 (median). Log rank test: Females: r vs c p-value<0.0001; rt vs c p-value<0.0001; t-low vs c p-value= 0.0255; t-high vs c p-value= 0.0430. Males: r vs cl p-value<0.0001; rt vs c p-value<0.0001; t-high vs c p-value<0.0001. Data are expressed as *P < 0.05 and ****P < 0.0001.

3.2.2.2. Healthspan assessment under joint treatment with trametinib and rapamycin

Given the additive effect of the combined administration of trametinib and rapamycin on mouse lifespan, we next assessed whether there are any combinatorial effects of these drugs on the health of mice.

3.2.2.2.1. Rapamycin alone and in combination with trametinib maintains cardiac function with age and rapamycin mildly improves motor function at old age

Heart rate evaluation revealed that rapamycin alone and in combination with trametinib ameliorated the decline in heart rate levels with age in male mice (Figure 3.3 B). In females, only mice receiving trametinib at 1.44 mg/kg showed significantly increased heart rate compared to controls at 22 months and rapamycin-treated mice showed the same very strong trend (Figure 3.3 A). These findings are in line with previous work indicating that transient rapamycin treatment ameliorates age-related heart dysfunction (Dai et al. 2014; Flynn et al. 2013). At 12 months of age, male mice treated with rapamycin and trametinib showed significantly increased heart rate compared to all single drug treatments, suggesting a beneficial effect on cardiac function in middle-aged male mice from combinatorial treatment (Figure 3.3 B). At 20 months of age, males receiving rapamycin singly or in combination with trametinib showed a significantly higher heart rate compared to controls and trametinib-only treated mice, indicating no further benefit of the combination of rapamycin and trametinib over the rapamycin-only treatment (Figure 3.3 B). Therefore, at old age there is no additional benefit

to cardiac function of the combined trametinib and rapamycin treatment compared to rapamycin administration alone in male mice, suggesting that the improvement in heart function under the double drug treatment is most likely attributed to rapamycin.

We also assessed motor coordination. 20-month old male mice treated with rapamycin alone showed increased baseline motor performance compared to the controls (Figure 3.4 D), while mice receiving the combined trametinib and rapamycin treatment exhibited motor performance levels comparable to controls (Figure 3.4 D). Similar to the significant improvement in motor learning under rapamycin treatment at day 3 of the training at 12 months, mice receiving rapamycin exhibited a sharp increase in motor learning at day 3 of the rotarod test compared to day 1 at 20 months (Figure 3.4 D). Further, rapamycin-treated mice maintained increased motor function both at the start and towards the end of the training period compared to controls (day 1 and 3), t-low (day 1) and rt mice (day 3) (Figure 3.4 D). In sharp contrast to the males, no differences were observed in females (Figure 3.4 B). Although the effects of trametinib on motor coordination are largely unexplored, previous work has implicated mTOR signalling and rapamycin in motor learning capacity in mice (Qi et al. 2010; Bergeron et al. 2014). Studies on rapamycin-treated male and female mice at young age (Bai et al. 2015), as well as on 20-month old mice under a lifespan extending transient rapamycin treatment (Bitto et al. 2016) support our findings of increased latency to fall and motor learning in males. Overall, these results suggest that, while trametinib administration did not improve motor function, rapamycin administration is associated with mild improvements in motor performance at the start of the training (i.e. baseline) and motor learning (later stages of the training) in old males. No additive effect of the combination of rapamycin and trametinib on motor function or learning was observed.

3.2.2.2.2. Trametinib and rapamycin combination enhances exploratory behaviour in old females

Rapamycin ameliorates anxiety-like behaviour and enhances exploratory capacity in mice (J. Halloran et al. 2012; Zhai et al. 2018). Although trametinib single treatment was not associated with any increases in mouse exploration or reductions in anxiety, the combination of trametinib with rapamycin may exert a beneficial effect on these behaviours. To address this hypothesis, we included the r and the rt mice in the open field test. We detected significantly increased locomotor speed and total distance travelled at 5 min of the open field test in female rt mice compared to control mice at 22 months of age (Figure 3.5 A-B). Given the absence of an anxiety-like phenotype (Supplementary Figure 3.4 E-F), the increased speed in combination with the increased distance that these mice travelled are indicative of an elevated exploratory capacity under rt treatment (Langford-Smith et al. 2011). No differences were detected in males (Figure 3.5 C-D) or in any of the sexes at 10 min of the open field test (Supplementary Figure 3.4 A-D). Consistent with the increased exploration of female rt mice, we observed a trend of increased endurance only in female mice at 22 months of age (Supplementary Figure 3.4 G-H). Collectively, our results suggest that, while the single administration of rapamycin or trametinib is not able to exert a beneficial effect on mouse exploratory capacity, their combination leads to increased exploration in old female mice.

Taken together, our findings suggest that trametinib single administration did not have an effect on motor coordination and exploratory or endurance capacity, but its combination with rapamycin significantly enhanced exploration in female mice at old age. Nonetheless, similar

to the single administration of trametinib and rapamycin, their combination only elicited very mild improvements in the behavioural parameters we checked, and these were not consistent between the sexes. Therefore, trametinib, rapamycin or their combination do not induce marked improvements in these aspects of mouse health.

3.2.2.3. Pathology assessment under joint treatment with trametinib and rapamycin

Given that trametinib and rapamycin treatments did not seem to generally improve the health status of the mice, we next examined whether these drugs extended lifespan by protecting against organ pathologies typically observed in ageing mice. For that purpose, we performed histopathological examination of several organs, including liver, heart, kidney, spleen, WAT, ovaries and testes in 24-month-old mice.

3.2.2.3.1. Trametinib and rapamycin combination reduces non-neoplastic and neoplastic pathologies in old mice

First, we analysed the total number of organs affected by neoplastic and non-neoplastic pathologies at time of death (Figure 3.7). Rapamycin and trametinib combination significantly decreased the number of organs with pathological findings compared to controls (Figure 3.7 A-B). In females, none of the single treatments showed a difference in pathological burden compared to controls, whereas rt mice showed reduced number of organs with pathologies compared to t-low and t-high mice (Figure 3.7 A). Similarly, there was a strong trend for reduced pathological burden of rt compared to r females (Figure 3.7 A), suggesting that, while single administration of trametinib or rapamycin cannot alleviate pathological burden, there was a beneficial effect of their combination. Consistent with the findings in females, in males, single trametinib-treated mice did not exhibit reduced pathological burden compared to controls and rt mice showed a significant reduction in organ pathology compared to t-low mice (Figure 3.7 B). However, rapamycin only treated male mice showed a reduction in the number of organs affected by pathologies compared to controls to a similar extent as rt mice (Figure 3.7 B). Therefore, we can speculate that the beneficial effects of the combination of trametinib and rapamycin on male organ pathology are most likely attributed to rapamycin treatment alone. This was not the case for female mice, where the combined trametinib and rapamycin treatment seemed to improve pathological burden compared to trametinib and rapamycin single treatments, indicative of a potentiation effect (i.e. trametinib enhances the effect of rapamycin without exerting any effect on its own). The beneficial effect of rt treatment on organ pathology compared both to the control and trametinib-only treated female mice was robust, as it was corroborated in an independent, albeit smaller, mouse cohort (Supplementary Figure 3.6 A). This effect seems to be stronger in females than males, given that no differences could be detected on the independent male mouse cohort, probably due to limited statistical power (Supplementary Figure 3.6 B). Therefore, these results point towards a more efficient alleviation of total organ pathology by combining trametinib and rapamycin, as compared to administering each drug alone, in females and a comparable alleviation of organ pathology under administration of rapamycin alone or together with trametinib in male mice.

We next evaluated the effects of trametinib and rapamycin on non-neoplastic and neoplastic pathologies separately in different organs. With respect to non-neoplastic pathologies, we did

not detect any differences in the occurrence of kidney and heart pathologies under single trametinib administration or its combination with rapamycin in either sex (Supplementary Figure 3.6 C-F). Postmortem macro-pathological inspection in an independent mouse cohort showed a significant decline in liver pathologies in males and a similar trend in females under the combined trametinib and rapamycin treatment (Supplementary Figure 3.6 I-J). However, these results were not consistent with the liver histopathological assessment (Supplementary Figure 3.6 G-H). Interestingly, histopathological analysis of spleens in c, r, t-low, t-high and rt male and female mice, after scoring for extramedullary hematopoiesis and hyperplasia revealed that the combined trametinib and rapamycin treatment significantly reduced the occurrence of spleen pathologies in male and female mice (Figure 3.7 C-D). Rapamycin alone could alleviate spleen pathologies compared to controls in males and there was no significant interaction with the combined treatment, suggesting that there is no additive effect of the combination with trametinib (Figure 3.7 D). In females, r, t-low and t-high treatments did not show a significant reduction in spleen pathologies (Figure 3.7 C). We also detected a strong trend towards reduction in spleen pathological appearance in female rt mice after postmortem macro-pathological inspection in an independent mouse cohort (Supplementary Figure 3.7 E). Previous work has demonstrated that rapamycin strongly ameliorates splenomegaly and associated spleen pathologies in rats (Y. Chen et al. 2016), thereby corroborating our results. Similarly, trametinib has been shown to enhance myeloid cell abundance in the spleen, which might have implications for spleen pathologies (Kerstjens et al. 2018). In contrast, while no differences in reproductive organ pathologies were detected in females (Figure 3.7 E), the rapamycin containing treatments, r and rt, showed significantly higher percentages of testicular degeneration and atrophy compared to control male mice (Figure 3.7 F). This is a well-documented side effect of rapamycin administration (Neff et al. 2013; Wilkinson et al. 2012) and it was not observed under the single trametinib administration, which exhibited comparable levels of these pathologies to controls (Figure 3.7 F). Thus, these results suggest that the trametinib and rapamycin co-administration could not alleviate the rapamycin-induced testicular pathologies. Taken together, trametinib single and combined administration with rapamycin could not alleviate kidney, liver (inconsistent results) or heart non-neoplastic pathologies or limit the rapamycin-induced testicular pathologies in males. Nonetheless, trametinib and rapamycin showed a potentiation effect in alleviating spleen pathologies.

Regarding neoplastic pathologies, which are amongst the predominant causes of death in mice (Ettlin, Stirnimann, and Prentice 1994; Brayton, Treuting, and Ward 2012), we detected tumours in the kidney, liver and spleen of female and male mice at old age. The formation of kidney tumours was not affected by the trametinib or rapamycin treatments in female or male mice (Supplementary Figure 3.7 A-B). On the contrary, histological and macro-pathological post-mortem examination of livers in male and female mice from two independent cohorts showed that the combination of trametinib with rapamycin significantly reduced the percentage of mice with liver tumours and liver tumour severity (Figure 3.7 G-H, Supplementary Figure 3.7 C-D). Similarly, histopathological analysis in the spleen revealed that the co-administration of trametinib and rapamycin significantly reduced the percentage of male mice with spleen tumours compared to controls (Figure 3.7 J) and the same trend was observed in female mice (Figure 3.7 I). Ras-Erk signalling has been largely implicated in cancer and previous work demonstrates that trametinib can slow, amongst others, non-small lung, colorectal and liver tumour growth and leukaemia progression in mice (Fujishita et al. 2015; Kerstjens et al. 2018; Wabitsch et al. 2021; C. Kim and Giaccone 2018). Overall, these results implicate trametinib

as a promising drug to reduce spleen tumour formation and corroborate the anti-tumour effects of trametinib on the mouse liver.

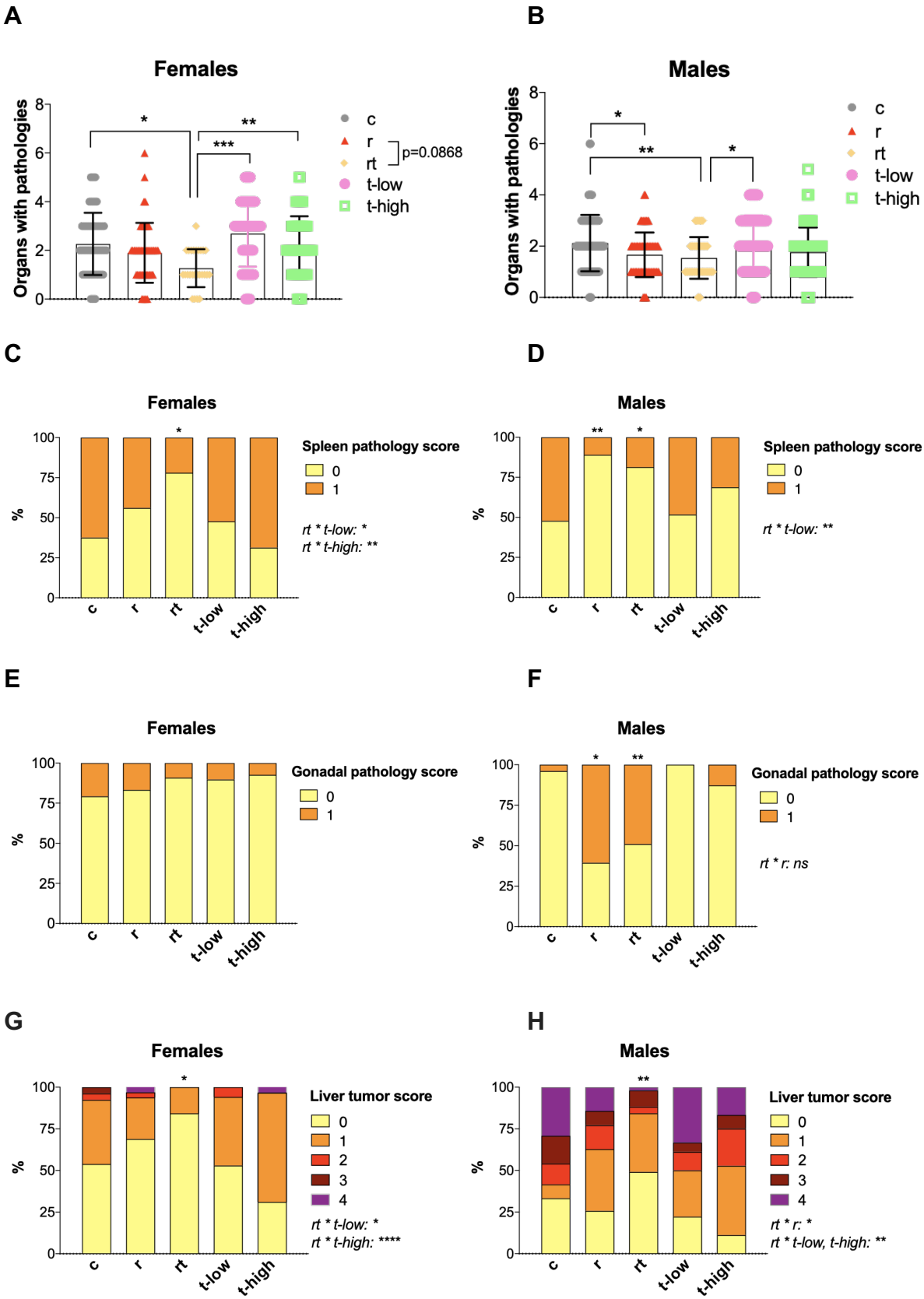

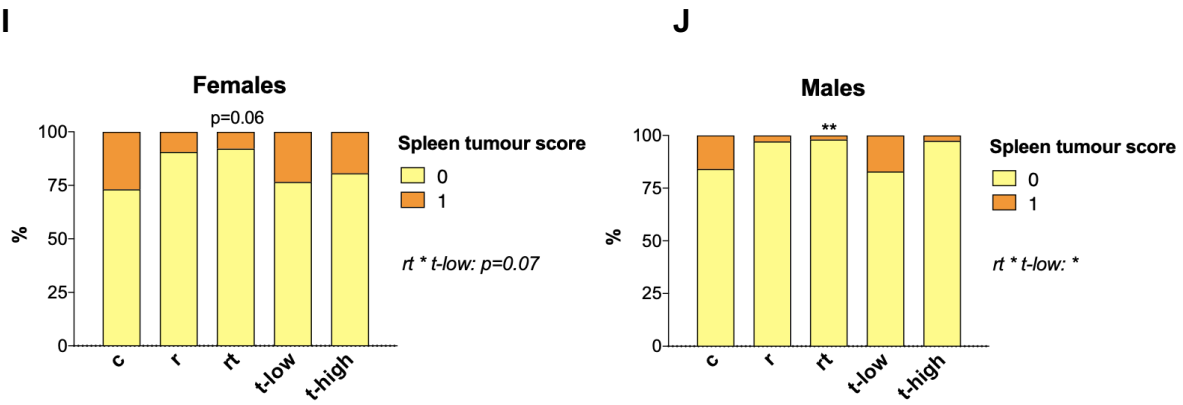

Figure 3.7. Trametinib and rapamycin double treatment reduces organ pathologies in old female and male mice. (A-B) Examination of organs with non-neoplastic and neoplastic pathologies in **(A)** female and **(B)** male mice at time of death. The following treatments were included: control (c, grey, ♂ n=25, ♀ n=26), rapamycin at 42 mg/kg (r, red, ♂ n=35, ♀ n=30), trametinib at 0.58 mg/kg (t-low, dark green, ♂ n=36, ♀ n=34), and trametinib at 1.44 mg/kg (t-high, green, ♂ n=39, ♀ n=31), as well as rapamycin and trametinib at 1.44 mg/kg (rt, yellow, ♂ n=51, ♀ n=38). Rapamycin combination with trametinib reduced the number of organs affected by pathologies compared to controls in female and male mice, but only in females none of the drugs could reduce pathological burden when administered alone. Data are presented as mean ± SD. Statistical analyses were performed using One-Way ANOVA with post hoc Bonferroni test. Females: rt vs c p-value= 0.0138; rt vs r p-value= 0.0868; rt vs t-low p-value= 0.0003; rt vs t-high p-value= 0.0042. Males: r vs c p-value= 0.0492; rt vs c p-value= 0.0071; rt vs t-low p-value= 0.0026. **(C-F)** Histopathological analysis in the **(C-D)** spleen and **(E-F)** reproductive organs of **(C, E)** female and **(D, F)** male mice. The following treatments were included: control (c, ♂ n=33, ♀ n=24), rapamycin at 42 mg/kg (r, ♂ n=33, ♀ n=30), rapamycin and trametinib at 1.44 mg/kg (rt, ♂ n=51, ♀ n=33), trametinib at 0.58 mg/kg (t-low, ♂ n=29, ♀ n=29), and trametinib at 1.44 mg/kg (t-high, ♂ n=32, ♀ n=27). The presence or absence of extramedullary hematopoiesis and hyperplasia (spleen) and testicular atrophy and ovarian cysts (reproductive organs) was scored with 1 or 0, respectively. Rt mice showed a significant reduction in spleen pathologies and r and rt mice showed a significant increase in testicular pathologies. Data are presented as percentage over total and analysis was performed by Chi-square test and Poisson regressions. Females: spleen rt vs c p-value=0.0101; spleen rt * r interaction p-value=0.1270; spleen rt * t-low interaction p-value=0.0394; spleen rt * t-high interaction p-value=0.0051. Males: spleen r vs c p-value=0.0016; spleen rt vs c p-value=0.0154; spleen rt * r interaction p-value=0.4065; spleen rt * t-low interaction p-value=0.0092; spleen rt * t-high interaction p-value=0.2087; gonads r vs c p-value=0.0382; gonads rt vs c p-value=0.0068; gonads rt * r interaction p-value=0.2997. **(G-J)** Histopathological analysis in the **(G-H)** liver and **(I-J)** spleen of **(G, I)** female and **(H, J)** male mice. The following treatments were included: control (c, ♂ n=25, ♀ n=26), rapamycin at 42 mg/kg (r, ♂ n=35, ♀ n=32), rapamycin and trametinib at 1.44 mg/kg (rt, ♂ n=51, ♀ n=38), trametinib at 0.58 mg/kg (t-low, ♂ n=36, ♀ n=34), and trametinib at 1.44 mg/kg (t-high, ♂ n=38, ♀ n=31). The absence of liver tumours was scored with 0 and the presence of low, moderate, high and very high severity tumours was scored with 1, 2, 3 and 4, respectively and the absence or presence of spleen lymphomas or sarcomas was scored with 0 or 1, respectively. Data are presented as percentage over total and analysis was performed by Chi-square test and Poisson regressions. Females: liver rt vs c p-value=0.0444; liver rt * r interaction p-value=0.2751; liver rt * t-low interaction p-value=0.0126; liver rt * t-high interaction p-value<0.0001; spleen rt vs c p-value=0.0644; spleen rt * r interaction p-value=0.8542; spleen rt * t-low interaction p-value=0.0778; spleen rt * t-high interaction p-value=0.1721. Males: liver rt vs c p-value=0.0023; liver rt * r interaction p-value=0.0357; liver rt * t-low interaction p-value=0.0012; liver rt * t-high interaction p-value=0.0027; spleen rt vs c p-value=0.0047; spleen rt * r interaction p-value=0.7985; spleen rt * t-low interaction p-value=0.0361; spleen rt * t-high interaction p-value=0.8444. Data are expressed as *P < 0.05; **P < 0.01; ***P < 0.001; ****P < 0.0001.

3.2.2.3.2. Trametinib and rapamycin combination slows spleen tumour progression

To address whether rapamycin and trametinib can slow tumour progression over time, we performed Positron emission tomography (PET) with 2-deoxy-2-[fluorine-18] fluoro-D-glucose (18F-FDG) (Rahman et al. 2019) in female mice, where we observed consistent effects on macro- and histo-pathology alleviation by rt (Figure 3.7, Supplementary Figure 3.6, 3.7). As only a limited number of animals could be used for this test, we performed 18F-FDG PET/CT in control, trametinib at 1.44 mg/kg and rapamycin and trametinib at 1.44 mg/kg treated mice, based on the robust lifespan extension and consistent effects on organ pathology alleviation that these treatments showed. To follow-up tumour progression over time, we repeated 18F-FDG PET/CT at 12, 18 and 24 months of age. All mice were sacrificed after the 18F-FDG PET/CT measurements at 24 months and their organs were macroscopically inspected. Although in several organs identification of tumours as hypermetabolic regions was confounded by the inherent glucose uptake of the organs themselves (e.g. kidney, bladder), CT and PET data from the same imaging session in the spleen allowed for accurate localization of tumours at 24 months of age, that could be traced back to 18 and 12 months of age (Figure 3.8 A-I). Even though 18F-FDG PET/CT identified tumours in other organs, including the liver and uterus, due to the very low number of control animals for which we could reliably retrieve tumour progression data over time, we were only able to quantify tumours in the spleen (Figure 3.8 J). Control mice showed a tendency towards more advanced spleen tumours already at 18 months of age (Figure 3.8 D, J) and further tumour progression at 24 months (Figure 3.8 G, J) compared to 12 months (Figure 3.8 A, J), whereas the tumours only started to appear at 24 months in the mice under t-high and rt treatments (Figure 3.8 H-I, J). Although there was no difference in the presence of spleen tumours at 12 months of age between the treatments, t-high and rt treatments displayed a strong tendency in alleviating the age-relating increase in tumour development between 12 and 18 months of age and there was a very strong trend of reduction in spleen tumours in rt compared to c mice at 24 months (Figure 3.8 J). Therefore, these findings indicate that the combined administration of trametinib with rapamycin, and potentially trametinib alone, slowed tumour progression in the spleen of female mice.

After combining the 18F-FDG PET/CT data with macro-pathological inspection of the organs in the same mice at 24 months, we found a significant reduction in spleen tumours by trametinib alone, as well as by its combination with rapamycin to a similar extent (Figure 3.8 K), consistent with the histopathological analysis of spleen tumours (Figure 3.7 I). Further, and in line with the protective effect of rapamycin against endometrial cancer in old mice (Bajwa et al. 2017), rt mice did not develop uterine tumours until 24 months of age, as opposed to control and t-high mice that were affected by uterus tumour formation at 24 months to a similar degree (Supplementary Figure 3.8 A). Lastly, in contrast to reports suggesting that trametinib can slow liver tumour progression (Wabitsch et al. 2021), no differences in the presence of liver tumours were detected in t-high or rt mice compared to control mice at 24 months of age (Supplementary Figure 3.8 B). On the whole, our findings suggest that the combination of trametinib and rapamycin slowed tumour progression between 12 and 24 months of age in the spleen and significantly reduced spleen and uterine tumours at 24 months of age.

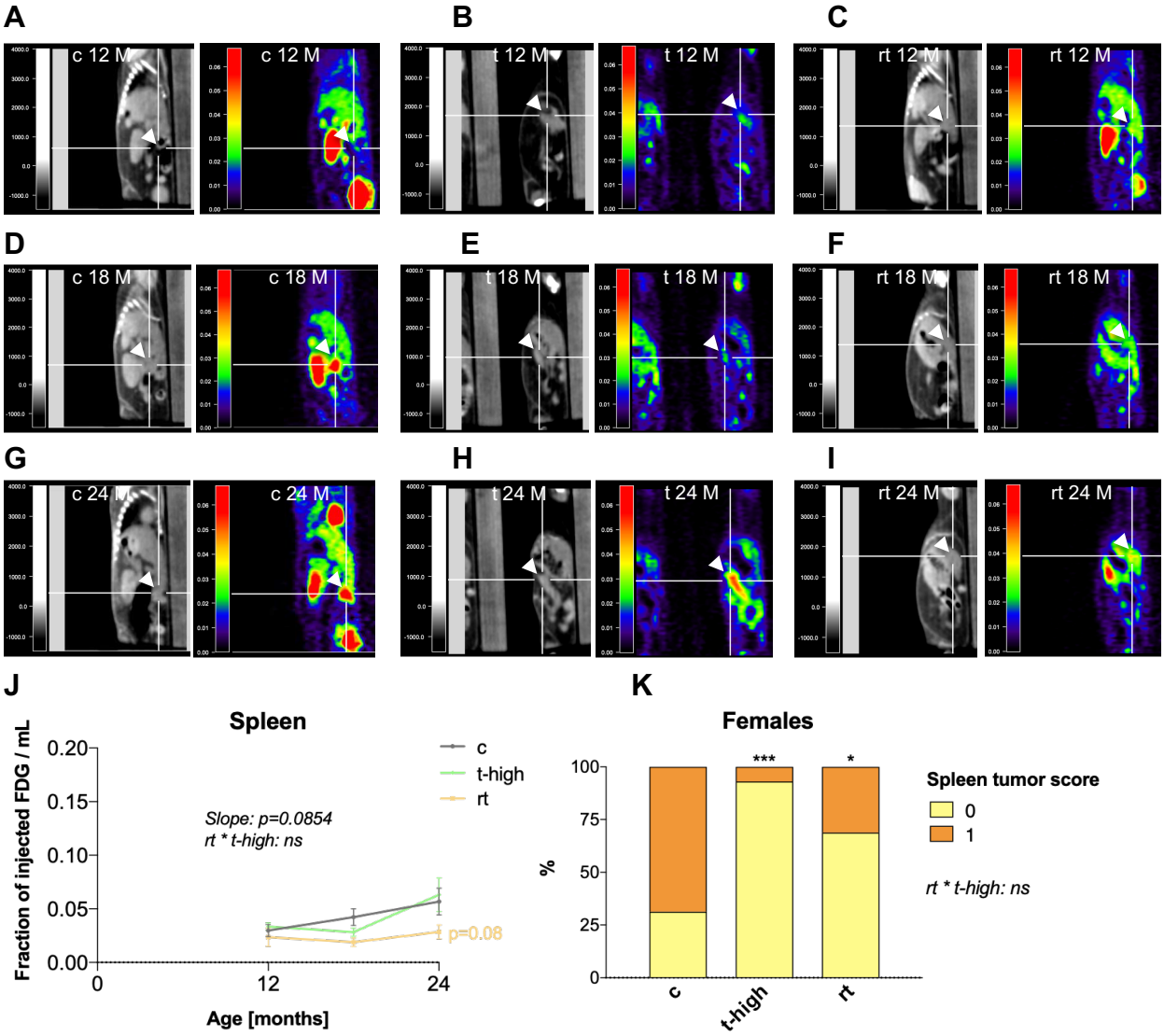

Figure 3.8. Rapamycin and trametinib combination slows tumours in the spleen of female mice. **(A-I)** Representative 18-FDG CT (left panels) and PET (right panels) images showing hypermetabolic activity in the spleen (coronal) at **(A-C)** 12 months of age, **(D-F)** 18 months of age and **(G-I)** 24 months of age in **(A, D, G)** control, **(B, E, H)** trametinib at 1.44 mg/kg and **(C, F, I)** rapamycin and trametinib at 1.44 mg/kg animals. Heatmap keys indicate a range of no 18-FDG uptake (dark blue) to very intense 18-FDG uptake (dark red). **(J)** Quantification of spleen tumour progression data from **(A-I).** Data are presented as mean ± SD. Statistical analyses were performed using Two-Way ANOVA with post hoc Bonferroni test and simple linear regression. rt treatment slowed spleen tumour progression between 12 and 24 months of age. Slope of change in 18-FDG uptake between 12 and 18 months between t-high and rt vs c p-value= 0.0854; 18-FDG uptake of rt versus c at 24 months p-value= 0.08; rt * t interaction p-value=0.2475. **(K)** Hypermetabolic regions in the spleen were identified as tumours and scored for their presence (1) or absence (0) in control female mice (c, n=20), female mice treated with trametinib at 1.44 mg/kg (t-high, n=14), and with rapamycin and trametinib at 1.44 mg/kg (rt, n=16) after cross-reference with macro-pathological inspection at 24 months of age. t-high and rt mice showed a significant reduction in spleen tumour formation compared to c at 24 months. Data are presented as percentage over total and analysis was performed by Chi-square test. t-high vs c p-value= 0.0006; rt vs c p-value= 0.0339; rt * t interaction p-value=0.1288. Data are expressed as *P < 0.05; ***P < 0.001.

3.2.2.3.3. Combined treatment with rapamycin and trametinib attenuates the age-related increase in glucose uptake in the brain

In mice, ageing is accompanied by an increased glucose uptake in the brain (J. Zhao et al. 2021) and this uptake has been linked to impaired cognitive function (Rosenzweig and Barnes 2003). Given the beneficial effects of combined trametinib and rapamycin treatment on exploratory drive in female mice (Figure 3.5 A-B), we next addressed whether trametinib and rapamycin can attenuate the age-related increase in glucose uptake in the mouse brain. Therefore, we performed a longitudinal analysis and measured the uptake of 18F-FDG in the brain of the same female mice via PET/CT scans at 12, 18 and 24 months of age. As the focus of this analysis was to measure the effect of trametinib and only a limited number of mice could be measured, we restricted the analysis to control mice and mice treated with trametinib at 1.44 mg/kg, and rapamycin and trametinib at 1.44 mg/kg. All measurements and initial analyses were performed by our collaboration partner Dr. Heiko Backes from the Max-Planck Institute for Metabolism, Cologne. Consistent with a previous study (J. Zhao et al. 2021), we detected a very strong trend of an increase in whole brain 18F-FDG uptake with age in control animals, when comparing 18F-FDG uptake between 12 and 24 months of age (Figure 3.9 A). There was no significant difference in 18F-FDG uptake between 12- and 18-months old control animals, suggesting that this phenotype only manifests late in life between 18 and 24 months of age (Figure 3.9 A). Although we found a significant increase in 18F-FDG uptake in the brains of trametinib-treated animals between 12 and 18 months of age, there was no difference in 18F-FDG uptake between 18 and 24 months of age (Figure 3.9 A). Interestingly, and in contrast to control animals, there was no significant age-related increase in 18F-FDG uptake in brains of animals treated with both trametinib and rapamycin (Figure 3.9 A). Further, quantification of the increase in 18F-FDG uptake between 12 and 24 months and comparison between treatments showed a significant difference in 18F-FDG uptake change of trametinib and the double drug treatment compared to the increase in 18F-FDG uptake in controls with age (Figure 3.9). Similarly, measurements of glucose utilisation using the cerebral metabolic rate of glucose (CMRglc) (Hutchinson et al. 2009; Jalloh et al. 2015) showed a lower glucose utilisation in 12- compared to 24-months old control and trametinib treated mice, primarily in the cortex and striatum (Supplementary Figure 3.9 A-B), while mice treated with trametinib and rapamycin displayed no changes between 12 and 24 months in the same brain areas (Supplementary Figure 3.9 C). We next investigated whether age and drug-related changes in 18F-FDG were specific to certain brain regions. Similar to the findings in the whole brain, control mice showed a significant increase in 18F-FDG uptake between 12 and 24 months of age in the striatum and cerebellum (Figure 3.9 B, D), whereas in the cortex no age-related change in 18F-FDG uptake was detected (Figure 3.9 C). We also found a significant increase in 18F-FDG uptake in trametinib-treated animals between 12 and 18 months of age in the striatum, cortex and cerebellum, but no difference in 18F-FDG uptake between 18 and 24 months of age (Figure 3.9 B-D). Conversely, no differences in 18F-FDG uptake were found in animals treated with trametinib and rapamycin in 24 months compared to 12 months of age in the striatum, cortex or cerebellum (Figure 3.9 B-D). Further, the 18F-FDG uptake increase in the cerebellum, cortex and striatum of control animals between 12 and 24 months was significantly different compared to mice receiving the combined trametinib and rapamycin treatment (Figure 3.9). Although, we found no differences in 18F-FDG uptake between the treatments at 24 months of age globally or in any of the brain regions (Figure 3.9 A-D), by measuring CMRglc levels, we found a strikingly elevated glucose utilisation in control animals compared to animals treated with trametinib and rapamycin at 24 months of age, manifesting

in most brain areas, including the striatum and cortex (Figure 3.9 F). In contrast, there was no difference in glucose utilisation between trametinib-treated and control animals at 24 months of age (Figure 3.9 E). Taken together, our findings suggest that trametinib combination with rapamycin attenuates the age-related increase of glucose uptake globally in the mouse brain and in specific brain areas, including the striatum and cerebellum and reduces glucose utilisation at old age.

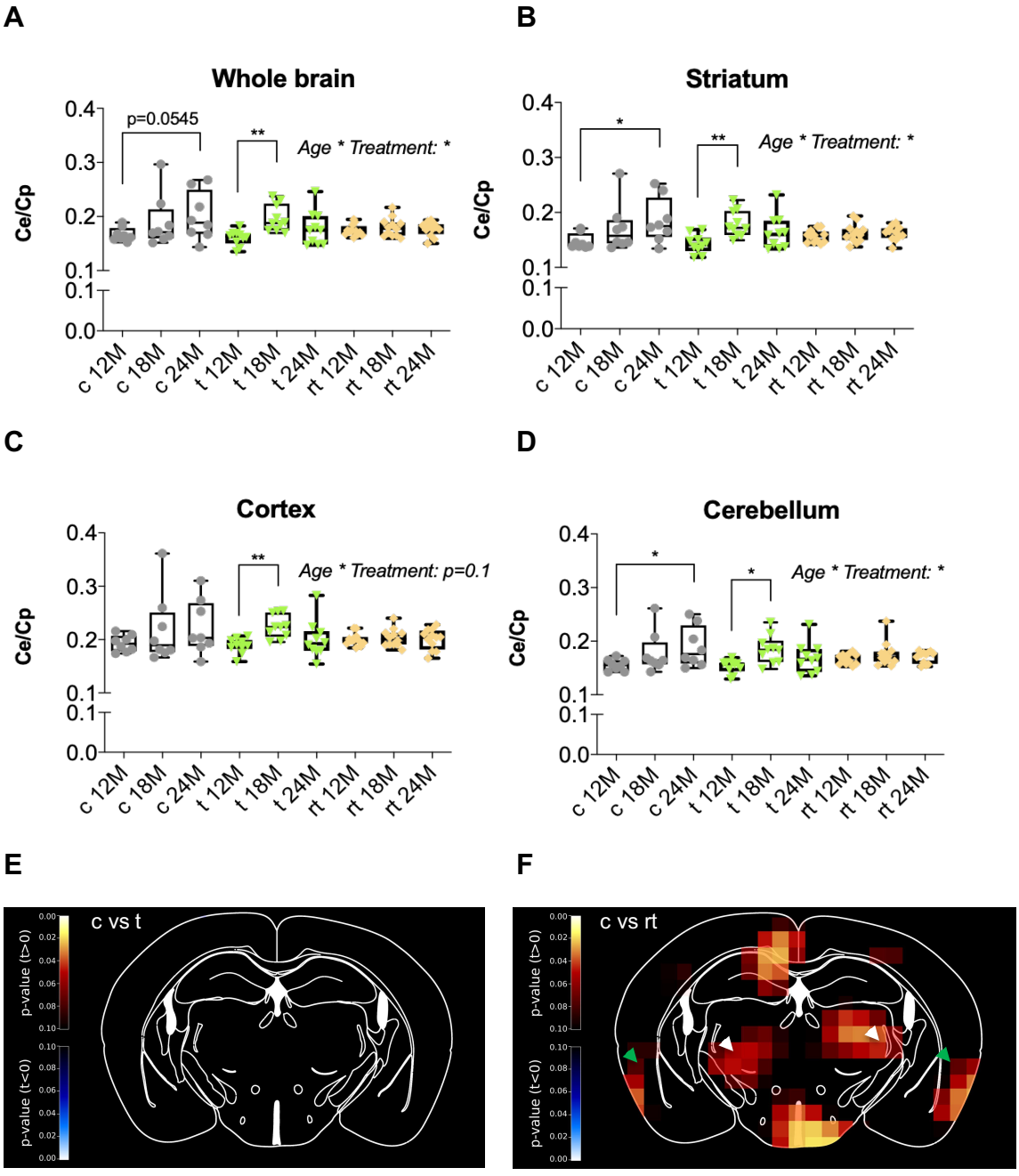

Figure 3.9. Trametinib and rapamycin combination slows the increase of glucose uptake with age in the brain of female mice. (A-D) Glucose uptake quantification by Ce/Cp ratio in the **(A)** whole brains of **(B)** striatum, **(C)** cortex and **(D)** cerebellum of control female mice (c, grey, n=8), female mice treated with trametinib at 1.44 mg/kg (t, green, n=10), and rapamycin and trametinib at 1.44 mg/kg (rt, yellow, n=12) at 12, 18 and 24 months of age. The combination of trametinib and rapamycin showed stable brain glucose uptake with age. Data are presented as median (line), max and min (whiskers) in a box plot and statistical analyses were performed using Two-Way ANOVA with post hoc Bonferroni

test. Whole brain: c at 24 months vs c at 12 months p-value= 0.0545; t at 18 months vs t at 12 months p-value= 0.0060; Age*Treatment Interaction p-value= 0.0283; c at 12-24 months vs t at 12-24 months p-value= 0.0506; c at 12-24 months vs rt at 12-24 months p-value= 0.0028. Striatum: c at 24 months vs c at 12 months p-value= 0.0134. t at 18 months vs t at 12 months p-value= 0.0023; Age*Treatment Interaction p-value= 0.0143; c at 12-24 months vs t at 12-24 months p-value= 0.0511; c at 12-24 months vs rt at 12-24 months p-value= 0.0024. Cortex: t at 18 months vs t at 12 months p-value= 0.0086; Age*Treatment Interaction p-value= 0.1070 c at 12-24 months vs t at 12-24 months p-value= 0.1372; c at 12-24 months vs rt at 12-24 months p-value= 0.0281. Cerebellum: c at 24 months vs c at 12 months p-value= 0.0234; t at 18 months vs t at 12 months p-value= 0.0146; Age*Treatment Interaction p-value= 0.0375 c at 12-24 months vs t at 12-24 months p-value= 0.0328; c at 12-24 months vs rt at 12-24 months p-value= 0.0018. **(E-F)** Representative coronal images of differential 18-FDG uptake based on CMRglc statistics in the brains of **(E)** c versus t and **(F)** c versus rt female mice at 24 months. Arrows indicate the cortex (green) and striatum (white) regions. Heatmap keys are based on p-value<0.05 and the red and blue scales indicate increased or decreased 18-FDG uptake in controls compared to the drug treatments, respectively. Data are expressed as *P < 0.05 and **P < 0.01.

3.2.2.3.4. Combined trametinib and rapamycin treatment reduces age-related brain inflammation

Age-related increase in glucose uptake in the brain might be caused by changes in neuronal metabolism or the presence of inflammation, which increases the requirements for glucose and results in greater 18F-FDG uptake (Safaie, Matthews, and Bergamaschi 2015). Systemic inflammation in the brain is characterised by a state of activated microglia and increased microglia density and has been associated with synapse loss and late-onset neurodegeneration (Ayata et al. 2018; Motori et al. 2013). Interestingly, Ras signalling has been implicated in microglia activation (Ayata et al. 2018). Thus, we hypothesised that trametinib, as a potent inhibitor of Ras-Erk signalling, might reduce inflammation in the brain. To address this hypothesis and investigate whether the attenuation of the age-related glucose uptake in the brain by trametinib and its combination with rapamycin can be attributed to reduced brain inflammation, we performed immunohistological stainings using antibodies against GFAP and Iba-1 for astrocytes and activated microglia, respectively (Figure 3.10). As the strongest changes in 18F-FDG uptake upon drug treatment were at old age, we performed the immunohistological analysis on brains of 24-months old control, rapamycin, trametinib at 1.44 mg/kg and rapamycin and trametinib at 1.44 mg/kg mice. To document age-related changes, we also stained brains of 6-months old control mice, which serve as a reference for a healthy young brain. We observed an age-related increase in activated microglial and astrocyte density in the striatum, hippocampus and cortex of 24-months old mice compared to 6-months old mice, (Figure 3.10 A-B & F, H, Supplementary Figure 3.10 A-B, I-J), consistent with increased age-related brain inflammation. Noteworthy, we did not observe age-related changes in activated microglial and astrocyte density in the cerebellum (Supplementary Figure 3.10 E-F), suggesting that these effects are brain region specific. We next investigated the effects of the drugs on age-related brain inflammation. Interestingly, double treatment with rapamycin and trametinib significantly reduced the density of activated microglia and astrocytes in the striatum of 24-months old mice (Figure 3.10 E, G, I). There was also a trend for the single drug-treatments to reduce the activated microglia density (Figure 3.10 G), albeit not significant. Further, there was more variance between individual drug treated brains when compared to the double treatment, suggesting an additive beneficial effect of rapamycin and trametinib on age-related inflammation in the striatum. In the other brain regions this effect

was not as prominent. There was a trend for the double drug treatment to attenuate age-related microglial accumulation in the cortex, while there was no clear effect of the drugs on microglial or astrocyte accumulation in the hippocampus (Supplementary Figure 3.10 L, C-D). In summary, the immunohistological analysis indicated that double treatment with rapamycin and trametinib reduced brain inflammation in a brain-region-specific manner. Consistent with the 18F-FDG uptake data (Figure 3.9), trametinib administration as a single treatment showed no attenuation in microglial and astrocyte accumulation with age in any of the brain regions we examined (Figure 3.10 and Supplementary Figure 3.10). In contrast to the immunohistological results, 18F-FDG uptake was increased in multiple brain regions (striatum and cerebellum), suggesting that other mechanisms apart from changes in the brain inflammation state might also contribute to the observed changes in 18F-FDG uptake.

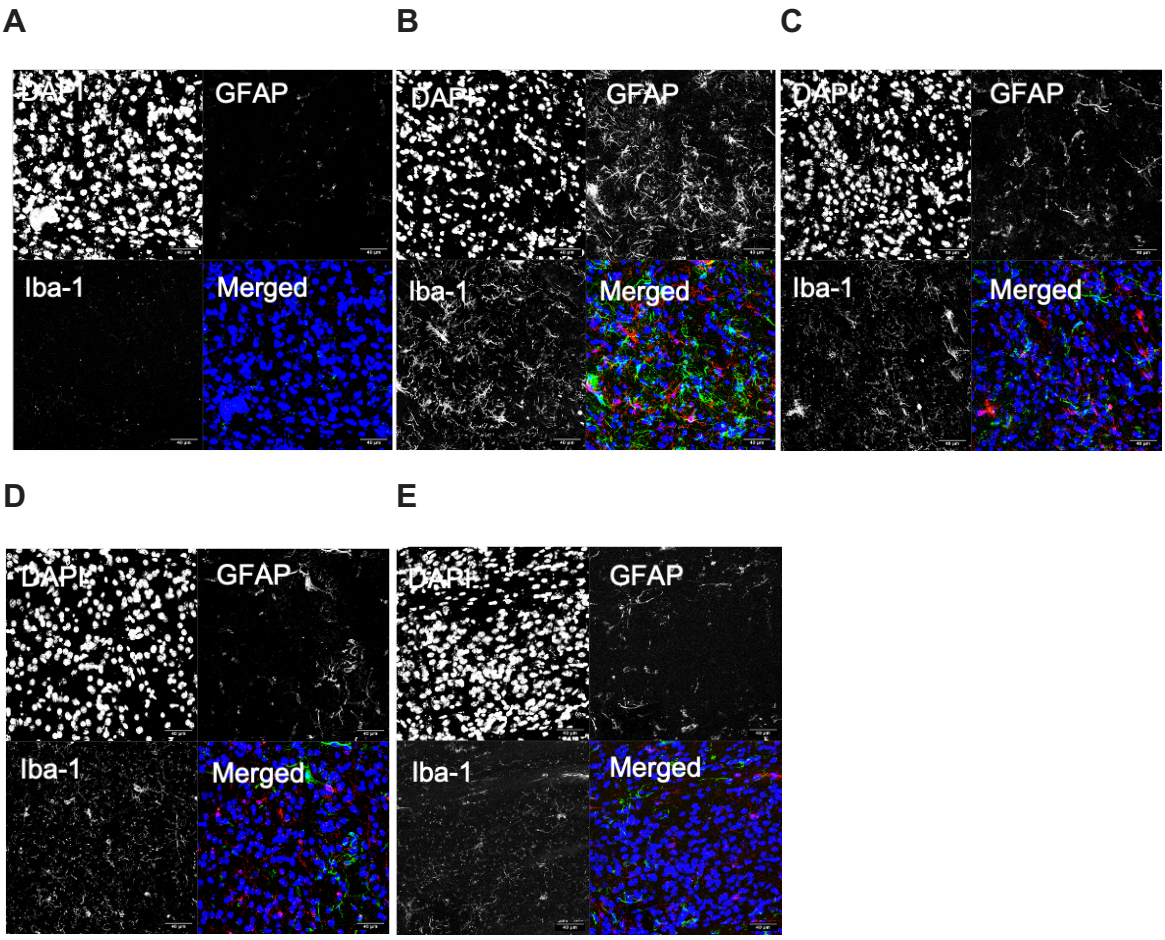

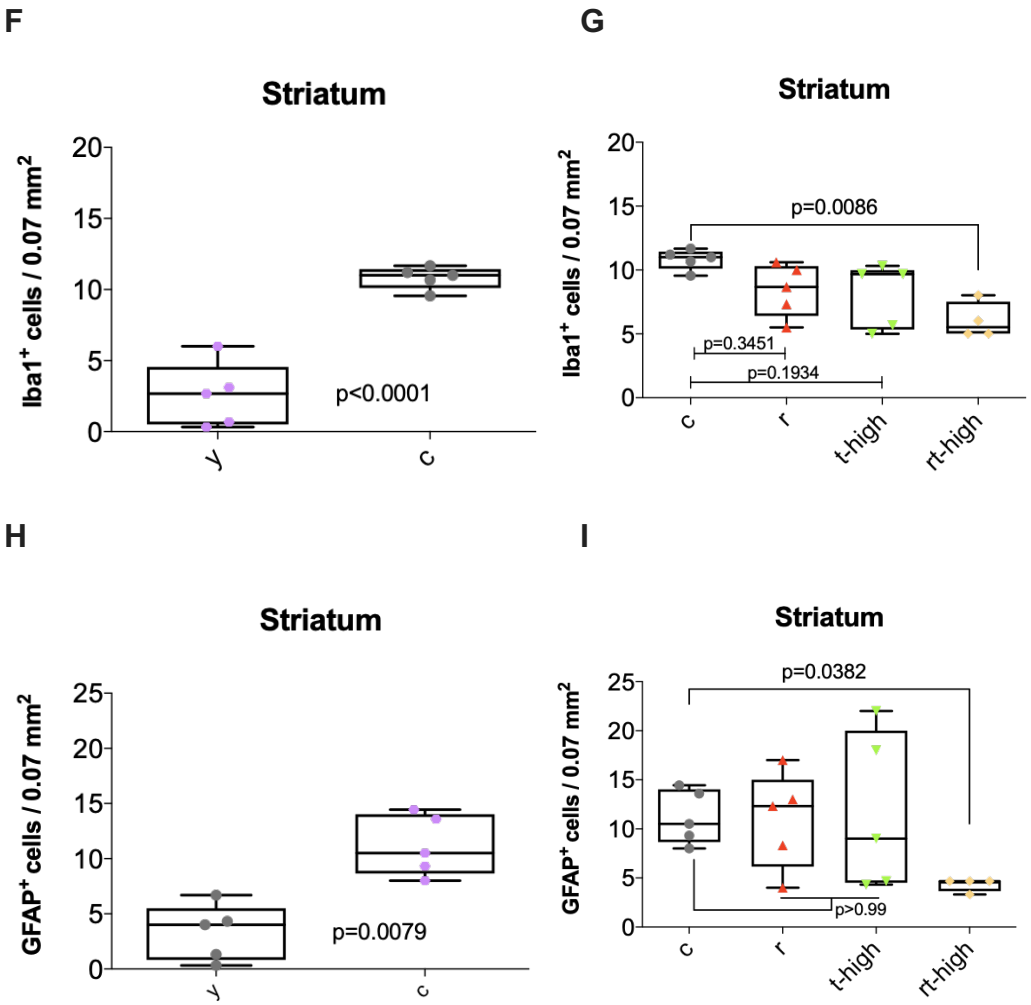

Figure 3.10. Combined trametinib and rapamycin administration attenuates inflammation in the striatum. Representative confocal composite images in grey scale of **(A) control** 6-month old, **(B)** 24-month old, **(C)** rapamycin-treated, **(D)** trametinib-treated (1.44 mg/kg) and **(E)** combined rapamycin and trametinib at 1.44 mg/kg treated female mice. Nuclei were stained with DAPI (left, upper panel, blue), astrocytes with GFAP (right upper panel, green) and activated microglia by Iba-1 (left lower panel, red). The right lower panel shows the merged image in RGB. **(F-I)** Quantification of the average number of double DAPI-Iba-1 positive cells (microglia density) and double DAPI-GFAP positive cells (astrocytes density) of 10-15 confocal images per mouse striatum of control (c, grey: 24 month old, y, purple: 6 month old, n=5), rapamycin-treated (r, red, n=5), trametinib-treated (1.44 mg/kg) (t-high, green, n=5), and rapamycin and trametinib at 1.44 mg/kg (rt, yellow, n=5) treated female mice. Rt mice showed a significant reduction in the accumulation of microglia and astrocytes in the ageing brain striatum. Data are presented as median (line), max and min (whiskers) in a box plot and statistical analyses were performed using **(F, H)** Mann-Whitney U test or **(G, I)** One-Way ANOVA with post hoc Bonferroni test.

3.2.2.3.5. Combined rapamycin and trametinib treatment reduces inflammation in the kidney

Ageing is characterised by increased levels of inflammation in multiple organs, that manifest in a low-level systemic pro-inflammatory phenotype, termed ‘inflammaging’ (Salminen, Kaarniranta, and Kauppinen 2012). Additionally, previous work has shown that inflammation activates both mTOR and Erk signalling (Laplante and Sabatini 2009; Collins et al. 2019; Jager et al. 2010). Based on the finding that rapamycin and trametinib double treatment reduced brain inflammation, we next asked whether this effect also extended to peripheral tissues. To address whether tissue inflammation can be ameliorated by trametinib and/or rapamycin, we

performed a histopathological analysis of the kidney and the WAT, two tissues known to be affected by age-related tissue inflammation, in 24-months old female and male mice. The ageing kidney is characterised by a functional decline associated with chronic inflammation (Lefèvre et al. 2021). There was no obvious effect of trametinib on kidney inflammation in male or female mice and rapamycin treatment induced only a non-significant decline (Figure 3.11 A-B). Interestingly, the combination of both drugs significantly reduced kidney inflammation compared to controls and the single trametinib treatments in female and male mice (Figure 3.11 A-B). Our findings were further supported by the results obtained from macro-pathological inspection of kidneys collected from a separate cohort of mice after their death (Supplementary Figure 3.11). While no differences in kidney pathologies were found in females under any of the treatments (Supplementary Figure 3.11 A), in males rt treatment significantly reduced the collective pathologies present in the kidney, including pathologies related to inflammation, such as enlargement and discoloration (Supplementary Figure 3.11 B). Additionally, and consistent with the kidney inflammation data, there was a strong trend towards reduction of kidney pathology in male rapamycin-treated mice (Supplementary Figure 3.11 B). Therefore, these results in combination with the absence of significant differences or interaction between the rt and r treatments suggest that the reduction in kidney pathology under the combination of the drugs is most likely attributed to rapamycin effects on kidney health (Liu 2006; Lieberthal and Levine 2009).

The WAT is another organ that is known to undergo an age-associated increase in inflammation. In mice, WAT inflammaging manifests with marked changes in the distribution and function of WAT, which lead to an increased inflammatory gene expression (Schaum et al. 2020; Mancuso and Bouchard 2019). This, in turn, triggers infiltration of the tissue by macrophages that further exacerbate the pro-inflammatory state (Mancuso and Bouchard 2019). Therefore, to address whether the age-related inflammation in the WAT can be attenuated by the combined trametinib and rapamycin treatment at old age, the presence of inflammation was assessed histopathologically in the WAT of 24-months old female and male mice (Figure 3.11 C-D). While we observed no significant differences in the percentage of mice with WAT inflammation among treatment groups, there was a trend for reduced WAT inflammation for most drug treatments except for t-low in female mice (Figure 3.11 C-D). Thus, further experiments including imaging of macrophage infiltration or measurements of inflammatory gene expression would be necessary to confirm whether treatment with rapamycin and trametinib can also reduce inflammation in the WAT.

On the whole, our findings demonstrate that the combined trametinib and rapamycin treatment reduced kidney inflammation and future work should investigate whether trametinib and rapamycin can exert an anti-inflammatory effect in other peripheral tissues.

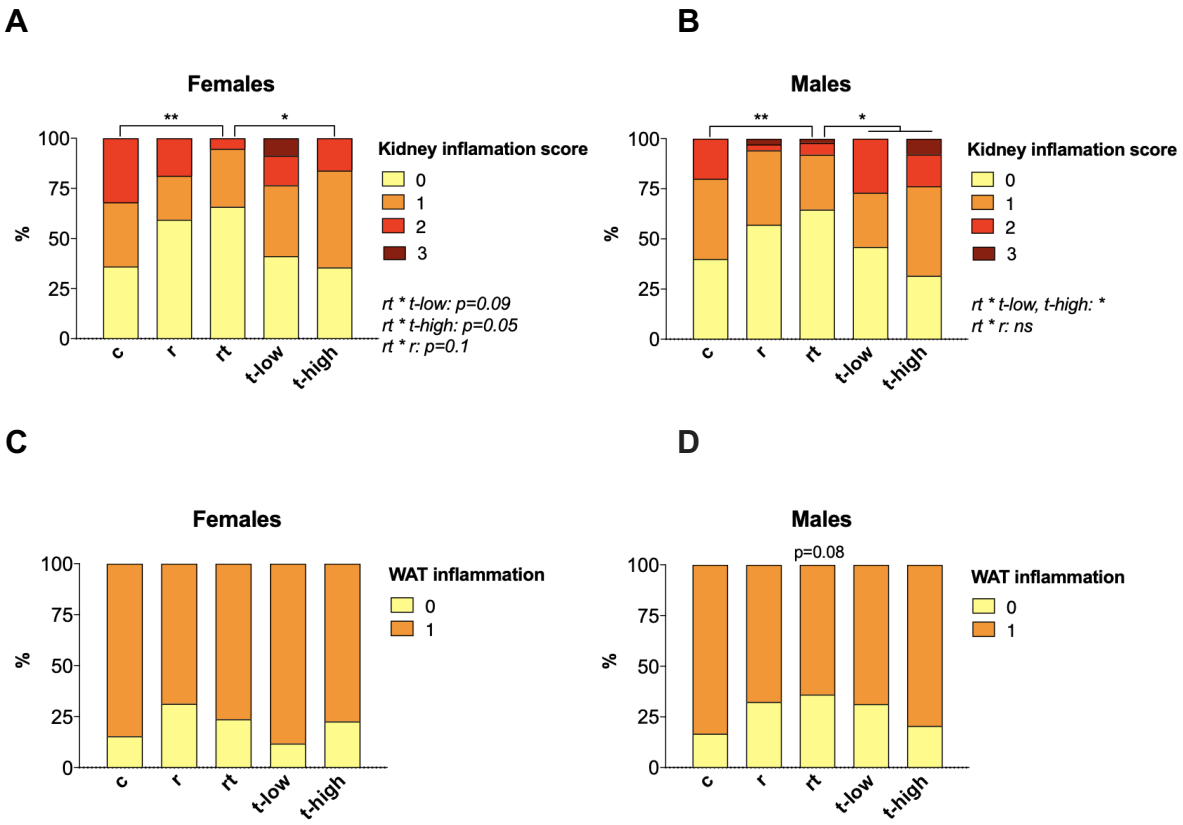

Figure 3.11. Combined trametinib and rapamycin treatment reduces kidney inflammation. (A-B) Histopathological analysis of kidney samples of **(A)** female and **(B)** male mice. The following treatments were included: control (c, ♂ n=25, ♀ n=25), rapamycin at 42 mg/kg (r, ♂ n=35, ♀ n=32), rapamycin and trametinib at 1.44 mg/kg (rt, ♂ n=51, ♀ n=38), trametinib at 0.58 mg/kg (t-low, ♂ n=37, ♀ n=34), and trametinib at 1.44 mg/kg (t-high, ♂ n=38, ♀ n=31). The presence of mild, moderate and severe inflammation was scored with 1, 2 and 3, respectively, whereas the absence of inflammation was scored with 0. Rt treatment showed a significant decline in the percentage of mice affected by inflammation and in the severity of inflammation in males and females. **(C-D)** Histopathological analysis in the WAT of **(C)** female and **(D)** male control mice (c, ♂ n=24, ♀ n=26), mice treated with rapamycin at 42 mg/kg (r, ♂ n=34, ♀ n=32), rapamycin and trametinib at 1.44 mg/kg (rt, ♂ n=50, ♀ n=38), trametinib at 0.58 mg/kg (t-low, ♂ n=35, ♀ n=34), and trametinib at 1.44 mg/kg (t-high, ♂ n=39, ♀ n=31). The presence or absence of inflammation was scored with 1 and 0, respectively. Rt treatment showed a tendency towards reduced inflammation in the WAT of male mice. Data are presented as percentage over total and analysis was performed by Chi-square test and Poisson regressions. Females kidney: rt vs c p-value=0.0095; rt vs t-low p-value=0.0649; rt vs t-high p-value=0.0350; rt vs r p-value= 0.2002; rt * r interaction p-value=0.1151; rt * t-low interaction p-value=0.0967; rt * t-high interaction p-value=0.0567. Males kidney: rt vs c p-value=0.0035; rt vs t-low p-value=0.0360; rt vs t-high p-value=0.0154; rt vs r p-value= 0.7306; rt * r interaction p-value=0.6151; rt * t-low interaction p-value=0.0170; rt * t-high interaction p-value=0.0392. WAT: rt vs c p-value=0.0885. Data are expressed as **P < 0.01.

3.3. Discussion

Living in a world of increasingly aged humans poses substantial socio-economic threats and an enormous challenge to develop effective strategies to improve lifelong human health (Nikolich-Žugich et al. 2016). One promising approach to improve health at old age is to target pathways that directly affect the ageing process. The evolutionarily conserved IIS/mTOR network is a prime candidate for this approach, because downregulation of IIS/mTOR network activity increases life- and health span in diverse organisms ranging from worms and flies to mammals (Castillo-Quan, Kinghorn, and Bjedov 2015; Slack 2017; Campisi et al. 2019). Importantly, the IIS/mTOR/Ras signalling network includes multiple drug targets for pharmacological interventions to increase healthy lifespan. One such example is the drug rapamycin, which directly inhibits the TORC1 node of the network, and extends lifespan in flies and mice (Bjedov et al. 2010; Harrison et al. 2009). Another is the MEK inhibitor trametinib, which can cause lifespan extension in flies (Slack et al. 2015). Here, we showed that administration of trametinib also significantly increased lifespan in female and male mice, establishing it as a gero-protective drug in mammals. Furthermore, we showed that trametinib and rapamycin exert a combinatorial effect on lifespan, by providing a greater lifespan prolongation compared to the single treatments in both male and female mice. Although we only found mild effects of rapamycin and its combination with trametinib on age-related health parameters, we demonstrated that the double drug treatment reduced tumour formation in the spleen and liver and spleen tumour progression. Additionally, we found evidence for reduced brain inflammation and inflammation of peripheral organs, such as the kidney, upon the combined trametinib and rapamycin treatment, suggesting that reduced systemic inflammation might contribute to the extended lifespan of these animals.

Treating mice with trametinib produced a median lifespan extension of approximately 7-10% in female and male mice, which is comparable with the lifespan extension under trametinib administration in female flies (Castillo-Quan et al. 2019; Slack et al. 2015). Consistent with the results in flies (Slack et al. 2015), both trametinib doses significantly extended lifespan to a similar extent in female mice, whereas in males we found a dose-dependent response of lifespan. Sex-specific effects have been also reported under rapamycin administration. Typically, at a given dose, rapamycin leads to greater lifespan prolongation in female mice compared to males (Harrison et al. 2021; Richard A. Miller et al. 2014), which is also what we observed in the current work for rapamycin treatment (sex*rapamycin treatment p-value<0.0001). Conversely, male mice showed a relatively greater lifespan prolongation than females under trametinib administration at 1.44 mg/kg (sex*trametinib treatment p-value<0.0001). The sex-specificity of rapamycin-mediated lifespan extension seems to be at least in part attributable to drug bioavailability differences between males and females, because blood levels of rapamycin were higher in females than in males receiving equal amounts of rapamycin in the food (Richard A. Miller et al. 2014). Here, we only observed increased plasma levels of trametinib in females compared to males at concentrations of 1.44 mg/kg and above. Therefore, we can speculate that these plasma level differences might be indicative of an increased metabolism and/or elimination of rapamycin and trametinib only at high doses in males. Alternatively, sexual dimorphism of immune responses and sex hormones might play a role (Richard A. Miller et al. 2014; Waxman and Holloway 2009). These gender-specific effects suggest that sex differences need to be carefully considered and

evaluated by future studies examining the effects of known and novel pharmacological treatments on healthspan.

Repurposing already existing therapeutics as gero-protectors can play a key role in developing effective strategies to combat human ageing. Trametinib is currently used in the clinic for the treatment of metastatic melanomas (Hoffner and Benchich 2018) and in a phase I clinical trial for the treatment of patients with advanced solid tumours, including non-small-cell lung, colorectal and pancreatic cancer (Infante et al. 2012). Trametinib has been typically administered at doses of 2 mg daily and although it was shown to be generally well tolerated, the most common adverse effects and toxicities reported were skin rash, diarrhoea, fatigue and retinopathy (Infante et al. 2012). In the current work, the plasma levels in both female and male mice under the various trametinib doses were found to be between 40- to 150-fold lower than plasma levels of cancer patients daily treated with trametinib in the clinic (Research and Case Medical Research 2019). Additionally, no adverse effects on body weight or organ toxicity were observed for trametinib doses ≤ 2.88 mg/kg of diet. Therefore, trametinib administration at 2.88 mg/kg or higher is likely to produce an even greater lifespan extension than the one we observed under 1.44 mg/kg. Overall, trametinib can be used as a gero-protective drug in mice and could possibly be a viable option to promote healthy ageing in humans. In mice, future work on optimising dosing of trametinib regimes to produce maximum effects on lifespan should investigate the impact of higher trametinib doses on lifespan in both females and males. Additionally, it would be interesting to determine whether short-term trametinib administration (such as late-onset or intermittent feeding) recapitulates the effects of continuous trametinib on mouse lifespan, as this would be key to enhance adherence and feasibility of trametinib treatment in humans. Importantly, evidence from trials in companion dogs and human clinical trials on the effects of trametinib on ageing or age-related chronic diseases would contribute to establishing trametinib as an anti-ageing intervention in humans.

The current study also showed that the combination of trametinib with rapamycin produced an even greater lifespan extension compared to each drug alone, in both sexes. In *Drosophila*, double treatment with trametinib and rapamycin also extended lifespan more than the single treatments, as did the combinations of each compound with lithium (Castillo-Quan et al. 2019). However, lithium was not included in this work, since it was recently shown that the lithium-mediated lifespan extension in flies was not conserved in mice (Nespital et al. 2021). Previous work on combinatorial drug treatments in mice showed that a combination of rapamycin at the same dose used in this study with metformin increased mouse lifespan by 26% and 23% in females and males, respectively (Bitto et al. 2016; Strong et al. 2016). However, this lifespan extension was comparable to the one under rapamycin single administration reported in previous work (Richard A. Miller et al. 2014), which represents the greatest median lifespan extension observed under single rapamycin treatment (26%). More recently, coadministration of rapamycin and acarbose in 9-months old female and male mice led to a 28% and 34% increase in median lifespan in females and males, respectively (Strong et al. 2022). Importantly however, this study was lacking a rapamycin single treatment control and therefore, it is not clear whether the lifespan extension was further promoted by the combination of rapamycin and acarbose as compared to rapamycin administration alone. The lifespan extension under rapamycin and acarbose combination was greater than the one reported earlier by Miller and colleagues under single rapamycin administration at the same dose (Richard A. Miller et al. 2014) in males, but not in females, where no additive effect of

the drugs was seen (Strong et al. 2022). Here, we demonstrated that trametinib could further improve the prolonged lifespan under rapamycin single treatment in females and males, extending median lifespan by approximately 29% and 27%, respectively. This magnitude of lifespan extension is comparable to the one observed under rapamycin and acarbose coadministration (Strong et al. 2022), as well as to the lifespan extension typically observed under DR (Green, Lamming, and Fontana 2022). Nevertheless, it is worth noting that comparison of quantitative effects between studies is complicated due to the differences in experimental design, genetic background and/or housing conditions. Yet, we have identified for the first time a drug treatment combination that elicits additive effects on lifespan in both sexes, paving the way to further research on combinatorial drug effects to design effective prolongevity interventions. Genetic and dietary prolongevity interventions are often dependent on genetic background and gender, and thus, future studies on multiple mouse strains and both sexes with consistent feeding regimes and housing conditions will shed more light on the interpretation of the sex- and strain-specificity of lifespan responses to single and combined drug treatments.

In the ageing field, it is becoming apparent that prolonged lifespan is not the sole aspect that needs to be considered in the context of anti-ageing interventions. To evaluate whether a pharmacological intervention extends lifespan by protecting against pathologies associated with mouse morbidity (e.g. tumours) or by generally improving organismal health, it is important to investigate its effects on multiple tissues. We hypothesised that the improved lifespan under trametinib alone and its combination with rapamycin would be, at least partly, attributable to improvements in phenotypes that are known to decline with age, and partly to inhibition of carcinogenesis. Regarding the ageing phenotypes, we examined the effects of trametinib and rapamycin on locomotor activity, exploration and cardiac function, all typically undergoing an age-associated decline (Kennard and Woodruff-Pak 2011; Murphy, Rahnama, and Silva 2006; Barreto, Huang, and Giffard 2010; Shoji et al. 2016; Piantoni et al. 2021). Here, we report only mild effects of trametinib and rapamycin combination in cardiac and motor function and exploration, that were not consistent between males and females and did not reflect the additive effect of the drugs in extending lifespan. Although previous work is indicative of improved locomotion and exploration across C57BL/6J and UM-HET3 mouse strains and genders under rapamycin treatment at old age (Bai et al. 2015; Neff et al. 2013; Richard A. Miller et al. 2011), we only observed mild improvements in motor function and no changes in exploration under rapamycin administration, possibly due to differences in genetic background. Interestingly, previous studies documented these improvements also in young mice (Neff et al. 2013). Therefore, these studies might be quantifying ageing-independent effects of rapamycin rather than attenuation of motor function decline with age. Similarly, since we did not include measurements of these phenotypes at young age, we cannot rule out the possibility of non-ageing-modulating effects in the current work. Thus, to disentangle the ageing-independent drug effects from the ageing-modulating effects and confirm the validity of existing findings, healthspan assessment of young mice from various genetic backgrounds should be included.

Several factors might account for the discrepancies between the striking effects of the drugs on mouse lifespan and their very limited healthspan improvements. A plausible explanation could be that other processes that we have not identified are likely to contribute to the lifespan effects. Here, we did not address metabolic regulation under the trametinib and rapamycin

treatments, even though previous work in flies and mice suggests that insulin sensitivity is normalised after combining rapamycin with lithium (Castillo-Quan et al. 2019) or with metformin (Reifsnyder et al. 2022). Interestingly, Ras-Mek-Erk signalling has been previously linked to insulin resistance in flies (W. Zhang et al. 2011) and administration of MEK inhibitors, including trametinib has been shown to reduce insulin resistance in obese wild type and genetically obese mice (A. S. Banks et al. 2015; Ozaki et al. 2016). Furthermore, elevated basal Erk activity has been reported in human type 2 diabetes (Carlson et al. 2003), suggesting that it would be worth investigating whether a combination of trametinib and rapamycin is beneficial for metabolic regulation and if it could explain the prolonged lifespan of the mice receiving the double treatment as compared to the single trametinib and rapamycin treatments. Similarly, major determinants of ageing, such as genomic instability and compromised stem cell function (López-Otín et al. 2013), have been associated with aberrant activation of Ras-Mek-Erk pathway (Aliper et al. 2015; Ying et al. 2008) and thereby justify further investigation in the context of trametinib-mediated lifespan extension. Additionally, we did not examine the effects of trametinib and rapamycin on the bones and the skeletal system, which are known to undergo marked changes with age (Flynn et al. 2013; B. P. Halloran et al. 2002). Ras-MAPK signalling has been extensively linked to osteogenesis (Ge et al. 2007) and Ras-Mek-Erk inhibition was shown to enhance osteogenic differentiation in *in-vitro* models (Nakayama et al. 2003; Higuchi et al. 2002; Hu et al. 2003). On the other hand, rapamycin treatment could attenuate some of the age-related changes in the tendons of old mice (Wilkinson et al. 2012). Thus, studies examining the direct effects of trametinib administration alone and in combination with rapamycin on bone and skeletal health are required. Alternatively, the lack of marked health improvements under the trametinib and rapamycin treatments despite their robust lifespan benefits, might be attributed to the fact that lifespan and healthspan are correlated but can be uncoupled. This has been previously shown for various long-lived IIS pathway mutants in *C. elegans* (Bansal et al. 2015) and dietary interventions in mice (R. T. Wu et al. 2017; Mitchell et al. 2018). As healthspan assessment is highly complex and the most relevant healthspan parameters to assess ageing in each organism are yet to be identified (Kaeberlein 2018), future studies are required to comprehensively assess the effects of trametinib and rapamycin on various healthspan parameters. Obvious candidates would be processes that have been shown to be modulated by trametinib and rapamycin, such as glucose metabolism, stem cell and skeletal health or others that represent known side-effects of the drugs, such as insulin resistance and dyslipidemia.

We also explored the possibility of trametinib single and combined treatment with rapamycin prolonging lifespan by eliciting specific effects on the tissue level rather than on the whole organism level. We hypothesised that the lifespan-extension benefits of trametinib and rapamycin combination would be partly attributed to inhibition of life-limiting pathologies, such as carcinogenesis. This is a plausible scenario given the anti-tumour effects of trametinib and rapamycin, both in slowing cancer progression and de novo tumour formation (Wabitsch et al. 2021; C. Kim and Giaccone 2018; Kauffman et al. 2005; Kopelovich et al. 2007). Additionally, cancer represents a major cause of death in mice (Ettlin, Stirnimann, and Prentice 1994; Brayton, Treuting, and Ward 2012). Indeed, we showed that the combination of trametinib and rapamycin reduced tumour formation and progression. More specifically, we found that liver tumours, which are typically present in the mouse strain used in this study as a result of ageing (Drews, 2021), and spleen tumours, were significantly reduced upon co-administration of

trametinib and rapamycin. Based on analysis of interaction between treatments, there was no interaction between the reduction of liver tumours under rapamycin single treatment and the double drug treatment. On the contrary, there was a significant interaction between the combined and single trametinib treatments in female mice and liver tumours were not reduced upon administering trametinib singly. Therefore, we speculate that the reduction in liver tumours under the combined trametinib and rapamycin treatment is most likely explained by rapamycin in females. On the contrary, in male mice, the double drug treatment showed a combinatorial effect in reducing liver tumours compared to the single treatments (significant interactions between the treatments). In the spleen, although only the combined trametinib and rapamycin administration showed a significant reduction of tumour formation, the same trend was observed under the single drug treatments and no significant interactions were detected. Therefore, we can conclude that there is no additive effect upon the combination of trametinib and rapamycin in reducing spleen tumours and the absence of effects under the single trametinib and rapamycin treatments might be attributed to the limited statistical power. Nonetheless, we identified a reduction in spleen tumour formation at 24-months in old females under the double drug treatment also by using 18F-FDG PET/CT. Therefore, this observation is robust, as it was confirmed by two independent techniques (histopathology and PET/CT) in different sets of mice. Consistent with the histopathological analysis that indicated the same trend for the single trametinib treatment, 18F-FDG PET/CT showed that trametinib alone also reduced spleen tumours at 24 months of age. Additionally, by making use of 18F-FDG PET/CT as an invaluable tool to examine tumour progression, we found that the combined treatment with trametinib and rapamycin and potentially trametinib treatment alone (no significant interaction between the two treatments) slowed tumour progression in the spleen in old females. Thus, we speculate that the reduction of tumours in the spleen and possibly in the liver might contribute to the lifespan extension elicited by trametinib and rapamycin treatments. However, other aspects besides carcinogenesis are likely to be involved, as the effect of the trametinib and rapamycin single treatments was not clear.

The total burden of organ pathologies, including both neoplastic and non-neoplastic pathologies, was also reduced under trametinib combination with rapamycin in both sexes. However, only in females the combined trametinib and rapamycin treatment reduced this burden more efficiently compared to the single treatments. Nonetheless, these results were largely influenced by the presence of tumours, since the assessment of various organs for non-neoplastic pathologies showed beneficial effects of trametinib and rapamycin combination only in the spleen. Consistent with previous work showing no beneficial effects of rapamycin in kidney glomerulopathy and heart hypertrophy (Neff et al. 2013), we did not find any effects of the single or combined rapamycin and trametinib treatments in these tissues. However, the collective kidney pathologies seemed to be reduced under rapamycin single and combined administration with trametinib in males. The fact that there was no significant interaction between the two treatments indicates that the reduction in kidney pathologies upon co-administration of rapamycin with trametinib is likely attributed to rapamycin. This speculation is supported by previous work demonstrating that rapamycin inhibits kidney inflammation and attenuates renal fibrosis (Liu 2006; Lieberthal and Levine 2009). Nonetheless, trametinib-treated male mice have been shown to exhibit an attenuation in kidney fibrosis, partly due to a reduction in mTORC1 activity, as revealed by studying the effects of trametinib in mouse models of renal fibrosis and human renal fibroblasts (Andrikopoulos et al. 2019). Therefore, a more detailed histopathological examination in the kidney tubule epithelial cells for

hyperplasia, fibrosis and other pathologies is needed to grasp the effects of trametinib and rapamycin in renal function. Our findings on testicular pathologies also confirmed previous findings demonstrating a rapamycin-induced testicular degeneration and atrophy (Wilkinson et al. 2012; Neff et al. 2013), that was not counteracted by coadministration with trametinib. As opposed to previous work indicating that liver lipidosis is reduced under rapamycin treatment in males (Wilkinson et al. 2012), we detected increased lipidosis in the livers of our rapamycin only-treated male mice, which could be due to mouse strain differences. Nonetheless, male mice receiving rapamycin and trametinib treatments showed decreased liver pathologies including visible fatty liver, thereby complicating the interpretation of these findings.

Collectively, our findings on neoplastic and non-neoplastic pathologies indicated an amelioration in liver and spleen carcinogenesis, as well as spleen and kidney pathologies under the single rapamycin and combined administration with trametinib. However, there was no robust evidence of combinatorial effects of the drugs or clear effects of the trametinib treatment alone. Therefore, taking into account the trametinib- and rapamycin-mediated lifespan extension data and their clear additive effect on longevity, we can speculate that neoplastic and non-neoplastic pathologies do not directly contribute to the effects of trametinib and rapamycin on lifespan. One likely explanation would be that tumours and pathologies in organs other than the ones investigated in the current work could explain the additive effect of these drugs on lifespan. Assessment of major tumours, including lymphomas and hematopoietic tumours (Lipman et al. 2004) and histological analysis of the thyroid gland, where rapamycin has been shown to exert protective effects (Neff et al. 2013) should be included in future studies. Although a general score for lymphomas and hematopoiesis abnormalities was not included in this study, we histologically examined extramedullary hematopoiesis, lymphomas, sarcomas and hyperplasia in the spleen of the female and male mice. Here, we found that rapamycin alone and in combination with trametinib ameliorated these spleen pathologies (no significant interaction between the single and combined rapamycin treatments). Trametinib alone had no effect in females (significant interaction between both trametinib doses and the combined treatment), but showed effects comparable to rapamycin and the combined treatment in males (no significant interaction between the higher trametinib dose and the double drug treatment). Overall, the effects of the drug treatments in spleen pathologies in males were clearer, possibly due to greater statistical power compared to females. Yet, as these findings cannot be directly linked to lymphomas, it is imperative that future studies explore the effects of trametinib and its combination with rapamycin in lymphomas and other hematopoietic tumours. Further, histological analysis of more tissues is necessary to pinpoint which organs are likely to account for the lifespan extension under trametinib single administration and the additive effect upon its combination with rapamycin.

In the female mouse, we found that joint treatment with trametinib and rapamycin attenuated the age-related increase in glucose uptake globally in the brain and in the striatum and cerebellum regions. Further, trametinib and rapamycin double treatment reduced the activation of microglia and astrocytes in the striatum of old females. Our findings are supported by studies highlighting the importance of both Ras-Mek-Erk and mTOR signalling in microglia activation in neurodegeneration and ageing. Previous work in Alzheimer's disease (AD) models, where microglia is among the main players in the pro-inflammatory mechanisms of

AD pathogenesis (Hickman et al. 2018; Lambert et al. 2013), has revealed a crucial role for Ras-Mek-Erk signalling. Transcriptomic profiling of primary microglia cultures from AD mice has shown that Erk phosphorylation is a critical enactor of pro-inflammatory activation of microglia by regulating interferon-γ- (INF-γ) mediated microglia activation (M. J. Chen et al. 2021). Interestingly, *in-vitro* studies have demonstrated that Erk inhibition is able to counteract this INF-γ-mediated pro-inflammatory microglia activation (Wood et al. 2015; Zheng, Zhou, and Wang 2016). Similar to the importance of Ras-Mek-Erk signalling in microglia-driven neurodegeneration, mTOR activation has been implicated in aged mouse microglial activation. Microglia from 23-months old mice showed increased mTOR activation that correlated with increased levels of pro-inflammatory cytokines, such as tumour necrosis factor (TNF), interleukin-1β (IL-1β) and interleukin-6 (IL-6) (Keane et al. 2021). Importantly, genetic inhibition of mTOR signalling reduced microglia activation and cytokine levels (Keane et al. 2021). Therefore, we would expect that, upon co-administration of trametinib and rapamycin, which reduce the activity of these crucial pathways in microglia activation, we would observe stronger effects compared to the single treatments. Additionally, the fact that trametinib has been shown to poorly cross the blood-brain barrier in mice (Vaidhyanathan et al. 2014; de Gooijer et al. 2018), as opposed to rapamycin (S. Banerjee et al. 2011; A.-L. Lin et al. 2013; Kaeberlein and Galvan 2019) might also account for the combinatorial effect of the two drugs. Even though we just detected a trend for reduced microglia activation under the single rapamycin and trametinib administration, this is likely attributed to the limited statistical power, high variability in the response to the single drug treatments and the absence of effects of trametinib and rapamycin alone. Thus, it would be crucial for future experiments to ensure that enough animals and measurements of brain levels of trametinib and rapamycin are included to detect the effects of these drugs in microglia activation and validate our findings of a strong effect upon double drug treatment. Importantly, the factors influencing the brain distribution of trametinib, including co-administration with rapamycin should be identified. Further, it would be interesting to examine whether the effects of trametinib singly and combined with rapamycin administrations in microglia activation can impact animal behaviour. Given the crucial role of striatum in the regulation of social learning and motor control (Báez-Mendoza and Schultz 2013), it would seem plausible that the alleviation of microglia and astrocytes accumulation we observed under combined treatment with trametinib and rapamycin in this region might be linked to the enhanced exploration under the double drug treatment. More elegant experiments, with microglia accumulation and exploratory capacity measured in the same mice before and after receiving the trametinib and rapamycin double treatments are required to establish this link. Importantly, mouse models with impaired exploratory drive, such as 3xTg-AD (Roda et al. 2020) should be used to test the response to the combined trametinib and rapamycin treatment in a state of severe microglia accumulation.

The fact that we did not detect solid evidence of reduced microglial accumulation in the trametinib-only treated mice compared to the mice receiving the combined trametinib and rapamycin treatment was puzzling. As indicated by the glucose uptake results, there was an age-related increase in the global uptake of glucose, which was very prominent in the striatum and cerebellum, but not in the cortex, and trametinib seemed to attenuate this increase between 18 and 24 months of age globally and in the striatum and cerebellum. However, in the cerebellum we could not detect a corresponding age-related increase in microglial or astrocyte accumulation, whereas in the cortex there was a significant accumulation of both astrocytes and microglia with age. Yet, in the cortex, the single trametinib treatment only

showed a minor trend in reduction of astrocytes accumulation and not of microglia. Although microglia have been considered the main driver of 18F-FDG uptake alterations in the brain (Xiang et al. 2021), based on our findings, it is possible that there might be another contributor to the increase in global, striatal and cortex glucose uptake of control animals with age. Neuronal activity is known to account for glucose metabolism uptake changes in the mouse brain (Acarin, González, and Castellano 2000; Chu et al. 2016). Neurons require high glucose utilisation to ensure proper brain function (Dienel 2019) and there is a decline in neuronal glucose uptake with age (Yin et al. 2016), suggesting that the age-related increase in glucose uptake we observed in controls cannot be attributed to alterations in neuronal activity. Other major players in glucose uptake changes in the brain include immune cells. Among immune cells, macrophages have been shown to exhibit increased 18F-FDG uptake in states of brain inflammation (Treglia 2019; Jamar et al. 2013). Ageing is characterised by increased inflammation levels in multiple organs, including the brain (Sparkman and Johnson 2008), and brain inflammation in the aged mouse manifests with increased nuclear factor 'kappa-light-chain-enhancer' of activated B-cells (NF-kb) signalling and IL-6 production (S. M. Ye and Johnson 2001). Activation of Erk signalling has been shown to coordinate synthesis of pro-inflammatory cytokines and a growing body of evidence indicates that Erk and NF-kb signalling act in concert to promote inflammation (Collins et al. 2019; Guma et al. 2011; Lu and Malemud 2019). Therefore, it would be important to examine whether accumulation of macrophages and increased production of pro-inflammatory cytokines are contributors to the increased glucose uptake in the ageing mouse brain. Importantly, additional studies should address whether Ras-Merk-Erk signalling inhibition via trametinib can alleviate the age-related changes in macrophage accumulation and cytokine production in the brain. For this purpose, future work should include macrophage markers, such as TomL next to microglia and astrocytes markers in brain immunostainings and transcriptionally examine cytokine levels to pinpoint which brain cell subsets are the primary contributors to the attenuated glucose uptake increase under trametinib and rapamycin treatments.

Although macrophage accumulation alterations might at least partly explain the discrepancy between the changes in glucose uptake and microglia activation with age and under the single and combined drug treatments, it remains unclear whether trametinib and rapamycin have an impact on astrocytes, microglia or macrophages in other brain areas. Hypothalamus could be interesting to explore further based on the CMRglc 18-FDG data, indicating that this region showed a prominent glucose uptake increase with age. Further, hypothalamus is a key regulator of metabolism (Schwartz et al. 2013) and increased mTOR signalling in hypothalamic neurons has been previously linked to age-associated obesity (S.-B. Yang et al. 2012). Similarly, microglia NF-kb-dependent inflammatory activation was shown to regulate a hypothalamic response that increased susceptibility to obesity in mice (Valdearcos et al. 2017). Further studies should investigate the role of the hypothalamic microglia in the response to trametinib and rapamycin treatments during ageing.

Brain inflammation typically manifests with activation of microglia and astrocytes (Ayata et al. 2018; Göbel et al. 2020; Khakh and Sofroniew 2015; Motori et al. 2013). Under neuroinflammation, microglial activation is caused through NF-kb-, MAPK- (including Erk) and toll-like receptors- (TLRs) mediated signalling (Kreutzberg 1996; E.-A. Kim et al. 2014) and activated microglia can further exacerbate the pro-inflammatory state in the brain by increased production of cytokines, such as IL-6, TNF-α and prostaglandin E2 (PGE2) (Amor et al. 2010).

Thus, inhibiting the aberrant microglia activation through Erk activation suppression may alleviate neuroinflammation (Lim et al. 2018). Indeed, based on our finding that the combined trametinib and rapamycin treatment reduced the activation of microglia and astrocytes in the striatum of old females, we speculate that this double drug treatment might reduce inflammation in the ageing mouse brain. To further confirm the link between microglia activation and brain inflammation, protein levels or immunostainings for IL-6, TNF-α and PGE2 expression in the brains of mice treated with trametinib and rapamycin are required. Although we did not perform such experiments due to unavailability of brain tissue, we examined whether trametinib and rapamycin can ameliorate inflammation in peripheral organs. By performing histopathological and macro-pathological examinations in the kidney, we found that trametinib and rapamycin co-administration reduced kidney inflammation at old age and this effect is likely explained by rapamycin (no significant interaction between the rapamycin containing treatments, whereas there was an interaction between the trametinib treatments). Similarly, by studying the WAT, we found a trend towards reduced inflammation upon trametinib and rapamycin co-administration and a less clear trend for their single administration, and thus, further studies are needed to confirm whether the joint treatment with trametinib and rapamycin can elicit anti-inflammatory effects in the WAT. Our findings provide preliminary evidence of beneficial effects of trametinib and rapamycin combination on systemic inflammation that would be interesting to explore further. Future work should confirm our indications of a reduction of age-related inflammation in the brain, kidney and WAT of mice treated with trametinib and rapamycin combination and extend this evidence by studying other tissues undergoing inflammaging. Importantly, in-depth analysis of the molecular regulators of the anti-inflammatory effects of mTOR and Ras-Mek-Erk signalling inhibition can provide crucial insights on the mechanisms by which trametinib and rapamycin affect tissue inflammation. A growing body of literature has implicated Erk activation in various inflammatory diseases, such as rheumatoid arthritis, osteoarthritis and alcoholic liver disease (Malemud 2015; Mandrekar and Szabo 2009). The main players in Erk-mediated inflammation identified include innate immunity dysregulation manifesting with TLR activation (Lang, Hammer, and Mages 2006) and aberrant pro-inflammatory cytokine production via increased NF-kb, activator protein-1 (AP-1) (Mandrekar and Szabo 2009) and tumour progression locus 2 (TPL2) signalling (D. Xu et al. 2018). Next to local inflammation, systemic inflammatory responses can be triggered through members of the dual-specificity phosphatase (DUSP) gene family (Lang, Hammer, and Mages 2006), that are known to selectively bind to Erk1/2, controlling inflammatory and immune responses (Lang and Raffi 2019). On the other hand, rapamycin has been shown to exert anti-inflammatory responses via suppression of TNF-α and IL-6 (Weichhart, Hengstschläger, and Linke 2015). Therefore, measurements of NF-kb, AP-1, TPL2 and DUSP1, DUSP2, IL-1β, IL-6 and TNF-α at the transcriptome or proteome level in multiple tissues, including the liver, muscle and bones under trametinib and rapamycin administrations should be included in future studies. Although reduced inflammation in multiple tissues could be indicative of a systemic anti-inflammatory effect of these drugs, measurements of cytokine levels in the mouse plasma would be required to support this conclusion and confirm that targeting Ras-Mek-Erk and mTOR networks modulates local and systemic inflammatory responses.

Apart from inflammation, other processes may be involved in the response to trametinib and rapamycin treatments. Previous work on transcriptomic changes under rapamycin administration has provided insights on altered regulation of mitochondrial function, protein ubiquitination and stress response in the mouse liver and kidney (Fok et al. 2014; Shindyapina

et al. 2022). Further, functional assays have revealed a role for rapamycin in attenuating the functional decline observed in old hematopoietic stem cells and in reversing geriatric satellite cell senescence, ultimately leading to an enhanced tissue regenerative capacity (García-Prat et al. 2016; C. Chen et al. 2009). Similarly, trametinib treatment has been shown to reduce cell senescence in in-vitro models (Latorre et al. 2017). Age-associated immune senescence was also shown to be attenuated under rapamycin treatment, which counteracted the age-related increase in plasma immunoglobulin concentrations and frequency of activated T cells (Neff et al. 2013). Therefore, future studies utilising comprehensive transcriptome analyses or histological and functional assays in a vast array of tissues are required to explore the involvement of mitochondrial function, protein ubiquitination, stress responses and cellular and immune senescence in the lifespan-extending effects of trametinib and rapamycin.

In conclusion, our study provides robust evidence that trametinib single administration increases lifespan in female and male mice and that its combination with rapamycin produces a greater lifespan prolongation compared to the single treatments in both sexes. Our comprehensive, large-scale assessment of a wide range of functional and histological ageing phenotypes across 9 different tissues reveals mild effects of trametinib and its combination with rapamycin in the mouse health, but substantial anti-carcinogenic effects liver and spleen. The combination of trametinib with rapamycin attenuates the increase in glucose uptake increase and activation of microglia and astrocytes in the brain of old female mice, indicative of a reduced brain inflammation. We speculate that these drugs might elicit a systemic anti-inflammatory response after finding preliminary evidence of a reduced inflammation in the kidney and possibly WAT. Yet, the contributors to the trametinib-mediated lifespan extension and the maximised longevity upon its coadministration with rapamycin remain unclear. Future investigation on the causal involvement of various cellular processes in the trametinib and rapamycin-induced longevity using functional assays in multiple tissues can greatly expand our understanding of the mechanisms of lifespan extension upon modulation of Ras/Erk and mTOR networks.

3.4. Supplementary figures

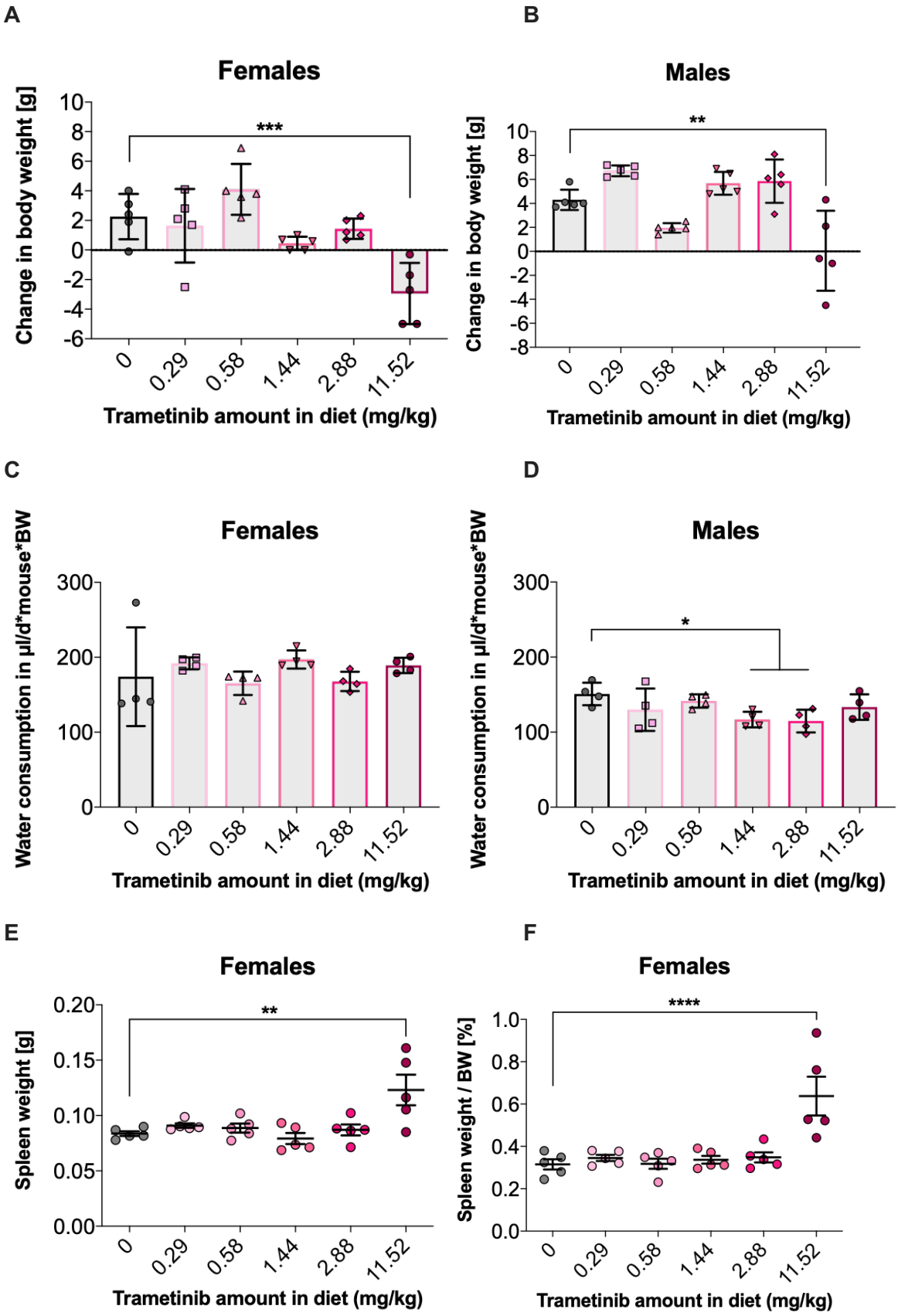

G

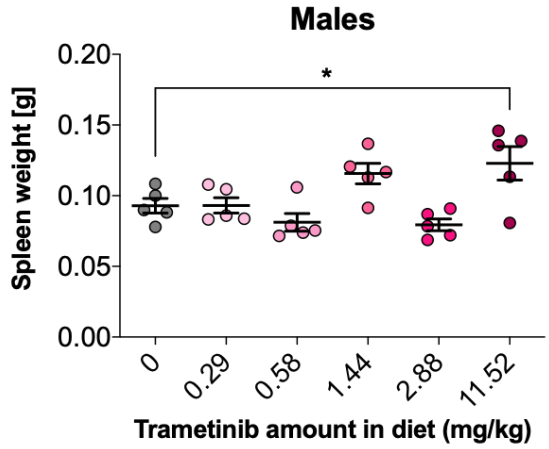
Males
Spleen weight [g]
0.20
0.15
0.10
0.05
0.00
*
0
0.29
0.58
1.44
2.88
11.52
Trametinib amount in diet (mg/kg)

H

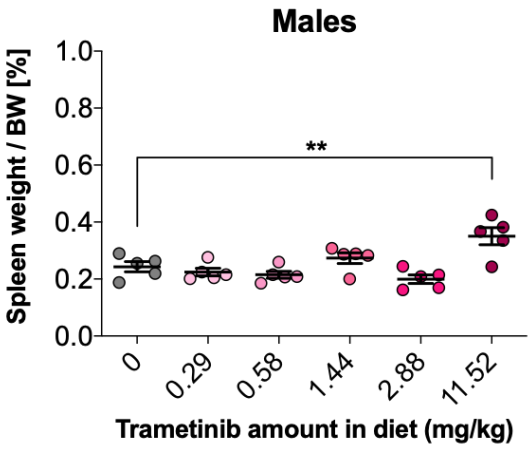
Males
Spleen weight / BW [%]
1.0
0.8
0.6
0.4
0.2
0.0
**
0
0.29
0.58
1.44
2.88
11.52
Trametinib amount in diet (mg/kg)

I

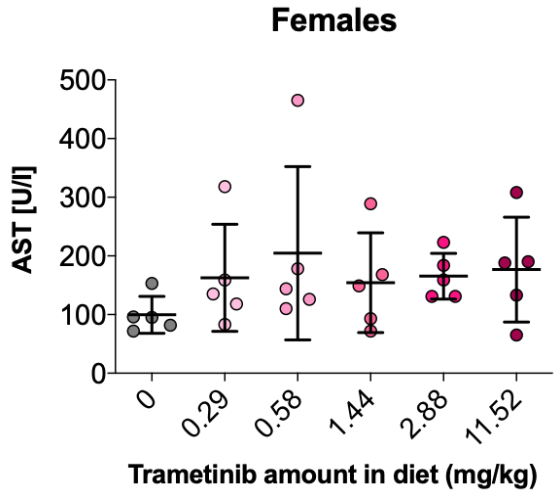
Females
AST [U/l]
500
400
300
200
100
0
0
0.29
0.58
1.44
2.88
11.52
Trametinib amount in diet (mg/kg)

J

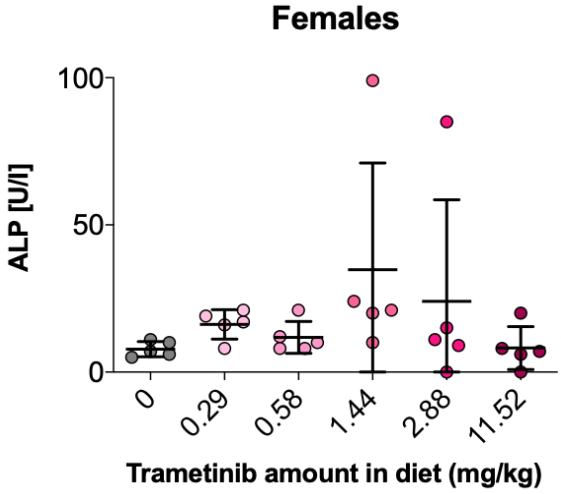
Females
ALP [U/l]
100
50
0
0
0.29
0.58
1.44
2.88
11.52
Trametinib amount in diet (mg/kg)

K

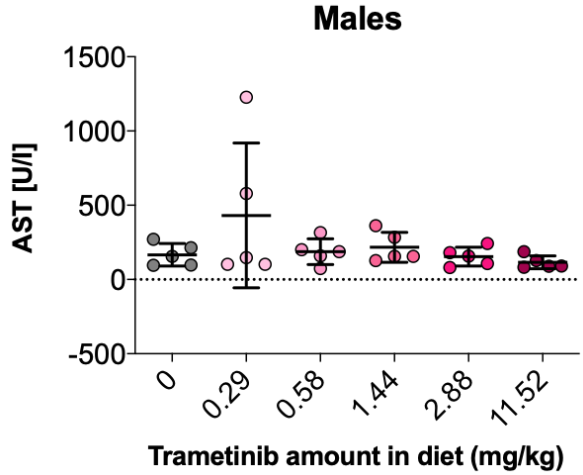
Males
AST [U/l]
1500
1000
500
0
-500
0
0.29
0.58
1.44
2.88
11.52
Trametinib amount in diet (mg/kg)

L


Males
ALP [U/l]
60
40
20
0
-20
0
0.29
0.58
1.44
2.88
11.52
Trametinib amount in diet (mg/kg)

M

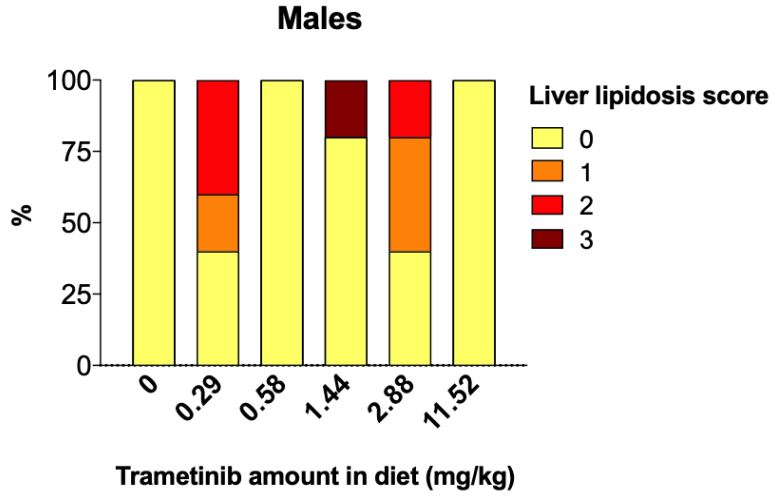

Supplementary Figure 3.1. Trametinib dose levels of 0.05-0.5 mg/kg of diet did not adversely affect mouse organismal health. (A-B) Body weight changes of **(A)** female and **(B)** male mice fed with 0, 0.29, 0.58, 1.44, 2.88 or 11.52 mg/kg of trametinib for 4 weeks. Trametinib at 11.52 mg/kg reduced weight gain in females (p-value= 0.0002) and males (p-value= 0.0023). Data are presented as mean ± SD. Statistical analyses were performed using One-Way ANOVA with post hoc Bonferroni test. **(C-D)** Water consumption of **(C)** female and **(D)** male mice fed with 0, 0.29, 0.58, 1.44, 2.88 or 11.52 mg/kg of trametinib for 4 weeks. Trametinib did not affect water consumption in females, whereas trametinib at 1.44 and 2.88 mg/kg reduced water consumption in males (p-value= 0.0423 and p-value= 0.0302, respectively). Data are presented as mean ± SD. Statistical analyses were performed using One-Way ANOVA with post hoc Bonferroni test. **(E-H)** Spleen **(E,G)** weight and spleen (F,H) as a percentage of mouse body weight in **(E-F)** female and **(G-H)** male mice fed with 0, 0.29, 0.58, 1.44, 2.88 or 11.52 mg/kg of trametinib for 4 weeks. Trametinib at 11.52 mg/kg increased spleen weight and percentage of mouse body weight in females (p-value= 0.0017and p-value<0.0001) and males (p-value=0.0342 and p-value=0.0026). Data are presented as mean ± SD. Statistical analyses were performed using One-Way ANOVA with post hoc Bonferroni test. **(I-M)** Plasma levels of **(I,K)** AST, **(J,L)** ALP in **(I,K)** female and **(J,L)** male mice fed with 0, 0.29, 0.58, 1.44, 2.88 or 11.52 mg/kg of trametinib for 4 weeks. **(M)** Liver lipidosis score of male mice fed with 0, 0.29, 0.58, 1.44, 2.88 or 11.52 mg/kg of trametinib for 4 weeks as determined by histopathological inspection of mouse livers. Scores range from 0 (no lipidosis) to 1 (mild), 2 (moderate) and 3 (marked), whereas none of the female mice showed liver lipidosis. Trametinib had no impact on AST, ALP or liver lipidosis at any of the doses. Data are presented as mean ± SD. Statistical analyses were performed using **(I-L)** One-Way ANOVA with post hoc Bonferroni test and **(M)** Chi-square test and Poisson Regressions. Data are expressed as *P < 0.05; **P < 0.01; ***P < 0.001 and ****P < 0.0001.

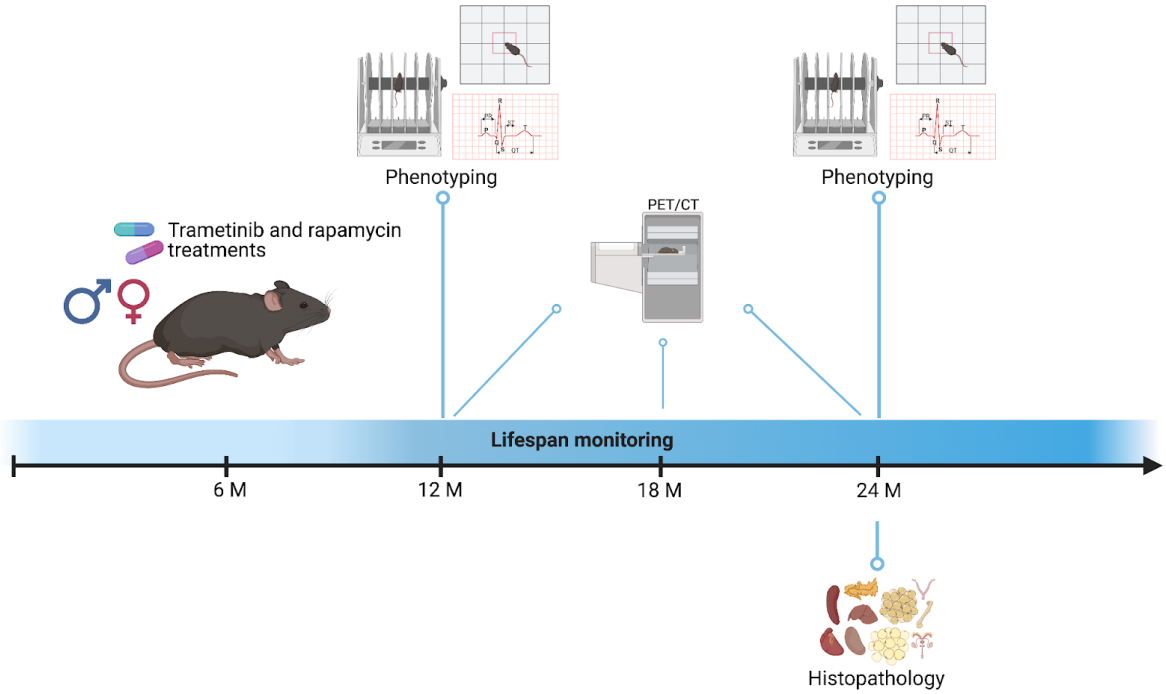

Supplementary Figure 3.2. Combined trametinib and rapamycin study design. 6-month old male and female mice were orally dosed with rapamycin weekly intermittently at 42 mg/kg, trametinib at 0.58 mg/kg, trametinib at 1.44 mg/kg, as well as with double combinations of rapamycin and trametinib at 1.44 mg/kg. Survival assessment (n=50/treatment group), phenotyping assessment (electrocardiogram, rotarod, open maze, treadmill, n=7-15/treatment group) and organ glucose uptake (PET/CT, n=14-16/treatment group) at middle and old age, as well as organ collection for histopathological examination (n=26-90/treatment group) at old age were performed.

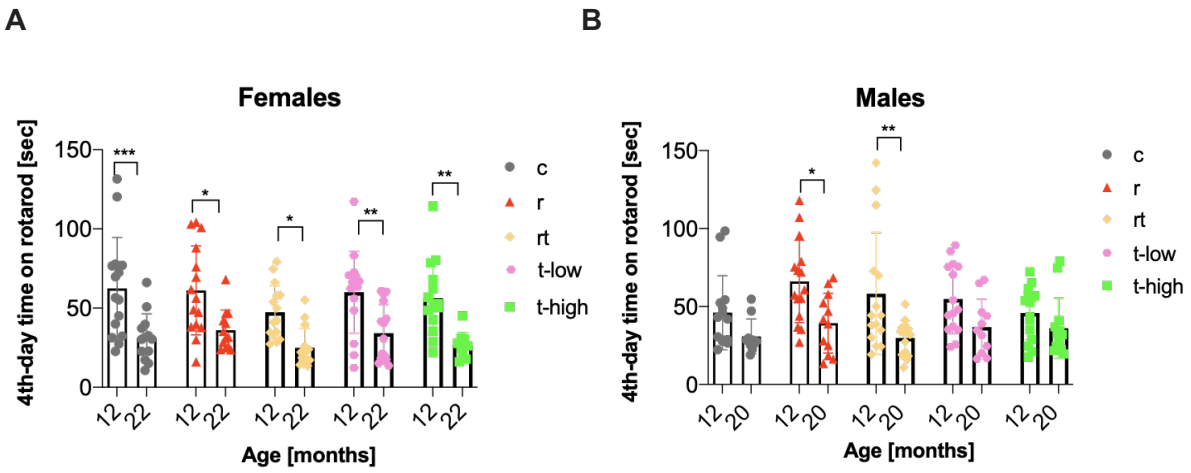

Supplementary Figure 3.3. Motor performance declines with age irrespective of drug treatment. **(A-B)** Total spent on the rod at day 4 of the rotarod test for **(A)** female and **(B)** male control mice (c, grey, ♂ n=10-14, ♀ n=13-15), mice treated with single rapamycin at 42 mg/kg (r, red, ♂ n=12-15, ♀ n=13-15), mice treated with trametinib at 0.58 mg/kg (t-low, pink, ♂ n=11-15, ♀ n=15), and trametinib at 1.44 mg/kg (t-high, green, ♂ n=13-15, ♀ n=10-15), as well as mice receiving double combinations of rapamycin and trametinib at 1.44 mg/kg (rt, yellow, ♂ n=15, ♀ n=15) at 12 and 20-22 months of age. Latency to fall was reduced in 20-22 month old compared to 12 month-old male and female mice. Data are presented as mean ± SD. Statistical analyses were performed using Two-Way ANOVA with post hoc Bonferroni test. Females: c at 12 vs c at 22 months p-value= 0.0008; r at 12 vs r at 22 months p-value= 0.0103; rt at 12 vs rt at 22 months p-value= 0.0210; t-low at 12 vs t-low at 22 months p-value= 0.0051; t-high at 12 vs t-high at 22 months p-value= 0.0037; Males: r at 12 vs r at 22 months p-value= 0.0135; rt at 12 vs rt at 22 months p-value= 0.0040. Data are expressed as *P < 0.05; **P < 0.01; ***P < 0.001.

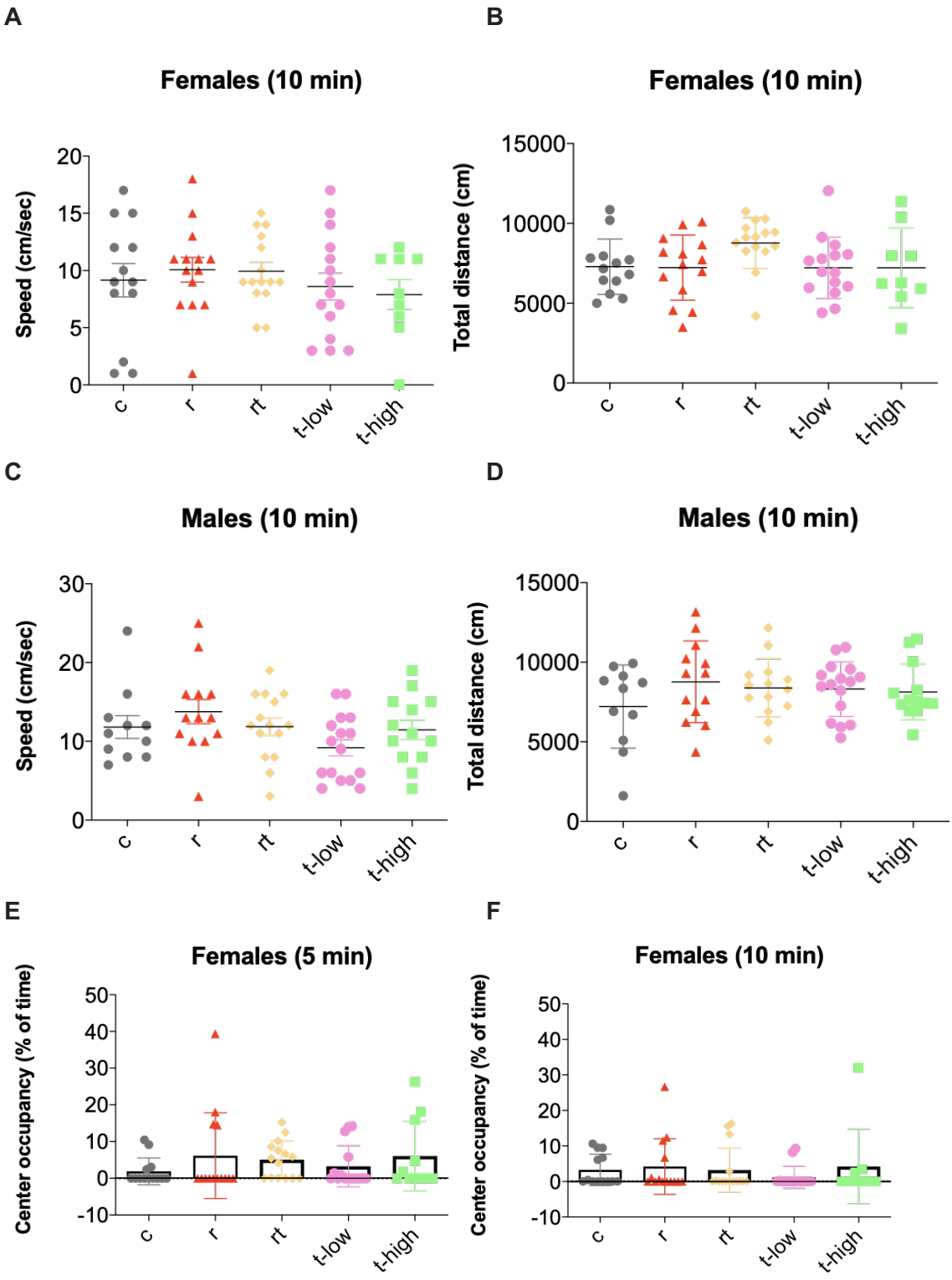
A
Females (10 min)
Speed (cm/sec)
20
15
10
5
0
c
r
rt
t-low
t-high
B
Females (10 min)
Total distance (cm)
15000
10000
5000
0
c
r
rt
t-low
t-high
C
Males (10 min)
Speed (cm/sec)
30
20
10
0
c
r
rt
t-low
t-high
D
Males (10 min)
Total distance (cm)
15000
10000
5000
0
c
r
rt
t-low
t-high
E
Females (5 min)
Center occupancy (% of time)
50
40
30
20
10
0
-10
c
r
rt
t-low
t-high
F
Females (10 min)
Center occupancy (% of time)
50
40
30
20
10
0
-10
c
r
rt
t-low
t-high

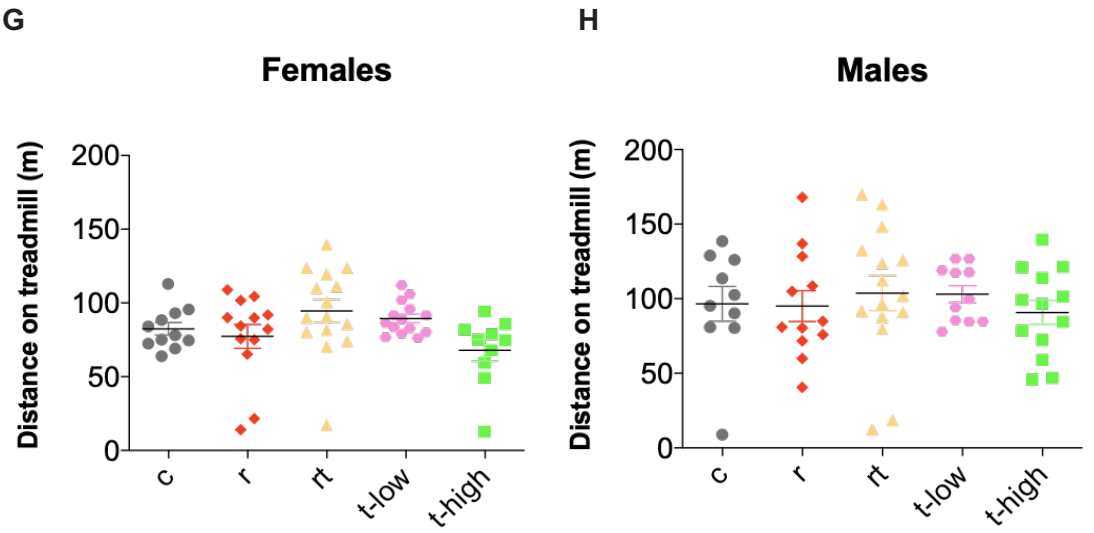

Supplementary Figure 3.4. Trametinib and rapamycin double treatment has no effect on male mouse exploration or endurance. (A-C) Locomotion speed, **(B-D)** total distance travelled, **(E-F)** percentage of time spent on the centre normalised to total time spent on the open field test at 10 min and **(G-H)** distance run on treadmill for **(A-B, E-F, G)** female and **(C-D, H)** male control mice (grey, ♂ n=10-11, ♀ n=12-13), mice treated with single rapamycin at 42 mg/kg (r, red, ♂ n=12-13, ♀ n=13-14), mice treated with trametinib at 0.58 mg/kg (t-low, pink, ♂ n=11-15, ♀ n=15), and trametinib at 1.44 mg/kg (t-high, green, ♂ n=13, ♀ n=10-12), as well as double combinations of rapamycin and trametinib at 1.44 mg/kg (rt, yellow, ♂ n=15, ♀ n=15) at **(A-B, E, G)** 22 and **(C-D, F, H)** 20 months of age. No significant differences were detected in locomotion speed, total distance travelled in open field or treadmill or centre occupancy between trametinib-treated and control 20-22 month old mice. Data are presented as mean ± SD. Statistical analyses were performed using One-Way ANOVA with post hoc Bonferroni test.

A

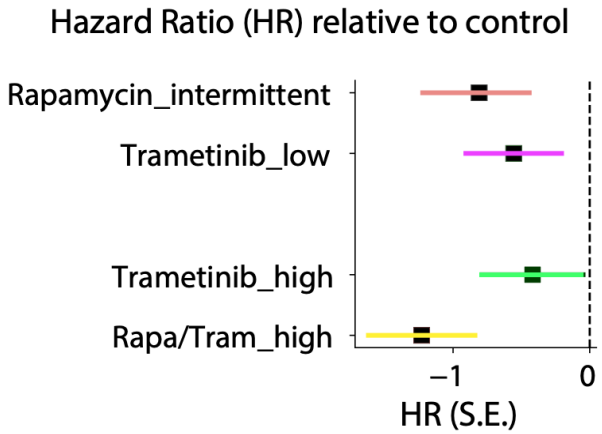

comparison	lowerCI	upperCI	coef	p-value
Rapa/Tram_high	-1.636872	-0.822338	-1.229605	3.200000e-09
Trametinib_high	-0.805394	-0.030949	-0.418172	3.429200e-02
Trametinib_low	-0.923990	-0.188579	-0.556284	3.025000e-03
Rapamycin_intermittent	-1.189824	-0.428282	-0.809053	3.100000e-05

B

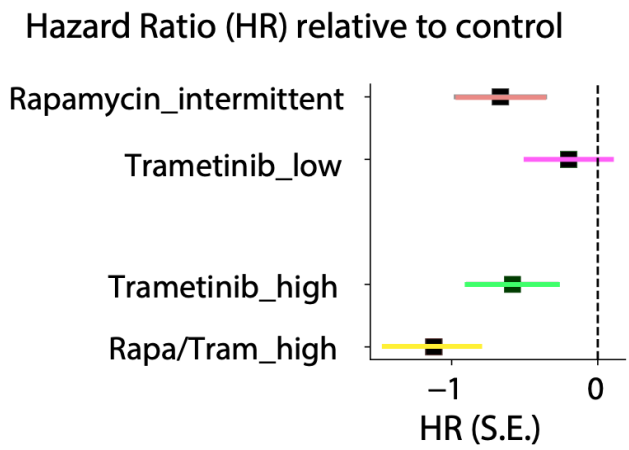

comparison	lowerCI	upperCI	coef	p-value
Rapa/Tram_high	-1.477601	-0.766539	-1.122070	6.180000e-10
Trametinib_high	-0.901640	-0.266588	-0.584114	3.120000e-04
Trametinib_low	-0.507309	0.109871	-0.198719	2.069010e-01
Rapamycin_intermittent	-0.985499	-0.347127	-0.666313	4.300000e-05

Supplementary Figure 3.5. Cox Proportional Hazard analysis of trametinib and rapamycin single and combined treatments on mouse longevity. Hazard ratio presented as mean ± SE (upper panel) and cox proportional hazard analysis output (lowe panel) of female **(A)** and **(B)** male mice treated with single, weekly intermediate rapamycin at 42 mg/kg (Rapamycin_intermittent, red, ♂ n=119, ♀ n=97), single trametinib at 0.58 mg/kg (Trametinib_low, pink, ♂ n=120, ♀ n=97), and trametinib at 1.44 mg/kg (Trametinib_high, green, ♂ n=121, ♀ n=97), or with double combinations of rapamycin and trametinib at 1.44 mg/kg (Rapa/Tram_high, yellow, ♂ n=120, ♀ n=97) compared to control mice. Cox proportional

hazard showed a significant Sex*Treatment effect for Rapa/Tram_high vs control (p-value= 2.144566e-08), Trametinib_high vs control (p-value= 0.000004), Trametinib_low vs control (p-value= 1.433227e-09) and Rapamycin_intermittent vs control (p-value= 6.748339e-08).

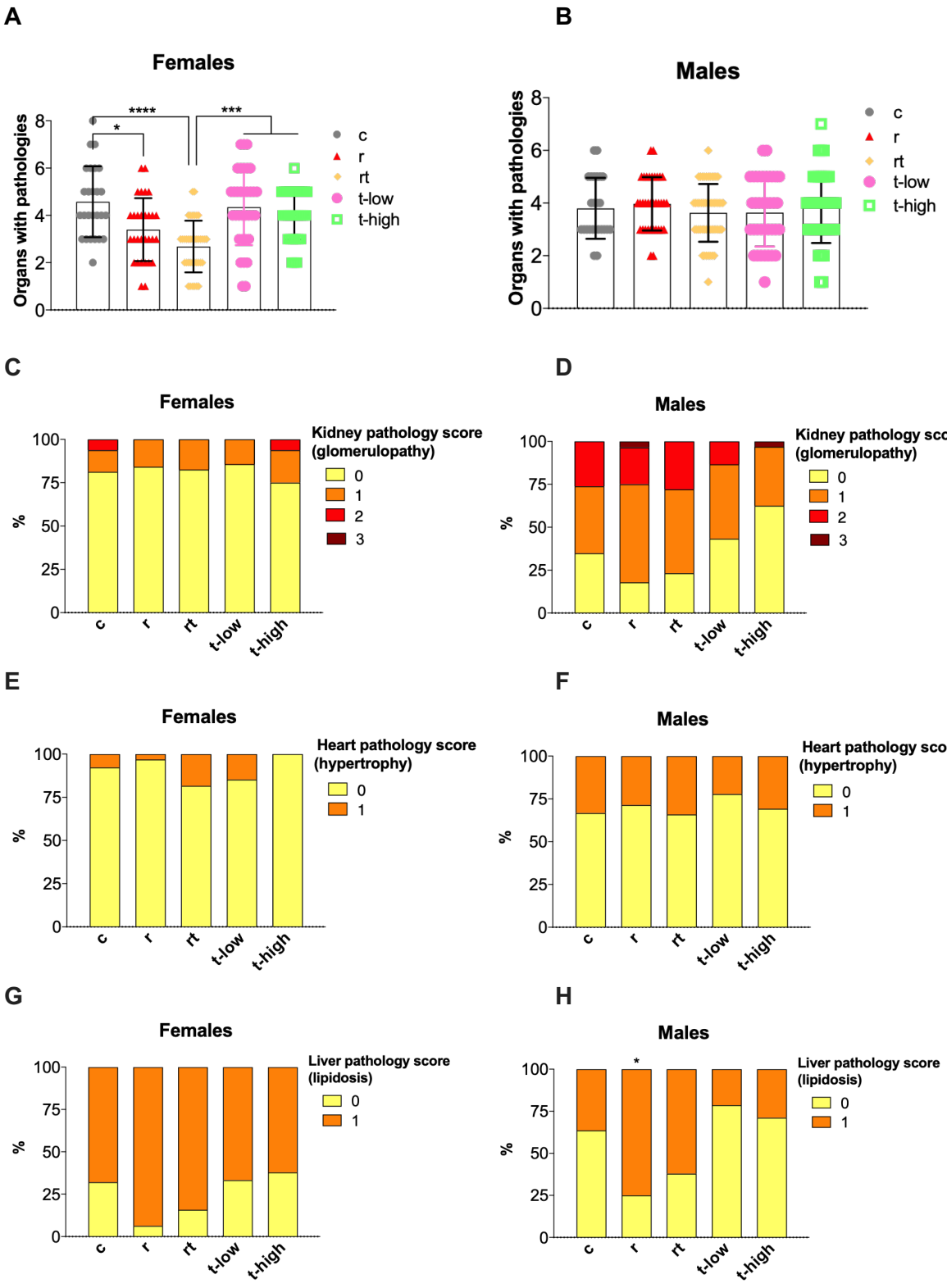
A
Females
Organs with pathologies
****
***
*
c
r
rt
t-low
t-high
B
Males
C
Females
Kidney pathology score (glomerulopathy)
%
D
Males
E
Females
Heart pathology score (hypertrophy)
F
Males
G
Females
Liver pathology score (lipidosis)
H
Males
*

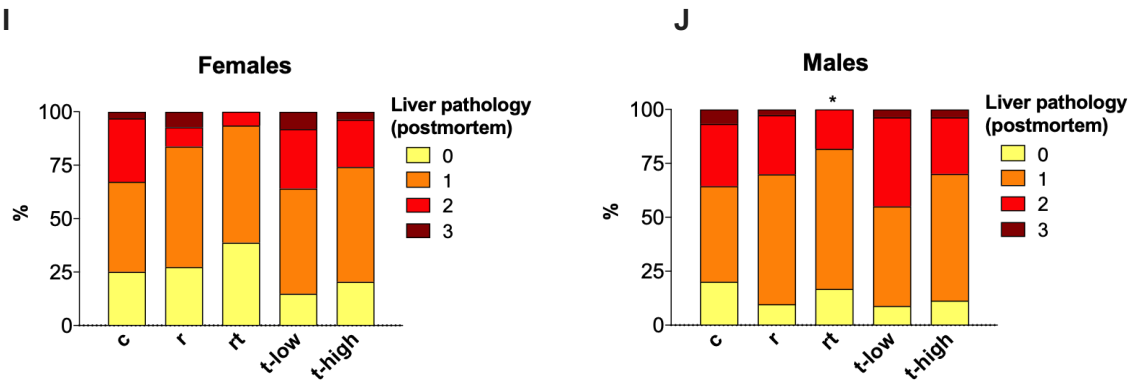

Supplementary Figure 3.6. Effects of trametinib and rapamycin on total pathological burden and non-neoplastic pathologies in various organs. (A-B) Examination of organs with non-neoplastic and neoplastic pathologies in **(A)** female and **(B)** male control mice (c, grey, ♂ n=90, ♀ n=64), mice treated with rapamycin at 42 mg/kg (r, red, ♂ n=72, ♀ n=49), mice treated with trametinib at 0.58 mg/kg (t-low, dark green, ♂ n=80, ♀ n=61), and trametinib at 1.44 mg/kg (t-high, green, ♂ n=79, ♀ n=55), and rapamycin and trametinib at 1.44 mg/kg (rt, yellow, ♂ n=55, ♀ n=26) at time of death. Rapamycin combination with trametinib reduced the number of organs affected by pathologies compared to controls in female mice, whereas no differences were detected in males. Data are presented as mean ± SD. Statistical analyses were performed using One-Way ANOVA with post hoc Bonferroni test. Females: r vs c p-value= 0.0137; rt vs c p-value>0.0001; rt vs t-low p-value= 0.0006; rt vs t-high p-value= 0.0007. **(C-H)** Histopathological analysis in the **(C-D)** kidney, **(E-F)** heart and **(G-H)** liver of **(C, E, G)** female and **(D, F, H)** male control mice (c, ♂ n=33, ♀ n=25), mice treated with rapamycin at 42 mg/kg (r, ♂ n=40, ♀ n=32), rapamycin and trametinib at 1.44 mg/kg (rt, ♂ n=58, ♀ n=38), trametinib at 0.58 mg/kg (t-low, ♂ n=42, ♀ n=30), and trametinib at 1.44 mg/kg (t-high, ♂ n=45, ♀ n=29). The presence or absence of glomerulopathy (kidney), hypertrophy (heart) and lipidosis (liver) was scored with 1 or 0, respectively. Trametinib alone or in combination with rapamycin did not affect kidney, heart and liver pathologies. Data are presented as percentage over total and analysis was performed by Chi-square test and Poisson regressions. Males: liver r vs c p-value=0.0203. **(I-J)** Macro-pathological analysis in the liver of **(I)** female and **(J)** male control mice (c, ♂ n=90, ♀ n=64), mice treated with rapamycin at 42 mg/kg (r, ♂ n=73, ♀ n=55), rapamycin and trametinib at 1.44 mg/kg (rt, ♂ n=60, ♀ n=31), trametinib at 0.58 mg/kg (t-low, ♂ n=79, ♀ n=61), and trametinib at 1.44 mg/kg (t-high, ♂ n=80, ♀ n=55). The presence or absence of enlarged or discoloured liver was scored with 1 or 0, respectively. Rt treatment significantly reduced liver pathologies in male mice, but no differences were observed in the females. Data are presented as percentage over total and analysis was performed by Chi-square test and Poisson regressions. Males: rt vs c p-value=0.0150. Data are expressed as *P < 0.05.

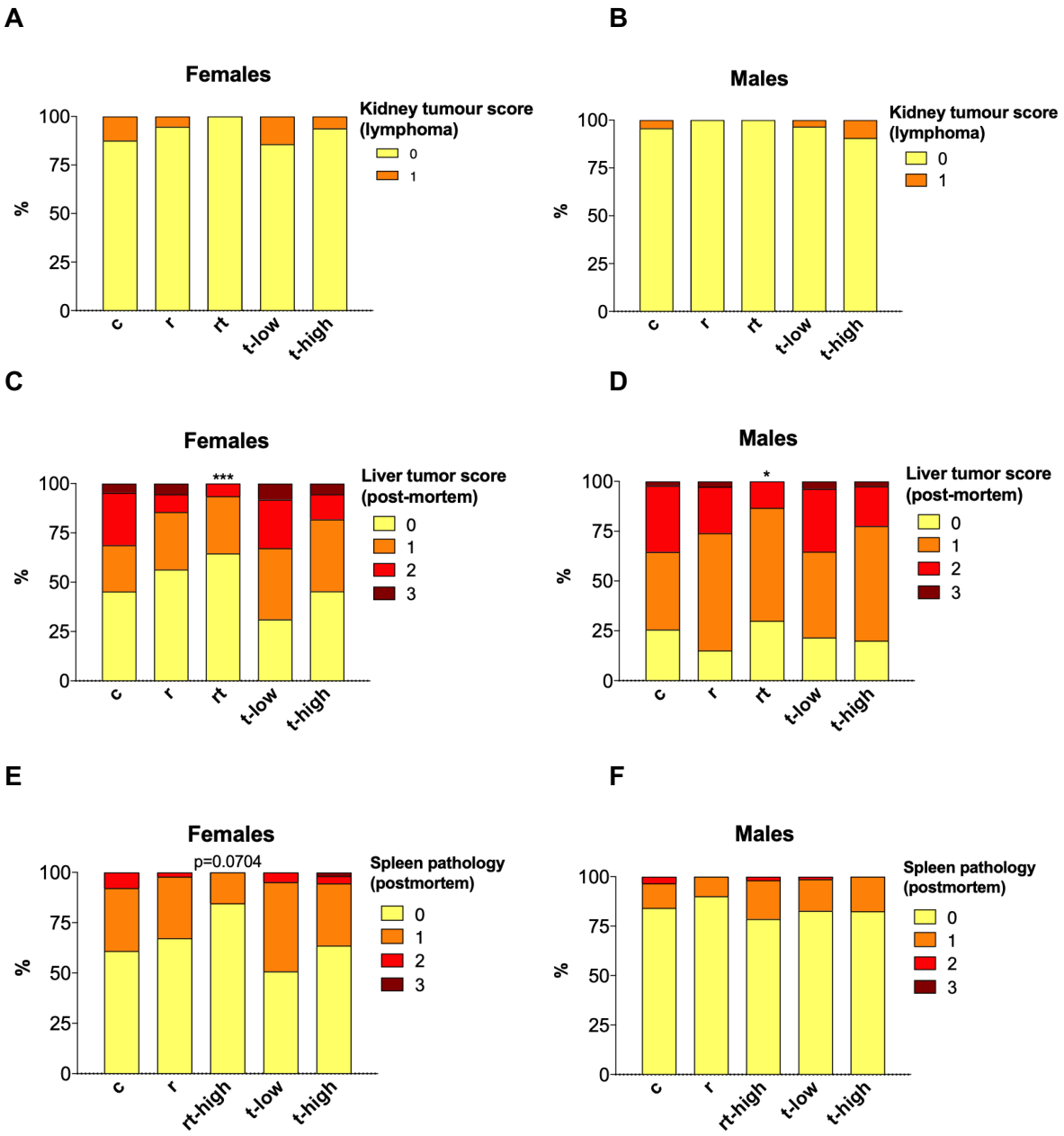

Supplementary Figure 3.7. Effects of trametinib and rapamycin on neoplastic pathologies in various organs. (A-B) Histopathological analysis in the kidney of **(A)** female and **(B)** male control mice (c, ♂ n=33, ♀ n=24), mice treated with rapamycin at 42 mg/kg (r, ♂ n=33, ♀ n=30), rapamycin and trametinib at 1.44 mg/kg (rt, ♂ n=51, ♀ n=33), trametinib at 0.58 mg/kg (t-low, ♂ n=29, ♀ n=30), and trametinib at 1.44 mg/kg (t-high, ♂ n=45, ♀ n=33). The presence or absence of kidney lymphomas was scored with 1 or 0, respectively. None of the trametinib and rapamycin treatments affected kidney tumour occurence. Data are presented as percentage over total and analysis was performed by Chi-square test and Poisson regressions. **(C-D)** Macro-pathological analysis in the liver of **(C)** female and **(D)** male control mice (c, ♂ n=90, ♀ n=64), mice treated with rapamycin at 42 mg/kg (r, ♂ n=73, ♀ n=55), rapamycin and trametinib at 1.44 mg/kg (rt, ♂ n=60, ♀ n=31), trametinib at 0.58 mg/kg (t-low, ♂ n=79, ♀ n=61), and trametinib at 1.44 mg/kg (t-high, ♂ n=80, ♀ n=55). The presence or absence and severity of tumours was scored with 0 (absence), 1 (one tumour), 2 (multiple tumours or metastasis in two organs), 3 (metastasis in 3 or more organs). Rt treatment showed a significant decline in the percentage of male and female mice with liver tumours. Data are presented as percentage over total and analysis was performed by Chi-square test and Poisson regressions. Females: rt vs c p-value=0.0009; Males: rt vs c p-value=0.0150. **(E-F)** Macro-pathological analysis in the spleen of **(E)**

female and **(F)** male control mice (c, ♂ n=89, ♀ n=64), mice treated with rapamycin at 42 mg/kg (r, ♂ n=71, ♀ n=49), rapamycin and trametinib at 1.44 mg/kg (rt, ♂ n=56, ♀ n=26), trametinib at 0.58 mg/kg (t-low, ♂ n=81, ♀ n=61), and trametinib at 1.44 mg/kg (t-high, ♂ n=80, ♀ n=54). The presence or absence and degree of pathologies, such as enlargement, discoloration and tumours were scored with 0 (absence), 1 (only enlargement or discoloration), 2 (multiple tumours or metastasis and enlargement or discoloration) and 3 (severe metastasis in three or more organs). Rt female mice showed a strong tendency of reduction in spleen pathologies. Data are presented as percentage over total and analysis was performed by Chi-square test and Poisson regressions. Females: rt vs c p-value=0.0704. Data are expressed as *P < 0.05 and ***P < 0.001.

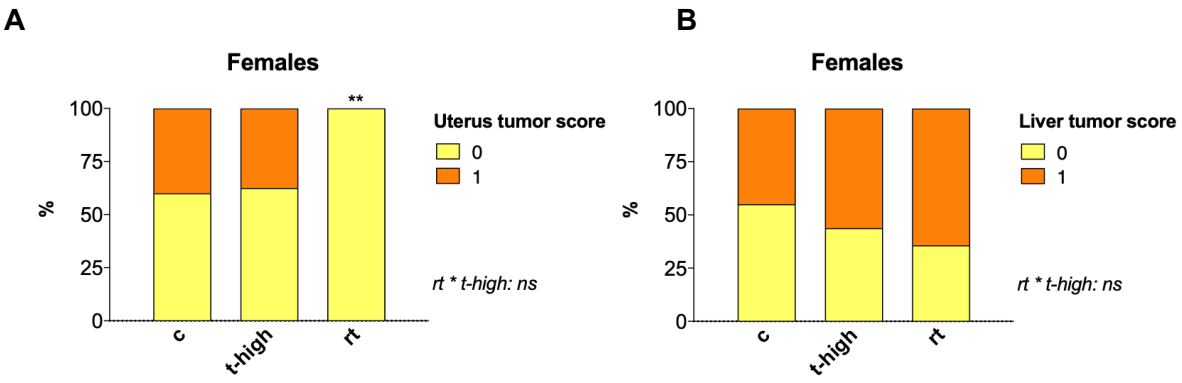

Supplementary Figure 3.8. Rapamycin and trametinib combination effects on uterine and liver tumours at old age. (A-B) Hypermetabolic regions in the **(A)** uterus and **(B)** liver were identified as tumours and scored for their presence (1) or absence (0) in control female mice (c, n=20), female mice treated with trametinib at 1.44 mg/kg (t-high, n=14), and with rapamycin and trametinib at 1.44 mg/kg (rt, n=16) after cross-reference with macro-pathological inspection at 24 months of age. Rt mice showed a significant reduction in uterine tumour presence at 24 months of age. Data are presented as percentage over total and analysis was performed by Chi-square test and Poisson regressions. Uterus: rt vs c p-value=0.0068; rt * t-high interaction p-value=0.9982. Liver: rt vs c p-value=0.2675; rt * t-high interaction p-value=0.6544. Data are expressed as **P < 0.01.

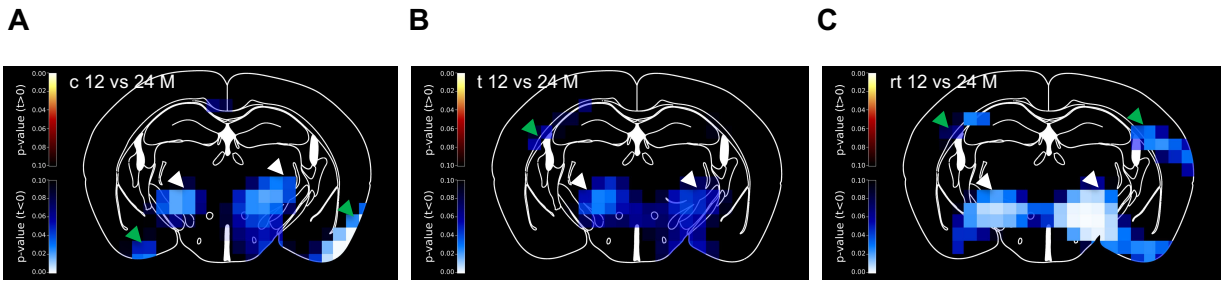

Supplementary Figure 3.9. Rapamycin and trametinib effects on differential glucose uptake in the brain. (A-C) Representative coronal image of differential 18-FDG uptake based on CMRglc statistics in the brains of **(A)** control mice at 12 versus 24 months of age (n=8), **(B)** trametinib at 1.44 mg/kg treated mice at 12 versus 24 months of age (n=10) and **(C)** rapamycin and trametinib at 1.44 mg/kg treated mice at 12 versus 24 months of age (n=12). Arrows indicate the cortex (green) and striatum (white) regions. Heatmap keys are based on p-value<0.05 and the red and blue scales indicate increased or decreased 18-FDG uptake in 12 compared to 24 months of age, respectively.

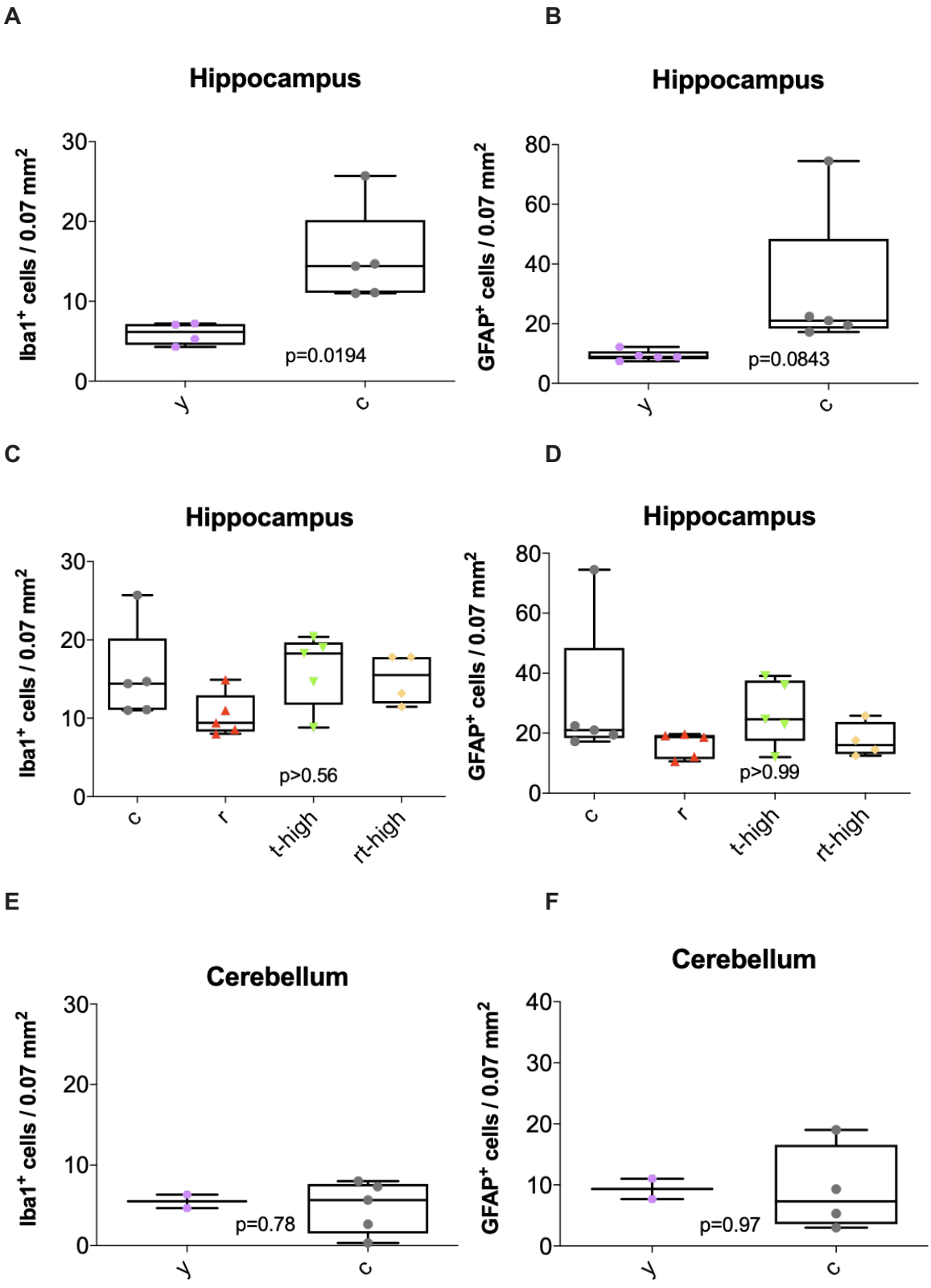
A
Hippocampus
Iba1+ cells / 0.07 mm2
30
20
10
0
p=0.0194
y
c
B
Hippocampus
GFAP+ cells / 0.07 mm2
80
60
40
20
0
p=0.0843
y
c
C
Hippocampus
Iba1+ cells / 0.07 mm2
30
20
10
0
p>0.56
c
r
t-high
rt-high
D
Hippocampus
GFAP+ cells / 0.07 mm2
80
60
40
20
0
p>0.99
c
r
t-high
rt-high
E
Cerebellum
Iba1+ cells / 0.07 mm2
30
20
10
0
p=0.78
y
c
F
Cerebellum
GFAP+ cells / 0.07 mm2
40
30
20
10
0
p=0.97
y
c

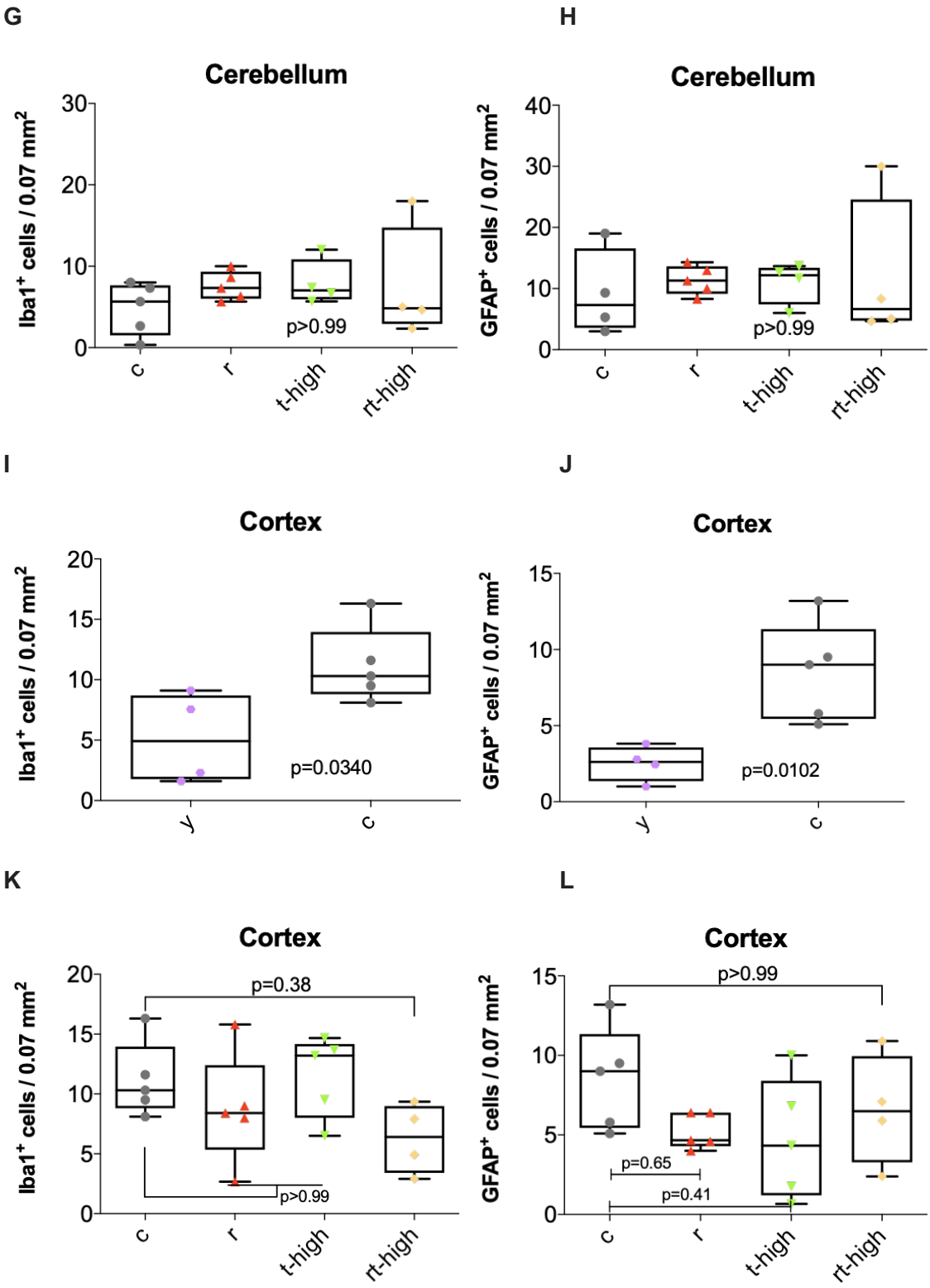

Supplementary Figure 3.10. Microglial and astrocyte density are not affected by trametinib and/or rapamycin treatments in the cerebellum, hippocampus or cortex of female 24-month old mice. (A-L) Quantification of the average number of double DAPI-Iba-1 positive cells (microglia density) and double DAPI-GFAP positive cells (astrocytes density) of 10-15 confocal images per female mouse brain region. The following treatments were included: young control (y, purple: 6 month old, n=2-5), old control (c, grey: 24 month old, n=5), trametinib at 1.44 mg/kg (t-high, green, n=5), and rapamycin and trametinib at 1.44 mg/kg (rt, yellow, n=5) in **(A-D)** hippocampus, **(E-H)** cerebellum, and **(I-L)** cortex of female mice. Data are presented as median (line), max and min (whiskers) in a box plot and statistical

analyses were performed using **(A-B, E-F, I-J)** Mann-Whitney U test or **(C-D, G-H, K-L)** One-Way ANOVA with post hoc Bonferroni test.

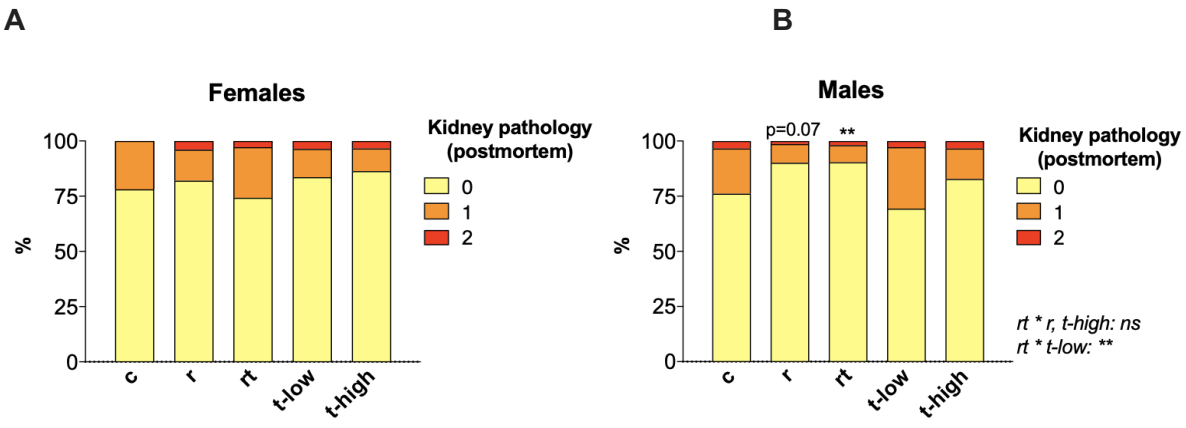

Supplementary Figure 3.11. Combined trametinib and rapamycin treatment reduces kidney pathologies in male mice. Macro-pathological analysis in the kidney of **(A)** female and **(B)** male control mice (c, ♂ n=88, ♀ n=64), mice treated with rapamycin at 42 mg/kg (r, ♂ n=71, ♀ n=50), mice receiving rapamycin and trametinib at 1.44 mg/kg (rt, ♂ n=52, ♀ n=35), mice treated with trametinib at 0.58 mg/kg (t-low, ♂ n=72, ♀ n=55), and trametinib at 1.44 mg/kg (t-high, ♂ n=87, ♀ n=59). The presence or absence and degree of pathologies, such as enlargement, discoloration and tumours were scored with 0 (absence), 1 (enlargement or discoloration) and 2 (tumours in one or both kidneys). Rt male mice showed a reduction in kidney pathologies and r males showed a strong tendency of reduction in pathologies in the kidney. Data are presented as percentage over total and analysis was performed by Chi-square test and Poisson regressions. Males: rt vs c p-value=0.0026; r vs c p-value=0.0702. rt * r interaction p-value=0.8287; rt * t-low interaction p-value=0.0081; rt * t-high interaction p-value=0.2682. Data are expressed as **P < 0.01.

4. Dietary restriction attenuates the age-related decline in mouse B cell receptor repertoire diversity

Author contributions:

Conception of the study predominantly by Carolina Monzó, Lisonia Gkioni, Sebastian Grönke, Dario Valenzano and Linda Partridge.

Tissues were provided by Lisa Drews and Sebastian Grönke.

Execution of experiments proportionally by Carolina Monzó and Lisonia Gkioni. Bioinformatic analysis and statistical evaluation of the data by Carolina Monzó. Graphical representation by Carolina Monzó.

Writing of the manuscript predominantly by Carolina Monzó and Lisonia Gkioni, with substantial contribution by Dario Valenzano, Sebastian Grönke and Linda Partridge.

Dietary restriction mitigates the age-associated decline in the mouse B cell receptor repertoire diversity

Authors:

Carolina Monzó[1,2]*, Lisonia Gkioni[1]*, Andreas Beyer[2], Dario Riccardo Valenzano[1], Sebastian Grönke[1] and Linda Partridge[1,3]

Affiliations:

1. Max Planck Institute for Biology of Ageing, Cologne, Germany

2. CECAD Research Centre, Cologne, Germany

3. Institute of Healthy Ageing, University College of London, United Kingdom

4.1. Introduction

4.1.1 Dietary interventions to delay ageing

Dietary restriction (DR) is the most effective environmental intervention to increase lifespan and late-life health in diverse animal species. DR ameliorates the effects of ageing in the nematode *Caenorhabditis elegans (C.elegans)*, the fruitfly *Drosophila melanogaster*, as well as rodents and non-human primates (Mattison et al. 2012; Colman et al. 2014; Fontana, Partridge, and Longo 2010; E. D. Smith et al. 2008; Chapman and Partridge 1996). DR is implemented as reduced nutrient intake without malnutrition and its benefits are not only limited to prolonged lifespan, but rather translate to an overall enhanced health status. In most organisms. DR delays the onset or slows progression of age-related pathologies, such as cardiovascular disease and dementia (Omodei and Fontana 2011; Colman et al. 2014; Mattison et al. 2012), neoplastic diseases (Ikeno et al. 2006) and dysregulated immune function (R. A. Miller 1996; Messaoudi et al. 2006; Shushimita et al. 2014). In humans, long-term DR can also exert substantial benefits, including prevention of diabetes and obesity and lower risk of developing cancer and cardiovascular disease (Fontana, Partridge, and Longo 2010; Fontana et al. 2004; Fontana and Klein 2007).

Despite the numerous benefits reported in model organisms and humans, extended periods of DR feeding have been accompanied by poor adherence in humans (Flatt and Partridge 2018; Redman et al. 2018; Tang et al. 2021). Therefore, less drastic dietary manipulations that recapitulate the full potential of DR but are not as hard to maintain are needed. The identification of DR effectors, which represent processes that contribute to the health benefits of DR, can be instrumental in designing effective dietary interventions to ameliorate ageing.

Extensive work in *Drosophila* and the mouse has revealed that specific macronutrients, rather than reduced calorie intake, are primarily responsible for the healthspan and lifespan benefits of DR (Solon-Biet et al. 2014; Grandison, Piper, and Partridge 2009). Accumulating evidence points towards a crucial role of the protein component of the diet in mediating these effects. In *Drosophila*, protein restriction extended lifespan, as opposed to carbohydrate or energy

restriction (Mair, Piper, and Partridge 2005), and a progressive reduction of protein-to-carbohydrate ratio in the mouse was associated with a corresponding increase in lifespan (Solon-Biet et al. 2014). Further, restriction of specific amino acids, such as methionine and tryptophan led to extended lifespan in flies and mice (Ables et al. 2014).

Besides dietary composition, the timing of food intake has been put forward as an important effector of DR (Fontana and Partridge 2015). Intermittent fasting (IF) has been shown to extend lifespan in *C. elegans* (Honjoh et al. 2009) and rodents (Mattson et al. 2014). Previous work has also indicated that IF has a protective effect against obesity and diabetes, the progression of neurodegenerative diseases and cancer (Mattson et al. 2014; Lee et al. 2012) and stem-cell exhaustion and impaired regeneration capacity (Cheng et al. 2014). Intriguingly, by controlling both the caloric intake and the timing of feeding, it was recently revealed that caloric restriction elicited a greater extension of mouse lifespan when feeding was restricted for at least 12 hours during the active phase of the mouse circadian cycle (Acosta-Rodríguez et al. 2022). In humans, a number of clinical trials have been investigating IF effects on metabolism, with promising findings against risk factors for obesity and cardiovascular disease (Harvie et al. 2011; Kroeger, Hoddy, and Varady 2014; Jakubowicz et al. 2013). Therefore, IF may be a powerful intervention to promote human health, and possibly longevity.

Overall, although DR is the most robust dietary intervention to extend healthy lifespan, its translational application in the context of human ageing is hindered by limited adherence. A thorough understanding of the complex interplay among DR, specific nutrient modifications, timing of food intake and other effectors involved in the benefits of DR in healthspan and lifespan is crucial. Therein lies the opportunity to develop efficient and sustainable interventions to promote healthy ageing.

4.1.2 The immune system as an effector of DR

One important effector, that needs to be carefully considered in the context of dietary anti-ageing interventions is the immune system. Disruptions in the capacity of the immune system to effectively clear pathogens and the reciprocal relationship of immunity with chronic inflammation and stem cell exhaustion contribute to the ageing process by altering intercellular communication and cellular senescence, two of the ageing hallmarks (López-Otín et al. 2013). In fact, targeting the ageing hallmarks can lead to alleviation of defective immune responses. One such example is restoring altered proteostasis via activation of autophagy, which was shown to enhance vaccination response in older individuals (Alsaleh et al. 2020). On the other hand, restoring defective immune responses themselves can be accompanied with healthspan and lifespan benefits. Of special interest is the modulation of the microbiome, which holds great promise to extend healthy lifespan (P. Smith et al. 2017; Bárcena et al. 2019; Parker et al. 2022) and is tightly linked to immunity. The microbiome controls the development, adaptation and maturation of the immune system and produces metabolites that elicit systemic effects, thereby interacting with the host (Sommer and Bäckhed 2013a; Schuijt et al. 2016; Kamada et al. 2013). In turn, the immune system reciprocates by controlling microbiome composition via a complex network of innate and adaptive immune responses (Sommer and Bäckhed 2013b). The indisputable links between immunity, senescence and inflammation, which are directly (inflammation) or indirectly (senescence) tied to the ageing hallmarks (Schmauck-Medina et al. 2022; López-Otín et al. 2013), further highlight the

importance of a thorough understanding of the effects of DR, a major anti-ageing intervention, on the immune system.

The adaptive immune system, which responds to antigen exposure by generating variable antibodies capable of identifying novel and known antigens, undergoes ageing-associated immune senescence. Immune senescence results in impaired protection against pathogens, and decreased vaccination efficiency, ultimately placing infectious diseases among the leading causes of morbidity and mortality in aged individuals (Wick et al. 2000a; Nikolich-Zugich 2005a; Ademokun, Wu, and Dunn-Walters 2010a). Next to age, the immune system is highly sensitive to diet-induced changes, including DR feeding. DR can partially attenuate or reverse some of the manifestations of age-associated immune senescence, exerting substantial improvements in T-cell-mediated responses and hematopoietic stem cell function (Messaoudi et al. 2006; White et al. 2016; Yan et al. 2021; Shushimita et al. 2014). However, whether DR has an impact on B-cell-mediated immune responses is currently unexplored.

Within the adaptive immune system, B-cell immune senescence with age does not manifest itself with a decline in B-cell abundance, but rather with a displacement of naïve B-cells by antigen-experienced (memory) B-cells, resulting in loss of B-cell receptor (BCR) repertoire diversity, and antigen-specificity (Oh, Lee, and Shin 2019a; Dunn-Walters 2016; Weiskopf, Weinberger, and Grubeck-Loebenstein 2009a; Dunn-Walters, Banerjee, and Mehr 2003; Wang et al. 2014; Hoehn et al. 2019). BCRs consist of two heavy chains (IgH), and two light chains (IgL). The heavy chains, which are sufficient to identify B cell clonal relationships (Zhou and Kleinstein 2019), have a variable domain encompassed by a combination of *IghV*, *IghD*, and *IghJ* genes, and a constant domain (*IghC*). After antigen identification by the variable domain, *IghC* regions undergo class-switch recombination, where *IghC* isotypes μ (IgM) and δ (IgD) are substituted by either γ, ε, or α heavy chains, giving rise to IgG, IgE and IgA isotypes with different effector functions, including opsonization and neutralisation of antigens (Schroeder and Cavacini 2010; Z. Xu et al. 2012). BCR sequencing can inform on the characteristics of the hypervariable loci responsible for antigen-identification and shed light on the different effector functions, by analysing the constant domains coding for immunoglobulin isotypes (Stavnezer, Guikema, and Schrader 2008; Turchaninova et al. 2016; Cook 2000). In fact, in humans, mice, and other model organisms, the age-dependent decline in BCR diversity, increased clonal expansions, impaired negative selection of autoreactive B cells and positive selection of high affinity B cells has been associated with poor health and frailty (V. Martin et al. 2015; Gibson et al. 2009; Booth and Toapanta 2021).

BCR diversity changes do not occur to the same extent in the major reservoirs of B cells. While a decline in the production of precursor B-cells mainly occurs in the mouse bone marrow, the mature B-cell population is maintained in the spleen (Frasca and Blomberg 2009). Nonetheless, exposure to an increasing amount of antigens with age leads to a compromised antigenic stimulation capacity and response to blood-borne antigens and pathogens in mice (Turner and Mabbott 2017; Ma et al. 2021). Similarly, ageing dramatically impairs the role of Peyer's patches; the well-defined lymphoid follicles in the small intestine that act as crucial portals through which antigens are sampled and tackled via specific mucosal immune responses (Donaldson, Shih, and Mabbott 2021). Although a comparable number of naïve B cells reach both the spleen and intestine (M. Banerjee et al. 2002b), profound tissue-specific differences in the BCRs are to be expected. These differences lie in the age-associated decline of B-cell selection processes, which occurs exclusively in the intestine (Dunn-Walters

2016) and on the rate of somatic hypermutation (SHM) (i.e. the process of diversification of B cell receptors by a high rate of point mutations on the immunoglobulin genes (McKean et al. 2008)). Regarding the latter, mucosal B-cells display a higher rate of mutations compared to those in the spleen, due to the much higher level of antigenic stimulation in the intestine (M. Banerjee et al. 2002b; Meng et al. 2017). Moreover, mouse SHM declines in splenic germinal centres with age (C. Miller and Kelsoe 1995; X. Yang, Stedra, and Cerny 1996), but increases in Peyer's patches germinal centres (Rogerson 2003; Lindner et al. 2012). Collectively, such intrinsic differences in immune responses require separate consideration of these tissues to grasp a complete picture of changes in BCR repertoire, and ultimately enhance immune function at old age.

DR initiation at older age is an attractive and viable option to enhance organismal function at old age, mainly due to the potential side effects of long-term DR feeding and limited adherence (Flatt and Partridge 2018; Redman et al. 2018; Tang et al. 2021). It has been previously shown that DR onset at 16 months of age was sufficient to recapitulate the lifespan extension seen with chronic DR in mice (Drews, 2021). However, initiating DR at 20-month-old mice did not extend lifespan (Drews, 2021). Several pathological parameters were improved in both groups, and it remains unclear what factors might explain the refractoriness of lifespan to DR initiated at 20 months.

In this study, we investigated whether DR delays age-related changes in the BCR that have been reported in mice, and whether it can do so when initiated later in life. We generated a BCR sequence dataset from ad libitum fed (AL) and DR mice, and from mice switched from AL to DR diet at 16 and 20 months of age. To assess systemic immune responses, we analysed the spleen, as the major secondary lymphoid organ. To evaluate the relationship between the host and the microbiome directly at mucosal organs, we analysed the ileum. We found that DR attenuated the age-associated decline of BCR repertoire diversity in the spleen. Further, the BCR profile of DR mice inversely correlated with morbidity, suggesting that BCR repertoire is associated with increased systemic health. The ileum BCR repertoire underwent only limited changes with age and DR treatment, mainly displaying a higher capacity for antigen binding under chronic DR. Mice subjected to DR at 16 months had spleen BCR diversity and clonal expansion rates indistinguishable from those under chronic DR, while mice switched to DR at 20 months of age showed BCR diversity and clonal expansion levels that remained in between the chronic AL and DR. These results suggested that these immunological traits may contribute to the response of lifespan to DR.

4.2. Results

To investigate how ageing and DR affect BCR repertoire, we sequenced the variable (*IghV, IghD, IghJ*) region of the BCR (Figure 4.1 A) of wild type, female C3B6F1 hybrid mice fed AL or DR (Figure 4.1 B). DR feeding was implemented by supplying 40% of the ad libitum (AL) food intake (Drews, 2021). To address whether any protection of the BCR repertoire can be achieved by DR implemented later in life, we included mice where DR was initiated at 16 (AL_DR16M) or 20 months of age (AL_DR20M) (Figure 4.1 B). Total RNA was isolated from the spleen and ileum to capture the systemic or gut-specific profiles, respectively, of five mice per treatment at 5, 20 and 24 months of age (Figure 4.1 B). Since sequencing protocols do not preserve Heavy:Light chain pairing, we limited our analysis to BCR-heavy chains, as they are sufficient to identify clonal relationships with high confidence (Zhou and Kleinstein 2019). BCR clones from the same naïve B cell ancestor were defined by sequences sharing the same *IghV* and *IghJ* gene, and having the same CDR3 length (Khan et al. 2016; Greiff et al. 2017; Koohy et al. 2018). BCR isotypes were identified by a template-switch adapter in the 5' of the *IghV* variable domain, and isotype-specific primers binding to the *IghC* effector domain (Figure 4.1 A) (Turchaninova et al. 2016).

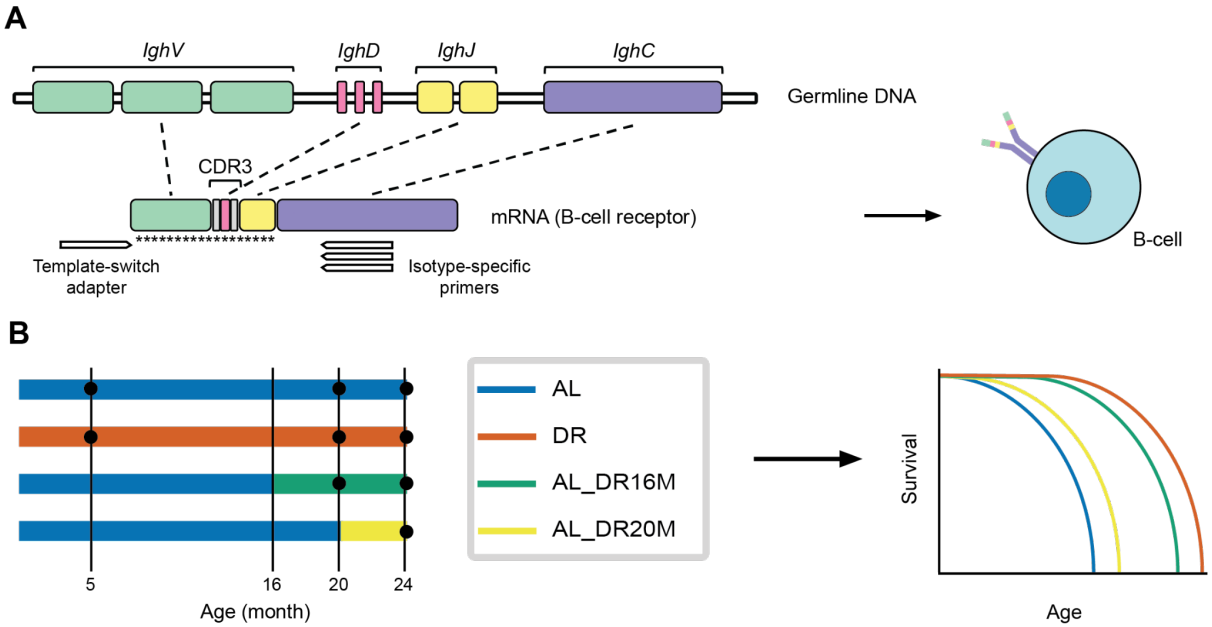

Figure 4.1: Study design. (A) Schematic of IgH heavy chain gene arrangement of B-cell receptors and location of BCR isotype-specific primers. Asterisks indicate the region modified by somatic hypermutations. **(B)** Scheme for DR switch and measurement of lifespans, adapted from (Drews, 2021). Black circles indicate time points when spleen and ileum samples were taken (n= 5 mice per treatment).

4.2.1 DR slows the age-associated decline of BCR repertoire diversity in the spleen

We first analysed data from the spleen. Abundances of BCR isotypes were quantified, and the majority of BCRs corresponded to IgM (~61%), a few to IgG (~23%), fewer to IgA (~13%), and yet fewer to IgD and IgE (~3%) (Figure 4.2 A) (Le Gallou et al. 2018). No age-dependent differences in relative abundances of IgM, IgA and IgE were detected in AL mice, but there

was a significant decline in IgD abundance with age (Figure 4.2 A), in line with previous studies in elderly humans (Colonna-Romano et al. 2006). Although the function of IgD is largely unknown, it may be involved in immune self-tolerance (Gutzeit, Chen, and Cerutti 2018; Nguyen 2022), and its decline with age may be associated with increased auto-reactivity. IgD abundance was higher in DR than in AL mice at 5 months and also declined with age, although it remained higher than in AL mice and declined at a slower rate (Figure 4.2 A). Therefore, DR not only ameliorated the age-related decline in IgD abundance, but also maintained higher levels of IgD throughout life compared to AL animals, indicating a tighter regulation of immune tolerance under DR.

High BCR within-individual diversity is associated with improved antigen recognition capacity and vaccination response (Dunn-Walters 2016; Ademokun et al. 2011a; de Bourcy et al. 2017). Thus, we hypothesised that DR mice would have higher BCR diversity. To measure this, we calculated Hill diversity spectra (Miho et al. 2018; Hill 1973). Clonal richness, i.e. the total number of different BCR clones, was stable in AL mice up to the age of 20 months, and then rapidly declined by 24 months of age (Figure 4.2 B). Unexpectedly, DR mice underwent a progressive decline in clonal richness with age (Figure 4.2 B), displaying significantly lower richness of B cell clones than AL mice at 20 months of age (Figure 4.2 B). However, analysis of the clonal richness of each isotype identified a significantly higher richness of IgE in DR mice at 24 months of age (Supplementary Figure 4.1 A). Therefore, contrary to our hypothesis, DR mice were generally characterised by lower within-mouse richness BCR diversity.

The diversity of the BCR repertoire is not only defined by the number (richness) of clones, but also the relative frequency of the subdivisions of the clonal population. We therefore determined whether DR mice had higher antigen-recognition capacity at old age as reflected by evenness in the size of each B cell clone (i.e. the subdivisions of the clonal population are evenly sized). To assess both clonal richness and population structure, we evaluated Shannon and Simpson diversity metrics. Shannon diversity is a measure of both clonal richness and population structure, mostly affected by rare clones, while Simpson diversity measures the distribution of the clonal population structure, mostly affected by large clones. AL mice displayed an age-related decline in both Shannon and Simpson indices (Figure 4.2 C and 4.2 D), mainly due to a decline in IgM, IgG and IgE isotypes (Supplementary Figure 4.1 B-C). The rare B cell clones of AL mice thus became less abundant with age, and the clonal population structure less uniform. DR mice also experienced an age-dependent decline in Shannon diversity, but to a lesser extent than AL mice (Figure 4.2 C). Thus, at 24 months of age, DR mice had higher Shannon diversity than AL mice (Figure 4.2 C), suggesting that DR slows the age-related change in the clonal population structure. In contrast to AL mice, Simpson diversity in DR mice was maintained until 20 months of age, with a rapid decline only at 24 months (Figure 4.2 D). Therefore, the strongest changes in clonal population structure of DR mice occurred between 20 and 24 months. Similarly, the most striking differences in diversity between AL and DR mice also appeared between 20 and 24 months of age, with DR retaining a more uniform clonal population structure, as indicated by the Shannon diversity. DR mice exhibited a significantly reduced Shannon and Simpson diversity with age in IgM (Supplementary Figure 4.1 B-C), and a less profound loss of IgG Shannon and Simpson diversity with age (Supplementary Figure 4.1 B-C). The ageing BCR repertoire thus showed loss of rare clones, and DR attenuated this change by maintaining a more uniform distribution of large clones. Thus, by maintaining a uniform B cell clonal population structure, DR mice

might exhibit a higher antigen-recognition capacity and possibly an enhanced vaccination response at old age (Okawa, Nagai, and Hase 2020).

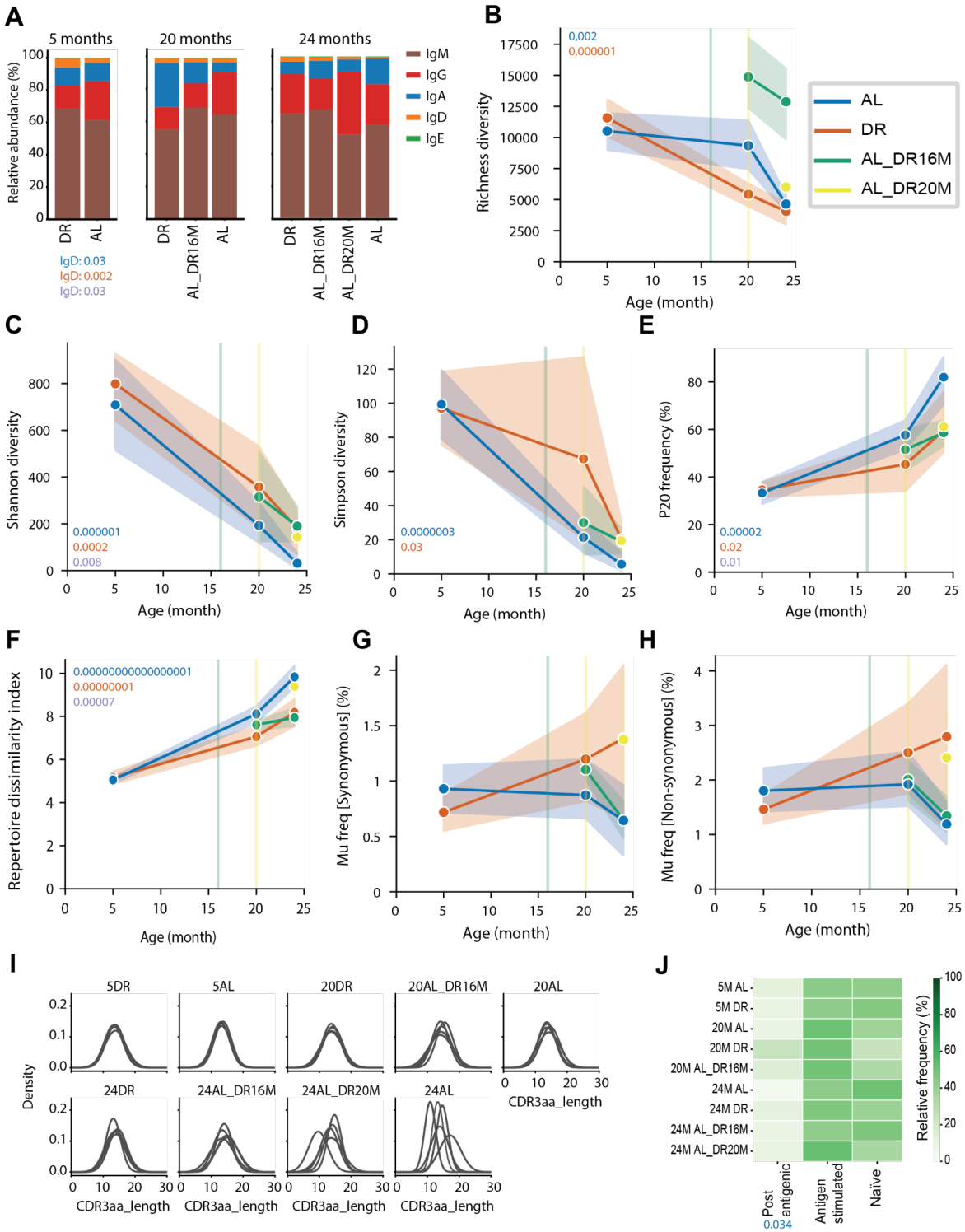

Figure 4.2. DR slows the age-associated decline of BCR repertoire in the spleen. (A) Relative abundance of antibody isotypes in the spleen. Significant differences at 5 months of age (Mann-Whitney U test): IgD (p-value AL vs DR = 0.036). Significant differences at 24 months of age (Mann-Whitney U test): IgD (p-value AL_DR16M vs AL = 0.036). **(B)** Richness within-individual diversity. Significant differences at 20 months of age (Mann-Whithey U test): DR vs AL p-value = 0.001. Significant differences at 24 months of age (Mann-Whitney U test): AL_DR16M vs AL p-value = 0.0003. **(C)**

Shannon within-individual diversity. Significant differences at 24 months of age (Mann-Whitney U test): DR vs AL p-value = 0.004; AL_DR16M vs AL p-value = 0.008. **(D)** Simpson within-individual diversity. Significant differences between 20 and 24 months of age (Mann-Whitney U test): DR p-value = 0.036. **(E)** Clonal expansion. Significant differences at 24 months of age (Mann-Whitney U test): AL_DR16M vs AL p-value = 0.002. Significant differences between 20 and 24 months of age (Mann-Whitney U test): DR p-value = 0.036. **(F)** Inter-individual dissimilarity. Significant differences at 24 months of age (Mann-Whitney U test): DR vs AL p-value = 0.002, AL vs AL_DR16M p-value = 2.0×10^{-4}, DR vs AL_DR20M p-value = 0.033, and AL_DR16M vs AL_DR20M p-value = 0.005. **(G)** Frequency of synonymous SHM. **(H)** Frequency of non-synonymous SHM. **(I)** Gaussian-fitted CDR3 length distribution per mouse in study. Significant differences in proportion of different CDR3 length distributions at 24 months of age (Fisher's test): DR vs AL p-value = 0.048; AL_DR16M vs AL p-value = 0.011. **(B-H)** Lines correspond to mean, and shaded areas to 95% confidence intervals. **(J)** Relative amounts of clones according to their class-switch status. Significant p-values for linear regression of AL age in blue and of DR age in red. Significant p-values for 2-way ANOVA of AL and DR throughout age in purple.

4.2.2 DR attenuates clonal expansions with age in the spleen

To determine whether the age-dependent decrease in within-individual antibody diversity was due to a B cell population skewed towards clonally expanded cells, we calculated clonal expansion as the percentage of the BCR repertoire taken up by the 20 most common clones (P20) (Figure 4.2 E). In line with previous work (Gibson et al. 2009; Oh, Lee, and Shin 2019a), clonal expansions increased progressively with age in AL mice (Figure 4.2 E). This expansion was most evident in the primary and long-term antigen response isotypes IgM and IgG (Supplementary Figure 4.1 D), suggesting a possible attenuation of memory immune response (Schroeder and Cavacini 2010). Clonal expansions also increased with age in DR mice (Figure 4.2 E), but to a significantly lesser extent than in AL animals (Figure 4.2 E). At 24 months of age, only ~60% of the total clonal population was occupied by expanded clones in DR mice, while in AL mice it reached ~80% (Figure 4.2 E). Further, DR mice maintained a stable rate of clonal expansions in IgM and IgG, only increasing at 24 months of age in IgM (Supplementary Figure 4.1 D). The age-dependent decrease in within-individual diversity was thus associated with a B cell population skewed towards clonally expanded B cells, an effect that was attenuated by DR.

Differences in clonal composition of B cells between individuals are accentuated by the proliferation of different clones in different individuals (Gibson et al. 2009; Weksler and Szabo 2000; Oh, Lee, and Shin 2019b; de Bourcy et al. 2017). We therefore hypothesised that there would be higher inter-individual dissimilarity at old than at young age. To quantify dissimilarity, we used the repertoire dissimilarity index (RDI) (Bolen et al. 2017), which calculates differences in *IghV*, *IghD* and *IghJ* gene usage and performs pairwise comparisons between BCR repertoires. Consistent with previous reports in mice and humans (de Bourcy et al. 2017; Gibson et al. 2009; Oh, Lee, and Shin 2019b), there was a progressive increase in RDI with age in AL mice (Figure 4.2 F). A lesser ageing-associated increase in inter-individual dissimilarity also occurred in DR mice (Figure 4.2 F). Isotype-specific analysis revealed that RDI increased with age in all isotypes in AL mice (Supplementary Figure 4.1 E) and in DR mice except for IgA (Figure 4.1 E). However, the slope of increasing RDI was significantly reduced under DR in all isotypes except IgE (Supplementary Figure 4.1 E).

IghV and *IghJ* gene usage are largely implicated in the ability of the BCR to bind to antigens, thereby affecting susceptibility to various diseases (Raposo et al. 2014). To determine whether the enhanced antigen recognition capacity of DR mice is further facilitated by selection of different *IghV* or *IghJ* genes than AL, we evaluated IghV and IghJ usage.. In concordance with previous studies (Muggen et al. 2019; Y.-C. Wu et al. 2010; V. Martin et al. 2015), the most commonly used *IghV* gene in AL mice was *IghV1* (Supplementary Figure 4.2 A). In humans, use of the *IghV1* gene family is reduced with age (Ghraichy et al. 2021), and AL mice also showed an age-related decline in the usage of *IghV1*, *IghV3*, *IghV4, IghV7*, and *IghV11* (Supplementary Figure 4.2 A).(Ghraichy et al. 2021) *IghV1* was the most commonly used *IghV* gene in DR mice, which showed a decline in usage of *IghV4*, *IghV6*, *IghV7* and *IghV11* with age (Supplementary Figure 4.2 A). However, DR treatment led to a significant increase in the usage of *IghV3*, and *IghV15* compared to AL (Supplementary Figure 4.2 A). There were no differences between AL and DR mice in *IghJ* gene usage (Supplementary Figure 4.2 B). DR thus led to changes in *IghV* gene usage that may have contributed to the age-related differences in clonal diversity between AL and DR spleen B cells.

4.2.3 DR maintains the somatic hypermutation rate and CDR3 length distribution at old age in the spleen

Clonal diversity is important for efficient antigen recognition (Dunn-Walters 2015), and we next determined whether antigen recognition capacity is affected by ageing and DR. We evaluated the somatic hypermutation (SMH) rate, which is the mechanism for affinity maturation of the BCR repertoire in response to antigen exposure, leading to clonal diversity (Dunn-Walters 2016; Schroeder and Cavacini 2010). The rate of synonymous substitutions indicates neutral evolution, providing a baseline for the nucleotide alteration capacity of the BCR sequence. Non-synonymous substitutions, on the other hand, accumulate during affinity maturation and become fixed under positive selection (Nielsen and Yang 1998). We quantified the frequency of synonymous and non-synonymous mutations in the BCR repertoire. Consistent with previous work (Dunn-Walters 2015), we did not detect any differences in synonymous or non-synonymous SHM rate with age in AL mice (Figure 4.2 G-H). Similarly, as previously reported (Hoehn et al. 2019), we did not find age-associated differences for the relative rate of amino acid changing substitutions versus synonymous substitutions or dN/dS ratio (Nielsen and Yang 1998) (Supplementary Figure 4.2 C). We found large dN/dS ratio values (>1), indicating strong positive selection, across all time points in the splenic BCR repertoire of all groups (Supplementary Figure 4.2 C). In contrast, after examining synonymous and non-synonymous SHM rates for each individual isotype, we uncovered an age-associated reduction in IgM synonymous SHM frequency in AL mice (Supplementary Figure 4.1 F), an age-associated increase in IgG synonymous SHM frequency in both AL and DR mice (Supplementary Figure 4.1 F), and an age-associated increase in IgA synonymous and non-synonymous SHMs in DR mice (Supplementary Figure 4.1 F-G). Only the synonymous and non-synonymous SHM rate in IgA was significantly different between AL and DR through age (Supplementary Figure 4.1 F-G), indicating that DR increases the affinity maturation of the IgA repertoire. Taken together, our results point towards a more stable and efficient SHM mechanism under DR treatment, indicating maintained antigen-recognition capacity; where IgM, IgG and IgA isotypes associated with primary and secondary B cell response are predominantly affected.

Class-switch recombination is the mechanism of diversification by which variable regions of heavy chains are juxtaposed to different constant chains, in order to generate different isotypes and confer different effector functions (Schroeder and Cavacini 2010; Booth and Toapanta 2021). To evaluate the effect of DR on class-switch recombination, clones with only IgM+IgD+SHM- segments were classified as naïve, IgM+IgD+SHM+ as antigen-stimulated, and those with IgM-IgD- where all isotypes had been class-switched, as post-antigenic (Wang et al. 2014). Very few post-antigenic BCR clones were found throughout age (Figure 4.2 J), which is not surprising given that the spleen is a secondary lymphoid organ, and the mice are not expected to have substantial encounters with potentially challenging/pathogenic antigens based on their housing conditions. The majority of the B cell population consisted of naïve and antigen-stimulated BCR clones (Figure 4.2 J). There was a significant loss in the post-antigenic BCR pool in AL mice with age (Figure 4.2 J). Conversely, DR mice displayed no differences in naïve, antigen-exposed or post-antigenic clones with age or compared to AL (Figure 4.2 J). Thus, these results suggest that ageing might impair the class-switch recombination capacity, while DR did not influence this process.

4.2.4 Midlife onset of DR has more positive effects on the BCR repertoire of the spleen than late-life onset DR

Previous work has shown that DR onset at 16 months of age (AL_DR16M) leads to a lifespan extension similar to the one observed under a chronic DR diet (Drews, 2021, Figure 4.1 B). In contrast, initiating DR at 20 months of age (AL_DR20M) did not lead to lifespan extension, indicating that the critical period of responsiveness to DR treatment lies between 16 and 20 months of age in mice (Drews, 2021, Figure 4.1 B). To address whether switching to DR later in life is sufficient to “rejuvenate” the BCR repertoire and recapitulate the immunological characteristics we observed under chronic DR, the midlife (AL_DR16M) and late-onset (AL_DR20M) DR groups were evaluated (Figure 4.1 B). To explore whether there are potential functionality alterations between BCR isotypes in AL_DR16M and AL_DR20M groups in comparison to chronic AL and DR groups, we evaluated relative abundances of antibody isotypes. IgD abundance in AL_DR16M was significantly higher compared to AL at 24 months of age, recapitulating the DR-specific levels of IgD abundance (Figure 4.2 A). In contrast, AL_DR20M mice remained unresponsive to the introduction of the new diet (Figure 4.2 A). Therefore, switching to DR as late as 16 months recapitulates the DR-specific igD abundance and the associated improved regulation of self-tolerance (Gutzeit, Chen, and Cerutti 2018; Nguyen 2022).

Next, we investigated whether DR onset at 16 or 20 months of age affected the BCR within-individual diversity. We computed Hill diversity spectra and identified a significantly higher richness and Shannon diversity in AL_DR16M compared to AL in 24-month-old mice (Figure 4.2 B-C). In other words, the AL_DR16M group had comparable diversity levels to DR, exhibiting a less dramatic loss in repertoire diversity in old age compared to AL (Figure 4.2 C). Conversely, the diversity of the AL_DR20M group remained in-between AL and DR; not mimicking the DR diversity profile with age (Figure 4.2 C). We then asked whether isotype-specific analysis might underpin the contributors to the effects on diversity in diet-switched mice. IgM and IgE isotypes displayed a profound increase in richness in AL_DR16M when compared to DR at 20 months of age, after the start of the new diet (Supplementary Figure 4.1 A). Similarly, IgD Shannon diversity was significantly higher in AL_DR16M compared to

DR in 20-month-old mice (Supplementary Figure 4.1 B). In addition, at 24 months of age, IgM and IgE Shannon and Simpson diversity, and only Simpson diversity in IgA, were elevated in AL_DR16M when compared to AL, pointing towards an acute primary response (Supplementary Figure 4.1 B-C). At 24 months, AL_DR20M mice also displayed a spike in IgE Shannon diversity in response to the diet change, leading to significantly higher IgE Shannon diversity levels compared to AL mice (Supplementary Figure 4.1 B). In contrast, IgG Shannon and Simpson diversity were significantly lower in AL_DR20M compared to DR mice, which was consistent with IgG diversity under AL (Supplementary Figure 4.1 B-C). Therefore, DR onset at 16 and 20 months of age affects the BCR within-individual diversity. Although starting DR at 20 months of age did not fully recapitulate the "younger-like" DR diversity, AL_DR16M mice recapitulated the DR diversity of primary (IgM) and hypersensibility (IgE) isotypes.

The relative frequency of expanded clones within the antibody repertoire increases with age (Gibson et al. 2009; Oh, Lee, and Shin 2019a). Our findings support this result and revealed that DR reduced the age-dependent clonal expansion rate compared to AL mice (Figure 4.2 E). Therefore, we next examined whether DR onset at 16 or 20 months of age can reduce the BCR repertoire clonal expansions in old age. Consistent with the findings in DR, there was lower clonal expansion in AL_DR16M compared to AL at 24 months of age (Figure 4.2 E). However, AL_DR20M mice remained in-between the AL and DR levels (Figure 4.2 E). Thus, DR onset at 16 months of age can reduce the portion of the BCR population occupied by expanded clones.

RDI increased with age at a slower rate in DR compared to AL (Figure 4.2 F). Thus, we evaluated whether AL_DR16M mice or AL_DR20M have lower RDI compared to AL. There was a clear separation in two groups: AL and AL_DR20M mice had significantly higher inter-individual dissimilarity than DR and AL_DR16M (Figure 4.2 F). This recapitulation of the lower repertoire divergence in DR by AL_DR16M, was already present 4 months after the start of DR, at 20 months of age (Figure 4.2 F). Moreover, AL_DR16M mice experienced a reduction in IgE RDI when compared to AL and DR at 20 months of age (Supplementary Figure 4.1 E), which stabilised to comparable levels with AL and DR 4 months later. At 24 months, RDI of IgA and IgM was lower in AL_DR16M than in AL and DR (Supplementary Figure 4.1 E). Similarly, 24-month-old AL_DR20M mice had reduced IgA and IgM RDI compared to AL (Supplementary Figure 4.1 E). Therefore, the effects of DR onset on the repertoire RDI highlighted an initial loss in inter-individual dissimilarity, mainly affecting AL_DR16M mice, consistent with the spike in diversity of IgE, IgA and IgM.

DR affected the different diversification and affinity maturation steps of the BCR development (Figure 4.2 E-F, Figure 4.2 I, Supplementary Figure 4.2 A). Thus, we evaluated repertoire characteristics of AL_DR16M and AL_DR20M mice. *IghV* and *IghJ* gene usage in AL_DR16M mice was comparable to DR (Supplementary Figure 4.2 A and 4.2 B). In line with the findings in DR mice, there were no changes in SHM or class-switch recombination in AL_DR16M or AL_DR20M mice (Figure 4.2 G, 4.2 H and 4.2 J). At 24 months of age, AL_DR16M but not AL_DR20M mice underwent a DR-like reduction in the proportion of different CDR3-length-distributions, which was significantly different from AL (Figure 4.2 I). However, the age-dependent skewing of IgA CDR3-length-distribution observed in AL mice was reduced in AL_DR20M mice (Supplementary Figure 4.1 H). On the whole, starting DR as late as 16 months of age reverted the general shift in the CDR3-length-distribution observed during ageing.

In summary, similar to the lifespan reports (Drews, 2021) (Figure 4.1 B), DR initiation as late as 16 months of age recapitulated the main effects of chronic DR on the BCR dynamics: within-individual diversity, inter-individual dissimilarity, and clonal expansion rate. More specifically, AL_DR16M displayed a profound acute response to DR initiation, generating a spike in IgM and IgE richness, and IgD Shannon diversity at 20-months. While AL_DR16M recapitulated DR-like levels by 24-months of age, the AL_DR20M group exhibited only a partial response, increasing IgE Shannon diversity and reducing the age-dependent skewing of the IgA CDR3-length-distribution.

4.2.5 Effects of DR and ageing on the intestinal BCR repertoire

DR modulates the composition of the gut microbiome in mice and humans (von Schwartzenberg et al. 2021; C. Zhang et al. 2013). As mucosal B-cells in the gut are in direct contact with the gut microbiome (Belkaid and Hand 2014a; Lindner et al. 2015a, 2012; Macpherson et al. 2018a), we asked whether DR-induced changes in the microbiome also affect the gut mucosal BCR repertoire. Within the small intestine, the highest accumulation of B-cells is found in the Peyer's patches in the ileum (Donaldson, Shih, and Mabbott 2021). Thus, we measured BCR repertoire dynamics in the ileum dependent on age and DR. Consistent with previous studies (Macpherson et al. 2018b; Lindner et al. 2012, [b] 2015), IgA was the predominant isotype in the ileum, accounting for up to 98% of all Ig isotypes in young animals (Figure 4.3 A). IgM, IgG, IgD, and IgE only accounted for 0.39, 0.33, 0.16 and 0.17% in young mice, respectively (Figure 4.3 A). In 20-month-old AL mice, the relative frequencies of IgM and IgG were significantly increased compared to 5-month-old mice, while there was a reduction in IgA (Figure 4.3 A). Therefore, in line with previous reports (Macpherson et al. 2018b), we observed an increase in IgM and IgG isotypes at the expense of IgA in old age, which could be important for maintaining homeostasis with the intestinal microbiome.

Next, we investigated whether ageing or DR affected the BCR within-individual diversity. Hill diversity spectra analysis of the BCR repertoire revealed an increased richness in DR mice compared to AL at 20 months of age, which was significantly lower than AL in 24-month-old mice (Figure 4.3 B). In addition, we detected a significantly higher richness of IgG in DR compared to AL in 24-month-old mice (Supplementary Figure 4.3 A). However, Shannon or Simpson diversity were not affected (Figure 4.3 C-D, Sup Figure 4.3 B-C). Similarly, the degree of clonal expansion was not significantly changed by age or DR diet (Figure 4.3 E, Supplementary Figure 4.3 D). Thus, although we did not observe strong ageing-associated effects on BCR within-individual diversity in the ileum (Figure 4.3 B-D), DR mildly increased the diversity of IgG small rare clones (Figure 4.3 B). Even in an IgA-dominated organ, IgG has been indirectly implicated in mucosal inflammation and commensal regulation (Castro-Dopico and Clatworthy 2019). Therefore, an increased IgG diversity could have implications for enhanced protection against enteropathogens and intestinal inflammation under DR.

To study the effect of age and evaluate whether DR generates a less dissimilar BCR repertoire between individuals, we studied differences in the ileum clonal composition using the RDI. RDI was rather stable with age in both AL and DR mice (Figure 4.3 F). However, in IgM, RDI showed a significant age-associated decline in AL, that was ameliorated in DR

(Supplementary Figure 4.3 E). In addition, RDI of IgD and IgG increased with age in AL mice but decreased in DR mice (Supplementary Figure 4.3 E). DR ameliorated the ageing-associated increase in inter-individual dissimilarity of the IgD and IgG repertoires with age (Supplementary Figure 4.3 E). Therefore, DR generates a more diverse and less dissimilar BCR repertoire between individuals, with higher chance to bind to known and novel antigens.

Previous studies have shown an age-associated decline in B cell selection processes in the gut, paired with declining SHM rate (McKean et al. 2008; Dunn-Walters 2015). We evaluated whether DR has an effect on class-switch recombination and SHM. As previously reported in humans (M. Banerjee et al. 2002a), 2002), the young gut BCR consisted primarily of post-antigenic clones (~73%), some antigen-stimulated clones (~25%) and very few naïve ones (~2%) (Figure 4.3 J). There were no differences in the proportions of BCR clones in each class-switch recombination stage with age or under DR (Figure 4.3 J). Consistent with previous work (Lindner et al. 2015a), the ratio between dN/dS was positive (>1) at all time points indicating positive selection through age (Supplementary Figure 4.4 C). In contrast, DR mice had significantly higher non-synonymous SHM compared to AL at 24 months of age (Figure 4.3 H). Further, we found an age-associated decline in synonymous and non-synonymous SHM in IgM (Supplementary Figure 4.3 F-G). In addition, IgA non-synonymous SHM declined with age in AL (Supplementary Figure 4.3 G), and synonymous IgA SHM increased with age in DR mice (Supplementary Figure 4.3 F). Finally, CDR3 length and variability were also not affected by age or DR (Figure 4.3 I, Supplementary Figure 4.3 H). Taken together, DR diversifies the ileal BCR repertoire and increases its affinity maturation by means of SHM of IgM and IgA isotypes.

In summary, age and DR have only minor effects on BCR composition in the ileum. However, SHM rates declined with age in AL mice, and this decline was mitigated by DR. As a peripheral organ, the ileum has more direct exposure to microbial antigens, which induce antibody maturation via SHM and class-switch recombination (Q. Zhao and Elson 2018). Our data imply that DR improves antibody maturation in the ileum through an increased SHM at old age.

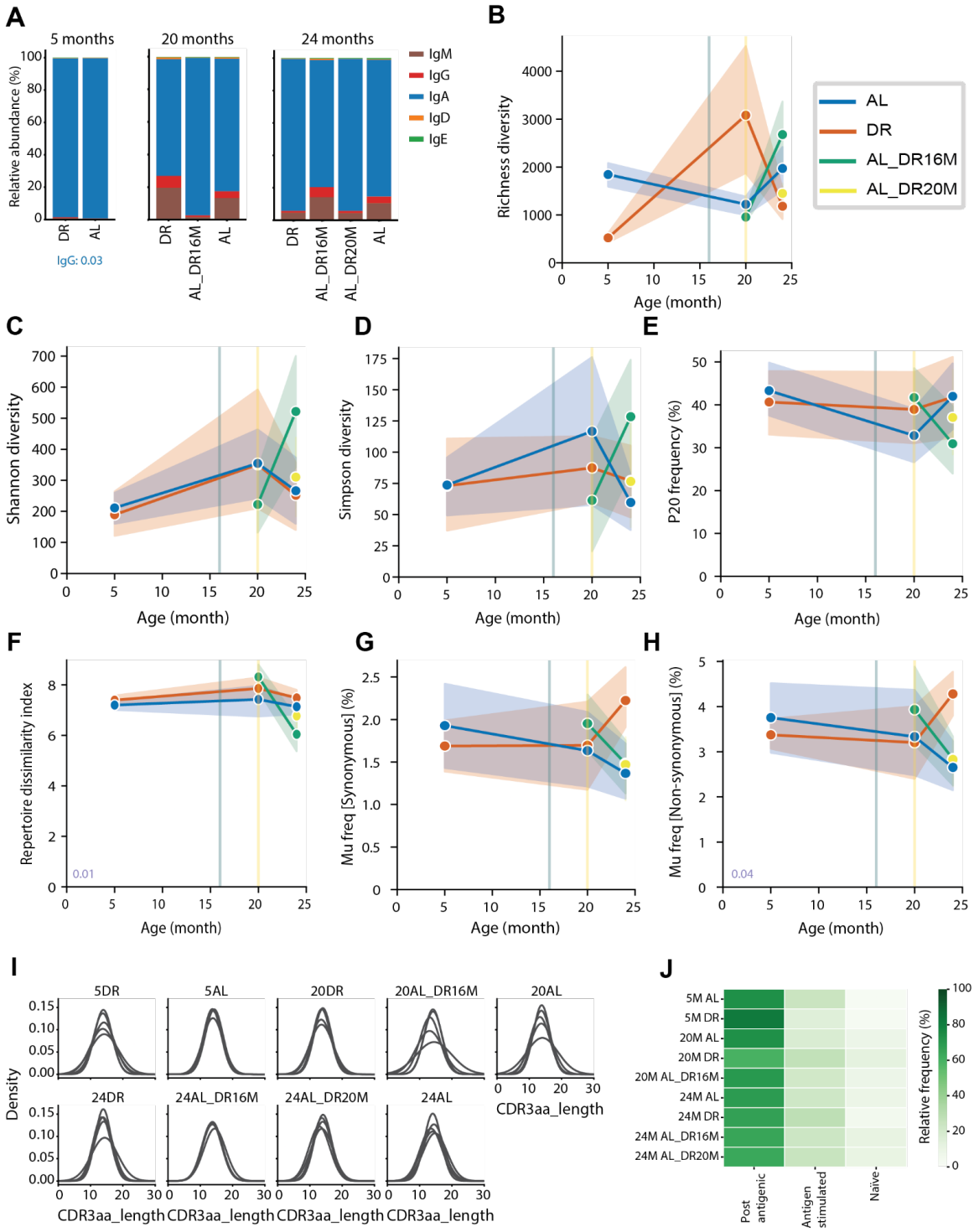

Figure 4.3: DR and ageing have only small effects on the intestinal BCR repertoire. (A) Relative abundance of antibody isotypes in the ileum. Significant differences between 5 and 20 months of age (Mann-Whitney U test): IgM (p-value AL = 0.036), IgG (p-value AL = 0.036), IgA (p-value AL = 0.024). **(B)** Richness within-individual diversity. Significant differences at 20 months of age (Mann-Whitney U test): DR vs AL p-value = 0.002; AL_DR16M vs DR p-value = 7.3×10^{-5}. Significant differences at 24 months of age (Mann-Whitney U test): DR vs AL p-value = 0.01; AL_DR16M vs DR p-value = 0.008. **(C)** Shannon within-individual diversity. **(D)** Simpson within-individual diversity. **(E)** Clonal expansion. **(F)** Inter-individual dissimilarity. Significant differences at 20 months of age (Mann-Whitney U test): AL_DR16M vs AL p-value = 0.04; AL_DR16M vs DR p-value = 0.009. **(G)** Frequency of synonymous SHM. **(H)** Frequency of non-synonymous SHM. Significant differences at 24 months of age (Mann-

Whitney U test): DR vs AL p-value = 0.043; AL_DR16M vs DR p-value = 0.043; AL_DR20M vs DR p-value = 0.043. **(I)** Gaussian-fitted CDR3 length distribution per mouse in study. **(B-H)** Lines correspond to mean, and shaded areas to 95% confidence intervals. **(J)** Relative amounts of clones according to their class-switch status. Significant p-values for linear regression of AL age in blue and significant p-values for 2-way ANOVA of AL and DR throughout age in purple.

4.2.6 Late-onset DR has no effect on the intestinal BCR repertoire

To address whether the ileum BCR repertoire in the AL_DR16M and AL_DR20M groups recapitulates the slightly improved BCR diversification under chronic DR, we first evaluated the relative abundances of immunoglobulin isotypes. No differences in isotype abundances were detected in AL_DR16M or AL_DR20M (Figure 4.3 A). By calculating Hill diversity spectra, we found a significantly lower richness in AL_DR16M and AL compared to DR in 20-month-old mice (Figure 4.3 B). However, at 24 months of age, AL_DR16M and AL mice exhibited a significantly higher richness than DR (Figure 4.3 B), suggesting that the presence of rare clones remained unaffected in AL_DR16M mice. On the other hand, AL_DR20M mice represented an in-between state, with no distinction from either AL or DR (Figure 4.3 B). Thus, we did not observe a recapitulation of the DR-like diversification in mice switched to DR late in life. However, we detected an acute response to DR initiation in AL_DR16M through an elevated total number of distinct BCR clones.

We next questioned whether this acute increase in the AL_DR16M diversity translated into other characteristics of the ileal BCR repertoire. No changes in clonal expansion were observed as a response to late DR onset (Figure 4.3 E). However, RDI was significantly higher in AL_DR16M 20-month-old mice when compared to AL (Figure 4.3 F). Yet, at 24 months of age, AL_DR16M mice had significantly lower dissimilarity than DR mice (Figure 4.3 F), indicating a strong loss of inter-individual dissimilarity in AL_DR16M mice. We found an acute spike in inter-individual dissimilarity of AL_DR16M at 20 months of age in IgA, IgD and IgG, when compared to AL and DR (Supplementary Figure 4.3 E). We further detected a significantly lower IgA, IgM and IgE RDI in AL_DR16M at 24 months compared to AL and DR (Supplementary Figure 4.3 E). These changes in AL_DR16M suggest that the gut BCR repertoire is somewhat responsive to DR initiation at 16 months of age. On the other hand, the IgM RDI of AL_DR20M mice was lower than AL (Supplementary Figure 4.3 E). RDI of AL_DR20M was lower in IgA, and higher in IgG than both AL and DR (Supplementary Figure 4.3 E). Thus, the isotype inter-individual dissimilarity as a response to the introduction of DR diet was highly dependent on the age of DR onset.

To examine whether DR initiation at 16 and 20 months of age recaptured the SHM rate preservation under chronic DR treatment, we evaluated SHM rates in AL_DR16M and AL_DR20M mice. Surprisingly, non-synonymous SHM in 24-month-old mice was significantly lower in AL_DR16M, AL_DR20M and AL compared to DR (Figure 4.3 G and 4.3 H). This was consistent with SHM findings in IgA (Supplementary Figure 4.3 G), indicating that late-onset of DR did not impact affinity maturation. Finally, CDR3-length-distribution variability of IgD at 20 months was higher in AL_DR16M and AL compared to DR (Supplementary Figure 4.3 H), and significantly decreased in AL_DR16M when compared to both AL and DR at 24 months in IgM (Supplementary Figure 4.3 H).

Taken together, AL_DR16M and AL_DR20M did not recapitulate the DR-like BCR dissimilarity, or SHM rate in the ileum. This refractoriness of response to DR initiation was in line with previous studies in mice and killifish, where diet changes or antibiotics exposure had a minor impact on the gut BCR repertoire (Lindner et al. 2015c; Bradshaw et al. 2022). AL_DR16M and AL_DR20M mice manifested little to no effect on the ileum BCR repertoire; they maintained a repertoire similar to chronic AL, even after dietary switch.

4.2.7 The ageing microbiome responds to late-onset DR

Previous work has shown that the gut microbiome undergoes significant changes with age (Badal et al. 2020) (Monzó, 2022), primarily reflected in a marked age-dependent decline in within-individual diversity. This decline is accompanied by loss of beneficial bacteria and extensive occupation by commensal and pathogenic bacteria (Nagpal et al. 2018; van der Lugt et al. 2018). Caloric restriction maintains a high abundance of bacteria considered to be beneficial for colonic health (Kok et al. 2018). Having observed mild differences between AL and DR in the ageing ileum BCR repertoire, we questioned whether the microbiome composition was as stable as the ileum BCR repertoire, given the direct contact between ileum and microbiome (Belkaid and Hand 2014b; Lindner et al. 2015b, 2012; Macpherson et al. 2018a). To address this question, we performed V4-16S rRNA amplicon sequencing of caecal contents. Consistent with our findings in the ileum BCR repertoire (Figure 4.3 B-D), we found no difference in microbial within-individual diversity with age or between AL and DR. In contrast, inter-individual dissimilarity in the microbiome, measured using the Unweighted UniFraq diversity index, was significantly higher in AL when compared to DR at 20 and 24 months of age (Figure 4.4).

Given that the microbiome inter-individual dissimilarity increased with age to a larger extent in AL than in DR mice, we next asked whether the caecal microbiome would respond to DR switch at 16 and 20 months of age by converging towards a DR-like microbiome. As opposed to the mild response of the gut BCR repertoire in AL_DR16M and AL_DR20M (Figure 4.3), the gut microbiome of AL_DR16M diverged from the microbiome of AL mice already at 20 months of age (Figure 4.4). These differences persisted up to 24 months, where the inter-individual variability of AL_DR16M and AL_DR20M mice was significantly different from AL (Figure 4.4). Therefore, contrary to the ileum BCR repertoire, the caecal microbiome rapidly responded to the switch from AL to DR, even when initiated at 20 months of age.

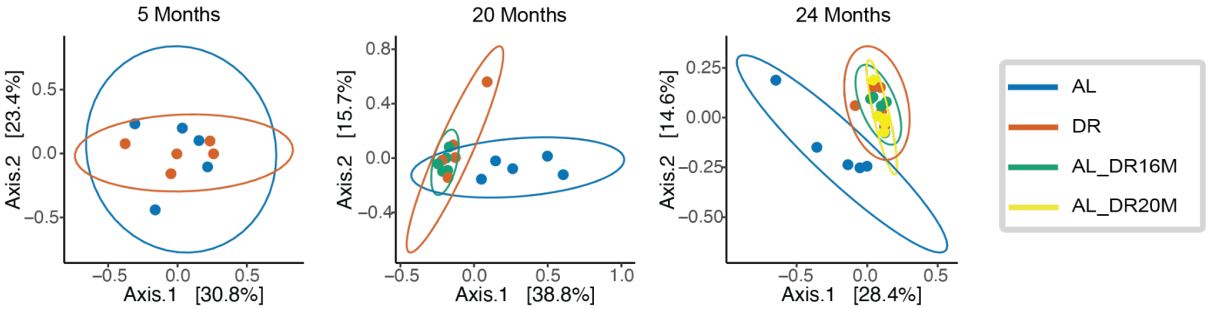

Figure 4.4. The ageing microbiome responds to late-onset DR. Bray Curtis Principal coordinates analysis; inter-individual dissimilarity. Significant differences at 20 months of age (Mann-Whitney U-test) AL vs DR p-value = 0.009; AL_DR16M vs DR p-value = 0.01. Significant changes at 24 months of age (Mann-Whitney U-test) AL vs DR p-value = 0.01; AL_DR16M vs AL p-value = 0.009; AL_DR20M vs AL p-value = 0.01.

4.2.8 DR-related BCR metrics are associated with healthier phenotypes

Finally, to characterise the observed BCR repertoire dynamics patterns, and understand how they are reflected in host health, we tested the correlation between morbidity and BCR metrics, in both the spleen and ileum (Figure 4.5 A-B). The 'macromorbidity index' developed in the present work was adapted from (Ikeno et al. 2009; Bokov et al. 2011; Treuting et al. 2008) to encompass the collected macro-pathology of these mice, previously described in detail by (Drews, 2021). For each mouse, the morbidity index was calculated as the sum of non-neoplastic pathology burden and neoplasia grade. A degree of 1 was assigned to each non-neoplastic pathological finding at dissection, while neoplasia were graded as 0 (absence of tumours), 1 (1 organ affected by tumours), or 2 (2 or more organs affected by tumours, representing metastatic cancer). Different models of morbidity index calculation were tested, yielding similar associations to BCR metrics in all cases (Supplementary Figure 4.5 A-B).

Of all the metrics obtained from the spleen BCR repertoire, clonal expansion (P20), inter-individual dissimilarity (RDI_uniqueness) and mean CDR3 length (cdr3_mu) were positively associated with the macromorbidity index. Shannon and Simpson diversity displayed a negative association (Figure 4.5 A), indicating that higher within-individual diversity is associated with healthier mice. Further, we asked which isotypes showed strongest correlation with morbidity, and found that IgM and IgG underpin the strongest association between morbidity and BCR characteristics (Figure 4.5 C). With respect to the ileal BCR repertoire metrics, only Simpson diversity was negatively associated with morbidity; high Simpson values were found in healthier mice (Figure 4.5 B, Supplementary Figure 4.5 C).

Having found lower clonal expansion and RDI in DR mice, paired with increased Shannon and Simpson diversity (Figure 4.2 C-F), our findings suggest that DR might delay the systemic functional decline of the BCR repertoire with age, and be associated with younger and healthier BCR repertoire. Similarly, decreased clonal expansion and RDI, and increased Shannon diversity in AL_DR16M mice, might suggest that initiating DR as late as 16 months could rejuvenate the BCR repertoire and be associated with lower morbidity.

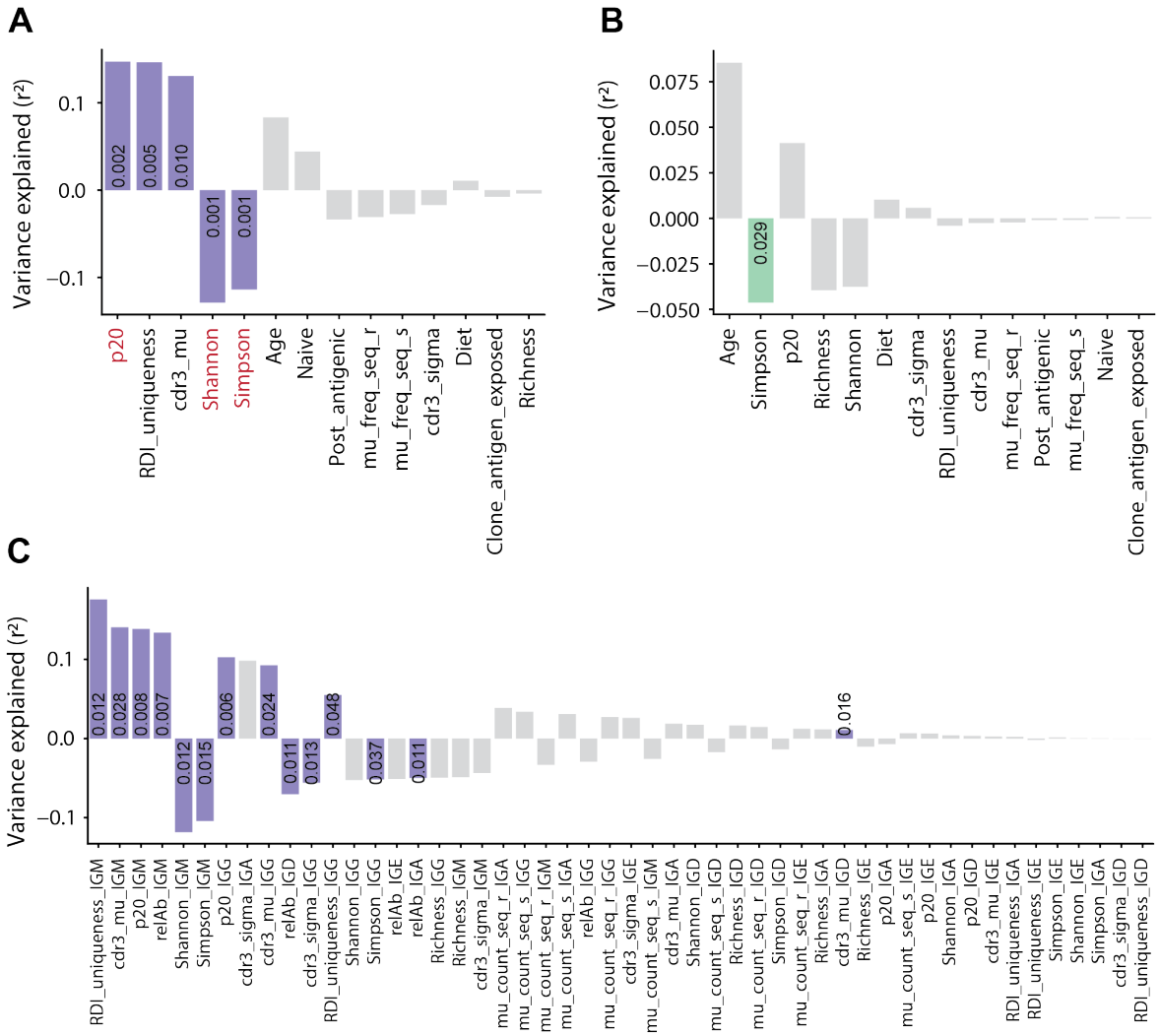

Figure 4.5: DR-associated BCR metrics are associated with healthier phenotypes. Percentage of variance explained in 'macromorbidity index' by **(A)** general BCR spleen metrics, **(B)** general BCR ileum metrics, **(C)** isotype-specific BCR spleen metrics. Coloured bars are spearman p-value < 0.05. Significant p-values are included and red metrics represent Bonferroni corrected p-values < 0.05.

4.3. Discussion

Establishing and maintaining a tight and life-long regulation of immune responses is vital for host homeostasis. The profound impairment of immune function with ageing is well documented (Wick et al. 2000b; Nikolich-Zugich 2005b; Ademokun, Wu, and Dunn-Walters 2010b; Weiskopf, Weinberger, and Grubeck-Loebenstein 2009b), and thereby strategies that can ameliorate the age-associated immune dysregulation may be holding a great promise to delay ageing. We asked whether the most robust anti-ageing intervention known to date (dietary restriction, or DR) has an impact on immune homeostasis, or whether it exerts its function independently from the immune system. Furthermore, DR can beneficially impact host health- and lifespan when started as late as 16 months of age (Drews, 2021). To investigate how the B cell receptor (BCR) repertoire changes with age, under chronic DR, and under midlife- and late-life onset of DR diet in the mouse spleen and ileum, we performed BCR sequencing. In addition, we test whether the critical temporal window within which DR beneficially impacts host health- and lifespan is consistent with a remodelling of the BCR repertoire dependent on age of DR onset. To our knowledge, this is the first study to use BCR sequencing to explore the mouse B cell clonal population dynamics with age in response to anti-ageing interventions. Our dataset allowed us to not only investigate the general characteristics of the BCR repertoire in the spleen and ileum, but also the corresponding changes on BCR isotypes. Here, we show for the first time that DR mitigates the ageing of the BCR repertoire in both spleen and ileum. Further, we find a recapitulation of the splenic DR-like BCR repertoire in mice where DR was started at 16 months of age, but not at 20 months. In the current work, we also provide associations of BCR repertoire characteristics to a novel macromorbidity index. We report an association of AL-like BCR repertoire characteristics with high morbidity, and DR-like characteristics with improved health.

The ageing BCR repertoire in the spleen of AL-fed mice followed the classically described pattern in both mice and humans: decreased within-individual diversity, coupled with increased clonal expansion rate and inter-individual dissimilarity (de Bourcy et al. 2017; Gibson et al. 2009; Weksler and Szabo 2000; Nagpal et al. 2018; Booth and Toapanta 2021). On the other hand, although ageing in chronic DR mice was also accompanied by a decline in within-individual BCR variability, increased clonal expansions and inter-individual dissimilarity, these effects were mitigated compared to AL. Importantly, low within-individual diversity, high clonal expansions and high inter-individual dissimilarity correlated with high macromorbidity index. Thereby, the DR-mediated mitigation of the age-associated BCR repertoire dysregulation might, at least partly, contribute to the beneficial effects of DR on mouse health. Furthermore, there is growing evidence that maintenance of a high BCR diversity translates to enhanced ability to generate robust antibody responses to novel antigens and possibly an enhanced vaccination response at old age (Dunn-Walters 2015; Okawa, Nagai, and Hase 2020). In fact, loss of BCR repertoire diversity in older individuals has been associated with poor vaccination response against pneumococcus and influenza (Ademokun et al. 2011b; Tas et al. 2016; de Bourcy et al. 2017). Thus, the observed age-associated decline in within-individual diversity and post-antigenic BCR clones in AL mice, suggests a decrease in high-affinity class-switched isotypes, and might also contribute to the impaired vaccination response in old age (Oh, Lee, and Shin 2019b). The amelioration of the ageing splenic BCR dysregulation by DR indicates that DR maintains a healthier, younger-like BCR repertoire. However, a limitation of the current

study is the lack of information on the B cell subsets (i.e. marginal, follicular, B-1, etc) encompassing the sequenced cell pool. Future studies performing fluorescence-activated cell sorting should not only investigate the B cell types involved in the DR response, but also causally address whether DR improves vaccination outcomes due to “enrichment” of the BCR repertoire.

Genome variation in the BCR loci is instrumental for mounting adequate immune responses and *IghV* and *IghJ* gene usage have been shown to be largely implicated, thereby affecting susceptibility to various diseases (Raposo et al. 2014). Results from a study in splenocytes showed an age-related increase in *IghV2*, *IghV11*, *IghJ1*, as well as reduction in *IghJ2* gene usage (Holodick et al. 2016). Here, we found a more pronounced decline in *IghV*-gene usage with age in AL compared to DR, especially in *IghV4*. Although very little is known about the functional relevance of these changes in ageing, differential *IghV* gene usage has been implicated in age-related diseases, such as rheumatoid arthritis and multiple sclerosis, in both mice and humans (Vencovský et al. 2002; Raposo et al. 2014; Walter et al. 1991). Further, previous work is indicative of a role of *IghV* gene usage in polyreactivity, especially in HIV and influenza virus antibody responses; polyreactivity is defined as the ability of an antibody molecule or of a BCR to bind to multiple distinct antigenic targets (Dimitrov et al. 2013). While polyreactivity is thought to dramatically increase with age in mice (Gunti and Notkins 2015), the decline in usage of some *IghV* genes, including the *IghV4* observed in this study, would be indicative of a reduced polyreactivity in our AL mice with age that was attenuated by DR. Increased polyreactivity has beneficial effects, including the diversification of immune repertoires and clearance of defective apoptotic cells, preventing inflammatory responses (Dimitrov et al. 2013). Therefore, we speculate that compared to AL, DR treatment might help retain some levels of polyreactivity and its corresponding benefits for longer periods of time.

During B cell development in the bone marrow, there is preferential removal of B cells expressing BCRs with long CDR3s (Wardemann et al. 2003). Studies in human peripheral blood have associated long CDR3 length with old age and increased autoreactivity, suggesting that there is a selection against BCRs with long CDR3s in the aged immune system (Wang et al. 2014). Similarly, in this study long CDR3s correlated with high macromorbidity index. Although the mean CDR3 length was not different between AL and DR, there was increased skewing of CDR3 length production in AL mice, generating BCRs of a smaller length range than both DR and AL_DR16M mice. Even though long CDR3s were found in mice with high macromorbidity, we did not observe a significant reduction under DR anti-ageing intervention. Future studies including higher numbers of mice should evaluate CDR3 lengths and determine whether DR maintains selection against BCRs with long CDR3s, to protect from the ageing-associated increased autoreactivity.

Our results highlight the importance of global splenic BCR repertoire dynamic metrics, such as within-individual variability, inter-individual dissimilarity, clonal expansions and CDR3 length distribution in enhanced health under DR. Moreover, we also uncover intriguing ageing- and DR-associated changes in immunoglobulin isotypes, which have been thus far unexplored in the context of anti-ageing interventions. With respect to ageing-associated changes, we found that IgM, known for their role in the primary immune response as poly-reactive antibodies involved in opsonization of antigens (Schroeder and Cavacini 2010), underwent a decline in within-individual diversity with age in both AL and DR. Similarly, IgG, which is involved in long-term protection and neutralisation of toxins and viruses (Schroeder and

Cavacini 2010), showed a decline in within-individual diversity with age in AL. In line with these results, previous studies have shown an association between age-related decline in IgM and IgG levels and BCR repertoire diversity, with impaired vaccination response (Ademokun et al. 2011b; Jiang et al. 2013; Shi et al. 2005). In addition, we found that the low within-individual diversity of both IgM and IgG isotypes was inversely associated with morbidity, suggesting that preservation of IgM and IgG diversity is one of the features of a 'younger', healthier BCR repertoire. Further, regarding DR-associated changes, we observed an amelioration of the ageing-associated increase in IgM clonal expansion rate. Although the implications of this change are unknown, we speculate that DR might offer a tighter regulation of the primary immune response, and thereby the maintenance of IgM clonal expansion rate might be a contributor to DR-mediated beneficial effects. This is corroborated by the fact that high IgM clonal expansion was associated with morbidity. Collectively, although the repertoire trajectories described in this work strictly reflect non-pathogen exposure conditions, as any type of infection is highly unlikely in the current cohort of mice, our results highlight the potential involvement of IgM and IgG in DR-associated healthspan and lifespan benefits. Nevertheless, in light of the macromorbidity-associated isotype-specific observations, future studies where isotypes are evaluated in the context of healthy ageing are necessary to more comprehensively reveal the implications of these changes on adaptive immune function and DR-associated beneficial effects.

Here, we demonstrate that DR and AL_DR16M mice have "healthier" repertoires than AL and AL_DR20M, especially affecting the splenic within-individual variability, and clonal expansion. The improvement of the immune health in DR and AL_DR16M mice, is the first reported molecular phenotype consistent with the recapitulation of the lifespan extension under DR by AL_DR16M mice (Drews, 2021). These findings indicate that the enhanced splenic B cell adaptive immune system of DR mice can be recapitulated in an age-dependent manner, by switching to a DR feeding regime as late as 16 months of age. More specifically, AL_DR16M displayed an increased IgM, IgE and IgA Shannon and Simpson within-individual diversity, recapitulating DR levels. IgM spike under AL_DR16M could be indicative of a greater hematopoietic stem cells (HSC) capacity. A previous study on HSCs on chronic and midlife-onset DR mice, showed that chronic DR feeding reduced the loss of repopulating capacity of HSCs observed with age in AL. Furthermore, the onset of DR at 15 months of age improved the hematopoietic regeneration of ageing HSCs (Tao et al. 2020). Thus, an improved regeneration of HSCs would be likely to facilitate the AL_DR16M BCR repertoire responsiveness under dietary switch. Future studies on bone marrow HSCs on midlife- and late-onset DR are necessary to evaluate a possible causal association of an age-of-onset-dependent start of DR with BCR repertoire responsiveness.

Noteworthy, we found that AL_DR16M responded to DR initiation through an increase in IgE diversity in spleen. Although elevated IgE levels are primarily implicated in allergic reactions (Gould and Sutton 2008; Saunders et al. 2019; Schroeder and Cavacini 2010), it is highly unlikely that food or other allergens are contributing to the increased IgE diversity levels after DR onset at 16 months, given the housing conditions and the unchanged chow food composition of our mice. Interestingly, high IgE levels have been previously documented in germ-free or antibiotic-treated mice that are typically characterised by low microbiome diversity, suggesting a regulatory role of the microbiome in controlling systemic IgE levels (Cahenzli et al. 2013). Similarly, a previous study evaluating the longitudinal microbiome characteristics of 50 AL, DR, AL_DR16M and AL_DR20M mice, reported an initial decline in

within-individual microbial diversity of AL_DR16M mice before recapitulating diversity levels similar to DR by 18 months of age (Monzó, 2022). Therefore, the spike in IgE in the AL_DR16M mice might reflect this acute loss of microbial within-individual diversity after DR onset. Nonetheless, future studies are necessary to confirm and comprehensively assess the changes and potential contributors in IgE responses in the context of dietary switches.

Despite the importance of the gut B cells, and the increasing number of studies examining mucosal antibodies and their interaction with the microbiome (Lindner et al. 2015c, 2012; Macpherson et al. 2018b; Belkaid and Hand 2014a), to the best of our knowledge, the effect of anti-ageing interventions on the gut BCR repertoire are yet to be reported. Here, we show that the ileum BCR repertoire undergoes very few changes with age and under chronic or late onset DR. On the contrary, the microbiome was found to rapidly respond to the switch to DR, even when DR was initiated at 20 months of age. In line with other studies where short-term antibiotics, microbiome transfers, or introduction of new diets did not result in changes in the ileum B cell compartment (Bradshaw et al. 2022; Lindner et al. 2015c), the switch to DR diet, independently of age-of-onset, did not strongly affect the gut BCR repertoire. Nonetheless, the SHM mechanism was found to be highly influenced by both age and diet in the ileum, which is not surprising given the constant microbial antigenic exposure in this organ (Q. Zhao and Elson 2018). More specifically, a declining ageing SHM capacity was observed in AL mice, affecting predominantly the IgA isotype. Previous analysis of IgA repertoire in human colon and mouse small intestine revealed that neither antibiotic treatment nor diet modulate the IgA clonal composition (Lindner et al. 2015c). It was postulated that, to maintain homeostasis through the interaction of the host and its microbiome, the IgA repertoire undergoes diversification of existing memory B cells, instead of generating new B cell clones (Lindner et al. 2015c). Elevated SHM in Peyer patches is critical for the generation of a diverse repertoire that can undergo affinity maturation and selection at a later phase (Macpherson et al. 2018b). Therefore, the decline in IgA SHM with age we observed under AL feeding may be associated with impaired diversification and affinity maturation capacity, which might ultimately lead to disruption of host-microbiome symbiosis and compromised mucosal defence (Wei et al. 2011; Lindner et al. 2015c). On the contrary, DR buffered the age-associated SHM decline observed in the AL mice ileum, indicating that DR feeding might offer an advantage in preserving diverse mucosal immune responses and gut homeostasis for extended periods.

In conclusion, in this study we not only show mitigation of the age-associated decline in within-individual diversity of the BCR repertoire in the spleen and ileum of mice under DR, correlating with improved mouse health, but also provide the first evidence that the splenic BCR repertoire responds to a mid/late-life start of DR in an age-dependent manner. Our findings highlight the immune responsiveness of the mice where DR was initiated at 16 months of age as one of the contributing factors to extended lifespan.

4.4. Supplementary figures

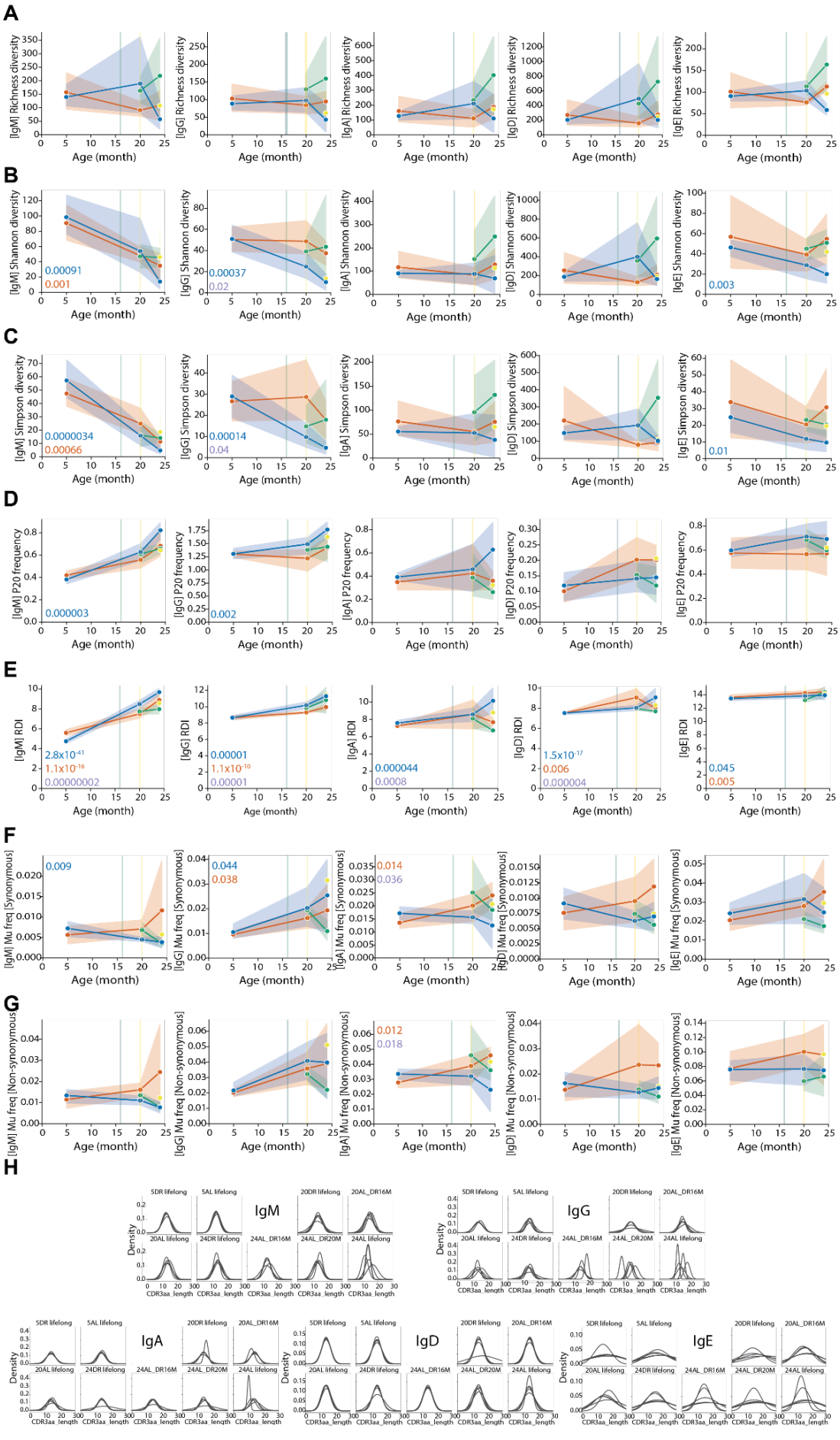
A
[IgM] Richness diversity
[IgG] Richness diversity
[IgA] Richness diversity
[IgD] Richness diversity
[IgE] Richness diversity
Age (month)
B
[IgM] Shannon diversity
0.00091
0.001
[IgG] Shannon diversity
0.00037
0.02
[IgA] Shannon diversity
[IgD] Shannon diversity
[IgE] Shannon diversity
0.003
C
[IgM] Simpson diversity
0.0000034
0.00066
[IgG] Simpson diversity
0.00014
0.04
[IgA] Simpson diversity
[IgD] Simpson diversity
[IgE] Simpson diversity
0.01
D
[IgM] P20 frequency
0.000003
[IgG] P20 frequency
0.002
[IgA] P20 frequency
[IgD] P20 frequency
[IgE] P20 frequency
E
[IgM] RDI
2.8x10-41
1.1x10-16
0.00000002
[IgG] RDI
0.00001
1.1x10-10
0.00001
[IgA] RDI
0.000044
0.0008
[IgD] RDI
1.5x10-17
0.006
0.000004
[IgE] RDI
0.045
0.005
F
[IgM] Mu freq [Synonymous]
0.009
[IgG] Mu freq [Synonymous]
0.044
0.038
[IgA] Mu freq [Synonymous]
0.014
0.036
[IgD] Mu freq [Synonymous]
[IgE] Mu freq [Synonymous]
G
[IgM] Mu freq [Non-synonymous]
[IgG] Mu freq [Non-synonymous]
[IgA] Mu freq [Non-synonymous]
0.012
0.018
[IgD] Mu freq [Non-synonymous]
[IgE] Mu freq [Non-synonymous]
H
IgM
IgG
IgA
IgD
IgE
5DR lifelong
5AL lifelong
20DR lifelong
20AL_DR16M
20AL lifelong
24DR lifelong
24AL_DR16M
24AL_DR20M
24AL lifelong
Density
CDR3aa_length

Supplementary figure 4.1. Spleen isotype-specific BCR repertoire metrics. (A) Richness within-individual diversity. Significant differences at 20 months of age (Mann-Whitney U test): IgM (AL_DR16M vs DR p-value = 0.04), IgE (AL_DR16M vs DR p-value = 0.04). Significant differences at 24 months of age (Mann-Whitney U test): IgE (DR vs AL p-value = 0.005). **(B)** Shannon within-individual diversity. Significant differences at 20 months of age (Mann-Whitney U test): IgD (AL_DR16M vs DR p-value = 0.02). Significant differences at 24 months of age (Mann-Whitney U test): IgM (AL_DR16M vs DR p-value = 0.04), IgG (AL_DR20M vs DR p-value = 0.01), IgE (AL_DR16M vs DR p-value = 0.002; AL_DR20M vs AL p-value = 0.02). **(C)** Simpson within-individual diversity. Significant differences at 24 months of age (Mann-Whitney U test): IgM (AL_DR16M vs AL p-value = 0.02), IgG (AL_DR20M vs DR p-value = 0.02), IgA (AL_DR16M vs AL p-value = 0.03), IgE (AL_DR16M vs AL p-value = 0.04). **(D)** Clonal expansion. **(E)** Inter-individual dissimilarity. Significant differences at 20 months of age (Mann-Whitney U test): IgE (AL_DR16M vs AL p-value = 0.011; AL_DR16M vs DR p-value = 0.00005). Significant differences at 24 months of age (Mann-Whitney U test): IgM (AL_DR16M vs AL p-value = $1.0x10^{-6}$; AL_DR16M vs DR p-value = 0.005; AL_DR20M vs AL p-value = 0.035), IgA (AL_DR16M vs AL p-value = $1.0x10^{-6}$; AL_DR16M vs DR p-value = 0.0005; AL_DR20M vs AL p-value = 0.049). **(F)** Frequency of synonymous SHM. **(G)** Frequency of non-synonymous SHM. **(H)** CDR3-length distribution Significant differences in CDR3-length distribution variability at 24 months of age (Kolmogorov-Smirnov): IgG (AL vs DR p-value = 0.0061), IgA (AL vs DR p-value = 0.015; AL_DR20M vs AL p-value = 0.024). **(A-G)** Blue represents AL, red DR, green AL_DR16M, and yellow AL_DR20M. Lines correspond to mean, and shaded area to 95% confidence intervals.

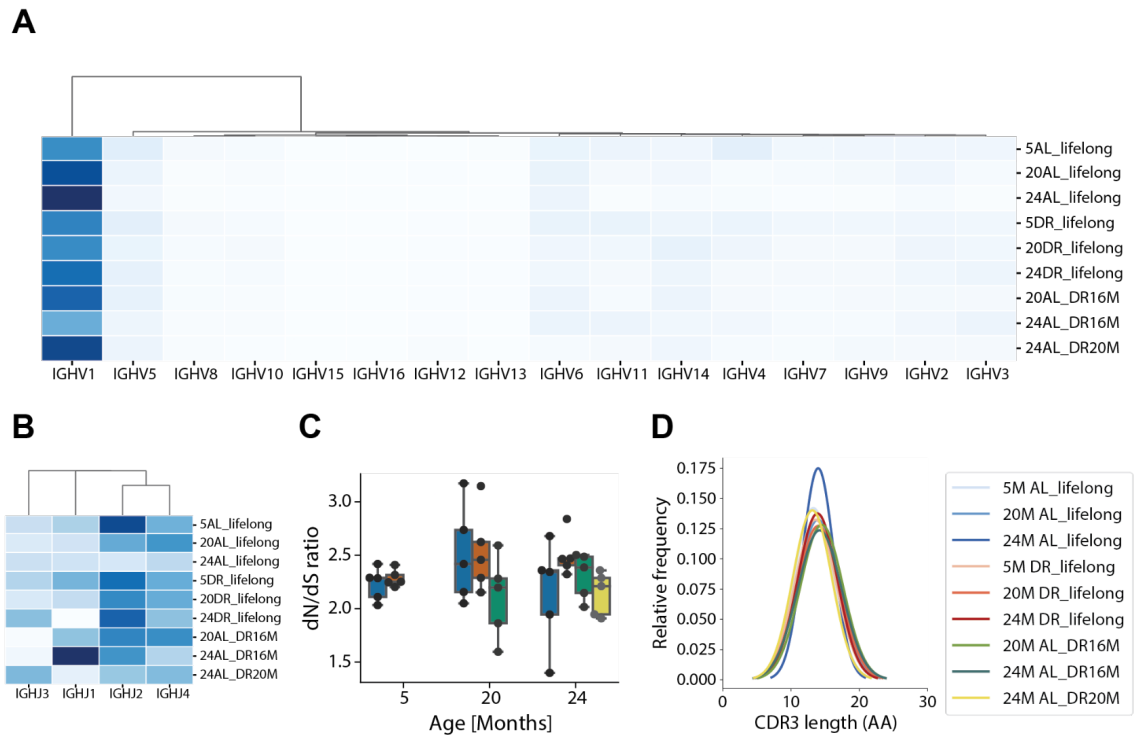

Supplementary figure 4.2. Spleen IGHV and IGHJ gene usage and CDR3 length. (A) Mean relative IGHV gene usage in the spleen BCR. Age-related decline in the usage of *IghV1*, *IghV3*, *IghV4, IghV7*, and *IghV11* in AL-fed mice (linear regression, p-value = 0.03, $8.2x10^{-5}$, 0.001, 0.02, and 0.049). Age-related decline in usage of *IghV4*, *IghV6*, *IghV7*, and *IghV11* in DR mice (linear regression, p-value = 0.001, 0.02, 0.02 and 0.03). Significantly higher usage of *IghV3* and *IghV15* in DR compared to AL mice (2-way ANOVA, p-value = 0.01 and 0.02). **(B)** Mean relative IGHJ gene usage in the spleen BCR. **(A-B)** Darker blue corresponds to higher gene usage, and white to lower. **(C)** Ratio of non-synonymous to synonymous mutations in spleen. **(D)** CDR3 length gaussian distribution in the spleen.

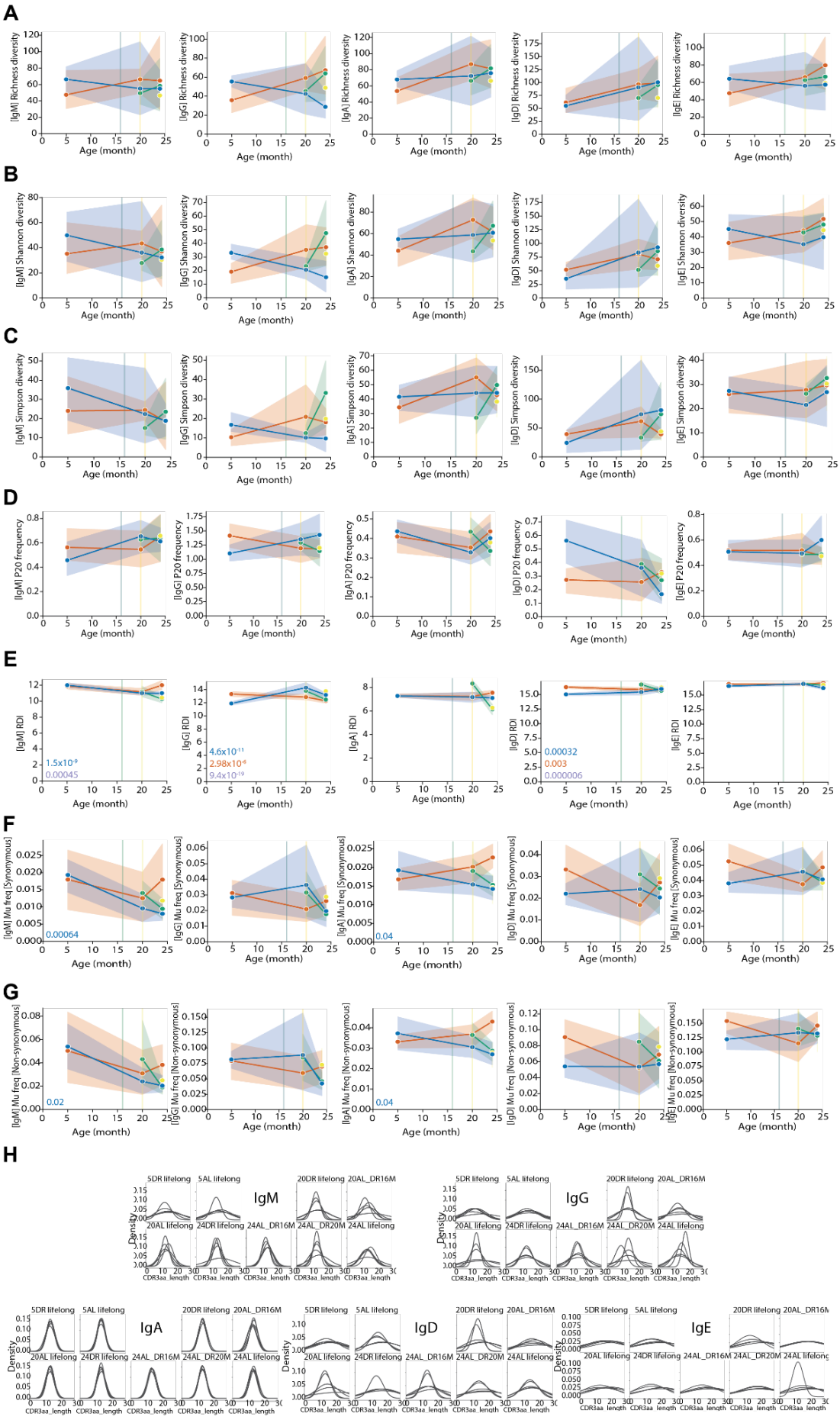
A
[IgM] Richness diversity
[IgG] Richness diversity
[IgA] Richness diversity
[IgD] Richness diversity
[IgE] Richness diversity
B
[IgM] Shannon diversity
[IgG] Shannon diversity
[IgA] Shannon diversity
[IgD] Shannon diversity
[IgE] Shannon diversity
C
[IgM] Simpson diversity
[IgG] Simpson diversity
[IgA] Simpson diversity
[IgD] Simpson diversity
[IgE] Simpson diversity
D
[IgM] P20 frequency
[IgG] P20 frequency
[IgA] P20 frequency
[IgD] P20 frequency
[IgE] P20 frequency
E
[IgM] RDI
1.5x10⁻⁹
0.00045
[IgG] RDI
4.6x10⁻³¹
2.98x10⁻⁶
9.4x10⁻¹⁹
[IgA] RDI
[IgD] RDI
0.00032
0.003
0.000006
[IgE] RDI
F
[IgM] Mu freq [Synonymous]
0.00064
[IgG] Mu freq [Synonymous]
[IgA] Mu freq [Synonymous]
0.04
[IgD] Mu freq [Synonymous]
[IgE] Mu freq [Synonymous]
G
[IgM] Mu freq [Non-synonymous]
0.02
[IgG] Mu freq [Non-synonymous]
[IgA] Mu freq [Non-synonymous]
0.04
[IgD] Mu freq [Non-synonymous]
[IgE] Mu freq [Non-synonymous]
Age (month)
H
IgM
IgG
IgA
IgD
IgE
5DR lifelong
5AL lifelong
20DR lifelong
20AL_DR16M
20AL lifelong
24DR lifelong
24AL_DR16M
24AL_DR20M
24AL lifelong
Density
CDR3aa_length

Supplementary figure 4.3. Ileum isotype-specific BCR repertoire metrics. (A) Richness within-individual diversity. Significant differences at 24 months of age (Mann-Whitney U test): IgG (p-value DR vs AL = 0.01). **(B)** Shannon within-individual diversity. **C)** Simpson within-individual diversity. **(D)** Clonal expansion **(E)** Inter-individual dissimilarity. Significant differences through age (linear regression): IgM (AL p-value = 1.5x10-9), IgG (AL p-value = $4.6x10^{-11}$; DR p-value = $2.9x10^{-6}$), IgD (AL p-value = 0.0003; DR p-value = 0.003). Significant differences through age and diet (2-way ANOVA): IgM (DR vs AL p-value = 0.00045), IgG (DR vs AL p-value = $9.4x10^{-19}$), IgD (DR vs AL p-value = 0.000006). Significant differences at 20 months of age (Mann-Whitney U test): IgA (AL_DR16M vs AL p-value = $2.0x10^{-5}$; AL_DR16M vs DR p-value = $5.1x10^{-17}$), IgD (AL_DR16M vs AL p-value = $6.7x10^{-4}$; AL_DR16M vs DR p-value = 0.007), IgG (AL_DR16M vs AL p-value = 0.01; AL_DR16M vs DR p-value = 0.00002). Significant differences at 24 months of age (Mann-Whitney U test): IgA (AL_DR16M vs AL p-value = $4.1x10^{-6}$; AL_DR16M vs DR p-value = $2.4x10^{-8}$; AL_DR20M vs AL p-value = $3.12x10^{-8}$; AL_DR20M vs DR p-value = $2.2x10^{-5}$), IgM (AL_DR16M vs AL p-value = 0.00018; AL_DR16M vs DR p-value = $6.6x10^{-7}$; AL_DR20M vs AL p-value = 0.00015), IgE (AL_DR16M vs AL p-value = $7.7x10^{-5}$; AL_DR16M vs DR p-value = 0.00013; AL_DR20M vs AL p-value = 0.015), IgG (AL_DR20M vs AL p-value = 0.003; AL_DR20M vs DR p-value = $4.3x10^{-7}$). **(F)** Frequency of synonymous SHM. Significant differences through age (linear regression): IgM (AL p-value = 0.0006), IgA (AL p-value = 0.04). **(G)** Frequency of non-synonymous SHM. Significant differences through age (linear regression): IgM (AL p-value = 0.02), IgA (AL p-value = 0.04). Significant differences at 24 months of age (Mann-Whitney U test): IgA (DR vs AL p-value = 0.024; AL_DR16M vs DR p-value = 0.024; AL_DR20M vs DR p-value = 0.024). **H)** CDR3-length distribution. Significant differences at 20 months of age (Kolmogorov-Smirnov): IgD (DR vs AL p-value = 0.036; AL_DR16M vs DR p-value = 0.036). Significant differences at 24 months of age (Kolmogorov-Smirnov): IgM (DR vs AL p-value = 0.015; AL_DR16M vs DR p-value = 0.015). **(A-G)** Blue represents AL, red DR, green AL_DR16M, and yellow AL_DR20M. Lines correspond to mean, and shaded area to 95% confidence intervals.

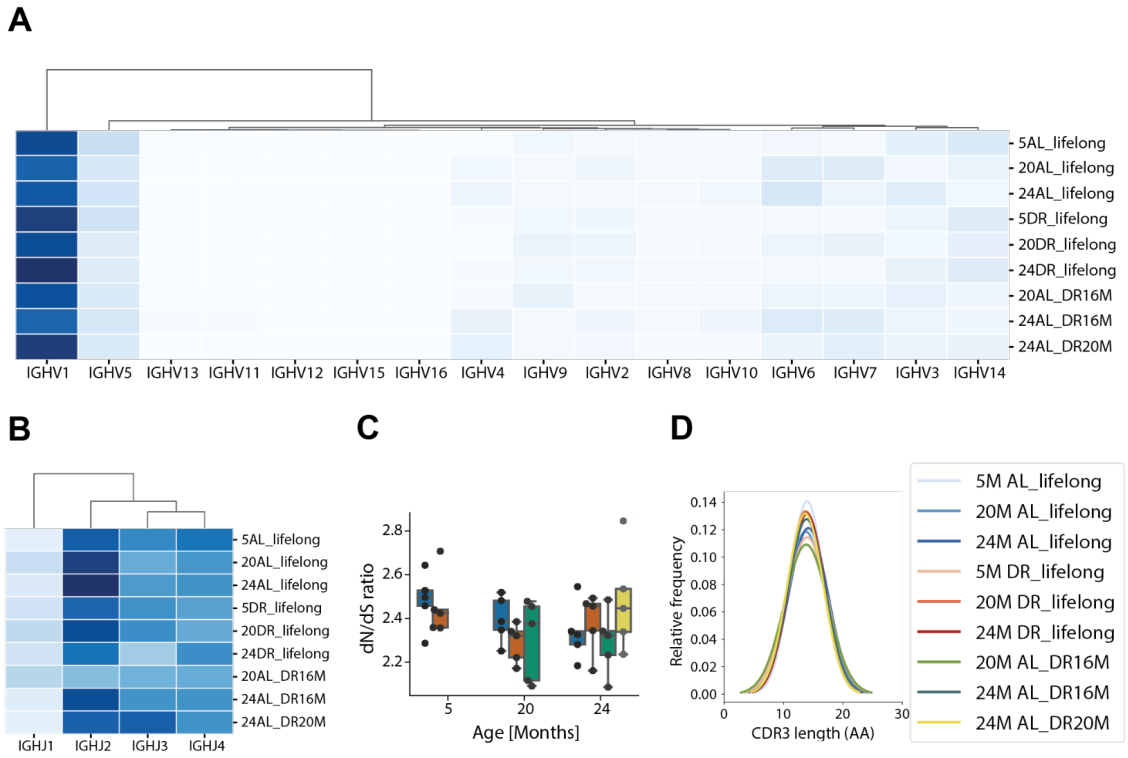

Supplementary figure 4.4. Ileal IGHV and IGHJ gene usage and CDR3 length. (A) Mean relative *IghV* gene usage in the ileum BCR. **(B)** Mean relative *IghJ* gene usage in the ileum BCR. **(A-B)** Darker blue corresponds to higher gene usage, and white to lower. **(C)** Ratio of non-synonymous to synonymous mutations in ileum. **(D)** CDR3 length gaussian distribution in the ileum.

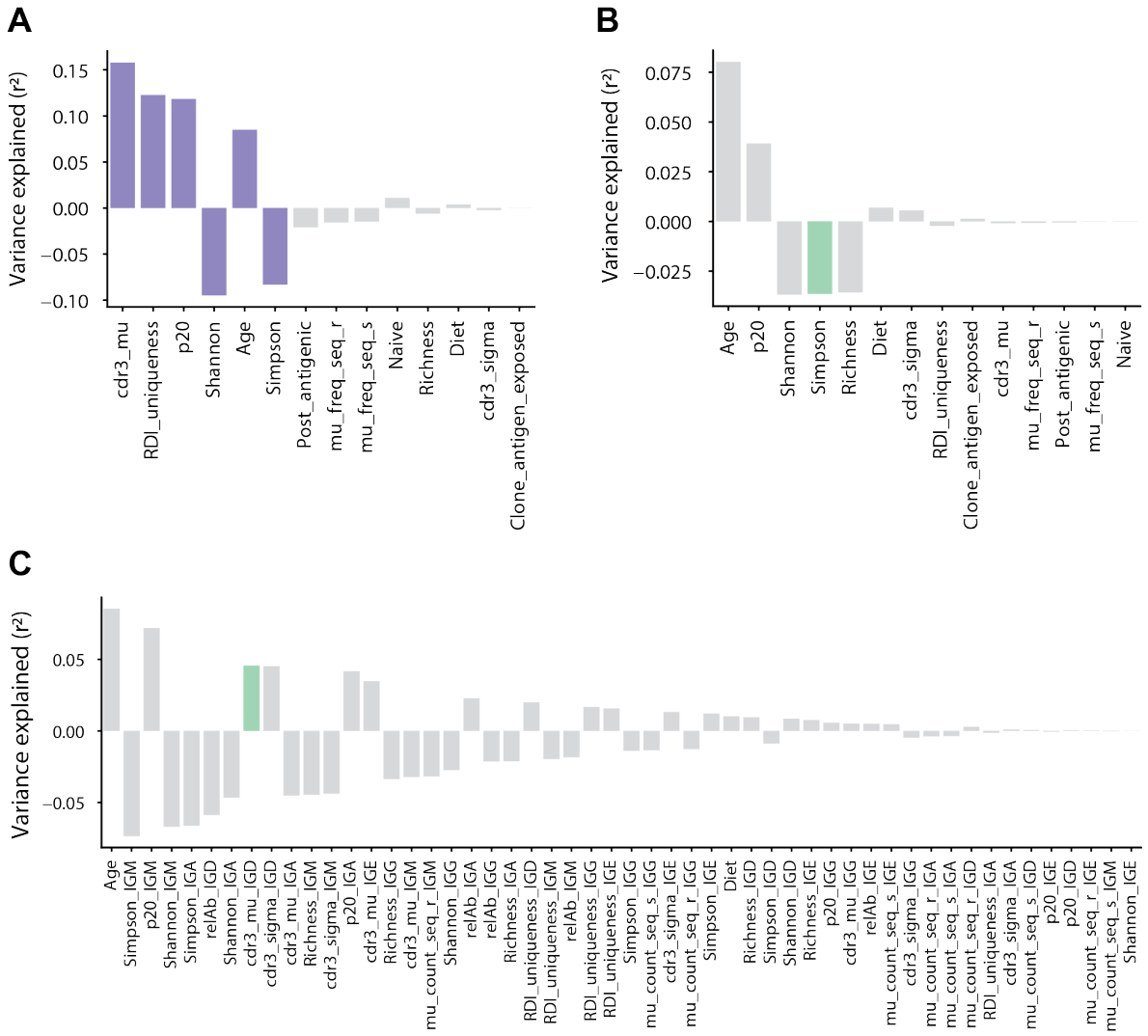

Supplementary figure 4.5. Association of BCR characteristics with morbidity. (A-B) Percentage of variance explained by variation of 'macromorbidity index' where the total number of pathologies detected per individual was divided by 3, thus making the accumulation of pathologies equal to the value of presence of cancer for **(A)** general BCR spleen metrics, and **(B)** general BCR ileum metrics. **(C)** Percentage of variance explained by standard 'macromorbidity index' for isotype-specific BCR ileum metrics. Coloured bars are spearman p-value < 0.05.

5. Appendix: Primers used for BCR Sequencing

5.1. Isotype-specific primers

Sequence	Target isotype	Source
CCAGGTCACATTCATCGTG	mIGA_r1	(Turchaninova et al. 2016)
GCCATTTCTCATTTCAGAGG	mIGD_r1	(Turchaninova et al. 2016)
GTTCACAGTGCTCATGTTC	mIGE_r1	(Turchaninova et al. 2016)
GTACAGTCACCAAGCTGCT	mIGG3_r1	(Turchaninova et al. 2016)
KKACAGTCACTGAGCTGCT	mIGG12_r1	(Turchaninova et al. 2016)
CTGGATGACTTCAGTGTTGT	mIGM_r1	(Turchaninova et al. 2016)

5.2. Template switch adaptor oligo

Sequence	Oligo	Source
AAGCAGUGGTAUCAACGCAGAGUNNNNUNNNNUNNNNUCTTrGrGrGrG	SmartNNNa	(Turchaninova et al. 2016)

5.3. First PCR primers

Sequence	Target isotype	Source
AAGCAGTGGTATCAACGCA	M1SS (mix)	(Turchaninova et al. 2016)
ATTGGGCAGCCCTGATTTCAGTGGGTAGATGGTG	mIGA_r2	(Turchaninova et al. 2016)
ATTGGGCAGCCCTGATTCTCTGAGAGGAGGAAC	mIGD_r2	(Turchaninova et al. 2016)

ATTGGGCAGCCCTGATTAAGGGGTAGAGCTGAG	mIGE_r2	(Turchaninova et al. 2016)
ATTGGGCAGCCCTGATTAAGGGATAGACAGATG	mIGG3_r2	(Turchaninova et al. 2016)
ATTGGGCAGCCCTGATTAGTGGATAGACMGATG	mIGG12_r2	(Turchaninova et al. 2016)
ATTGGGCAGCCCTGATTGGGGGAAGACATTTGG	mIGM_r2	(Turchaninova et al. 2016)

5.4. Second PCR primers

Sequence	Primer name	Source
(N)4–6(XXXXX)CAGTGGTATCAACGCAGAG	M1S	(Turchaninova et al. 2016)
(N)4-6(XXXXX)ATTGGGCAGCCCTGATT	Z	(Turchaninova et al. 2016)

6. List of Figures

7. Bibliography

Ables, Gene P., Holly M. Brown-Borg, Rochelle Buffenstein, Christopher D. Church, Amany K. Elshorbagy, Vadim N. Gladyshev, Tsang-Hai Huang, et al. 2014. “The First International Mini-Symposium on Methionine Restriction and Lifespan.” *Frontiers in Genetics* 5 (May): 122.

Acarin, L., B. González, and B. Castellano. 2000. “Neuronal, Astroglial and Microglial Cytokine Expression after an Excitotoxic Lesion in the Immature Rat Brain.” *The European Journal of Neuroscience* 12 (10): 3505–20.

Acosta-Rodríguez, Victoria, Filipa Rijo-Ferreira, Mariko Izumo, Pin Xu, Mary Wight-Carter, Carla B. Green, and Joseph S. Takahashi. 2022. “Circadian Alignment of Early Onset Caloric Restriction Promotes Longevity in Male C57BL/6J Mice.” *Science*, May, e.

Ademokun, Alexander, Yu-Chang Wu, and Deborah Dunn-Walters. 2010a. “The Ageing B Cell Population: Composition and Function.” *Biogerontology* 11 (2): 125–37.

———. 2010b. “The Ageing B Cell Population: Composition and Function.” *Biogerontology* 11 (2): 125–37.

Ademokun, Alexander, Yu-Chang Wu, Victoria Martin, Rajive Mitra, Ulrich Sack, Helen Baxendale, David Kipling, and Deborah K. Dunn-Walters. 2011a. “Vaccination-Induced Changes in Human B-Cell Repertoire and Pneumococcal IgM and IgA Antibody at Different Ages.” *Aging Cell*. https://doi.org/10.1111/j.1474-9726.2011.00732.x.

———. 2011b. “Vaccination-Induced Changes in Human B-Cell Repertoire and Pneumococcal IgM and IgA Antibody at Different Ages.” *Aging Cell* 10 (6): 922–30.

Alic, Nazif, Maria E. Giannakou, Irene Papatheodorou, Matthew P. Hoddinott, T. Daniel Andrews, Ekin Bolukbasi, and Linda Partridge. 2014. “Interplay of dFOXO and Two ETS-Family Transcription Factors Determines Lifespan in Drosophila Melanogaster.” *PLoS Genetics* 10 (9): e1004619.

Aliper, Alexander M., Antonei Benjamin Csoka, Anton Buzdin, Tomasz Jetka, Sergey Roumiantsev, Alexy Moskalev, and Alex Zhavoronkov. 2015. “Signaling Pathway Activation Drift during Aging: Hutchinson-Gilford Progeria Syndrome Fibroblasts Are Comparable to Normal Middle-Age and Old-Age Cells.” *Aging* 7 (1): 26–37.

Alsaleh, Ghada, Isabel Panse, Leo Swadling, Hanlin Zhang, Felix Clemens Richter, Alain Meyer, Janet Lord, et al. 2020. “Autophagy in T Cells from Aged Donors Is Maintained by Spermidine and Correlates with Function and Vaccine Responses.” *eLife* 9 (December). https://doi.org/10.7554/eLife.57950.

Altintas, Ozlem, Sangsoon Park, and Seung-Jae V. Lee. 2016. “The Role of insulin/IGF-1 Signaling in the Longevity of Model Invertebrates, C. Elegans and D. Melanogaster.” *BMB Reports*. https://doi.org/10.5483/bmbrep.2016.49.2.261.

Amor, Sandra, Fabiola Puentes, David Baker, and Paul van der Valk. 2010. “Inflammation in Neurodegenerative Diseases.” *Immunology* 129 (2): 154–69.

Andrikopoulos, Petros, Julius Kieswich, Sabrina Pacheco, Luxme Nadarajah, Steven Michael Harwood, Caroline E. O’Riordan, Christoph Thiemermann, and Muhammad M. Yaqoob. 2019. “The MEK Inhibitor Trametinib Ameliorates Kidney Fibrosis by Suppressing ERK1/2 and mTORC1 Signaling.” *Journal of the American Society of Nephrology: JASN* 30 (1): 33–49.

Atella, Vincenzo, Andrea Piano Mortari, Joanna Kopinska, Federico Belotti, Francesco Lapi, Claudio Cricelli, and Luigi Fontana. 2019. “Trends in Age-Related Disease Burden and Healthcare Utilization.” *Aging Cell* 18 (1): e12861.

Ayata, Pinar, Ana Badimon, Hayley J. Strasburger, Mary Kaye Duff, Sarah E. Montgomery, Yong-Hwee E. Loh, Anja Ebert, et al. 2018. “Epigenetic Regulation of Brain Region-Specific Microglia Clearance Activity.” *Nature Neuroscience* 21 (8): 1049–60.

Badal, Varsha D., Eleonora D. Vaccariello, Emily R. Murray, Kasey E. Yu, Rob Knight, Dilip V. Jeste, and Tanya T. Nguyen. 2020. “The Gut Microbiome, Aging, and Longevity: A Systematic Review.” *Nutrients* 12 (12). https://doi.org/10.3390/nu12123759.

Báez-Mendoza, Raymundo, and Wolfram Schultz. 2013. “The Role of the Striatum in Social

Behavior.” *Frontiers in Neuroscience* 7 (December): 233.
Bai, Xiang, Margaret Chia-Ying Wey, Elizabeth Fernandez, Matthew J. Hart, Jonathan Gelfond, Alex F. Bokov, Sheela Rani, and Randy Strong. 2015. “Rapamycin Improves Motor Function, Reduces 4-Hydroxynonenal Adducted Protein in Brain, and Attenuates Synaptic Injury in a Mouse Model of Synucleinopathy.” *Pathobiology of Aging & Age Related Diseases* 5 (August): 28743.
Bajwa, Preety, Sarah Nielsen, Janine M. Lombard, Loui Rassam, Pravin Nahar, Bo R. Rueda, J. Erby Wilkinson, Richard A. Miller, and Pradeep S. Tanwar. 2017. “Overactive mTOR Signaling Leads to Endometrial Hyperplasia in Aged Women and Mice.” *Oncotarget*. https://doi.org/10.18632/oncotarget.13919.
Banerjee, Monica, Ramit Mehr, Alex Belelovsky, Jo Spencer, and Deborah K. Dunn-Walters. 2002a. “Age- and Tissue-Specific Differences in Human Germinal Center B Cell Selection Revealed by Analysis of IgVH Gene Hypermutation and Lineage Trees.” *European Journal of Immunology*. https://doi.org/10.1002/1521-4141(200207)32:7<1947::aid-immu1947>3.0.co;2-1.
———. 2002b. “Age- and Tissue-Specific Differences in Human Germinal Center B Cell Selection Revealed by Analysis of IgVH Gene Hypermutation and Lineage Trees.” *European Journal of Immunology* 32 (7): 1947–57.
Banerjee, Sutapa, Scott M. Gianino, Feng Gao, Uwe Christians, and David H. Gutmann. 2011. “Interpreting Mammalian Target of Rapamycin and Cell Growth Inhibition in a Genetically Engineered Mouse Model of *Nf1*-Deficient Astrocytes.” *Molecular Cancer Therapeutics*. https://doi.org/10.1158/1535-7163.mct-10-0654.
Banks, Alexander S., Fiona E. McAllister, João Paulo G. Camporez, Peter-James H. Zushin, Michael J. Jurczak, Dina Laznik-Bogoslavski, Gerald I. Shulman, Steven P. Gygi, and Bruce M. Spiegelman. 2015. “An ERK/Cdk5 Axis Controls the Diabetogenic Actions of PPARγ.” *Nature* 517 (7534): 391–95.
Banks, Mary, Karen Crowell, Amber Proctor, and Brian C. Jensen. 2017. “Cardiovascular Effects of the MEK Inhibitor, Trametinib: A Case Report, Literature Review, and Consideration of Mechanism.” *Cardiovascular Toxicology* 17 (4): 487–93.
Bansal, Ankita, Lihua J. Zhu, Kelvin Yen, and Heidi A. Tissenbaum. 2015. “Uncoupling Lifespan and Healthspan in Caenorhabditis Elegans Longevity Mutants.” *Proceedings of the National Academy of Sciences of the United States of America* 112 (3): E277–86.
Baquer, Najma Z., Asia Taha, Pardeep Kumar, P. McLean, S. M. Cowsik, R. K. Kale, R. Singh, and Deepak Sharma. 2009. “A Metabolic and Functional Overview of Brain Aging Linked to Neurological Disorders.” *Biogerontology* 10 (4): 377–413.
Bárcena, Clea, Rafael Valdés-Mas, Pablo Mayoral, Cecilia Garabaya, Sylvère Durand, Francisco Rodríguez, María Teresa Fernández-García, et al. 2019. “Healthspan and Lifespan Extension by Fecal Microbiota Transplantation into Progeroid Mice.” *Nature Medicine* 25 (8): 1234–42.
Baroja-Mazo, Alberto, Beatriz Revilla-Nuin, Pablo Ramírez, and José A. Pons. 2016. “Immunosuppressive Potency of Mechanistic Target of Rapamycin Inhibitors in Solid-Organ Transplantation.” *World Journal of Transplantation* 6 (1): 183–92.
Barreto, George, Ting-Ting Huang, and Rona G. Giffard. 2010. “Age-Related Defects in Sensorimotor Activity, Spatial Learning, and Memory in C57BL/6 Mice.” *Journal of Neurosurgical Anesthesiology* 22 (3): 214–19.
Belkaid, Yasmine, and Timothy W. Hand. 2014a. “Role of the Microbiota in Immunity and Inflammation.” *Cell*. https://doi.org/10.1016/j.cell.2014.03.011.
———. 2014b. “Role of the Microbiota in Immunity and Inflammation.” *Cell*. https://doi.org/10.1016/j.cell.2014.03.011.
Bergeron, Yan, Laure Chagniel, Geneviève Bureau, Guy Massicotte, and Michel Cyr. 2014. “mTOR Signaling Contributes to Motor Skill Learning in Mice.” *Frontiers in Molecular Neuroscience* 7 (April): 26.
Bitto, Alessandro, Takashi K. Ito, Victor V. Pineda, Nicolas J. LeTexier, Heather Z. Huang, Elissa Sutlief, Herman Tung, et al. 2016. “Transient Rapamycin Treatment Can Increase Lifespan and Healthspan in Middle-Aged Mice.” *eLife* 5 (August).

https://doi.org/10.7554/eLife.16351.
Bjedov, Ivana, Janne M. Toivonen, Fiona Kerr, Cathy Slack, Jake Jacobson, Andrea Foley, and Linda Partridge. 2010. “Mechanisms of Life Span Extension by Rapamycin in the Fruit Fly Drosophila Melanogaster.” *Cell Metabolism* 11 (1): 35–46.
Blüher, Matthias, Barbara B. Kahn, and C. Ronald Kahn. 2003. “Extended Longevity in Mice Lacking the Insulin Receptor in Adipose Tissue.” *Science* 299 (5606): 572–74.
Bokov, Alex F., Neha Garg, Yuji Ikeno, Sachin Thakur, Nicolas Musi, Ralph A. DeFronzo, Ning Zhang, et al. 2011. “Does Reduced IGF-1R Signaling in Igf1r+/- Mice Alter Aging?” *PloS One* 6 (11): e26891.
Bolen, Christopher R., Florian Rubelt, Jason A. Vander Heiden, and Mark M. Davis. 2017. “The Repertoire Dissimilarity Index as a Method to Compare Lymphocyte Receptor Repertoires.” *BMC Bioinformatics* 18 (1): 155.
Booth, Jayaum S., and Franklin R. Toapanta. 2021. “B and T Cell Immunity in Tissues and Across the Ages.” *Vaccines*. https://doi.org/10.3390/vaccines9010024.
Borrás, Consuelo, Daniel Monleón, Raul López-Grueso, Juan Gambini, Leonardo Orlando, Federico V. Pallardó, Eugenio Santos, José Viña, and Jaime Font de Mora. 2011. “RasGrf1 Deficiency Delays Aging in Mice.” *Aging* 3 (3): 262–76.
Bourcy, Charles F. A. de, Cesar J. Lopez Angel, Christopher Vollmers, Cornelia L. Dekker, Mark M. Davis, and Stephen R. Quake. 2017. “Phylogenetic Analysis of the Human Antibody Repertoire Reveals Quantitative Signatures of Immune Senescence and Aging.” *Proceedings of the National Academy of Sciences of the United States of America* 114 (5): 1105–10.
Bradshaw, William John, Michael Poeschla, Aleksandra Placzek, Samuel Kean, and Dario Riccardo Valenzano. 2022. “Extensive Age-Dependent Loss of Antibody Diversity in Naturally Short-Lived Turquoise Killifish.” *eLife* 11 (February). https://doi.org/10.7554/eLife.65117.
Brayton, C. F., P. M. Treuting, and J. M. Ward. 2012. “Pathobiology of Aging Mice and GEM: Background Strains and Experimental Design.” *Veterinary Pathology* 49 (1): 85–105.
Cahenzli, Julia, Yasmin Köller, Madeleine Wyss, Markus B. Geuking, and Kathy D. McCoy. 2013. “Intestinal Microbial Diversity during Early-Life Colonization Shapes Long-Term IgE Levels.” *Cell Host & Microbe* 14 (5): 559–70.
Callahan, Benjamin J., Paul J. McMurdie, Michael J. Rosen, Andrew W. Han, Amy Jo A. Johnson, and Susan P. Holmes. 2016. “DADA2: High-Resolution Sample Inference from Illumina Amplicon Data.” *Nature Methods* 13 (7): 581–83.
Campisi, Judith, Pankaj Kapahi, Gordon J. Lithgow, Simon Melov, John C. Newman, and Eric Verdin. 2019. “From Discoveries in Ageing Research to Therapeutics for Healthy Ageing.” *Nature* 571 (7764): 183–92.
Caporaso, J. Gregory, J. Gregory Caporaso, Christian L. Lauber, William A. Walters, Donna Berg-Lyons, Catherine A. Lozupone, Peter J. Turnbaugh, Noah Fierer, and Rob Knight. 2011. “Global Patterns of 16S rRNA Diversity at a Depth of Millions of Sequences per Sample.” *Proceedings of the National Academy of Sciences*. https://doi.org/10.1073/pnas.1000080107.
Carlson, Christian J., Sandra Koterski, Richard J. Sciotti, German Braillard Poccard, and Cristina M. Rondinone. 2003. “Enhanced Basal Activation of Mitogen-Activated Protein Kinases in Adipocytes from Type 2 Diabetes: Potential Role of p38 in the Downregulation of GLUT4 Expression.” *Diabetes* 52 (3): 634–41.
Castillo-Quan, Jorge Iván, Kerri J. Kinghorn, and Ivana Bjedov. 2015. “Genetics and Pharmacology of Longevity: The Road to Therapeutics for Healthy Aging.” *Advances in Genetics* 90 (July): 1–101.
Castillo-Quan, Jorge Iván, Luke S. Tain, Kerri J. Kinghorn, Li Li, Sebastian Grönke, Yvonne Hinze, T. Keith Blackwell, Ivana Bjedov, and Linda Partridge. 2019. “A Triple Drug Combination Targeting Components of the Nutrient-Sensing Network Maximizes Longevity.” *Proceedings of the National Academy of Sciences of the United States of America* 116 (42): 20817–19.
Castro-Dopico, Tomas, and Menna R. Clatworthy. 2019. “IgG and Fcγ Receptors in

Intestinal Immunity and Inflammation." *Frontiers in Immunology* 10 (April): 805.
Chapman, T., and L. Partridge. 1996. "Female Fitness in Drosophila Melanogaster: An Interaction between the Effect of Nutrition and of Encounter Rate with Males." *Proceedings. Biological Sciences / The Royal Society* 263 (1371): 755–59.
Chen, Chong, Yu Liu, Yang Liu, and Pan Zheng. 2009. "mTOR Regulation and Therapeutic Rejuvenation of Aging Hematopoietic Stem Cells." *Science Signaling* 2 (98): ra75.
Cheng, Chia-Wei, Gregor B. Adams, Laura Perin, Min Wei, Xiaoying Zhou, Ben S. Lam, Stefano Da Sacco, et al. 2014. "Prolonged Fasting Reduces IGF-1/PKA to Promote Hematopoietic-Stem-Cell-Based Regeneration and Reverse Immunosuppression." *Cell Stem Cell* 14 (6): 810–23.
Chen, Michael J., Supriya Ramesha, Laura D. Weinstock, Tianwen Gao, Lingyan Ping, Hailian Xiao, Eric B. Dammer, et al. 2021. "Extracellular Signal-Regulated Kinase Regulates Microglial Immune Responses in Alzheimer's Disease." *Journal of Neuroscience Research* 99 (6): 1704–21.
Chen, Yunyang, Weijie Wang, Huakai Wang, Yongjian Li, Minmin Shi, Hongwei Li, and Jiqi Yan. 2016. "Rapamycin Attenuates Splenomegaly in Both Intrahepatic and Prehepatic Portal Hypertensive Rats by Blocking mTOR Signaling Pathway." *PloS One* 11 (1): e0141159.
Chu, Chun-Hsien, Shijun Wang, Chia-Ling Li, Shih-Heng Chen, Chih-Fen Hu, Yi-Lun Chung, Shiou-Lan Chen, et al. 2016. "Neurons and Astroglia Govern Microglial Endotoxin Tolerance through Macrophage Colony-Stimulating Factor Receptor-Mediated ERK1/2 Signals." *Brain, Behavior, and Immunity* 55 (July): 260–72.
Chueh, Shih-Chieh J., and Barry D. Kahan. 2005. "Clinical Application of Sirolimus in Renal Transplantation: An Update." *Transplant International*. https://doi.org/10.1111/j.1432-2277.2004.00039.x.
Clancy, D. J., D. Gems, L. G. Harshman, S. Oldham, H. Stocker, E. Hafen, S. J. Leevers, and L. Partridge. 2001. "Extension of Life-Span by Loss of CHICO, a Drosophila Insulin Receptor Substrate Protein." *Science* 292 (5514): 104–6.
Collins, Patricia E., Domenico Somma, David Kerrigan, Felicity Herrington, Karen Keeshan, Robert J. B. Nibbs, and Ruaidhrí J. Carmody. 2019. "The IκB-Protein BCL-3 Controls Toll-like Receptor-Induced MAPK Activity by Promoting TPL-2 Degradation in the Nucleus." *Proceedings of the National Academy of Sciences of the United States of America* 116 (51): 25828–38.
Colman, Ricki J., T. Mark Beasley, Joseph W. Kemnitz, Sterling C. Johnson, Richard Weindruch, and Rozalyn M. Anderson. 2014. "Caloric Restriction Reduces Age-Related and All-Cause Mortality in Rhesus Monkeys." *Nature Communications* 5 (April): 3557.
Colonna-Romano, Giuseppina, Alessandra Aquino, Matteo Bulati, Gabriele Di Lorenzo, Florinda Listì, Salvatore Vitello, Domenico Lio, Giuseppina Candore, Gioacchino Clesi, and Calogero Caruso. 2006. "Memory B Cell Subpopulations in the Aged." *Rejuvenation Research* 9 (1): 149–52.
Comelli, Martina, Marianna Meo, Daniel O. Cervantes, Emanuele Pizzo, Aaron Plosker, Peter J. Mohler, Thomas J. Hund, Jason T. Jacobson, Olivier Meste, and Marcello Rota. 2020. "Rhythm Dynamics of the Aging Heart: An Experimental Study Using Conscious, Restrained Mice." *American Journal of Physiology. Heart and Circulatory Physiology* 319 (4): H893–905.
Cook, Graham. 2000. "Immunobiology: The Immune System in Health and Disease (4th Edn) by C.A. Janeway, P. Travers, M. Walport and J.D. Capra." *Immunology Today*. https://doi.org/10.1016/s0167-5699(00)01613-3.
Dai, Dao-Fu, Pabalu P. Karunadharma, Ying A. Chiao, Nathan Basisty, David Crispin, Edward J. Hsieh, Tony Chen, et al. 2014. "Altered Proteome Turnover and Remodeling by Short-Term Caloric Restriction or Rapamycin Rejuvenate the Aging Heart." *Aging Cell* 13 (3): 529–39.
Dienel, Gerald A. 2019. "Brain Glucose Metabolism: Integration of Energetics with Function." *Physiological Reviews* 99 (1): 949–1045.
Dimitrov, Jordan D., Cyril Planchais, Lubka T. Roumenina, Tchavdar L. Vassilev, Srinivas V.

Kaveri, and Sebastien Lacroix-Desmazes. 2013. “Antibody Polyreactivity in Health and Disease: Statu Variabilis.” *Journal of Immunology* 191 (3): 993–99.
Donaldson, David S., Barbara B. Shih, and Neil A. Mabbott. 2021. “Aging-Related Impairments to M Cells in Peyer’s Patches Coincide With Disturbances to Paneth Cells.” *Frontiers in Immunology*. https://doi.org/10.3389/fimmu.2021.761949.
Dunn-Walters, D. K. 2015. “The Ageing Human B Cell Repertoire: A Failure of Selection?” *Clinical and Experimental Immunology*. https://doi.org/10.1111/cei.12700.
———. 2016. “The Ageing Human B Cell Repertoire: A Failure of Selection?” *Clinical & Experimental Immunology*. https://doi.org/10.1111/cei.12700.
Dunn-Walters, D. K., M. Banerjee, and R. Mehr. 2003. “Effects of Age on Antibody Affinity Maturation.” *Biochemical Society Transactions* 31 (2): 447–48.
Ettlin, R. A., P. Stirnimann, and D. E. Prentice. 1994. “Causes of Death in Rodent Toxicity and Carcinogenicity Studies.” *Toxicologic Pathology* 22 (2): 165–78.
Fabrizio, Paola, Lee-Loung Liou, Vanessa N. Moy, Alberto Diaspro, Joan Selverstone Valentine, Edith Butler Gralla, and Valter D. Longo. 2003. “SOD2 Functions Downstream of Sch9 to Extend Longevity in Yeast.” *Genetics* 163 (1): 35–46.
Feng, Xiaofeng, Jianying Pan, Junyan Li, Chun Zeng, Weizhong Qi, Yan Shao, Xin Liu, et al. 2020. “Metformin Attenuates Cartilage Degeneration in an Experimental Osteoarthritis Model by Regulating AMPK/mTOR.” *Aging* 12 (2): 1087–1103.
Flatt, Thomas, and Linda Partridge. 2018. “Horizons in the Evolution of Aging.” *BMC Biology* 16 (1): 93.
Flynn, James M., Monique N. O’Leary, Christopher A. Zambataro, Emmeline C. Academia, Michael P. Presley, Brittany J. Garrett, Artem Zykovich, et al. 2013. “Late-Life Rapamycin Treatment Reverses Age-Related Heart Dysfunction.” *Aging Cell* 12 (5): 851–62.
Fok, Wilson C., Yidong Chen, Alex Bokov, Yiqiang Zhang, Adam B. Salmon, Vivian Diaz, Martin Javors, et al. 2014. “Mice Fed Rapamycin Have an Increase in Lifespan Associated with Major Changes in the Liver Transcriptome.” *PloS One* 9 (1): e83988.
Fontana, Luigi, Brian K. Kennedy, Valter D. Longo, Douglas Seals, and Simon Melov. 2014. “Medical Research: Treat Ageing.” *Nature*. https://doi.org/10.1038/511405a.
Fontana, Luigi, and Samuel Klein. 2007. “Aging, Adiposity, and Calorie Restriction.” *JAMA: The Journal of the American Medical Association* 297 (9): 986–94.
Fontana, Luigi, Timothy E. Meyer, Samuel Klein, and John O. Holloszy. 2004. “Long-Term Calorie Restriction Is Highly Effective in Reducing the Risk for Atherosclerosis in Humans.” *Proceedings of the National Academy of Sciences of the United States of America* 101 (17): 6659–63.
Fontana, Luigi, and Linda Partridge. 2015. “Promoting Health and Longevity through Diet: From Model Organisms to Humans.” *Cell* 161 (1): 106–18.
Fontana, Luigi, Linda Partridge, and Valter D. Longo. 2010. “Extending Healthy Life Span—From Yeast to Humans.” *Science* 328 (5976): 321–26.
Frasca, Daniela, and Bonnie B. Blomberg. 2009. “Effects of Aging on B Cell Function.” *Current Opinion in Immunology*. https://doi.org/10.1016/j.coi.2009.06.001.
Fujishita, Teruaki, Rie Kajino-Sakamoto, Yasushi Kojima, Makoto Mark Taketo, and Masahiro Aoki. 2015. “Antitumor Activity of the MEK Inhibitor Trametinib on Intestinal Polyp Formation in Apc(Δ716) Mice Involves Stromal COX-2.” *Cancer Science* 106 (6): 692–99.
Gadala-Maria, Daniel, Gur Yaari, Mohamed Uduman, and Steven H. Kleinstein. 2015. “Automated Analysis of High-Throughput B-Cell Sequencing Data Reveals a High Frequency of Novel Immunoglobulin V Gene Segment Alleles.” *Proceedings of the National Academy of Sciences of the United States of America* 112 (8): E862–70.
García-Prat, Laura, Marta Martínez-Vicente, Eusebio Perdiguero, Laura Ortet, Javier Rodríguez-Ubreva, Elena Rebollo, Vanessa Ruiz-Bonilla, et al. 2016. “Autophagy Maintains Stemness by Preventing Senescence.” *Nature* 529 (7584): 37–42.
Ge, Chunxi, Guozhi Xiao, Di Jiang, and Renny T. Franceschi. 2007. “Critical Role of the Extracellular Signal-Regulated Kinase-MAPK Pathway in Osteoblast Differentiation and

Skeletal Development." *The Journal of Cell Biology* 176 (5): 709–18.
Ghraichy, Marie, Valentin von Niederhäusern, Aleksandr Kovaltsuk, Jacob D. Galson, Charlotte M. Deane, and Johannes Trück. 2021. "Different B Cell Subpopulations Show Distinct Patterns in Their IgH Repertoire Metrics." *eLife* 10 (October). https://doi.org/10.7554/eLife.73111.
Giannakou, Maria E., Martin Goss, Martin A. Jünger, Ernst Hafen, Sally J. Leevers, and Linda Partridge. 2004. "Long-Lived Drosophila with Overexpressed dFOXO in Adult Fat Body." *Science* 305 (5682): 361.
Giannini, Edoardo G., Roberto Testa, and Vincenzo Savarino. 2005. "Liver Enzyme Alteration: A Guide for Clinicians." *CMAJ: Canadian Medical Association Journal = Journal de l'Association Medicale Canadienne* 172 (3): 367–79.
Gibson, Kate L., Yu-Chang Wu, Yvonne Barnett, Orla Duggan, Robert Vaughan, Elli Kondeatis, Bengt-Olof Nilsson, Anders Wikby, David Kipling, and Deborah K. Dunn-Walters. 2009. "B-Cell Diversity Decreases in Old Age and Is Correlated with Poor Health Status." *Aging Cell* 8 (1): 18–25.
Giudicelli, V. 2004. "IMGT/GENE-DB: A Comprehensive Database for Human and Mouse Immunoglobulin and T Cell Receptor Genes." *Nucleic Acids Research*. https://doi.org/10.1093/nar/gki010.
Goitre, Luca, Eliana Trapani, Lorenza Trabalzini, and Saverio Francesco Retta. 2014. "The Ras Superfamily of Small GTPases: The Unlocked Secrets." *Methods in Molecular Biology* 1120: 1–18.
Gooijer, Mark C. de, Ping Zhang, Ruud Weijer, Levi C. M. Buil, Jos H. Beijnen, and Olaf van Tellingen. 2018. "The Impact of P-Glycoprotein and Breast Cancer Resistance Protein on the Brain Pharmacokinetics and Pharmacodynamics of a Panel of MEK Inhibitors." *International Journal of Cancer. Journal International Du Cancer* 142 (2): 381–91.
Gould, Hannah J., and Brian J. Sutton. 2008. "IgE in Allergy and Asthma Today." *Nature Reviews Immunology*. https://doi.org/10.1038/nri2273.
Grandison, Richard C., Matthew D. W. Piper, and Linda Partridge. 2009. "Amino-Acid Imbalance Explains Extension of Lifespan by Dietary Restriction in Drosophila." *Nature* 462 (7276): 1061–64.
Green, Cara L., Dudley W. Lamming, and Luigi Fontana. 2022. "Molecular Mechanisms of Dietary Restriction Promoting Health and Longevity." *Nature Reviews. Molecular Cell Biology* 23 (1): 56–73.
Greiff, Victor, Cédric R. Weber, Johannes Palme, Ulrich Bodenhofer, Enkelejda Miho, Ulrike Menzel, and Sai T. Reddy. 2017. "Learning the High-Dimensional Immunogenomic Features That Predict Public and Private Antibody Repertoires." *Journal of Immunology* 199 (8): 2985–97.
Grönke, Sebastian, David-Francis Clarke, Susan Broughton, T. Daniel Andrews, and Linda Partridge. 2010. "Molecular Evolution and Functional Characterization of Drosophila Insulin-like Peptides." *PLoS Genetics* 6 (2): e1000857.
Guma, Monica, Dariusz Stepniak, Helena Shaked, Martina E. Spehlmann, Steve Shenouda, Hilde Cheroutre, Ildelfonso Vicente-Suarez, Lars Eckmann, Martin F. Kagnoff, and Michael Karin. 2011. "Constitutive Intestinal NF-κB Does Not Trigger Destructive Inflammation Unless Accompanied by MAPK Activation." *The Journal of Experimental Medicine* 208 (9): 1889–1900.
Gunti, Sreenivasulu, and Abner Louis Notkins. 2015. "Polyreactive Antibodies: Function and Quantification." *The Journal of Infectious Diseases* 212 Suppl 1 (July): S42–46.
Gupta, Namita T., Jason A. Vander Heiden, Mohamed Uduman, Daniel Gadala-Maria, Gur Yaari, and Steven H. Kleinstein. 2015. "Change-O: A Toolkit for Analyzing Large-Scale B Cell Immunoglobulin Repertoire Sequencing Data." *Bioinformatics* 31 (20): 3356–58.
Gutzeit, Cindy, Kang Chen, and Andrea Cerutti. 2018. "The Enigmatic Function of IgD: Some Answers at Last." *European Journal of Immunology* 48 (7): 1101–13.
Göbel, Jana, Esther Engelhardt, Patric Pelzer, Vignesh Sakthivelu, Hannah M. Jahn, Milica Jevtic, Kat Folz-Donahue, et al. 2020. "Mitochondria-Endoplasmic Reticulum Contacts in Reactive Astrocytes Promote Vascular Remodeling." *Cell Metabolism* 31 (4): 791–

808.e8.
Hahn, Oliver, Lisa F. Drews, An Nguyen, Takashi Tatsuta, Lisonia Gkioni, Oliver Hendrich, Qifeng Zhang, et al. 2019. “A Nutritional Memory Effect Counteracts Benefits of Dietary Restriction in Old Mice.” *Nature Metabolism* 1 (11): 1059–73.
Hahn, Oliver, Sebastian Grönke, Thomas M. Stubbs, Gabriella Ficz, Oliver Hendrich, Felix Krueger, Simon Andrews, et al. 2017. “Dietary Restriction Protects from Age-Associated DNA Methylation and Induces Epigenetic Reprogramming of Lipid Metabolism.” *Genome Biology* 18 (1): 56.
Haller, Samantha, Subir Kapuria, Rebeccah R. Riley, Monique N. O’Leary, Katherine H. Schreiber, Julie K. Andersen, Simon Melov, et al. 2017. “mTORC1 Activation during Repeated Regeneration Impairs Somatic Stem Cell Maintenance.” *Cell Stem Cell* 21 (6): 806–18.e5.
Halloran, Bernard P., Virginia L. Ferguson, Steven J. Simske, Andrew Burghardt, Laura L. Venton, and Sharmila Majumdar. 2002. “Changes in Bone Structure and Mass with Advancing Age in the Male C57BL/6J Mouse.” *Journal of Bone and Mineral Research: The Official Journal of the American Society for Bone and Mineral Research* 17 (6): 1044–50.
Halloran, J., S. A. Hussong, R. Burbank, N. Podlutskaya, K. E. Fischer, L. B. Sloane, S. N. Austad, et al. 2012. “Chronic Inhibition of Mammalian Target of Rapamycin by Rapamycin Modulates Cognitive and Non-Cognitive Components of Behavior throughout Lifespan in Mice.” *Neuroscience* 223 (October): 102–13.
Harrison, David E., Randy Strong, Peter Reifsnyder, Navasuja Kumar, Elizabeth Fernandez, Kevin Flurkey, Martin A. Javors, et al. 2021. “17-a-Estradiol Late in Life Extends Lifespan in Aging UM-HET3 Male Mice; Nicotinamide Riboside and Three Other Drugs Do Not Affect Lifespan in Either Sex.” *Aging Cell* 20 (5): e13328.
Harrison, David E., Randy Strong, Zelton Dave Sharp, James F. Nelson, Clinton M. Astle, Kevin Flurkey, Nancy L. Nadon, et al. 2009. “Rapamycin Fed Late in Life Extends Lifespan in Genetically Heterogeneous Mice.” *Nature* 460 (7253): 392–95.
Harvie, M. N., M. Pegington, M. P. Mattson, J. Frystyk, B. Dillon, G. Evans, J. Cuzick, et al. 2011. “The Effects of Intermittent or Continuous Energy Restriction on Weight Loss and Metabolic Disease Risk Markers: A Randomized Trial in Young Overweight Women.” *International Journal of Obesity* 35 (5): 714–27.
Heiden, Jason A. Vander, Jason A. Vander Heiden, Gur Yaari, Mohamed Uduman, Joel N. H. Stern, Kevin C. O’Connor, David A. Hafler, Francois Vigneault, and Steven H. Kleinstein. 2014. “pRESTO: A Toolkit for Processing High-Throughput Sequencing Raw Reads of Lymphocyte Receptor Repertoires.” *Bioinformatics*. https://doi.org/10.1093/bioinformatics/btu138.
Hernández-Vicente, Adrián, David Hernando, Alejandro Santos-Lozano, Gabriel Rodríguez-Romo, Germán Vicente-Rodríguez, Esther Pueyo, Raquel Bailón, and Nuria Garatachea. 2020. “Heart Rate Variability and Exceptional Longevity.” *Frontiers in Physiology* 11 (September): 566399.
Hickman, Suzanne, Saef Izzy, Pritha Sen, Liza Morsett, and Joseph El Khoury. 2018. “Microglia in Neurodegeneration.” *Nature Neuroscience* 21 (10): 1359–69.
Higuchi, Chikahisa, Akira Myoui, Nobuyuki Hashimoto, Kohji Kuriyama, Kiyoko Yoshioka, Hideki Yoshikawa, and Kazuyuki Itoh. 2002. “Continuous Inhibition of MAPK Signaling Promotes the Early Osteoblastic Differentiation and Mineralization of the Extracellular Matrix.” *Journal of Bone and Mineral Research: The Official Journal of the American Society for Bone and Mineral Research* 17 (10): 1785–94.
Hill, M. O. 1973. “Diversity and Evenness: A Unifying Notation and Its Consequences.” *Ecology*. https://doi.org/10.2307/1934352.
Hoehn, Kenneth B., Jason A. Vander Heiden, Julian Q. Zhou, Gerton Lunter, Oliver G. Pybus, and Steven H. Kleinstein. 2019. “Repertoire-Wide Phylogenetic Models of B Cell Molecular Evolution Reveal Evolutionary Signatures of Aging and Vaccination.” *Proceedings of the National Academy of Sciences of the United States of America* 116 (45): 22664–72.

Hoffner, Brianna, and Katherine Benchich. 2018. “Trametinib: A Targeted Therapy in Metastatic Melanoma.” *Journal of the Advanced Practitioner in Oncology* 9 (7): 741–45.
Holodick, Nichol E., Teresa Vizconde, Thomas J. Hopkins, and Thomas L. Rothstein. 2016. “Age-Related Decline in Natural IgM Function: Diversification and Selection of the B-1a Cell Pool with Age.” *Journal of Immunology* 196 (10): 4348–57.
Holzenberger, Martin, Joëlle Dupont, Bertrand Ducos, Patricia Leneuve, Alain Géloën, Patrick C. Even, Pascale Cervera, and Yves Le Bouc. 2003. “IGF-1 Receptor Regulates Lifespan and Resistance to Oxidative Stress in Mice.” *Nature* 421 (6919): 182–87.
Honjoh, Sakiko, Takuya Yamamoto, Masaharu Uno, and Eisuke Nishida. 2009. “Signalling through RHEB-1 Mediates Intermittent Fasting-Induced Longevity in C. Elegans.” *Nature* 457 (7230): 726–30.
Hutchinson, Peter J., Mark T. O’Connell, Alex Seal, Jurgens Nortje, Ivan Timofeev, Pippa G. Al-Rawi, Jonathan P. Coles, et al. 2009. “A Combined Microdialysis and FDG-PET Study of Glucose Metabolism in Head Injury.” *Acta Neurochirurgica* 151 (1): 51–61; discussion 61.
Hu, Yuanyu, Emily Chan, Sherry X. Wang, and Baojie Li. 2003. “Activation of p38 Mitogen-Activated Protein Kinase Is Required for Osteoblast Differentiation.” *Endocrinology* 144 (5): 2068–74.
Ikeno, Yuji, Gene B. Hubbard, Shuko Lee, Lisa A. Cortez, Christie M. Lew, Celeste R. Webb, Darlene E. Berryman, Edward O. List, John J. Kopchick, and Andrzej Bartke. 2009. “Reduced Incidence and Delayed Occurrence of Fatal Neoplastic Diseases in Growth Hormone Receptor/binding Protein Knockout Mice.” *The Journals of Gerontology. Series A, Biological Sciences and Medical Sciences* 64 (5): 522–29.
Ikeno, Yuji, Christie M. Lew, Lisa A. Cortez, Celeste R. Webb, Shuko Lee, and Gene B. Hubbard. 2006. “Do Long-Lived Mutant and Calorie-Restricted Mice Share Common Anti-Aging Mechanisms?--a Pathological Point of View.” *Age* 28 (2): 163–71.
Infante, Jeffrey R., Leslie A. Fecher, Gerald S. Falchook, Sujatha Nallapareddy, Michael S. Gordon, Carlos Becerra, Douglas J. DeMarini, et al. 2012. “Safety, Pharmacokinetic, Pharmacodynamic, and Efficacy Data for the Oral MEK Inhibitor Trametinib: A Phase 1 Dose-Escalation Trial.” *The Lancet Oncology* 13 (8): 773–81.
Jager, Jennifer, Thierry Grémeaux, Teresa Gonzalez, Stéphanie Bonnafous, Cyrille Debard, Martine Laville, Hubert Vidal, et al. 2010. “Tpl2 Kinase Is Upregulated in Adipose Tissue in Obesity and May Mediate Interleukin-1beta and Tumor Necrosis Factor-{alpha} Effects on Extracellular Signal-Regulated Kinase Activation and Lipolysis.” *Diabetes* 59 (1): 61–70.
Jakubowicz, Daniela, Maayan Barnea, Julio Wainstein, and Oren Froy. 2013. “Effects of Caloric Intake Timing on Insulin Resistance and Hyperandrogenism in Lean Women with Polycystic Ovary Syndrome.” *Clinical Science* 125 (9): 423–32.
Jalloh, Ibrahim, Keri L. H. Carpenter, Adel Helmy, T. Adrian Carpenter, David K. Menon, and Peter J. Hutchinson. 2015. “Glucose Metabolism Following Human Traumatic Brain Injury: Methods of Assessment and Pathophysiological Findings.” *Metabolic Brain Disease* 30 (3): 615–32.
Jamar, Francois, John Buscombe, Arturo Chiti, Paul E. Christian, Dominique Delbeke, Kevin J. Donohoe, Ora Israel, Josep Martin-Comin, and Alberto Signore. 2013. “EANM/SNMMI Guideline for 18F-FDG Use in Inflammation and Infection.” *Journal of Nuclear Medicine: Official Publication, Society of Nuclear Medicine* 54 (4): 647–58.
Jiang, Ning, Jiankui He, Joshua A. Weinstein, Lolita Penland, Sanae Sasaki, Xiao-Song He, Cornelia L. Dekker, et al. 2013. “Lineage Structure of the Human Antibody Repertoire in Response to Influenza Vaccination.” *Science Translational Medicine* 5 (171): 171ra19.
Kaeberlein, Matt. 2018. “How Healthy Is the Healthspan Concept?” *GeroScience* 40 (4): 361–64.
Kaeberlein, Matt, and Veronica Galvan. 2019. “Rapamycin and Alzheimer’s Disease: Time for a Clinical Trial?” *Science Translational Medicine* 11 (476). https://doi.org/10.1126/scitranslmed.aar4289.
Kamada, Nobuhiko, Grace Y. Chen, Naohiro Inohara, and Gabriel Núñez. 2013. “Control of

Pathogens and Pathobionts by the Gut Microbiota." *Nature Immunology* 14 (7): 685–90.
Kapahi, Pankaj, Brian M. Zid, Tony Harper, Daniel Koslover, Viveca Sapin, and Seymour Benzer. 2004. "Regulation of Lifespan in Drosophila by Modulation of Genes in the TOR Signaling Pathway." *Current Biology: CB* 14 (10): 885–90.
Kauffman, H. Myron, Wida S. Cherikh, Yulin Cheng, Douglas W. Hanto, and Barry D. Kahan. 2005. "Maintenance Immunosuppression with Target-of-Rapamycin Inhibitors Is Associated with a Reduced Incidence of de Novo Malignancies." *Transplantation* 80 (7): 883–89.
Keane, Lily, Ignazio Antignano, Sean-Patrick Riechers, Raphael Zollinger, Anaelle A. Dumas, Nina Offermann, Maria E. Bernis, et al. 2021. "mTOR-Dependent Translation Amplifies Microglia Priming in Aging Mice." *The Journal of Clinical Investigation* 131 (20). https://doi.org/10.1172/JCI155208.
Kennard, John A., and Diana S. Woodruff-Pak. 2011. "Age Sensitivity of Behavioral Tests and Brain Substrates of Normal Aging in Mice." *Frontiers in Aging Neuroscience* 3 (May): 9.
Kenyon, Cynthia. 2011. "The First Long-Lived Mutants: Discovery of the insulin/IGF-1 Pathway for Ageing." *Philosophical Transactions of the Royal Society of London. Series B, Biological Sciences* 366 (1561): 9–16.
Kenyon, Cynthia, Jean Chang, Erin Gensch, Adam Rudner, and Ramon Tabtiang. 1993. "A C. Elegans Mutant That Lives Twice as Long as Wild Type." *Nature*. https://doi.org/10.1038/366461a0.
Kerstjens, Mark, Sandra S. Pinhancos, Patricia Garrido Castro, Pauline Schneider, Priscilla Wander, Rob Pieters, and Ronald W. Stam. 2018. "Trametinib Inhibits RAS-Mutant MLL-Rearranged Acute Lymphoblastic Leukemia at Specific Niche Sites and Reduces ERK Phosphorylation in Vivo." *Haematologica* 103 (4): e147–50.
Khakh, Baljit S., and Michael V. Sofroniew. 2015. "Diversity of Astrocyte Functions and Phenotypes in Neural Circuits." *Nature Neuroscience* 18 (7): 942–52.
Khan, Tarik A., Simon Friedensohn, Arthur R. Gorter de Vries, Jakub Straszewski, Hans-Joachim Ruscheweyh, and Sai T. Reddy. 2016. "Accurate and Predictive Antibody Repertoire Profiling by Molecular Amplification Fingerprinting." *Science Advances* 2 (3): e1501371.
Kim, Chul, and Giuseppe Giaccone. 2018. "MEK Inhibitors under Development for Treatment of Non-Small-Cell Lung Cancer." *Expert Opinion on Investigational Drugs* 27 (1): 17–30.
Kim, Eun-A, A. Reum Han, Jiyoung Choi, Jee-Yin Ahn, Soo Young Choi, and Sung-Woo Cho. 2014. "Anti-Inflammatory Mechanisms of N-Adamantyl-4-Methylthiazol-2-Amine in Lipopolysaccharide-Stimulated BV-2 Microglial Cells." *International Immunopharmacology* 22 (1): 73–83.
Kok, Dieuwertje E. G., Fenni Rusli, Benthe van der Lugt, Carolien Lute, Luca Laghi, Stefano Salvioli, Gianfranco Picone, et al. 2018. "Lifelong Calorie Restriction Affects Indicators of Colonic Health in Aging C57Bl/6J Mice." *The Journal of Nutritional Biochemistry* 56 (June): 152–64.
Koohy, Hashem, Daniel J. Bolland, Louise S. Matheson, Stefan Schoenfelder, Claudia Stellato, Andrew Dimond, Csilla Várnai, et al. 2018. "Genome Organization and Chromatin Analysis Identify Transcriptional Downregulation of Insulin-like Growth Factor Signaling as a Hallmark of Aging in Developing B Cells." *Genome Biology* 19 (1): 126.
Kopelovich, Levy, Judith R. Fay, Caroline C. Sigman, and James A. Crowell. 2007. "The Mammalian Target of Rapamycin Pathway as a Potential Target for Cancer Chemoprevention." *Cancer Epidemiology, Biomarkers & Prevention: A Publication of the American Association for Cancer Research, Cosponsored by the American Society of Preventive Oncology* 16 (7): 1330–40.
Kreutzberg, G. W. 1996. "Microglia: A Sensor for Pathological Events in the CNS." *Trends in Neurosciences* 19 (8): 312–18.
Kroeger, Cynthia M., Kristin K. Hoddy, and Krista A. Varady. 2014. "Impact of Weight Regain on Metabolic Disease Risk: A Review of Human Trials." *Journal of Obesity* 2014

(August): 614519.
Kuningas, Maris, Reedik Mägi, Rudi G. J. Westendorp, P. Eline Slagboom, Maido Remm, and Diana van Heemst. 2007. “Haplotypes in the Human Foxo1a and Foxo3a Genes; Impact on Disease and Mortality at Old Age.” *European Journal of Human Genetics: EJHG* 15 (3): 294–301.
Lambert, J. C., C. A. Ibrahim-Verbaas, D. Harold, A. C. Naj, R. Sims, C. Bellenguez, A. L. DeStafano, et al. 2013. “Meta-Analysis of 74,046 Individuals Identifies 11 New Susceptibility Loci for Alzheimer’s Disease.” *Nature Genetics* 45 (12): 1452–58.
Langford-Smith, A., M. Malinowska, K. J. Langford-Smith, G. Wegrzyn, S. Jones, R. Wynn, J. E. Wraith, F. L. Wilkinson, and B. W. Bigger. 2011. “Hyperactive Behaviour in the Mouse Model of Mucopolysaccharidosis IIIB in the Open Field and Home Cage Environments.” *Genes, Brain, and Behavior* 10 (6): 673–82.
Lang, Roland, Michael Hammer, and Jörg Mages. 2006. “DUSP Meet Immunology: Dual Specificity MAPK Phosphatases in Control of the Inflammatory Response.” *Journal of Immunology* 177 (11): 7497–7504.
Lang, Roland, and Faizal A. M. Raffi. 2019. “Dual-Specificity Phosphatases in Immunity and Infection: An Update.” *International Journal of Molecular Sciences* 20 (11). https://doi.org/10.3390/ijms20112710.
Laplante, Mathieu, and David M. Sabatini. 2009. “mTOR Signaling at a Glance.” *Journal of Cell Science* 122 (Pt 20): 3589–94.
Larson, Eric D., Joshua R. St Clair, Whitney A. Sumner, Roger A. Bannister, and Cathy Proenza. 2013. “Depressed Pacemaker Activity of Sinoatrial Node Myocytes Contributes to the Age-Dependent Decline in Maximum Heart Rate.” *Proceedings of the National Academy of Sciences of the United States of America* 110 (44): 18011–16.
Latorre, Eva, Vishal C. Birar, Angela N. Sheerin, J. Charles C. Jeynes, Amy Hooper, Helen R. Dawe, David Melzer, et al. 2017. “Small Molecule Modulation of Splicing Factor Expression Is Associated with Rescue from Cellular Senescence.” *BMC Cell Biology* 18 (1): 31.
Lee, Changhan, Lizzia Raffaghello, Sebastian Brandhorst, Fernando M. Safdie, Giovanna Bianchi, Alejandro Martin-Montalvo, Vito Pistoia, et al. 2012. “Fasting Cycles Retard Growth of Tumors and Sensitize a Range of Cancer Cell Types to Chemotherapy.” *Science Translational Medicine* 4 (124): 124ra27.
Lefèvre, Lise, Jason S. Iacovoni, Hélène Martini, Julie Bellière, Damien Maggiorani, Marianne Dutaur, Dimitri J. Marsal, et al. 2021. “Kidney Inflammaging Is Promoted by CCR2 Macrophages and Tissue-Derived Micro-Environmental Factors.” *Cellular and Molecular Life Sciences: CMLS* 78 (7): 3485–3501.
Le Gallou, Simon, Zhicheng Zhou, Lan-Huong Thai, Remi Fritzen, Alba Verge de Los Aires, Jérôme Mégret, Philipp Yu, et al. 2018. “A Splenic IgM Memory Subset with Antibacterial Specificities Is Sustained from Persistent Mucosal Responses.” *The Journal of Experimental Medicine* 215 (8): 2035–53.
Le Pelletier, Laura, Matthieu Mantecon, Jennifer Gorwood, Martine Auclair, Roberta Foresti, Roberto Motterlini, Mireille Laforge, et al. 2021. “Metformin Alleviates Stress-Induced Cellular Senescence of Aging Human Adipose Stromal Cells and the Ensuing Adipocyte Dysfunction.” *eLife* 10 (September). https://doi.org/10.7554/eLife.62635.
Lieberthal, Wilfred, and Jerrold S. Levine. 2009. “The Role of the Mammalian Target of Rapamycin (mTOR) in Renal Disease.” *Journal of the American Society of Nephrology: JASN* 20 (12): 2493–2502.
Lim, Hye-Sun, Yu Jin Kim, Bu-Yeo Kim, Gunhyuk Park, and Soo-Jin Jeong. 2018. “The Anti-Neuroinflammatory Activity of Tectorigenin Pretreatment via Downregulated NF-κB and ERK/JNK Pathways in BV-2 Microglial and Microglia Inactivation in Mice With Lipopolysaccharide.” *Frontiers in Pharmacology* 9 (May): 462.
Lin, Ai-Ling, Wei Zheng, Jonathan J. Halloran, Raquel R. Burbank, Stacy A. Hussong, Matthew J. Hart, Martin Javors, et al. 2013. “Chronic Rapamycin Restores Brain Vascular Integrity and Function through NO Synthase Activation and Improves Memory in Symptomatic Mice Modeling Alzheimer’s Disease.” *Journal of Cerebral Blood Flow*

and Metabolism: Official Journal of the International Society of Cerebral Blood Flow and Metabolism 33 (9): 1412–21.
Lindner, Cornelia, Irene Thomsen, Benjamin Wahl, Milas Ugur, Maya K. Sethi, Michaela Friedrichsen, Anna Smoczek, et al. 2015a. “Diversification of Memory B Cells Drives the Continuous Adaptation of Secretory Antibodies to Gut Microbiota.” *Nature Immunology* 16 (8): 880–88.
———. 2015b. “Diversification of Memory B Cells Drives the Continuous Adaptation of Secretory Antibodies to Gut Microbiota.” *Nature Immunology* 16 (8): 880–88.
———. 2015c. “Diversification of Memory B Cells Drives the Continuous Adaptation of Secretory Antibodies to Gut Microbiota.” *Nature Immunology* 16 (8): 880–88.
Lindner, Cornelia, Benjamin Wahl, Lisa Föhse, Sebastian Suerbaum, Andrew J. Macpherson, Immo Prinz, and Oliver Pabst. 2012. “Age, Microbiota, and T Cells Shape Diverse Individual IgA Repertoires in the Intestine.” *Journal of Experimental Medicine*. https://doi.org/10.1084/jem.20111980.
Lin, K., J. B. Dorman, A. Rodan, and C. Kenyon. 1997. “Daf-16: An HNF-3/forkhead Family Member That Can Function to Double the Life-Span of Caenorhabditis Elegans.” *Science* 278 (5341): 1319–22.
Lipman, Ruth, Andrzej Galecki, David T. Burke, and Richard A. Miller. 2004. “Genetic Loci That Influence Cause of Death in a Heterogeneous Mouse Stock.” *The Journals of Gerontology. Series A, Biological Sciences and Medical Sciences* 59 (10): 977–83.
Liu, Y. 2006. “Rapamycin and Chronic Kidney Disease: Beyond the Inhibition of Inflammation.” *Kidney International*.
Longo, Valter D., Adam Antebi, Andrzej Bartke, Nir Barzilai, Holly M. Brown-Borg, Calogero Caruso, Tyler J. Curiel, et al. 2015. “Interventions to Slow Aging in Humans: Are We Ready?” *Aging Cell* 14 (4): 497–510.
López-Otín, Carlos, Maria A. Blasco, Linda Partridge, Manuel Serrano, and Guido Kroemer. 2013. “The Hallmarks of Aging.” *Cell*. https://doi.org/10.1016/j.cell.2013.05.039.
Lugt, Benthe van der, Fenni Rusli, Carolien Lute, Andreas Lamprakis, Ethel Salazar, Mark V. Boekschoten, Guido J. Hooiveld, et al. 2018. “Integrative Analysis of Gut Microbiota Composition, Host Colonic Gene Expression and Intraluminal Metabolites in Aging C57BL/6J Mice.” *Aging* 10 (5): 930–50.
Lu, Nathan, and Charles J. Malemud. 2019. “Extracellular Signal-Regulated Kinase: A Regulator of Cell Growth, Inflammation, Chondrocyte and Bone Cell Receptor-Mediated Gene Expression.” *International Journal of Molecular Sciences* 20 (15). https://doi.org/10.3390/ijms20153792.
Macpherson, Andrew J., Bahtiyar Yilmaz, Julien P. Limenitakis, and Stephanie C. Ganal-Vonarburg. 2018a. “IgA Function in Relation to the Intestinal Microbiota.” *Annual Review of Immunology*. https://doi.org/10.1146/annurev-immunol-042617-053238.
———. 2018b. “IgA Function in Relation to the Intestinal Microbiota.” *Annual Review of Immunology*. https://doi.org/10.1146/annurev-immunol-042617-053238.
Mair, William, Matthew D. W. Piper, and Linda Partridge. 2005. “Calories Do Not Explain Extension of Life Span by Dietary Restriction in Drosophila.” *PLoS Biology* 3 (7): e223.
Malemud, Charles J. 2015. “Biologic Basis of Osteoarthritis: State of the Evidence.” *Current Opinion in Rheumatology* 27 (3): 289–94.
Ma, Lina, Xinxin Tao, Xiaoyan He, Peng Wang, Long Ma, Bin Shi, and Xinsheng Yao. 2021. “Analysis of the Heterogeneity of the BCR H-CDR3 Repertoire in the Bone Marrow and Spleen of 3-, 12-, and 20-Month Old Mice.” *Immunity & Ageing: I & A* 18 (1): 17.
Mancuso, Peter, and Benjamin Bouchard. 2019. “The Impact of Aging on Adipose Function and Adipokine Synthesis.” *Frontiers in Endocrinology* 10 (March): 137.
Mandrekar, Pranoti, and Gyongyi Szabo. 2009. “Signalling Pathways in Alcohol-Induced Liver Inflammation.” *Journal of Hepatology* 50 (6): 1258–66.
Mangoni, Matteo E., and Joël Nargeot. 2008. “Genesis and Regulation of the Heart Automaticity.” *Physiological Reviews* 88 (3): 919–82.
Mannick, Joan B., Giuseppe Del Giudice, Maria Lattanzi, Nicholas M. Valiante, Jens Praestgaard, Baisong Huang, Michael A. Lonetto, et al. 2014. “mTOR Inhibition

Improves Immune Function in the Elderly." *Science Translational Medicine* 6 (268): 268ra179.
Mannick, Joan B., Melody Morris, Hans-Ulrich P. Hockey, Guglielmo Roma, Martin Beibel, Kenneth Kulmatycki, Mollie Watkins, et al. 2018. "TORC1 Inhibition Enhances Immune Function and Reduces Infections in the Elderly." *Science Translational Medicine* 10 (449). https://doi.org/10.1126/scitranslmed.aaq1564.
Martin, Marcel. 2011. "Cutadapt Removes Adapter Sequences from High-Throughput Sequencing Reads." *EMBnet.journal*. https://doi.org/10.14806/ej.17.1.200.
Martin, Victoria, Yu-Chang (bryan) Wu, David Kipling, and Deborah Dunn-Walters. 2015. "Ageing of the B-Cell Repertoire." *Philosophical Transactions of the Royal Society B: Biological Sciences*. https://doi.org/10.1098/rstb.2014.0237.
Mattison, Julie A., George S. Roth, T. Mark Beasley, Edward M. Tilmont, April M. Handy, Richard L. Herbert, Dan L. Longo, et al. 2012. "Impact of Caloric Restriction on Health and Survival in Rhesus Monkeys from the NIA Study." *Nature* 489 (7415): 318–21.
Mattson, Mark P., David B. Allison, Luigi Fontana, Michelle Harvie, Valter D. Longo, Willy J. Malaisse, Michael Mosley, et al. 2014. "Meal Frequency and Timing in Health and Disease." *Proceedings of the National Academy of Sciences of the United States of America* 111 (47): 16647–53.
McKay, M. M., and D. K. Morrison. 2007. "Integrating Signals from RTKs to ERK/MAPK." *Oncogene* 26 (22): 3113–21.
McKean, David, Konrad Huppi, Michael Bell, Louis Staudt, Walter Gerhard, and Martin Weigert. 2008. "Pillars Article: Generation of Antibody Diversity in the Immune Response of BALB/c Mice to Influenza Virus Hemagglutinin. Proc. Natl. Acad. Sci. USA, 81: 3180-3184, May 1984." *Journal of Immunology* 180 (9): 5765–69.
McMurdie, Paul J., and Susan Holmes. 2013. "Phyloseq: An R Package for Reproducible Interactive Analysis and Graphics of Microbiome Census Data." *PLoS ONE*. https://doi.org/10.1371/journal.pone.0061217.
Mendoza, Michelle C., E. Emrah Er, and John Blenis. 2011. "The Ras-ERK and PI3K-mTOR Pathways: Cross-Talk and Compensation." *Trends in Biochemical Sciences* 36 (6): 320–28.
Meng, Wenzhao, Bochao Zhang, Gregory W. Schwartz, Aaron M. Rosenfeld, Daqiu Ren, Joseph J. C. Thome, Dustin J. Carpenter, et al. 2017. "An Atlas of B-Cell Clonal Distribution in the Human Body." *Nature Biotechnology* 35 (9): 879–84.
Messaoudi, Ilhem, Jessica Warner, Miranda Fischer, Buyng Park, Brenna Hill, Julie Mattison, Mark A. Lane, et al. 2006. "Delay of T Cell Senescence by Caloric Restriction in Aged Long-Lived Nonhuman Primates." *Proceedings of the National Academy of Sciences of the United States of America* 103 (51): 19448–53.
Miho, Enkelejda, Alexander Yermanos, Cédric R. Weber, Christoph T. Berger, Sai T. Reddy, and Victor Greiff. 2018. "Computational Strategies for Dissecting the High-Dimensional Complexity of Adaptive Immune Repertoires." *Frontiers in Immunology* 9 (February): 224.
Miller, C., and G. Kelsoe. 1995. "Ig VH Hypermutation Is Absent in the Germinal Centers of Aged Mice." *Journal of Immunology* 155 (7): 3377–84.
Miller, R. A. 1996. "The Aging Immune System: Primer and Prospectus." *Science* 273 (5271): 70–74.
Miller, Richard A., David E. Harrison, Clinton M. Astle, Elizabeth Fernandez, Kevin Flurkey, Melissa Han, Martin A. Javors, et al. 2014. "Rapamycin-Mediated Lifespan Increase in Mice Is Dose and Sex Dependent and Metabolically Distinct from Dietary Restriction." *Aging Cell* 13 (3): 468–77.
Miller, Richard A., David E. Harrison, C. M. Astle, Joseph A. Baur, Angela Rodriguez Boyd, Rafael de Cabo, Elizabeth Fernandez, et al. 2011. "Rapamycin, But Not Resveratrol or Simvastatin, Extends Life Span of Genetically Heterogeneous Mice." *The Journals of Gerontology: Series A*. https://doi.org/10.1093/gerona/glq178.
Mirisola, Mario G., and Valter D. Longo. 2011. "Conserved Role of Ras-GEFs in Promoting Aging: From Yeast to Mice." *Aging*.

Mitchell, Sarah J., Michel Bernier, Miguel A. Aon, Sonia Cortassa, Eun Young Kim, Evandro F. Fang, Hector H. Palacios, et al. 2018. “Nicotinamide Improves Aspects of Healthspan, but Not Lifespan, in Mice.” *Cell Metabolism* 27 (3): 667–76.e4.
Moiseeva, Olga, Xavier Deschênes-Simard, Emmanuelle St-Germain, Sebastian Igelmann, Geneviève Huot, Alexandra E. Cadar, Véronique Bourdeau, Michael N. Pollak, and Gerardo Ferbeyre. 2013. “Metformin Inhibits the Senescence-Associated Secretory Phenotype by Interfering with IKK/NF-κB Activation.” *Aging Cell* 12 (3): 489–98.
Motori, Elisa, Julien Puyal, Nicolas Toni, Alexander Ghanem, Cristina Angeloni, Marco Malaguti, Giorgio Cantelli-Forti, et al. 2013. “Inflammation-Induced Alteration of Astrocyte Mitochondrial Dynamics Requires Autophagy for Mitochondrial Network Maintenance.” *Cell Metabolism* 18 (6): 844–59.
Muggen, Alice F., Madelon de Jong, Ingrid L. M. Wolvers-Tettero, Martine J. Kallemeijn, Cristina Teodósio, Nikos Darzentas, Ralph Stadhouders, et al. 2019. “The Presence of CLL-Associated Stereotypic B Cell Receptors in the Normal BCR Repertoire from Healthy Individuals Increases with Age.” *Immunity & Ageing: I & A* 16 (August): 22.
Murphy, Geoffrey G., Nancy P. Rahnama, and Alcino J. Silva. 2006. “Investigation of Age-Related Cognitive Decline Using Mice as a Model System: Behavioral Correlates.” *The American Journal of Geriatric Psychiatry: Official Journal of the American Association for Geriatric Psychiatry* 14 (12): 1004–11.
Nagpal, Ravinder, Rabina Mainali, Shokouh Ahmadi, Shaohua Wang, Ria Singh, Kylie Kavanagh, Dalane W. Kitzman, Almagul Kushugulova, Francesco Marotta, and Hariom Yadav. 2018. “Gut Microbiome and Aging: Physiological and Mechanistic Insights.” *Nutrition and Healthy Aging* 4 (4): 267–85.
Nakayama, Konosuke, Yasuhiro Tamura, Miyuki Suzawa, Shun-Ichi Harada, Seiji Fukumoto, Mitsuyasu Kato, Kohei Miyazono, Gideon A. Rodan, Yasuhiro Takeuchi, and Toshiro Fujita. 2003. “Receptor Tyrosine Kinases Inhibit Bone Morphogenetic Protein-Smad Responsive Promoter Activity and Differentiation of Murine MC3T3-E1 Osteoblast-like Cells.” *Journal of Bone and Mineral Research: The Official Journal of the American Society for Bone and Mineral Research* 18 (5): 827–35.
Neff, Frauke, Diana Flores-Dominguez, Devon P. Ryan, Marion Horsch, Susanne Schröder, Thure Adler, Luciana Caminha Afonso, et al. 2013. “Rapamycin Extends Murine Lifespan but Has Limited Effects on Aging.” *The Journal of Clinical Investigation* 123 (8): 3272–91.
Nespital, Tobias, Brit Neuhaus, Andrea Mesaros, André Pahl, and Linda Partridge. 2021. “Lithium Can Mildly Increase Health during Ageing but Not Lifespan in Mice.” *Aging Cell* 20 (10): e13479.
Nguyen, Tue Gia. 2022. “The Therapeutic Implications of Activated Immune Responses via the Enigmatic Immunoglobulin D.” *International Reviews of Immunology* 41 (2): 107–22.
Niccoli, Teresa, and Linda Partridge. 2012. “Ageing as a Risk Factor for Disease.” *Current Biology*. https://doi.org/10.1016/j.cub.2012.07.024.
Nielsen, Rasmus, and Ziheng Yang. 1998. “Likelihood Models for Detecting Positively Selected Amino Acid Sites and Applications to the HIV-1 Envelope Gene.” *Genetics*. https://doi.org/10.1093/genetics/148.3.929.
Nikolich-Zugich, Janko. 2005a. “T Cell Aging: Naive but Not Young.” *The Journal of Experimental Medicine* 201 (6): 837–40.
———. 2005b. “T Cell Aging: Naive but Not Young.” *The Journal of Experimental Medicine* 201 (6): 837–40.
Nikolich-Žugich, Janko, Dana P. Goldman, Paul R. Cohen, Denis Cortese, Luigi Fontana, Brian K. Kennedy, M. Jane Mohler, et al. 2016. “Preparing for an Aging World: Engaging Biogerontologists, Geriatricians, and the Society.” *The Journals of Gerontology. Series A, Biological Sciences and Medical Sciences* 71 (4): 435–44.
Oh, Soo-Jin, Jae Kyung Lee, and Ok Sarah Shin. 2019a. “Aging and the Immune System: The Impact of Immunosenescence on Viral Infection, Immunity and Vaccine Immunogenicity.” *Immune Network* 19 (6): e37.
———. 2019b. “Aging and the Immune System: The Impact of Immunosenescence on Viral

Infection, Immunity and Vaccine Immunogenicity." *Immune Network* 19 (6): e37.
Okawa, Takuma, Motoyoshi Nagai, and Koji Hase. 2020. "Dietary Intervention Impacts Immune Cell Functions and Dynamics by Inducing Metabolic Rewiring." *Frontiers in Immunology* 11: 623989.
Omodei, Daniela, and Luigi Fontana. 2011. "Calorie Restriction and Prevention of Age-Associated Chronic Disease." *FEBS Letters* 585 (11): 1537–42.
Ozaki, Kei-Ichi, Midori Awazu, Mayuko Tamiya, Yuka Iwasaki, Aya Harada, Satomi Kugisaki, Susumu Tanimura, and Michiaki Kohno. 2016. "Targeting the ERK Signaling Pathway as a Potential Treatment for Insulin Resistance and Type 2 Diabetes." *American Journal of Physiology. Endocrinology and Metabolism* 310 (8): E643–51.
Paolisso, G., D. Manzella, M. Barbieri, M. R. Rizzo, A. Gambardella, and M. Varricchio. 1999. "Baseline Heart Rate Variability in Healthy Centenarians: Differences Compared with Aged Subjects (>75 Years Old)." *Clinical Science* 97 (5): 579–84.
Parker, Aimée, Stefano Romano, Rebecca Ansorge, Asmaa Aboelnour, Gwenaelle Le Gall, George M. Savva, Matthew G. Pontifex, et al. 2022. "Fecal Microbiota Transfer between Young and Aged Mice Reverses Hallmarks of the Aging Gut, Eye, and Brain." *Microbiome* 10 (1): 68.
Partridge, Linda. 2010. "The New Biology of Ageing." *Philosophical Transactions of the Royal Society B: Biological Sciences*. https://doi.org/10.1098/rstb.2009.0222.
Partridge, Linda, Nazif Alic, Ivana Bjedov, and Matt D. W. Piper. 2011. "Ageing in Drosophila: The Role of the insulin/Igf and TOR Signalling Network." *Experimental Gerontology* 46 (5): 376–81.
Pawlikowska, Ludmila, Donglei Hu, Scott Huntsman, Andrew Sung, Catherine Chu, Justin Chen, Alexander H. Joyner, et al. 2009. "Association of Common Genetic Variation in the insulin/IGF1 Signaling Pathway with Human Longevity." *Aging Cell* 8 (4): 460–72.
Piantoni, Chiara, Luca Carnevali, David Molla, Andrea Barbuti, Dario DiFrancesco, Annalisa Bucchi, and Mirko Baruscotti. 2021. "Age-Related Changes in Cardiac Autonomic Modulation and Heart Rate Variability in Mice." *Frontiers in Neuroscience* 15 (May): 617698.
Piccirillo, G., C. Bucca, C. Bauco, A. M. Cinti, D. Michele, F. L. Fimognari, M. Cacciafesta, and V. Marigliano. 1998. "Power Spectral Analysis of Heart Rate in Subjects over a Hundred Years Old." *International Journal of Cardiology* 63 (1): 53–61.
Piper, Matthew D. W., and Linda Partridge. 2018. "Drosophila as a Model for Ageing." *Biochimica et Biophysica Acta, Molecular Basis of Disease* 1864 (9 Pt A): 2707–17.
Qi, Sihua, Makoto Mizuno, Kazuyoshi Yonezawa, Hiroyuki Nawa, and Nobuyuki Takei. 2010. "Activation of Mammalian Target of Rapamycin Signaling in Spatial Learning." *Neuroscience Research* 68 (2): 88–93.
Rahman, W. Tania, W. Tania Rahman, Daniel J. Wale, Benjamin L. Viglianti, Danyelle M. Townsend, Matthew S. Manganaro, Milton D. Gross, Ka Kit Wong, and Domenico Rubello. 2019. "The Impact of Infection and Inflammation in Oncologic 18F-FDG PET/CT Imaging." *Biomedicine & Pharmacotherapy*. https://doi.org/10.1016/j.biopha.2019.109168.
Rajalingam, Krishnaraj, Ralf Schreck, Ulf R. Rapp, and Stefan Albert. 2007. "Ras Oncogenes and Their Downstream Targets." *Biochimica et Biophysica Acta* 1773 (8): 1177–95.
Raposo, Bruno, Doreen Dobritzsch, Changrong Ge, Diana Ekman, Bingze Xu, Ingrid Lindh, Michael Förster, et al. 2014. "Epitope-Specific Antibody Response Is Controlled by Immunoglobulin V(H) Polymorphisms." *The Journal of Experimental Medicine* 211 (3): 405–11.
Redman, Leanne M., Steven R. Smith, Jeffrey H. Burton, Corby K. Martin, Dora Il'yasova, and Eric Ravussin. 2018. "Metabolic Slowing and Reduced Oxidative Damage with Sustained Caloric Restriction Support the Rate of Living and Oxidative Damage Theories of Aging." *Cell Metabolism* 27 (4): 805–15.e4.
Reifsnyder, Peter C., Kevin Flurkey, Rosalinda Doty, Nigel A. Calcutt, Robert A. Koza, and David E. Harrison. 2022. "Rapamycin/metformin Co-Treatment Normalizes Insulin

Sensitivity and Reduces Complications of Metabolic Syndrome in Type 2 Diabetic Mice." *Aging Cell* 21 (9): e13666.
Research, Case Medical, and Case Medical Research. 2019. "Human Medicines European Public Assessment Report (EPAR): Mekinist, Trametinib, Melanoma, Date of Authorisation: 30/06/2014, Revision: 16, Status: Authorised." *Case Medical Research*. https://doi.org/10.31525/cmr-c543df.
Robida-Stubbs, Stacey, Kira Glover-Cutter, Dudley W. Lamming, Masaki Mizunuma, Sri Devi Narasimhan, Elke Neumann-Haefelin, David M. Sabatini, and T. Keith Blackwell. 2012. "TOR Signaling and Rapamycin Influence Longevity by Regulating SKN-1/Nrf and DAF-16/FoxO." *Cell Metabolism* 15 (5): 713–24.
Roda, Alejandro R., Gisela Esquerda-Canals, Joaquim Martí-Clúa, and Sandra Villegas. 2020. "Cognitive Impairment in the 3xTg-AD Mouse Model of Alzheimer's Disease Is Affected by Aβ-ImmunoTherapy and Cognitive Stimulation." *Pharmaceutics* 12 (10). https://doi.org/10.3390/pharmaceutics12100944.
Rogerson, B. 2003. "Germinal Center B Cells in Peyer's Patches of Aged Mice Exhibit a Normal Activation Phenotype and Highly Mutated IgM Genes." *Mechanisms of Ageing and Development*. https://doi.org/10.1016/s0047-6374(02)00115-x.
Rosenzweig, Ephron S., and Carol A. Barnes. 2003. "Impact of Aging on Hippocampal Function: Plasticity, Network Dynamics, and Cognition." *Progress in Neurobiology* 69 (3): 143–79.
Safaie, E., R. Matthews, and R. Bergamaschi. 2015. "PET Scan Findings Can Be False Positive." *Techniques in Coloproctology* 19 (6): 329–30.
Salminen, Antero, Kai Kaarniranta, and Anu Kauppinen. 2012. "Inflammaging: Disturbed Interplay between Autophagy and Inflammasomes." *Aging* 4 (3): 166–75.
Saunders, Sean P., Erica G. M. Ma, Carlos J. Aranda, and Maria A. Curotto de Lafaille. 2019. "Non-Classical B Cell Memory of Allergic IgE Responses." *Frontiers in Immunology* 10 (April): 715.
Schaum, Nicholas, Benoit Lehallier, Oliver Hahn, Róbert Pálovics, Shayan Hosseinzadeh, Song E. Lee, Rene Sit, et al. 2020. "Ageing Hallmarks Exhibit Organ-Specific Temporal Signatures." *Nature* 583 (7817): 596–602.
Schlessinger, J. 2000. "Cell Signaling by Receptor Tyrosine Kinases." *Cell* 103 (2): 211–25.
Schmauck-Medina, Tomas, Adrian Molière, Sofie Lautrup, Jianying Zhang, Stefan Chlopicki, Helena Borland Madsen, Shuqin Cao, et al. 2022. "New Hallmarks of Ageing: A 2022 Copenhagen Ageing Meeting Summary." *Aging* 14 (16): 6829–39.
Schroeder, Harry W., Jr, and Lisa Cavacini. 2010. "Structure and Function of Immunoglobulins." *The Journal of Allergy and Clinical Immunology* 125 (2 Suppl 2): S41–52.
Schuijt, Tim J., Jacqueline M. Lankelma, Brendon P. Scicluna, Felipe de Sousa e Melo, Joris J. T. H. Roelofs, J. Daan de Boer, Arjan J. Hoogendijk, et al. 2016. "The Gut Microbiota Plays a Protective Role in the Host Defence against Pneumococcal Pneumonia." *Gut* 65 (4): 575–83.
Schwartzenberg, Reiner Jumpertz von, Jordan E. Bisanz, Svetlana Lyalina, Peter Spanogiannopoulos, Qi Yan Ang, Jingwei Cai, Sophia Dickmann, et al. 2021. "Caloric Restriction Disrupts the Microbiota and Colonization Resistance." *Nature* 595 (7866): 272–77.
Schwartz, Michael W., Randy J. Seeley, Matthias H. Tschöp, Stephen C. Woods, Gregory J. Morton, Martin G. Myers, and David D'Alessio. 2013. "Cooperation between Brain and Islet in Glucose Homeostasis and Diabetes." *Nature* 503 (7474): 59–66.
Seabold, Skipper, and Josef Perktold. 2010. "Statsmodels: Econometric and Statistical Modeling with Python." *Proceedings of the 9th Python in Science Conference*. https://doi.org/10.25080/majora-92bf1922-011.
Selman, Colin, Steven Lingard, Agharul I. Choudhury, Rachel L. Batterham, Marc Claret, Melanie Clements, Faruk Ramadani, et al. 2008. "Evidence for Lifespan Extension and Delayed Age-Related Biomarkers in Insulin Receptor Substrate 1 Null Mice." *FASEB Journal: Official Publication of the Federation of American Societies for Experimental*

Biology 22 (3): 807–18.
Selman, Colin, Jennifer M. A. Tullet, Daniela Wieser, Elaine Irvine, Steven J. Lingard, Agharul I. Choudhury, Marc Claret, et al. 2009. “Ribosomal Protein S6 Kinase 1 Signaling Regulates Mammalian Life Span.” *Science* 326 (5949): 140–44.
Sheridan, Paige E., Christine A. Mair, and Ana R. Quiñones. 2019. “Associations between Prevalent Multimorbidity Combinations and Prospective Disability and Self-Rated Health among Older Adults in Europe.” *BMC Geriatrics* 19 (1): 198.
Shindyapina, Anastasia V., Yongmin Cho, Alaattin Kaya, Alexander Tyshkovskiy, José P. Castro, Amy Deik, Juozas Gordevicius, et al. 2022. “Rapamycin Treatment during Development Extends Life Span and Health Span of Male Mice and.” *Science Advances* 8 (37): eabo5482.
Shi, Yuhui, Takashi Yamazaki, Yoshio Okubo, Yoshio Uehara, Kazuo Sugane, and Kazunaga Agematsu. 2005. “Regulation of Aged Humoral Immune Defense against Pneumococcal Bacteria by IgM Memory B Cell.” *Journal of Immunology* 175 (5): 3262–67.
Shoji, Hirotaka, Keizo Takao, Satoko Hattori, and Tsuyoshi Miyakawa. 2016. “Age-Related Changes in Behavior in C57BL/6J Mice from Young Adulthood to Middle Age.” *Molecular Brain* 9 (January): 11.
Shushimita, Shushimita Shushimita, Marjolein J. W. de Bruijn, Ron W. F. de Bruin, Jan N. M. IJzermans, Rudi W. Hendriks, and Frank J. M. Dor. 2014. “Dietary Restriction and Fasting Arrest B and T Cell Development and Increase Mature B and T Cell Numbers in Bone Marrow.” *PLoS ONE*. https://doi.org/10.1371/journal.pone.0087772.
Slack, Cathy. 2017. “Ras Signaling in Aging and Metabolic Regulation.” *Nutrition and Healthy Aging* 4 (3): 195–205.
Slack, Cathy, Nazif Alic, Andrea Foley, Melissa Cabecinha, Matthew P. Hoddinott, and Linda Partridge. 2015. “The Ras-Erk-ETS-Signaling Pathway Is a Drug Target for Longevity.” *Cell* 162 (1): 72–83.
Slack, Cathy, Maria E. Giannakou, Andrea Foley, Martin Goss, and Linda Partridge. 2011. “dFOXO-Independent Effects of Reduced Insulin-like Signaling in Drosophila.” *Aging Cell* 10 (5): 735–48.
Smith, Erica D., Tammi L. Kaeberlein, Brynn T. Lydum, Jennifer Sager, K. Linnea Welton, Brian K. Kennedy, and Matt Kaeberlein. 2008. “Age- and Calorie-Independent Life Span Extension from Dietary Restriction by Bacterial Deprivation in Caenorhabditis Elegans.” *BMC Developmental Biology* 8 (May): 49.
Smith, Patrick, David Willemsen, Miriam Popkes, Franziska Metge, Edson Gandiwa, Martin Reichard, and Dario Riccardo Valenzano. 2017. “Regulation of Life Span by the Gut Microbiota in the Short-Lived African Turquoise Killifish.” *eLife* 6 (August). https://doi.org/10.7554/eLife.27014.
Solon-Biet, Samantha M., Aisling C. McMahon, J. William O. Ballard, Kari Ruohonen, Lindsay E. Wu, Victoria C. Cogger, Alessandra Warren, et al. 2014. “The Ratio of Macronutrients, Not Caloric Intake, Dictates Cardiometabolic Health, Aging, and Longevity in Ad Libitum-Fed Mice.” *Cell Metabolism* 19 (3): 418–30.
Sommer, Felix, and Fredrik Bäckhed. 2013a. “The Gut Microbiota--Masters of Host Development and Physiology.” *Nature Reviews. Microbiology* 11 (4): 227–38.
———. 2013b. “The Gut Microbiota--Masters of Host Development and Physiology.” *Nature Reviews. Microbiology* 11 (4): 227–38.
Sparkman, Nathan L., and Rodney W. Johnson. 2008. “Neuroinflammation Associated with Aging Sensitizes the Brain to the Effects of Infection or Stress.” *Neuroimmunomodulation* 15 (4-6): 323–30.
Stavnezer, Janet, Jeroen E. J. Guikema, and Carol E. Schrader. 2008. “Mechanism and Regulation of Class Switch Recombination.” *Annual Review of Immunology* 26: 261–92.
Stephen, Andrew G., Dominic Esposito, Rachel K. Bagni, and Frank McCormick. 2014. “Dragging Ras Back in the Ring.” *Cancer Cell* 25 (3): 272–81.
Strong, Randy, Richard A. Miller, Adam Antebi, Clinton M. Astle, Molly Bogue, Martin S. Denzel, Elizabeth Fernandez, et al. 2016. “Longer Lifespan in Male Mice Treated with a

Weakly Estrogenic Agonist, an Antioxidant, an α-Glucosidase Inhibitor or a Nrf2-Inducer." *Aging Cell* 15 (5): 872–84.
Strong, Randy, Richard A. Miller, Catherine J. Cheng, James F. Nelson, Jonathan Gelfond, Shailaja Kesaraju Allani, Vivian Diaz, et al. 2022. "Lifespan Benefits for the Combination of Rapamycin plus Acarbose and for Captopril in Genetically Heterogeneous Mice." *Aging Cell*, September, e13724.
Tang, Duozhuang, Si Tao, Zhiyang Chen, Ievgen Oleksandrovich Koliesnik, Philip Gerald Calmes, Verena Hoerr, Bing Han, et al. 2021. "Correction: Dietary Restriction Improves Repopulation but Impairs Lymphoid Differentiation Capacity of Hematopoietic Stem Cells in Early Aging." *The Journal of Experimental Medicine* 218 (1). https://doi.org/10.1084/jem.2015110012042020C.
Tao, Si, Yiting Wang, Jianying Wu, Ting Zeng, Hui Cui, Zhendong Tao, Lang Lei, et al. 2020. "Long-Term Mid-Onset Dietary Restriction Rejuvenates Hematopoietic Stem Cells and Improves Regeneration Capacity of Total Bone Marrow from Aged Mice." *Aging Cell* 19 (10): e13241.
Tas, Jeroen M. J., Luka Mesin, Giulia Pasqual, Sasha Targ, Johanne T. Jacobsen, Yasuko M. Mano, Casie S. Chen, et al. 2016. "Visualizing Antibody Affinity Maturation in Germinal Centers." *Science* 351 (6277): 1048–54.
Tatar, M., A. Kopelman, D. Epstein, M. P. Tu, C. M. Yin, and R. S. Garofalo. 2001. "A Mutant Drosophila Insulin Receptor Homolog That Extends Life-Span and Impairs Neuroendocrine Function." *Science* 292 (5514): 107–10.
Thireau, J., B. L. Zhang, D. Poisson, and D. Babuty. 2008. "Heart Rate Variability in Mice: A Theoretical and Practical Guide." *Experimental Physiology* 93 (1): 83–94.
Treglia, Giorgio. 2019. "Diagnostic Performance of F-FDG PET/CT in Infectious and Inflammatory Diseases according to Published Meta-Analyses." *Contrast Media & Molecular Imaging* 2019 (July): 3018349.
Treuting, Piper M., Nancy J. Linford, Sue E. Knoblaugh, M. J. Emond, John F. Morton, George M. Martin, Peter S. Rabinovitch, and Warren C. Ladiges. 2008. "Reduction of Age-Associated Pathology in Old Mice by Overexpression of Catalase in Mitochondria." *The Journals of Gerontology. Series A, Biological Sciences and Medical Sciences* 63 (8): 813–22.
Turchaninova, M. A., A. Davydov, O. V. Britanova, M. Shugay, V. Bikos, E. S. Egorov, V. I. Kirgizova, et al. 2016. "High-Quality Full-Length Immunoglobulin Profiling with Unique Molecular Barcoding." *Nature Protocols* 11 (9): 1599–1616.
Turner, Vivian M., and Neil A. Mabbott. 2017. "Influence of Ageing on the Microarchitecture of the Spleen and Lymph Nodes." *Biogerontology* 18 (5): 723–38.
United Nations. 2019. *World Population Ageing 2019 Highlights*. United Nations.
Urban, Jörg, Alexandre Soulard, Alexandre Huber, Soyeon Lippman, Debdyuti Mukhopadhyay, Olivier Deloche, Valeria Wanke, et al. 2007. "Sch9 Is a Major Target of TORC1 in Saccharomyces Cerevisiae." *Molecular Cell* 26 (5): 663–74.
Vaidhyanathan, Shruthi, Rajendar K. Mittapalli, Jann N. Sarkaria, and William F. Elmquist. 2014. "Factors Influencing the CNS Distribution of a Novel MEK-1/2 Inhibitor: Implications for Combination Therapy for Melanoma Brain Metastases." *Drug Metabolism and Disposition: The Biological Fate of Chemicals* 42 (8): 1292–1300.
Valdearcos, Martin, John D. Douglass, Megan M. Robblee, Mauricio D. Dorfman, Daniel R. Stifler, Mariko L. Bennett, Irene Gerritse, et al. 2017. "Microglial Inflammatory Signaling Orchestrates the Hypothalamic Immune Response to Dietary Excess and Mediates Obesity Susceptibility." *Cell Metabolism* 26 (1): 185–97.e3.
Vander Heiden, Jason Anthony, Susanna Marquez, Nishanth Marthandan, Syed Ahmad Chan Bukhari, Christian E. Busse, Brian Corrie, Uri Hershberg, et al. 2018. "AIRR Community Standardized Representations for Annotated Immune Repertoires." *Frontiers in Immunology* 9 (September): 2206.
Vellai, Tibor, Krisztina Takacs-Vellai, Yue Zhang, Attila L. Kovacs, László Orosz, and Fritz Müller. 2003. "Influence of TOR Kinase on Lifespan in C. Elegans." *Nature*. https://doi.org/10.1038/426620a.

Vencovský, J., E. Zď árský, S. P. Moyes, A. Hajeer, S. Ruzicková, Z. Cimburek, W. E. Ollier, R. N. Maini, and R. A. Mageed. 2002. “Polymorphism in the Immunoglobulin VH Gene V1-69 Affects Susceptibility to Rheumatoid Arthritis in Subjects Lacking the HLA-DRB1 Shared Epitope.” *Rheumatology* 41 (4): 401–10.
Virtanen, Pauli, Ralf Gommers, Travis E. Oliphant, Matt Haberland, Tyler Reddy, David Cournapeau, Evgeni Burovski, et al. 2020. “SciPy 1.0: Fundamental Algorithms for Scientific Computing in Python.” *Nature Methods* 17 (3): 261–72.
Wabitsch, Simon, Mayank Tandon, Benjamin Ruf, Qianfei Zhang, Justin D. McCallen, John C. McVey, Chi Ma, et al. 2021. “Anti–PD-1 in Combination With Trametinib Suppresses Tumor Growth and Improves Survival of Intrahepatic Cholangiocarcinoma in Mice.” *Cellular and Molecular Gastroenterology and Hepatology* 12 (3): 1166–78.
Walter, M. A., W. T. Gibson, G. C. Ebers, and D. W. Cox. 1991. “Susceptibility to Multiple Sclerosis Is Associated with the Proximal Immunoglobulin Heavy Chain Variable Region.” *The Journal of Clinical Investigation* 87 (4): 1266–73.
Wang, Chen, Yi Liu, Lan T. Xu, Katherine J. L. Jackson, Krishna M. Roskin, Tho D. Pham, Jonathan Laserson, et al. 2014. “Effects of Aging, Cytomegalovirus Infection, and EBV Infection on Human B Cell Repertoires.” *The Journal of Immunology*. https://doi.org/10.4049/jimmunol.1301384.
Wardemann, Hedda, Sergey Yurasov, Anne Schaefer, James W. Young, Eric Meffre, and Michel C. Nussenzweig. 2003. “Predominant Autoantibody Production by Early Human B Cell Precursors.” *Science*. https://doi.org/10.1126/science.1086907.
Waxman, David J., and Minita G. Holloway. 2009. “Sex Differences in the Expression of Hepatic Drug Metabolizing Enzymes.” *Molecular Pharmacology* 76 (2): 215–28.
“Website.” n.d. http://support.illumina.com/documents/documentation/chemistry_documentation/16s/16s-metagenomic-library-prep-guide-15044223-b.pdf.
Weichhart, Thomas, Markus Hengstschläger, and Monika Linke. 2015. “Regulation of Innate Immune Cell Function by mTOR.” *Nature Reviews. Immunology* 15 (10): 599–614.
Wei, Min, Reiko Shinkura, Yasuko Doi, Mikako Maruya, Sidonia Fagarasan, and Tasuku Honjo. 2011. “Mice Carrying a Knock-in Mutation of Aicda Resulting in a Defect in Somatic Hypermutation Have Impaired Gut Homeostasis and Compromised Mucosal Defense.” *Nature Immunology*. https://doi.org/10.1038/ni.1991.
Weiskopf, Daniela, Birgit Weinberger, and Beatrix Grubeck-Loebenstein. 2009a. “The Aging of the Immune System.” *Transplant International: Official Journal of the European Society for Organ Transplantation* 22 (11): 1041–50.
———. 2009b. “The Aging of the Immune System.” *Transplant International: Official Journal of the European Society for Organ Transplantation* 22 (11): 1041–50.
Weksler, M. E., and P. Szabo. 2000. “The Effect of Age on the B-Cell Repertoire.” *Journal of Clinical Immunology* 20 (4): 240–49.
White, Matthew J., Charlotte M. Beaver, Martin R. Goodier, Christian Bottomley, Carolyn M. Nielsen, Asia-Sophia F. M. Wolf, Luisa Boldrin, et al. 2016. “Calorie Restriction Attenuates Terminal Differentiation of Immune Cells.” *Frontiers in Immunology* 7: 667.
Wick, G., P. Jansen-Dürr, P. Berger, I. Blasko, and B. Grubeck-Loebenstein. 2000a. “Diseases of Aging.” *Vaccine* 18 (16): 1567–83.
———. 2000b. “Diseases of Aging.” *Vaccine* 18 (16): 1567–83.
Wilkinson, John E., Lisa Burmeister, Susan V. Brooks, Chi-Chao Chan, Sabrina Friedline, David E. Harrison, James F. Hejtmancik, et al. 2012. “Rapamycin Slows Aging in Mice.” *Aging Cell* 11 (4): 675–82.
Willcox, Bradley J., Timothy A. Donlon, Qimei He, Randi Chen, John S. Grove, Katsuhiko Yano, Kamal H. Masaki, D. Craig Willcox, Beatriz Rodriguez, and J. David Curb. 2008. “FOXO3A Genotype Is Strongly Associated with Human Longevity.” *Proceedings of the National Academy of Sciences of the United States of America* 105 (37): 13987–92.
Wittinghofer, A., and N. Nassar. 1996. “How Ras-Related Proteins Talk to Their Effectors.” *Trends in Biochemical Sciences* 21 (12): 488–91.
Wood, Levi B., Ashley R. Winslow, Elizabeth A. Proctor, Declan McGuone, Daniel A.

Mordes, Matthew P. Frosch, Bradley T. Hyman, Douglas A. Lauffenburger, and Kevin M. Haigis. 2015. “Identification of Neurotoxic Cytokines by Profiling Alzheimer’s Disease Tissues and Neuron Culture Viability Screening.” *Scientific Reports* 5 (November): 16622.

Wright, Cameron J. M., and Paul L. McCormack. 2013. “Trametinib: First Global Approval.” *Drugs* 73 (11): 1245–54.

Wu, Ryan T., Lei Cao, Elliot Mattson, Kenneth W. Witwer, Jay Cao, Huawei Zeng, Xin He, Gerald F. Combs Jr, and Wen-Hsing Cheng. 2017. “Opposing Impacts on Healthspan and Longevity by Limiting Dietary Selenium in Telomere Dysfunctional Mice.” *Aging Cell* 16 (1): 125–35.

Wu, Yu-Chang, David Kipling, Hui Sun Leong, Victoria Martin, Alexander A. Ademokun, and Deborah K. Dunn-Walters. 2010. “High-Throughput Immunoglobulin Repertoire Analysis Distinguishes between Human IgM Memory and Switched Memory B-Cell Populations.” *Blood* 116 (7): 1070–78.

Xiang, Xianyuan, Karin Wind, Thomas Wiedemann, Tanja Blume, Yuan Shi, Nils Briel, Leonie Beyer, et al. 2021. “Microglial Activation States Drive Glucose Uptake and FDG-PET Alterations in Neurodegenerative Diseases.” *Science Translational Medicine* 13 (615): eabe5640.

Xu, Daqi, Marissa L. Matsumoto, Brent S. McKenzie, and Ali A. Zarrin. 2018. “TPL2 Kinase Action and Control of Inflammation.” *Pharmacological Research: The Official Journal of the Italian Pharmacological Society* 129 (March): 188–93.

Xu, Zhenming, Hong Zan, Egest J. Pone, Thach Mai, and Paolo Casali. 2012. “Immunoglobulin Class-Switch DNA Recombination: Induction, Targeting and beyond.” *Nature Reviews. Immunology* 12 (7): 517–31.

Yamaguchi, Takayuki, Reina Kakefuda, Nobuyuki Tajima, Yoshihiro Sowa, and Toshiyuki Sakai. 2011. “Antitumor Activities of JTP-74057 (GSK1120212), a Novel MEK1/2 Inhibitor, on Colorectal Cancer Cell Lines in Vitro and in Vivo.” *International Journal of Oncology* 39 (1): 23–31.

Yamamoto, Rochele, and Marc Tatar. 2011. “Insulin Receptor Substrate Chico Acts with the Transcription Factor FOXO to Extend Drosophila Lifespan.” *Aging Cell* 10 (4): 729–32.

Yang, Shi-Bing, An-Chi Tien, Gayatri Boddupalli, Allison W. Xu, Yuh Nung Jan, and Lily Yeh Jan. 2012. “Rapamycin Ameliorates Age-Dependent Obesity Associated with Increased mTOR Signaling in Hypothalamic POMC Neurons.” *Neuron* 75 (3): 425–36.

Yang, X., J. Stedra, and J. Cerny. 1996. “Relative Contribution of T and B Cells to Hypermutation and Selection of the Antibody Repertoire in Germinal Centers of Aged Mice.” *Journal of Experimental Medicine*. https://doi.org/10.1084/jem.183.3.959.

Yan, Xiaoxiang, Natsumi Imano, Kayoko Tamaki, Motoaki Sano, and Ken Shinmura. 2021. “The Effect of Caloric Restriction on the Increase in Senescence-Associated T Cells and Metabolic Disorders in Aged Mice.” *PloS One* 16 (6): e0252547.

Ye, Jian, Ning Ma, Thomas L. Madden, and James M. Ostell. 2013. “IgBLAST: An Immunoglobulin Variable Domain Sequence Analysis Tool.” *Nucleic Acids Research* 41 (Web Server issue): W34–40.

Ye, S. M., and R. W. Johnson. 2001. “Regulation of Interleukin-6 Gene Expression in Brain of Aged Mice by Nuclear Factor kappaB.” *Journal of Neuroimmunology* 117 (1-2): 87–96.

Yilmaz, Pelin, Laura Wegener Parfrey, Pablo Yarza, Jan Gerken, Elmar Pruesse, Christian Quast, Timmy Schweer, Jörg Peplies, Wolfgang Ludwig, and Frank Oliver Glöckner. 2014. “The SILVA and ‘All-Species Living Tree Project (LTP)’ Taxonomic Frameworks.” *Nucleic Acids Research*. https://doi.org/10.1093/nar/gkt1209.

Yin, Fei, Harsh Sancheti, Ishan Patil, and Enrique Cadenas. 2016. “Energy Metabolism and Inflammation in Brain Aging and Alzheimer’s Disease.” *Free Radical Biology & Medicine* 100 (November): 108–22.

Ying, Qi-Long, Jason Wray, Jennifer Nichols, Laura Batlle-Morera, Bradley Doble, James Woodgett, Philip Cohen, and Austin Smith. 2008. “The Ground State of Embryonic Stem Cell Self-Renewal.” *Nature* 453 (7194): 519–23.

Zhai, Baohui, Xueliang Shang, Jingxuan Fu, Fangjuan Li, and Tao Zhang. 2018. “Rapamycin Relieves Anxious Emotion and Synaptic Plasticity Deficits Induced by Hindlimb Unloading in Mice.” *Neuroscience Letters* 677 (June): 44–48.
Zhang, Chenhong, Shoufeng Li, Liu Yang, Ping Huang, Wenjun Li, Shengyue Wang, Guoping Zhao, et al. 2013. “Structural Modulation of Gut Microbiota in Life-Long Calorie-Restricted Mice.” *Nature Communications* 4: 2163.
Zhang, Wei, Barry J. Thompson, Ville Hietakangas, and Stephen M. Cohen. 2011. “MAPK/ERK Signaling Regulates Insulin Sensitivity to Control Glucose Metabolism in Drosophila.” *PLoS Genetics* 7 (12): e1002429.
Zhao, Jingmin, Chengbo Tan, Ryota Imai, Naoyuki Ukon, Saki Shimoyama, Yuko Maejima, Yuji Omiya, et al. 2021. “Evaluation of Organ Glucose Metabolism by 18F-FDG Accumulation with Insulin Loading in Aged Mice Compared with Young Normal Mice.” *Scientific Reports* 11 (1): 7421.
Zhao, Qing, and Charles O. Elson. 2018. “Adaptive Immune Education by Gut Microbiota Antigens.” *Immunology* 154 (1): 28–37.
Zheng, Cong, Xin-Wen Zhou, and Jian-Zhi Wang. 2016. “The Dual Roles of Cytokines in Alzheimer’s Disease: Update on Interleukins, TNF-α, TGF-β and IFN-γ.” *Translational Neurodegeneration* 5 (April): 7.
Zhou, Julian Q., and Steven H. Kleinstein. 2019. “Cutting Edge: Ig H Chains Are Sufficient to Determine Most B Cell Clonal Relationships.” *The Journal of Immunology*. https://doi.org/10.4049/jimmunol.1900666.

Erklärung zur Dissertation
gemäß der Promotionsordnung vom 12. März 2020

Diese Erklärung muss in der Dissertation enthalten sein.
(*This version must be included in the doctoral thesis*)

„Hiermit versichere ich an Eides statt, dass ich die vorliegende Dissertation selbstständig und ohne die Benutzung anderer als der angegebenen Hilfsmittel und Literatur angefertigt habe. Alle Stellen, die wörtlich oder sinngemäß aus veröffentlichten und nicht veröffentlichten Werken dem Wortlaut oder dem Sinn nach entnommen wurden, sind als solche kenntlich gemacht. Ich versichere an Eides statt, dass diese Dissertation noch keiner anderen Fakultät oder Universität zur Prüfung vorgelegen hat; dass sie - abgesehen von unten angegebenen Teilpublikationen und eingebundenen Artikeln und Manuskripten - noch nicht veröffentlicht worden ist sowie, dass ich eine Veröffentlichung der Dissertation vor Abschluss der Promotion nicht ohne Genehmigung des Promotionsausschusses vornehmen werde. Die Bestimmungen dieser Ordnung sind mir bekannt. Darüber hinaus erkläre ich hiermit, dass ich die Ordnung zur Sicherung guter wissenschaftlicher Praxis und zum Umgang mit wissenschaftlichem Fehlverhalten der Universität zu Köln gelesen und sie bei der Durchführung der Dissertation zugrundeliegenden Arbeiten und der schriftlich verfassten Dissertation beachtet habe und verpflichte mich hiermit, die dort genannten Vorgaben bei allen wissenschaftlichen Tätigkeiten zu beachten und umzusetzen. Ich versichere, dass die eingereichte elektronische Fassung der eingereichten Druckfassung vollständig entspricht."

Teilpublikationen:

07.09.2022, Lisonia Gkioni 
Datum, Name und Unterschrift

Erklärung zum Gesuch um Zulassung zur Promotion
gemäß der Promotionsordnung vom 12. März 2020

1. Zugänglichkeit von Daten und Materialien

Die Dissertation beinhaltet die Gewinnung von Primärdaten oder die Analyse solcher Daten oder die Reproduzierbarkeit der in der Dissertation dargestellten Ergebnisse setzt die Verfügbarkeit von Datenanalysen, Versuchsprotokollen oder Probenmaterial voraus.

☐ Trifft nicht zu
☒ Trifft zu.
In der Dissertation ist dargelegt wie diese Daten und Materialien gesichert und zugänglich sind (entsprechend den Vorgaben des Fachgebiets beziehungsweise der Betreuerin oder des Betreuers).

2. Frühere Promotionsverfahren

Ich habe bereits einen Doktortitel erworben oder ehrenhalber verliehen bekommen.
Oder: Für mich ist an einer anderen Fakultät oder Universität ein Promotionsverfahren eröffnet worden, aber noch nicht abgeschlossen.
Oder: Ich bin in einem Promotionsverfahren gescheitert.
☒ Trifft nicht zu
☐ Zutreffend
Erläuterung:

3. Straftat

Ich bin nicht zu einer vorsätzlichen Straftat verurteilt worden, bei deren Vorbereitung oder Begehung der Status einer Doktorandin oder eines Doktoranden missbraucht wurde.

Ich versichere, alle Angaben wahrheitsgemäß gemacht zu haben.

Datum	Name	Unterschrift
07.09.2022	Lisonia Gkioni